Highly Emissive Europium Complexes

JAMES WILLIAM WALTON

1. Introduction

1.1 Background to Luminescence

1.1.1 History

Luminescence, the spontaneous emission of radiation from an electronically excited species, is of great importance to many areas of science and technology. Various types of luminescence exist and are defined by their mode of excitation. Chemiluminescence, for example, is the emission of light following excitation via a chemical reaction. An early illustration of chemiluminescence comes from a Bolognian cobbler, Vincenzo Cascariolo, in 1602 who observed purple-blue light from a mineral which had been baked in a hot oven.[1] This light was later recognised as luminescence from the formation of impure barium sulphide. Photoluminescence, which is the main focus of this introduction, is the emission of light following direct photoexcitation of the emitting species. In 1565, Nicolás Mondardes, a Spanish physician, observed a peculiar blue colour in the infusion of a Mexican wood, *Lignum nephriticum*, used to treat urinary diseases. The colour is now known to originate from the photoluminescence of matlaline (*Figure 1.1*).[2] A final early example, which has relevance to the location in which this thesis is being written, is the sapphire blue photoluminescence of calcium fluoride crystals (*Figure 1.1*). Edward D. Clark, in 1819, commented that the crystals, found in Weardale, County Durham, surpassed in magnificence and beauty any other mineral he had ever seen.[3]

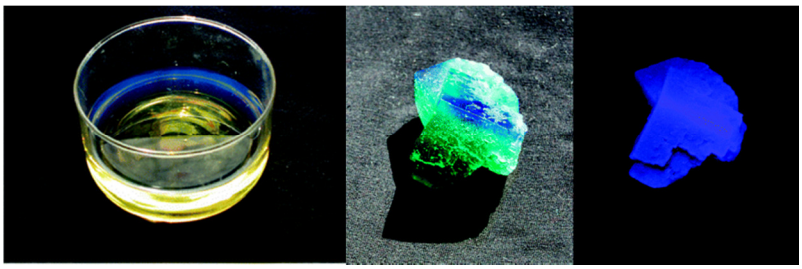

Figure 1.1 From left to right: blue photoluminescence from an aqueous solution of matlaline found in *Lignum nephriticum*; calcium fluoride crystals appearing emerald under direct sunlight and sapphire photoluminescence of the same crystal after UV excitation.

Photoluminescence was again responsible for observations made by Sir David Brewster in 1833, who described a red emission from a green alcoholic extract of leaves[4] (now known to be fluorescence from chlorophyll) and Sir John Herschel in 1845, who reported a celestial blue colour from an acidic solution of quinine.[5] In 1852, after experiments with a number of compounds, including quinine, George G. Stokes introduced the term fluorescence to describe the emission of light from a compound at a wavelength longer than that of the incident light.[6] He also noted that the dispersion of light took place in all directions. Many other contributions were made over the following years and today the application of photoluminescence ranges from fluorescence microscopy and plasma screens to counterfeit banknote detection.[7]

1.1.2 Fluorescence and Phosphorescence

Fluorescence and phosphorescence are both forms of photoluminescence and are best illustrated by a Jablonski diagram (*Figure 1.2*).[8] Following absorption of light by a molecule in its ground singlet state (S_0), fast relaxation occurs to its lowest lying singlet excited state (S_1) by internal conversion. From here, radiative emission (fluorescence), non radiative decay and intersystem crossing to the triplet excited state (T_1) can all take place. From the triplet state both radiative (phosphorescence) and non-radiative decay can occur to return the molecule to its ground state. Due to the dissipation of energy in the excited state, fluorescence always occurs at a longer wavelength than absorption. This is known as Stokes' shift.[6] The rate of internal conversion to the lowest lying vibrational level of S_1 or T_1 is typically much faster than the rate of radiative decay (10^{12} vs. 10^8 s^{-1}). As a result, the emission spectrum is generally independent of the excitation wavelength. The ability of a compound to absorb light is quantified by the molar extinction coefficient.

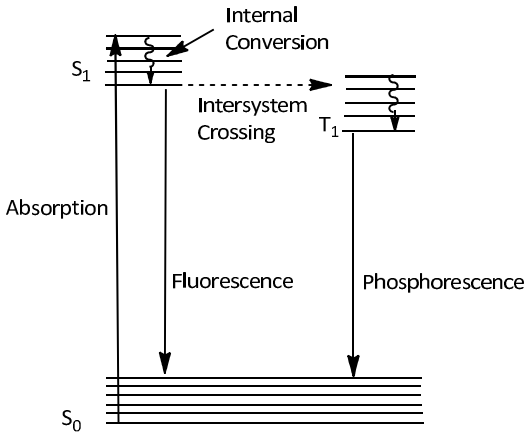

Figure 1.2 Jablonski diagram showing the important processes in photoluminescence.

1.1.3 Lifetime, Quantum Yield and Quenching

The lifetime of an excited state is defined by the average time a molecule spends in the excited state prior to returning to the ground state. Fluorescence lifetimes are of the order of 10 ns, whereas phosphorescence lifetimes are longer. The lifetime is often used to distinguish phosphorescence from fluorescence although, strictly, phosphorescence is defined by a change in spin multiplicity from the excited state to the ground state.

The quantum yield is the ratio of photons emitted to photons absorbed. The 'brightness' of a compound can be thought of as the product of the molar extinction coefficient, which defines the efficiency of absorption, and the quantum yield. The quantum yield is governed by the rate of radiative decay relative to all other non-radiative decay pathways. Quenching processes are those which decrease the overall emission by increasing the rate of non-radiative decay or providing alternative non-radiative decay pathways. These processes lead to a reduction in the quantum yield. Quenching processes can be collisional or static and include energy transfer, electron transfer and vibrational quenching. Quenching processes are of great importance when designing emissive molecules and are the subject of *Chapter 6*.

1.2 Luminescence in Biological Systems

1.2.1 Fluorescent Dyes

Fluorescent dyes are highly emissive organic molecules possessing large molar extinction coefficients and high quantum yields. They can be used to label, analyse and clarify the roles of biomolecules in living systems (*Figure 1.3*).[9] One of the most common dyes, fluorescein, and its derivatives, has found many applications in biological imaging as pH sensors,[10] calcium indicators,[11] and markers for the study of enzyme kinetics.[12] The sodium salt of fluorescein is also used extensively as a diagnostic tool in the field of optometry.

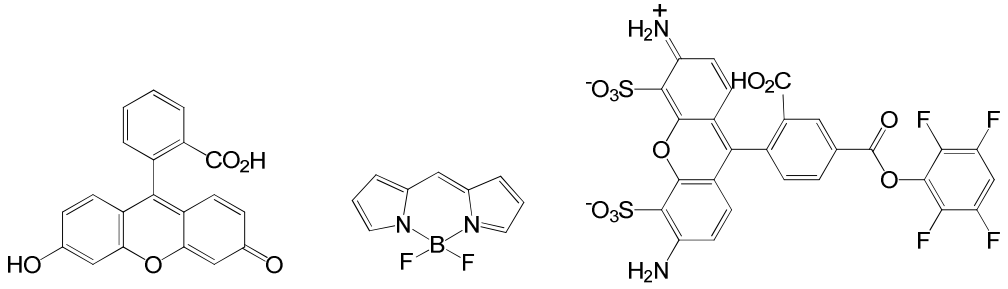

Figure 1.3 Examples of common commercially available fluorescent dyes.

Less desirable properties of fluorescein derivatives include a relatively high rate of photobleaching and broad emission bands. To address these issues, dyes based upon BODIPY and Alexa Fluor were developed.[13] These systems have increased resistance to photobleaching and have sharp emission bands. As with fluorescein, derivatives of the core structures lead to dyes with useful properties.

Despite their versatility, fluorescent dyes have a number of drawbacks, limiting their use in biological systems. These include: short lived excited states, making differentiation from background autofluorescence difficult; small Stokes' shifts, limiting their use in fluorescence microscopy and featureless, often broad emission spectra, which restrict their use as responsive probes.

1.2.2 Metal Complexes

A more in-depth discussion of lanthanide complexes as emissive compounds is given in *Section 1.3*. This section will focus only on the transition metal complexes, which make up a large class of optical probes. In general, these complexes combine a d^6 (Ru^{II}, Os^{II}, Re^{I} and Ir^{III}) or d^8 (Pt^{II}) metal with highly conjugated ligands, giving rise to intense ligand to metal (LMCT) or metal to ligand (MLCT) charge transfer bands.[14]

Low spin d^6 ruthenium polypyridyl complexes have been used to study biological systems for many years. Stereoselective binding of tris(phenanthroline)ruthenium(II) to DNA was monitored by changes in the MLCT emission as early as 1984.[15] A more recent example is shown in *Figure 1.4*, in which a ruthenium complex is able to permeate a myeloma cell, due to conjugation with a polypepide chain.[16]

The photophysical properties of this complex (λ_{ex} = 470 nm, λ_{em}= 600 nm, τ_{em} = 480 ns, Φ_{em} = 6 %) allow its visualisation by fluorescence microscopy. The emission lies outside the range of background fluorescence from endogenous species and the relatively high quantum yield and high molar extinction coefficient at 470 nm result in a bright complex.

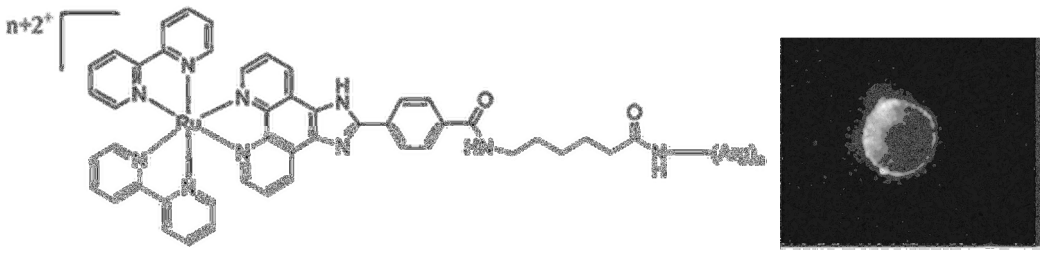

Figure 1.4 A ruthenium bipyridine complex conjugated to an arginine polypeptide, aiding fast uptake of the complex into a myeloma cell, visualised by fluorescence microscopy.

Many other metal complexes have been developed for use in cellular studies. As with the example above, these complexes typically have much larger Stokes' shifts than the fluorescent dyes and longer excited state lifetimes, making them amenable to time-resolved microscopy and fluorescence lifetime imaging. They also show good photostability. One limitation of these systems is their lack of responsiveness to their surroundings. Whilst this may be advantageous for some applications, they primarily function as cellular stains and do not report changes in their local environment.

1.2.3 Recombinant Fluorescent Proteins and Quantum Dots

Two final systems worthy of mention are the fluorescent proteins[17] and quantum dots.[18] Fluorescent proteins (FPs) consist of imidazolinone dyes within a β-barrel tertiary structure. They allow monitoring of live cells by fluorescence microscopy, due to their high quantum yield, stability within cells and resistance to quenching, thanks to the tertiary structure of the protein. Mutations of the protein have led to several 'colours' of fluorescent protein (green, cyan, yellow), which vary in their excitation and emission wavelengths. The limitations of FPs, as with the fluorescent dyes, are their short excited state lifetimes and small Stokes' shifts.

Quantum dots (QDs) are fluorescent semiconducting nanocrystals (common QDs include CdSe and ZnS) and are used as fluorescent tags due to their tuneable emission, high extinction coefficients and good photostability. Their application in living systems, however, is limited by the invasive nature of the large nanoparticles, which are likely to affect the physiology of dosed cells. Despite this drawback, the first clinical trial of quantum-dot technology in humans was recently approved by the U.S. Food and Drug Administration.[19]

1.3 Emissive Lanthanide Complexes

1.3.1 Introduction to Lanthanide Emission

Lanthanides form trivalent cations with partially filled 4*f* orbitals. The electronic energy levels of these ions are described by the Russell-Saunders coupling scheme.[20] The majority of the lanthanides have electronic excited states which radiatively decay to the ground state. Sm^{3+}, Eu^{3+}, Tb^{3+} and Dy^{3+} all emit in the visible region of the electromagnetic spectrum, while Nd^{3+}, Ho^{3+}, Er^{3+} and Yb^{3+} emit in the near-IR region. The most commonly studied lanthanides with respect to luminescence are Eu^{3+} and Tb^{3+}, whose excited states are $^5D_0$ (17,200 cm^{-1}) and $^5D_4$ (20,400 cm^{-1}), respectively.[21] Splitting of the ground state, due to spin-orbit coupling, leads to emission spectra with several bands, denoted by their ΔJ value. The emission spectrum of Eu^{3+} (*Figure 1.5*) has five manifolds due to splitting of the ^7F ground state. Within each manifold, further splitting is also observed. The *f* orbitals are fairly well penetrating and therefore show little interaction with the ligand field. As a result, Ln^{3+} emission spectra are sharp and generally independent of the coordination environment. Having said this, the form and fine splitting of the Eu^{3+} spectrum is known to be dependent upon the symmetry about the Eu^{3+} centre and the nature of coordinating species. In general, the higher the degree of symmetry about the Eu^{3+} centre, the simpler the spectrum appears (i.e. less fine splitting). Further details on the factors affecting the Eu^{3+} emission spectrum are given in *Section 3.1*.

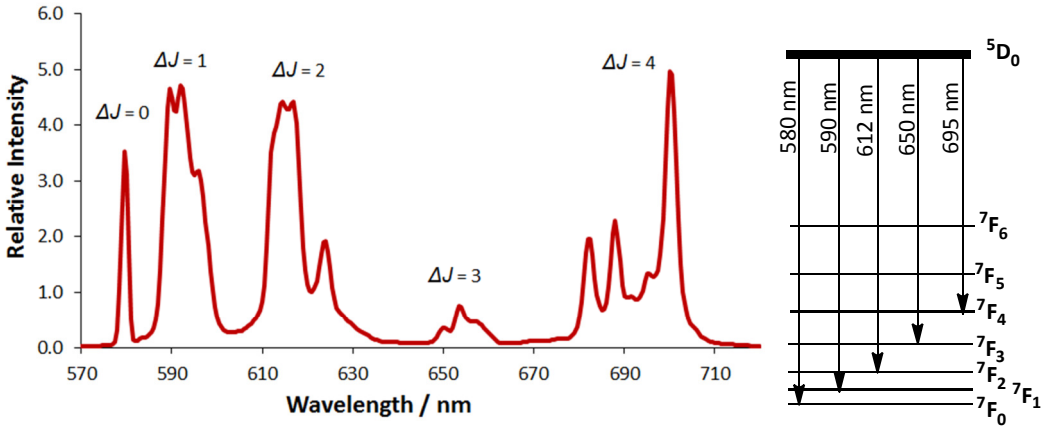

Figure 1.5 *left*) A typical europium emission spectrum, with five transitions denoted by their ΔJ value. Further splitting within each transition is also observed and *right*) the $^5D_0$ and ^7F_J energy levels, giving rise to the europium emission.

Transitions between *f* orbitals are very weak as they are formally Laporte forbidden. Unlike transition metal *d-d* transitions, this selection rule is not overcome by ligand field interactions, due to the contracted nature of the *f* orbitals. An advantage of the forbidden nature of these transitions is that the excited state lifetime is long (µs – ms), allowing time gated studies, which can distinguish the lanthanide emission from the background fluorescence present in most biological systems.

A disadvantage to the forbidden *f-f* transitions is the resulting low molar extinction coefficients (0.5-3 mol^{-1} dm^3 cm^{-1}),[22] leading to inefficient population of the excited states upon optical irradiation. Instead, sensitised emission is generally employed. This process utilises a proximal

chromophoric group, with a high molar extinction coefficient, which absorbs light energy and then transfers this energy to the lanthanide excited state. The processes involved are illustrated with a Jablonski diagram (*Figure 1.6*).

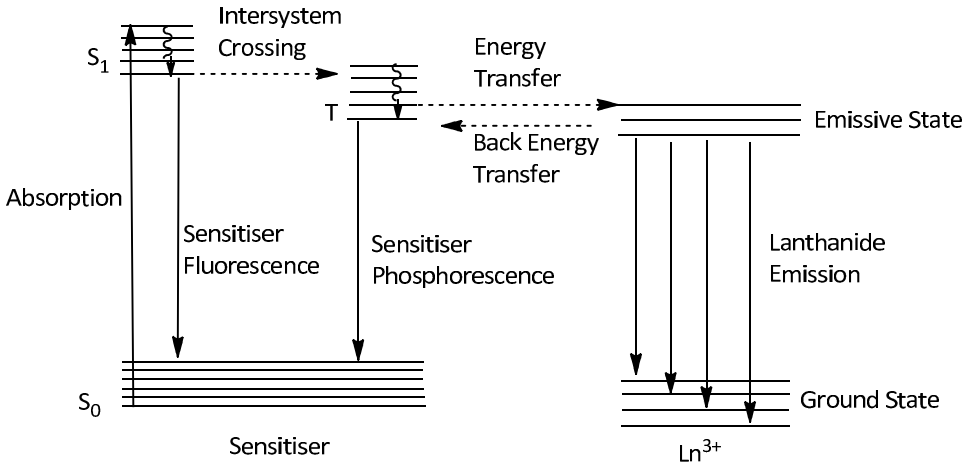

Figure 1.6 Jablonski diagram showing the processes of sensitised emission.

The energy transfer step is thought to proceed via either a Förster[23] or Dexter[24] mechanism. The former is a through-space, dipole-dipole interaction, which is strongly dependent upon the donor-acceptor spectral overlap and has an r^{-6} dependence, whereas the latter involves a short range electron-exchange energy transfer process. The reverse process, back energy transfer, can take place if the sensitiser triplet state is close enough in energy (within 1,500 cm^{-1}) to the Ln^{3+} excited state and results in a decrease in the lifetime and quantum yield of a Ln^{3+} complex. To maximise the quantum yield of a complex, the sensitiser triplet state must be high enough in energy to minimise back energy transfer, whilst remaining close enough in energy to maximise spectral overlap, assuming a Förster mechanism for energy transfer.

1.3.2 Quenching Processes

An appreciation of quenching processes is important when using lanthanide complexes in any luminescence application, especially in biological systems, where many endogenous quenchers are present. Quenching processes are those which reduce the overall quantum yield of lanthanide emission. The key quenching processes which can take place during sensitised emission of a lanthanide complex are shown in *Scheme 1.1*.[25] Quenching can occur at: the singlet excited state of the sensitiser, which can lose energy by fluorescence or be quenched by electron transfer; the sensitiser triplet state, which can lose energy by phosphorescence or be quenched by energy transfer to molecular oxygen and the lanthanide excited state, from where both energy (ET) and electron transfer (eT) can occur.

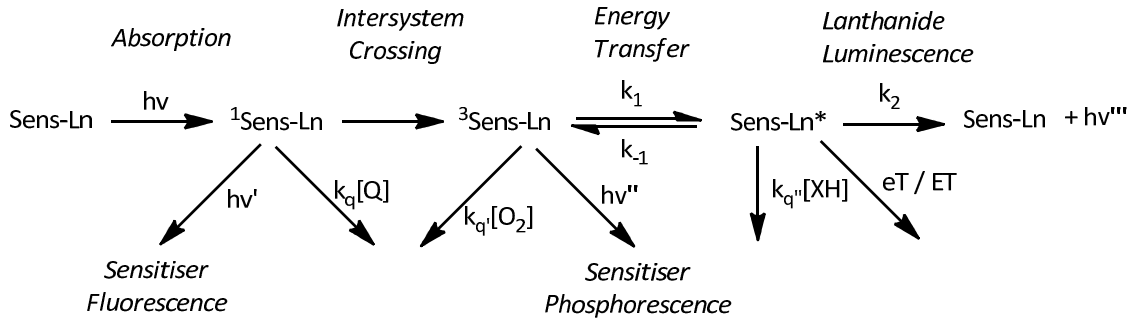

Scheme 1.1

The presence of inner sphere water molecules bound to the lanthanide metal also reduces the overall quantum yield of Eu^{3+} and Tb^{3+} complexes. The excited state energy levels of Eu^{3+} and Tb^{3+} approximately correspond in energy to some of the higher vibrational energy levels of water. As a result, nearby water molecules effectively quench the Eu^{3+} and Tb^{3+} excited states by populating the O-H vibrational energy levels. Other X-H oscillators, such as N-H and C-H, can have a similar quenching effect, in which the energy transfer process follows an r^{-6} dependence on distance. The quenching effect is not as efficient with D_2O, compared to H_2O, due to the lower energy of the O-D oscillation. By measuring the difference in lifetime of Eu^{3+} and Tb^{3+} emission in H_2O and D_2O, the number of inner sphere water molecules, q, can be estimated, according to *Equations 1.1* and *1.2*.[26]

$$q_{Eu} = 1.2\left(k_{H_2O} - k_{D_2O} - 0.25 - 0.075n\right) \quad [1.1]$$

$$q_{Tb} = 5.0\left(k_{H_2O} - k_{D_2O} - 0.06 - 0.010n\right) \quad [1.2]$$

where: q_{Ln} is the inner sphere hydration number; k is the inverse of the excited state lifetime, τ and n is the number of proximal NH oscillators, for the particular case of a secondary amide group, coordinated by the carbonyl oxygen.[26]

1.3.3 Ligands for Lanthanide Ions

As previously discussed, the *f* orbitals of the lanthanide ions are contracted and show little interaction with the ligand field. As a result, bonding between the ligand and metal is mostly electrostatic and non-directional, leading to the most common coordination numbers of 8 and 9. The ligand plays an important role in lanthanide complexes. Firstly, it provides a binding site for the central ion. A good ligand should minimise dissociation of the lanthanide, especially in biological media where some Ln^{3+} ions have moderately high toxicity levels.[27] The ligand also imparts function on the complex. Water solubility, localisation within biological systems and toxicity of the overall complex are all modulated by the choice of ligand. In terms of luminescence behaviour, the ligand is integral in determining the photophysical properties of the overall complex. For Eu^{3+} complexes, the ligand also affects the form of the emission spectrum.

While this thesis concentrates mainly on the properties of Eu^{3+} complexes, it is necessary to introduce at this stage complexes of Gd^{3+}, for which ligand design is a very important consideration. Gd^{3+} has an isotropic arrangement of 7 unpaired electrons in the 4*f* orbitals. As a result, it greatly enhances the rate of relaxation of proximal water protons in a magnetic field. This property is exploited in magnetic resonance imaging (MRI), which use Gd^{3+} complexes as contrast agents.[28] Free Gd^{3+} has a high toxicity in humans so it is necessary to design ligands whose complexes have very high stability constants and kinetic inertness. These ligands are equally applicable to Eu^{3+} binding, as the ionic radii of Eu^{3+} and Gd^{3+} are similar (1.09 and 1.08 Å, respectively for the nine-coordinate complexes).

For the purpose of this section, the ligand refers to the moieties directly bound to the Ln^{3+} centre. Sensitising groups are often directly bound to the Ln^{3+} to maximise energy transfer. An in-depth discussion on the choice of sensitising groups is given in *Section 1.3.4* and will not be discussed in detail in this section. One example, however, in which the sensitising group is also the ligand is the Eu^{3+} tris bipyridine complex, $[Eu{\cdot}L^{1.1}]^{3+}$.[29] This macrocyclic complex, first reported by J.-M. Lehn in 1987, exhibits high kinetic stability and allows sensitisation of Eu^{3+} at 303 nm. The quantum yield of this complex is only 2 % in aqueous solution. This is due to quenching of the Eu^{3+} excited state by two inner sphere water molecules, within the cryptate cavity.

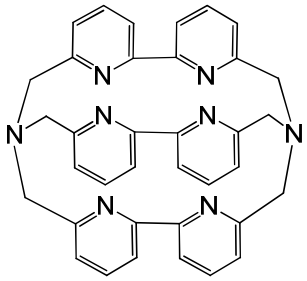

$L^{1.1}$

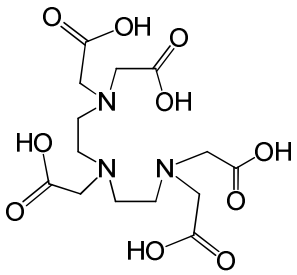

H_5DTPA, **$H_5L^{1.2}$**

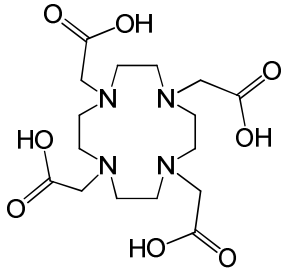

H_4DOTA, **$H_4L^{1.3}$**

Chelated ligands, such as ***L*^1.1^** form very stable complexes, as is expected by the unfavourable entropy changes required to displace such ligands. Two ligands commonly used for lanthanide complexation are DTPA (***L*^1.2^**) and DOTA (***L*^1.3^**). While both ligands make use of the chelate effect to form highly stable complexes, DOTA also benefits from the macrocyclic effect, in which the ligand is preorganised so that little change in conformation is required upon binding to Ln^{3+}. This is reflected in a higher binding constant for DOTA ($[Eu{\cdot}DOTA]^-$, $\log K = 23.5$)[30] compared to DTPA ($[Eu{\cdot}DTPA]^{2-}$, $\log K = 22.4$).[31] Due to their high stability, Gd^{3+} complexes of DTPA and DOTA are used commercially as contrast agents, under the trading names Magnevist[32] and Dotarem,[33] respectively.

DOTA is one of the most commonly used ligands for Ln^{3+} binding and, as a result, a good deal is known about its solution and solid state structures. The coordination geometry about the Ln^{3+} centre is approximately monocapped square-antiprismatic or twisted square-antiprismatic, where the four cyclen N atoms describe the basal plane and the four carboxyl O atoms form the apical place.[34] The capping ligand is typically a solvent molecule, such as H_2O. Complexes of DOTA exist as two enantiomeric pairs of diastereomers arising from two elements of chirality, associated with the sign of

the 12-N_4 ring N-C-C-N and the N-C-C-O torsion angles. The terms Δ (clockwise) and Λ (anticlockwise) are often used to represent the latter, whilst the terms δδδδ (positive torsion angle) and λλλλ (negative torsion angle), represent the former (*Figure 1.7*). The four possible solution state structures (*Figure 1.8*) may interconvert in aqueous solution but in the solid state [Eu·DOTA]$^-$ exists as a square antiprismatic Λ(δδδδ) / Δ(λλλλ) pair of enantiomers, with a capping H_2O molecule.[35]

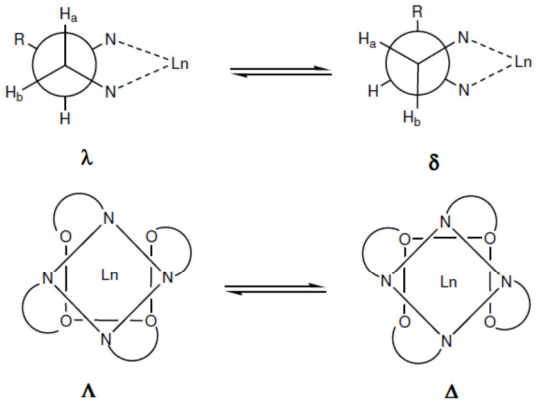

Figure 1.7 Conformations of Ln(III) complexes of DOTA showing the limiting orientations of the cyclen ring, and the layout of the acetate arms.

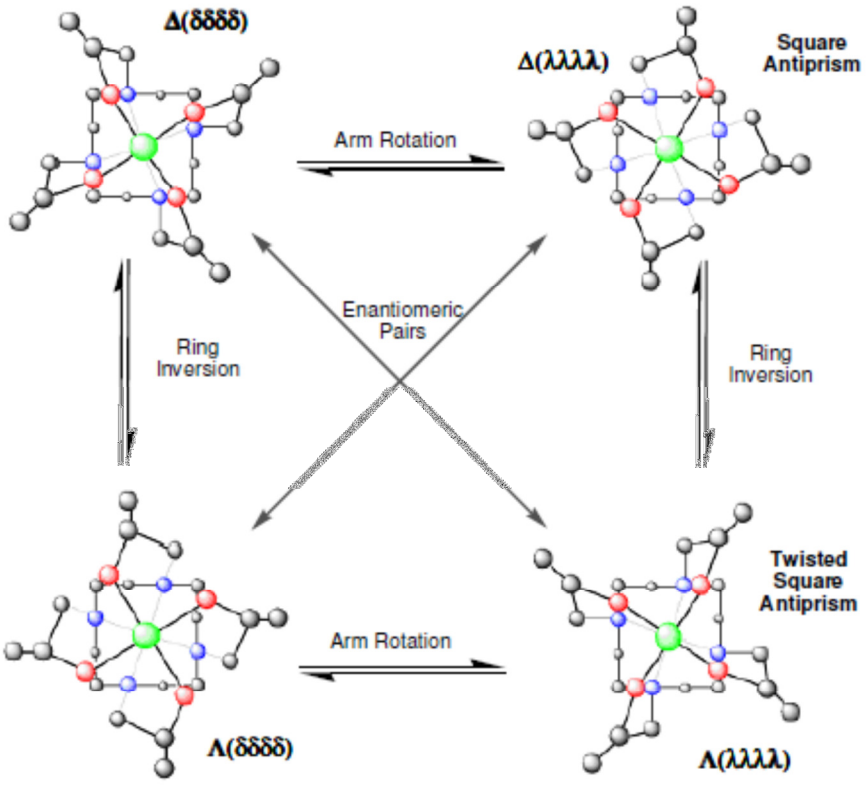

Figure 1.8 The four stereoisomers of [Ln·DOTA]$^-$ complexes. Interconversion between enantiomeric pairs is possible through successive arm rotation and ring inversion.

Due to their high stability, there are many examples of emissive Eu^{3+} complexes based on DOTA, in which at least one of the carboxylate pendent arms is replaced by a sensitising group or some other moiety to alter the characteristics of the complex.[36] Replacement of all four carboxylates for pyridyl

moieties gives the ligand ***L*^1.4**.[37] The complexes, $[Ln{\cdot}L^{1.4}]^{3+}$ crystallise in different geometries, depending upon the size of Ln^{3+}. The early lanthanides, including $[Eu{\cdot}L^{1.4}]^{3+}$, form twisted square antiprismatic structures, with the stereochemistry, Δ(δδδδ). In the solid state, this complex has a capping triflate anion. In aqueous solution, a *q* value of 0.4 was calculated from lifetime measurements. Such a value suggests an equilibrium between the $q = 0$ and $q = 1$ complexes on the millisecond timescale of the measurement. The stereochemistry of $[Eu{\cdot}L^{1.4}]^{3+}$ was investigated by ^{1}H-NMR and it was found that two diastereomers, Δ(δδδδ) and Δ(λλλλ), exist in solution in the ratio 85 : 15. Relative to DOTA, one disadvantage of this neutral ligand is its lower kinetic stability. In a competition assay, it was found that one equivalent of DTPA caused dissociation of the Eu^{3+} ion. This was confirmed by ^{1}H-NMR and a reduction in the europium luminescence lifetime upon dissociation. This result shows the need for charged donors, to increase thermodynamic stability and kinetic inertness.

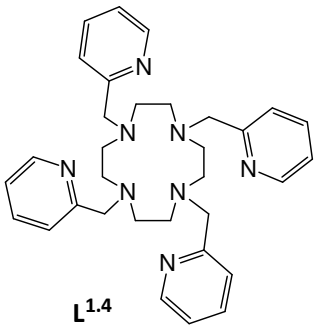

L^1.4

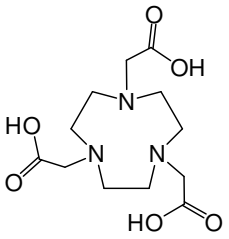

H$_3$L^1.5

Both ligand systems, ***L*^1.3** and ***L*^1.4** are based upon cyclen, a twelve member ring with four coordinating N atoms. This system can also be called 12-N_4. The ring system 9-N_3 makes up another class of ligands, which are less well studied for Ln^{3+} binding. Early work by Sherry and Geraldes investigated the NMR applications of $[Gd{\cdot}L^{1.5}]$.[38] The triacetate of 9-N_3, ***L*^1.5**, contains six donor atoms capable of binding a metal ion and has been used in binding studies of radioisotopes, ^{111}In and $^{67/68}$Ga.[39] In the solid state, these complexes are C_3 symmetric with an octahedral metal ion centre (*Figure 1.9*). The ^{111}In complex was found to retain C_3 symmetry in the solution state and was kinetically stable over the pH range -0.7 – 12.[40]

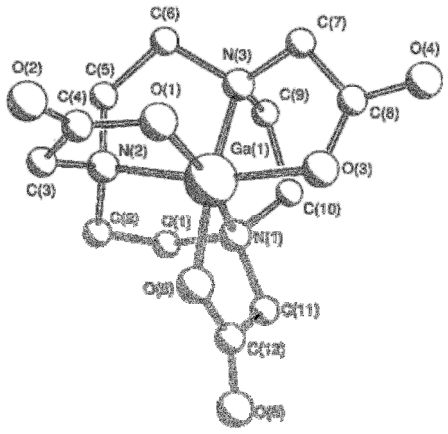

Figure 1.9 Crystal structure of the C_3 symmetric complex Ga**L**^1.5.[40]

As discussed above, Ln^{3+} ions favour a coordination number of 8 or 9. To allow the 9-N_3 core structure to accommodate Ln^{3+} ions, the tris(picolinate) ligand, ***L*$^{1.6}$** was developed.[41] The complex [Ln·L$^{1.6}$] is 9 coordinate, C_3 symmetric and, due to the electrostatic interaction between the positively charged Ln^{3+} ion and the three carboxylates, forms highly thermodynamically and kinetically stable complexes. The pyridyl group is a moiety which can be further functionalised to allow incorporation of a sensitising group. One example of this is the ligand ***L*$^{1.7}$**, which exchanges carboxylate for the isosteric tetrazole moiety, which are deprotonated at pH 7 (p$K_a \approx 4.9$).[42] The pyridyl-tetrazole unit is able to sensitise Eu^{3+} emission at a wavelength of 315 nm with a quantum yield of 20 % in the solid state. Solution state properties of [Eu·L$^{1.7}$] were not reported due to low solubility. A water soluble derivative, [Eu·L$^{1.7b}$], was found to bind Ln^{3+} ions and sensitise the emission of the near-IR emitters, Nd^{3+}, Er^{3+} and Yb^{3+}.[43]

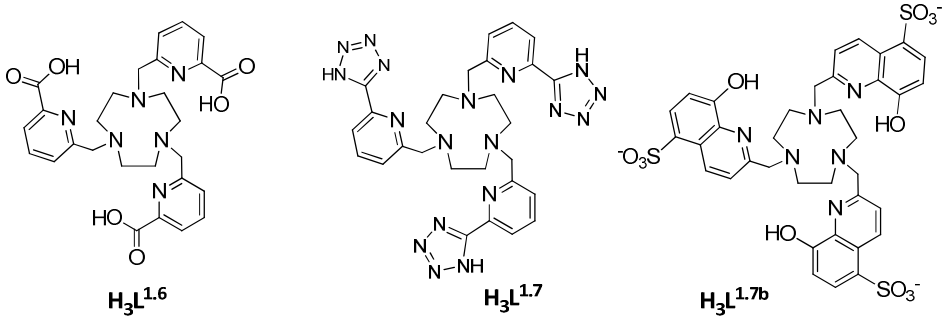

Towards the development of new ligands, exchange of the carboxylate ligating groups in ***L*$^{1.3}$** and ***L*$^{1.5}$** for phosphinate groups gives the ligands ***L*$^{1.8}$** and ***L*$^{1.9}$**.[44, 45] The advantages of phosphinates over carboxylates are threefold. Firstly, the pK_a of phosphinates are lower (1.38 for [Y·L$^{1.9}$] (R = Me) vs. 3.07 for [Y·L$^{1.5}$])[46], leading to complexes which are more kinetically stable towards acid dissociation. Secondly, upon phosphinate oxygen binding, the P centre becomes stereogenic. In octahedral complexes of the type [Ln·L$^{1.9}$], two diastereoisomers may result from co-operative binding of all six donor atoms (i.e. *RRR*/*SSS* and *RSR*/*SRS*). This extra degree of stereochemistry gives rise to a number of possibilities, such as differential chiral interactions. Finally, the pentavalency of P provides a position for further functionalisation, leading to improved solubility properties or conjugation to other moieties.

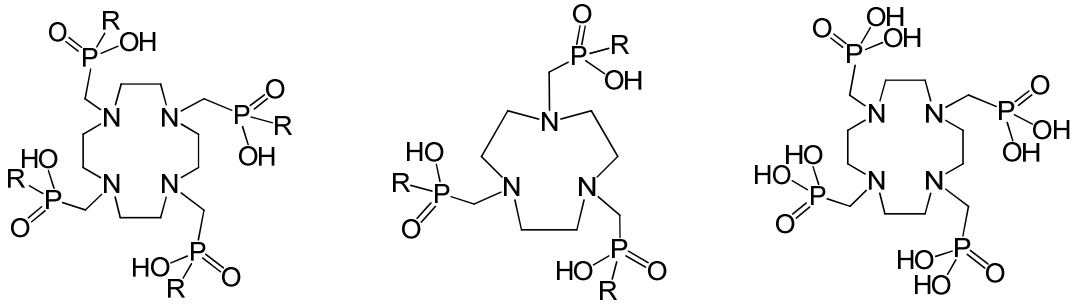

Examples of systems based on phosphinate ligands include the C_3 symmetric octahedral complexes [Co·L$^{1.9}$], [Ni·L$^{1.9}$] and [Ga·L$^{1.9}$] (R = Me in each case), which form enantiomers, and were found to be either *RRR* or *SSS* at P. For the [Ga·L$^{1.9}$] complex, the resultant racemic mixture was separated by

chiral-HPLC.[45] A second example of [Ga·$L^{1.9}$] (R = $CH_2CH_2CO_2^-$) was found to have log $K_{[GaL]}$ = 26.2, demonstrating its high thermodynamic stability.[47] One 12-N_4 example is the complex [Tb·$L^{1.8}$]$^-$ (R = CH_2Ph),[44] which is q = 0 (coordination number = 8), due to the more bulky nature of the phosphinate groups relative to carboxylates. Sensitised Tb emission via the benzyl group leads to a 44 % quantum yield for [Tb·$L^{1.8}$]$^-$ in water.

A brief mention of the related phosphonate complexes is also necessary. As with the phosphinate analogues, complexes of 12-N_4 tetra(phosphonate) (***L*$^{1.10}$**), are 8 coordinate (q = 0) and have very high kinetic and thermodynamic stability. An example is [Gd·$L^{1.10}$], which has been used as an outer sphere water relaxation agent for MRI.[48]

From this brief summary of some of the ligands which are used for Ln^{3+} binding, several conclusions can be made. Firstly, ligands should be kinetically and thermodynamically stable towards metal dissociation by competing ligands or extremes of pH. Macrocyclic chelating ligands serve this purpose well. The inclusion of charged donors, such as carboxylate O atoms, increases the stability of complexes due to strong electrostatic interactions. Phosphinates are an attractive alternative to carboxylates due to their additional steric bulk, shielding of the Ln^{3+} centre and the pentavalency, allowing functionalisation of the binding moiety. Pyridine donors are also useful, in that they can be modified to form sensitising groups, as revealed in the next section.

1.3.4 Chromophores for Lanthanide Sensitisation

The processes involved in sensitisation of the luminescent lanthanides were illustrated by a Jablonski diagram in *Figure 1.6*. The important steps were: sensitiser excitation ($S_0 \rightarrow S_1$) by absorption of incident light; intersystem crossing ($S_1 \rightarrow T_1$); energy transfer to the lanthanide excited state ($T_1 \rightarrow$ Ln*) and lanthanide emission (Ln* $\rightarrow$ Ln + hν). It follows that a good sensitiser should have the following properties: a high molar extinction coefficient with an excitation wavelength above 300 nm to avoid the excitation of endogenous biological fluorophores; a small singlet-triplet energy gap to maximise the rate of intersystem crossing; a triplet energy around 2000 cm^{-1} above that of the lanthanide excited state to allow efficient energy transfer but minimal thermally activated back energy transfer and a short distance between the sensitiser and the lanthanide ion to maximise the rate and efficiency of energy transfer. The term chromophore is often used in place of sensitiser as it describes the ability of the moiety to absorb light in the UV-visible wavelength range.

One of the compounds currently used commercially for Eu^{3+} sensitisation is the tris(bipyridine) complex, [Eu·$L^{1.1}$]$^{3+}$, which was introduced in *Section 1.3.3*. The excitation wavelength for the trisbipyridine sensitiser (λ_{abs} = 303 nm) is low compared to some of the more recently developed chromophores. However, with a molar extinction coefficient of 18,000 M^{-1} cm^{-1} and an absorption spectrum with a shallow tail into the longer wavelength region of the spectrum, excitation at 337 nm is possible, avoiding the excitation of biomolecules. From the lifetime values of [Eu·$L^{1.1}$]$^{3+}$ in H_2O and D_2O, a q value of 2 was calculated.[49] This leads to a low quantum yield due to quenching of the Eu^{3+} excited state by inner sphere water molecules. However, commercial assays which use this

complex are carried out in the presence of 0.4 M F^- ions, which almost completely displace the two inner sphere H_2O molecules, increasing the quantum yield to 10 %.[50] The structurally related terpyridine ligand ***L*^1.11^** forms complexes of the type $[Ln{\cdot}L_3]^{3+}$, which result in a 9 coordinate Ln^{3+} centre. Whilst both ***L*^1.11a^** and ***L*^1.11b^** are able to sensitise Eu^{3+} emission, it was found that the addition of the ^{t}Bu groups led to a 7 fold increase in quantum yield, due to an increase in the efficiency of the intersystem crossing process.[51]

A disadvantage to the terpyridines shown is their low aqueous solubility. Whilst modifications to the core structure have led to greater solubility, an alternative sensitiser is tetraazatriphenylene.[52] Complexes based on DOTA with the tetraazatriphenylene sensitiser ($[Ln{\cdot}L^{1.12}]$) are water soluble and have found application in fluorescence microscopy.[53] This sensitiser has a fast rate of intersystem crossing and a triplet energy suitable for sensitising both Eu^{3+} and Tb^{3+} emission. It is also electron-poor and so is difficult to oxidise, a process which can lead to quenching of the singlet excited state. As with the bi- and terpyridines, tetraazatriphenylene directly binds to the Ln^{3+} centre via a five-membered chelate. This leads to efficient energy transfer and a high quantum yield of 18 % for the complex $[Eu{\cdot}L^{1.12}]$. *Table 1.1* summarises the properties of complexes incorporating selected pyridine-based and tetraazatriphenylene chromophores.

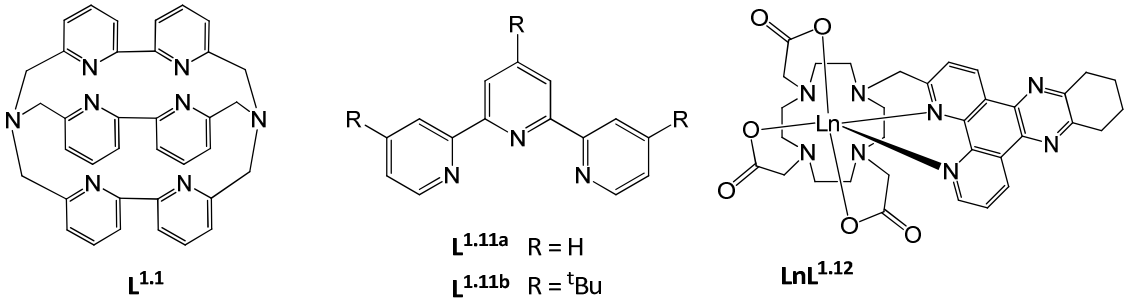

Table 1.1 Summary of the photophysical properties of complexes incorporating bipyridine, terpyridine and tetraazatriphenylene chromophores. All values measured at 298 K in H_2O unless stated. [a]Values measured in CH_3CN.

Complex	λ_{max} /nm	ε / M^{-1} cm^{-1}	$\tau^{Ln}_{H_2O}$ / *ms*	$\tau^{Ln}_{D_2O}$ / *ms*	$\Phi^{Ln}_{H_2O}$ / %	E_T^{Gd} / cm^{-1} (77*K*)
[Eu·L^1.1^]	303	18,000	0.34	1.54	2.0	29,200
[Eu·(L^1.11a^)$_3$]	305	9,300	2.31[a]	-	1.3[a]	22,900
[Eu·(L^1.11b^)$_3$]	305	7,700	2.14[a]	-	10[a]	22,750
[Eu·L^1.12^]	340	3,500	1.06	1.15	18	24,000

In contrast to the electron deficient tetraazatriphenylene choromphore, the 2-hydroxyisophthalamide based ligand (***L*^1.13^**) is electron rich and contains several oxygen donors.[54] One similarity to the pyridyl based sensitisers is that they both directly coordinate to the lanthanide centre in a multidentate manner. The ligand ***L*^1.13^** forms 1 : 1 complexes with Ln^{3+}, giving complexes which are $q = 0$ and, in the case of $[Tb{\cdot}L^{1.13}]^-$, has an exceptionally high quantum yield of 59 %. The quantum yield of $[Eu{\cdot}L^{1.13}]^-$ was 6 %. The large difference in quantum yield originates from the difference in Ln^{3+} excited state energy (Eu^{3+} ($^5D_0$) at 17,200 cm^{-1} and Tb^{3+} ($^5D_4$) at 20,400 cm^{-1}). The ligand has a triplet

energy of 23,350 cm^{-1} and therefore has better overlap with the Tb^{3+} excited state.[55] A density functional theory (DFT) calculation was used to identify the π-π* character of the lowest lying singlet and triplet excited states of ***L*$^{1.13}$**. With a view to enhancing the ability to sensitise Eu^{3+}, a screening process led to the use of 1-hydroxypyridin-2-one (***L*$^{1.14a}$**).[56] The triplet energy of this moiety lies lower in energy and the complex $[Eu{\cdot}(L^{1.14a})_4]^-$ (q = 0) has a quantum yield of 21 %. Interestingly, the complex $[Eu{\cdot}L^{1.14b}]^-$ has a much smaller quantum yield as a result of an inner sphere water molecule quenching the Eu^{3+} excited state. Sensitisation of Tb^{3+} by ***L*$^{1.14}$** has a very low efficiency due to back energy transfer to the sensitiser triplet state. Upon degassing a solution of $[Tb{\cdot}L^{1.14}]^-$, the emission intensity increases, due to a reduction in quenching of the triplet state by molecular oxygen. The two sensitisers in ***L*$^{1.13}$** and ***L*$^{1.14}$** are excellent sensitisers for Tb^{3+} and Eu^{3+} emission, respectively (*Table 1.2*). The presence of 4 sensitising groups per Ln^{3+} leads to high molar extinction coefficients. However, the ability to add further function to complexes based on these ligands is not straightforward. For example, introduction of a group which can conjugate to other biomolecules is non-trivial due to the highly symmetric nature of the ligands (i.e. can you functionalise one group only). Also, due to the electron rich nature of the chromophores, there may be biocompatibility issues involving oxidation processes within a biological environment.

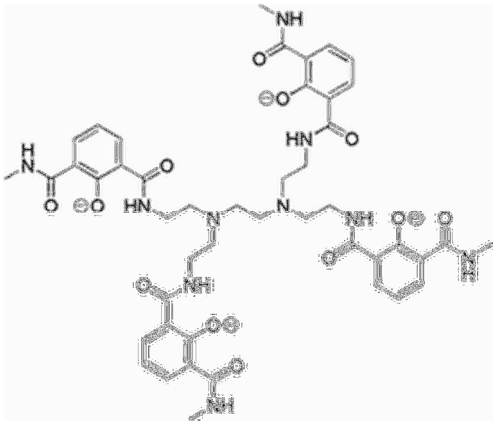

L$^{1.13}$

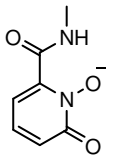

L$^{1.14a}$

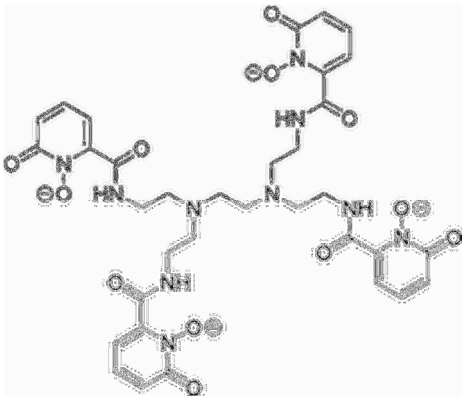

L$^{1.14b}$

Table 1.2 Summary of the photophysical properties of lanthanide complexes with 2-hydroxyisophthalamide and 1-hydroxypyridin-2-one chromophores. All values measured at 298 K in H_2O unless stated.

Complex	λ_{max} /nm	ε / M^{-1} cm^{-1}	$\tau^{Ln}_{H_2O}$ / *ms*	$\tau^{Ln}_{D_2O}$ / *ms*	$\Phi^{Ln}_{H_2O}$ / %	E_T^{Gd} / cm^{-1} (77*K*)
[Tb·L$^{1.13}$]	350	26,800	2.60	3.22	59	23,350
[Eu·(L$^{1.14a}$)$_4$]	345	18,800	0.74	0.98	21	21,260
[Eu·L$^{1.14b}$]	345	18,200	0.48	1.22	3.6	21,260

Another class of chromophores are the tricyclic heterocyclic aromatics. The properties of the Ln^{3+} complexes based on a DOTA ligand, with one carboxylate group exchanged for the sensitising moiety, are shown in *Table 1.3*. The phenanthridine complex $[Eu{\cdot}L^{1.15}]$ is able to sensitise Eu^{3+} emission in the protonated form shown. Above pH 6, the Eu^{3+} emission is switched off, due to photo-induced electron transfer at the phenanthridine N in the singlet excited state. The result is a probe which can report pH by a change in intensity of Eu^{3+} emission.[57] The disadvantage to this type of

on/off switch is that, intracellularly, the probe concentration is unknown and the measurement cannot be calibrated. Other applications of complexes incorporating the phenanthridine chromophore are limited by the pH dependence on emission intensity. The acridone based complex [Eu·$L^{1.16}$] appears to have favourable absorption properties (λ_{abs} = 410 nm, ε = 5,300 M^{-1} cm^{-1}).[58] However, the relative energies of the n-π* and π-π* transitions in the acridone sensitiser are sensitive to solvent polarity. In non-polar media, the energy of the singlet excited state is around 25,000 cm^{-1} and the quantum yield for fluorescence (Φ_f) and intersystem crossing (Φ_{isc}) are 2 % and 96 %, respectively. Upon moving to a polar solvent, the lowest lying singlet energy state drops in energy to around 23,500 cm^{-1}, due to the increasing contribution of the π-π* transition, and the values of Φ_f and Φ_{isc} become 98 % and 0.1 %, respectively. Consequently, the quantum yield for europium emission of [Eu·$L^{1.16}$] in aqueous media is low, and cannot be considered for use in the aqueous cellular environment.

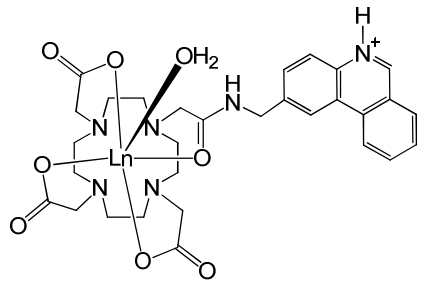

LnL$^{1.15}$

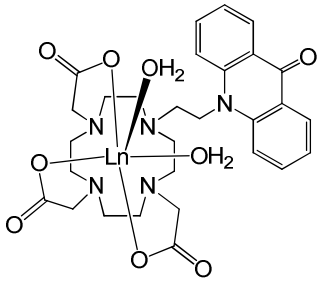

LnL$^{1.16}$

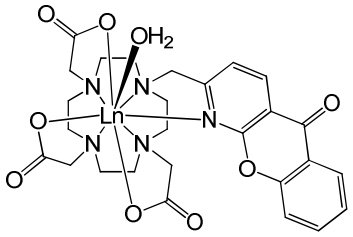

LnL$^{1.17}$

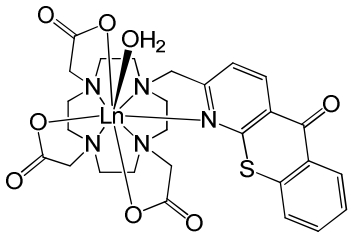

LnL$^{1.18}$

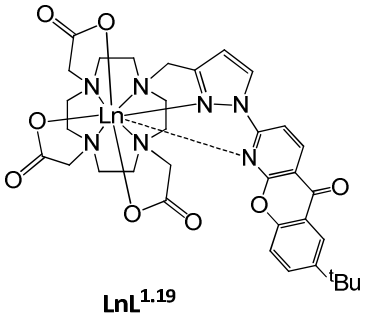

LnL$^{1.19}$

Table 1.3 Summary of the photophysical properties of tricyclic heterocyclic chromophores. All values measured at 298 K in H_2O unless stated.

Complex	λ_{max} /nm	ε / M^{-1} cm^{-1}	$\tau^{Ln}_{H_2O}$ / *ms*	$\tau^{Ln}_{D_2O}$ / *ms*	$\Phi^{Ln}_{H_2O}$ / %	E_T^{Gd} / cm^{-1}(77*K*)
[Eu·$L^{1.15}$]	365	5,000	1.48	0.41	1.4	22,000
[Eu·$L^{1.16}$]	410	5,300	0.35	1.20	5.3	21,500
[Eu·$L^{1.17}$]	330	6,900	1.75	0.50	6.9	23,700
[Eu·$L^{1.18}$]	375	5,360	1.96	0.62	2.2	24,800
[Tb·$L^{1.19}$]	355	15,050	2.24	2.65	15	23,450

More recently, lanthanide complexes containing the azaxanthone ([Ln·$L^{1.17}$]) and azathiaxanthone ([Ln·$L^{1.18}$]) sensitisers have been exploited in a number of analytical experiments.[59] In contrast to the acridone sensitiser, the quantum yield for intersystem crossing of azaxanthones remain high in polar media (Φ_{isc} = 82 %). A low fluorescence quantum yield (Φ_f = 1 %), along with an appropriate triplet energy (23,700 cm^{-1}), make azaxanthones excellent candidates for Eu^{3+} and Tb^{3+} sensitisation. In a

similar manner to ligands ***L*^1.11^ – *L*^1.14^**, the azaxanthone sensitiser can bind directly to the europium centre via the nitrogen lone pair, maximising the rate of energy transfer. Upon exchange of oxygen for sulphur, the excitation wavelength of the azaxanthone is red-shifted from 335 nm to 375 nm, while maintaining a relatively high molar extinction coefficient (~6,000 M^{-1} cm^{-1}). This benefit is offset by the increased fluorescence from the azathiaxanthone centred at 437 nm. Indeed, a related complex to [Eu·$L^{1.18}$] reports a fluorescence quantum yield of 44 % in aqueous media.[57] As with [Eu·$L^{1.16}$], the polarity of the solvent has an effect on the fluorescence. As the polarity decreases, fluorescence also decreases, with the maximum emission wavelength shifting to the blue. Such behaviour illustrates the sensitivity of the excited states to solvent effects.

While the azaxanthones and azathiaxanthones are effective sensitisers, their molar extinction coefficients are not as high as some of the previously reviewed chromophores, which make use of multiple chromophores per complex. To improve both the molar extinction coefficient and the excitation wavelength, the pyrazoyl-1-azaxanthone sensitiser (***L*^1.19^**) was synthesised.[60] Pyrazoyl groups are known to be effective donors in lanthanide complexes[61] and the increase in conjugation length enhances the photophysical properties of the established azaxanthone sensitiser. The terbium complex, [Tb·$L^{1.19}$], has a molar extinction coefficient of around 15,000 M^{-1} cm^{-1} in water, an excitation wavelength of 355 nm and a quantum yield of 15 %.[62] An analogue of [Tb·$L^{1.19}$], which varies only in the nature of the pendant arms, has a quantum yield of 61 % – an exceptionally high value for such complexes. The pyrazoyl-1-azaxanthone sensitiser clearly illustrates the benefit of increasing conjugation length on excitation wavelength and molar extinction coefficient. However, a balance must be maintained, as increasing conjugation length will naturally decrease the triplet energy of the sensitiser, thereby increasing the rate of thermally induced back energy transfer.

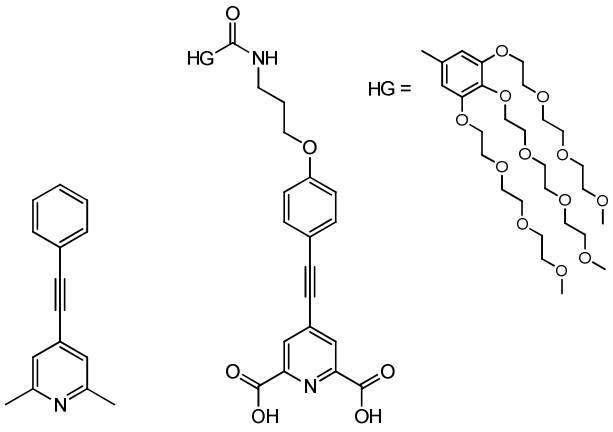

$L^{1.20}$ $H_2L^{1.21}$

The sensitisers discussed above predominantly have excited states which are believed to involve n-π* or π-π* transitions. These sensitisers typically have molar extinction coefficients around 5,000 – 10,000 M^{-1} cm^{-1} per chromophoric moiety. Another class of chromophores, whose lowest excited states involve an internal charge transfer (ICT) mechanism, are the pyridylalkynylaryl moieties, such as ***L*^1.21^**, in which the aryl group is electron rich.[63] The ICT arises due to flow of charge from the alkoxy O donor to the pyridyl N acceptor,[64] and is seen as a broad band in the absorption spectrum

centred at 332 nm. Chromophores of this type have large molar extinction coefficients around 25,000 M^{-1} cm^{-1}. $[Eu\cdot(L^{1.21})_3]^{3-}$, which contains three bound sensitisers, exhibits an overall molar extinction coefficient of 78,700 M^{-1} cm^{-1}, is $q = 0$ and has a quantum yield of 16 % in H_2O. The chromophore without the alkoxy donating group, ***L*$^{1.20}$**, has been known since 1988[65] and its use as a lanthanide sensitiser was reported shortly afterwards.[66] The addition of the O-alkyl group raises the λ_{abs} to a value which is suitable for biological applications.

One final class of sensitiser worthy of mention is the transition metal (TM) complexes.[67] In these systems, energy transfer occurs from a transition metal excited state (commonly a $Ru(bipyridine)_3$ MLCT state)[68] to the lanthanide excited state. This method is more relevant for the near-infrared emitting lanthanides such as Yb^{3+}, Nd^{3+} and Er^{3+}, as their emissive excited states lie fairly low in energy. A rare example of such a sensitisation pathway for Eu^{3+} emission utilises an Ir^{3+} complex as the sensitising moiety ($[Eu\cdot L^{1.22}]^-$).[69] The subsequent emission appears white, due to both Eu^{3+} red and Ir^{3+} blue emission. The system shown is likely to suffer from instability, as the Ir complexes are bound to the Eu^{3+} centre by a single conjugated carboxylate. This group will be easily displaced by competing ligands. In general, sensitisation of Eu^{3+} via transition metal complexes will always suffer from inefficient energy transfer, due to the large distances between the donor and acceptor complexes and competing processes, such as emission from the TM complex.

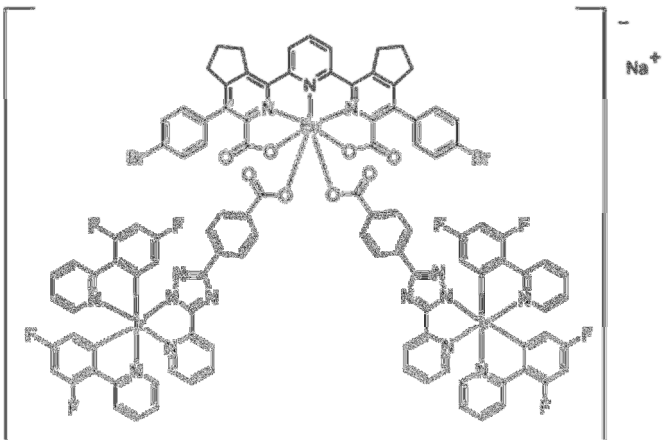

$[Eu\cdot L^{1.22}]^-$

From this summary of sensitising moieties, several important properties are apparent. Firstly, the chromophore should have a high molar extinction coefficient at an absorption wavelength above 300 nm. The rate of intersystem crossing must be fast and, importantly, the energy of the triplet state should be well matched in energy to the Ln^{3+} excited state (~2000 cm^{-1} above) to maximise the energy transfer step. The most common sensitisers are aromatic heterocycles with extended conjugation and typically include pyridyl donors, as they can bind directly to the lanthanide centre and are readily modified into useful chromophores.

1.4 Fluorescence Resonance Energy Transfer

1.4.1 Principles of Fluorescence Resonance Energy Transfer

Fluorescence resonance energy transfer (FRET) is a process commonly used to probe interactions between biomolecules. It can be used to signal the presence or absence of a certain molecule, to identify protein-protein interactions and may also be used to measure distances between molecules. FRET describes the transfer of energy between two fluorophores, a donor and an acceptor. The process begins with the absorption of light by the donor, promoting it to its excited state. Providing there is overlap between the donor emission spectrum and the acceptor absorption spectrum, and that the two species are close in space, energy transfer can occur. Note that the energy transfer is non-radiative but, instead, requires an interaction between the transition dipoles of the donor and the acceptor. Once energy transfer has occurred, emission from the acceptor is observed. *Figure 1.10a* shows the basic FRET experiment.[8]

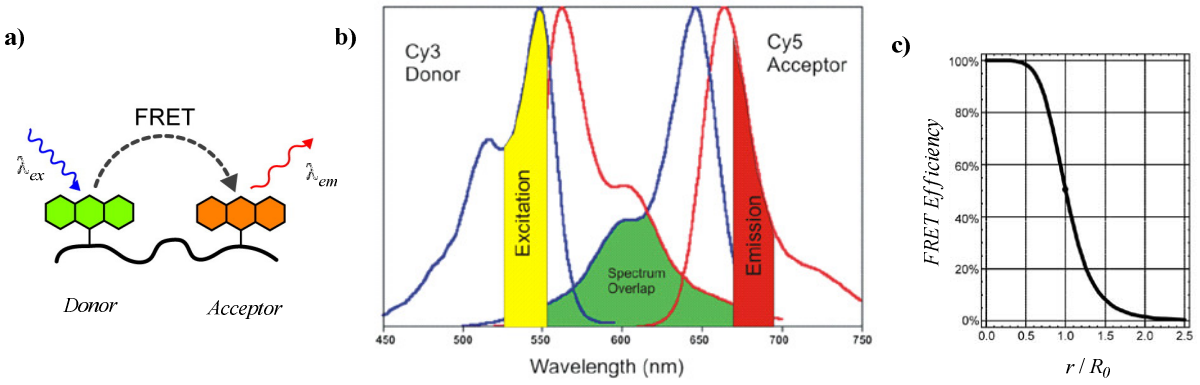

Figure 1.10 a) Schematic showing FRET between a donor and an acceptor, b) the excitation (*blue*) and emission (*red*) spectra of two cyanine dyes. The spectral overlap integral is highlighted in green. The yellow and red highlighted areas illustrate suitable wavelengths to excite the donor and measure acceptor emission, respectively and c) FRET efficiency as a function of r / R_0.

The rate of energy transfer, k_T, is given by the equation:

$$k_T = \frac{1}{\tau_0}\left(\frac{R_0}{r}\right)^6 \qquad [1.3]$$

where: τ_0 is the radiative lifetime of the donor in the absence of the acceptor; R_0 is the Förster radius – defined as the distance at which the extent of energy transfer is 50 % and r is the internuclear distance between the donor and acceptor. R_0 is constant for a specific donor-acceptor pair and depends upon the donor emissive quantum yield, the acceptor molar extinction coefficient, the overlap integral of the donor emission spectrum with the acceptor absorption spectrum (*Figure 1.10b*) and the orientation of the two transition dipole moments. In solution, the orientation of the dipole moments is the average of all possible orientations but when the fluorophores are in fixed orientations, for example within a protein, they may have a significant effect upon R_0. The FRET process is very sensitive to the distance between the donor and acceptor (r^{-6} dependence). By definition, when r is equal to R_0 energy transfer

is 50 % efficient. When r is twice R_0 the energy transfer drops to 1.5 % (*Figure 1.10c*). Due to this high sensitivity, the extent of energy transfer can be used as a 'spectroscopic ruler' to measure distances between sites on proteins.[70] FRET is usually only observed for values of r up to 10 nm.[71]

1.4.2 Examples of FRET in Biological Systems

Many examples of the use of FRET to gain information on biological systems are available in the literature. One such example which makes use of the fluorescent dyes fluorescein and rhodamine is illustrated in *Figure 1.11*.[72] Here, the activity of sortase, an enzyme essential for the colonisation and propagation of bacteria within a host, is monitored by FRET. When sortase is active, a transpeptidation reaction occurs and the emission of rhodamine, due to energy transfer from fluorescein, is observed.

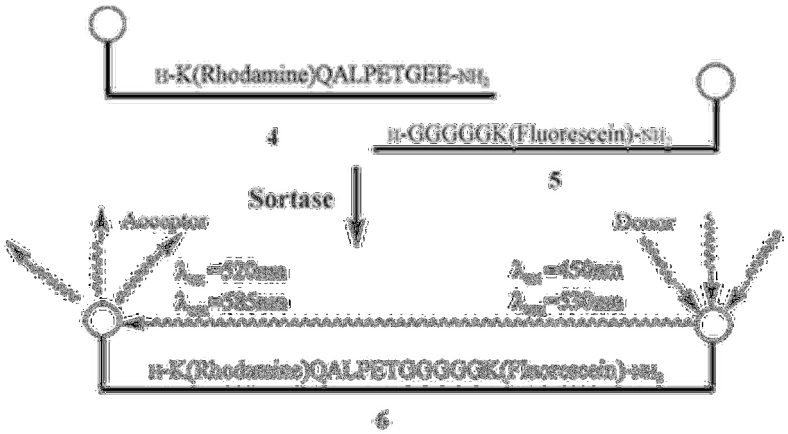

Figure 1.11 Analysis of the sortase-catalysed transpeptidase reaction with intramolecular FRET between fluorescein and rhodamine.

It is also possible to monitor levels of biomolecules by the absence of FRET between a donor and an acceptor. In the given example (*Figure 1.12*), a quantum dot acts as the donor while a gold nanoparticle acts as the acceptor. In the absence of glucose, FRET occurs and no donor emission is observed. However, in the presence of glucose, the gold nanoparticle is displaced and emission from the QD is seen, due to the absence of FRET.[73]

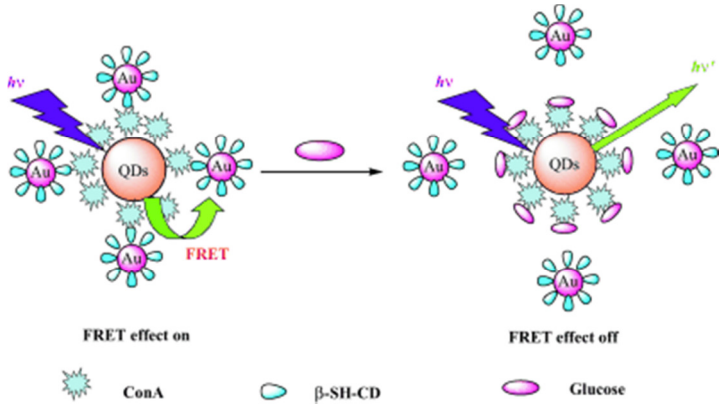

Figure 1.12 Schematic illustration of FRET between a QD and a gold nanoparticle which is inhibited by the presence of glucose.

Other examples of the use of FRET in biological imaging include the study of protein-protein interaction using different coloured fluorescent proteins as donors and acceptors.[74] Multiple FRET sensors acting simultaneously have also been designed in which several signalling events are monitored at the same time, giving information on the precise timing of cellular events within a single cell.[75] For this to be viable, several FRET donor-acceptor pairs must be used which are spatially and spectrally independent.

1.4.3 Homogeneous Time Resolved Fluorescence

Homogeneous Time Resolved Fluorescence (HTRF) is a technology which uses the properties of emissive Eu^{3+} and Tb^{3+} complexes to enhance the FRET experiment. The company CISbio Bioassays uses the Ln^{3+} complexes as donors in their commercial assays.[76] The large Stokes' shifts and sharp emission bands of these complexes aid the differentiation between donor and acceptor emission. The long luminescence lifetimes also allow time-gated detection methods to be employed, which avoid interference from background fluorescence. It is apparent that the observed lifetime of the acceptor is determined by the lifetime of the donor. Hence, a fluorescent dye acceptor (τ_0 ~ 10 ns) can have a much longer observed lifetime (τ_{obs} ~ 1 ms), due to FRET from the long lived donor excited state.

A schematic of the general antigen-antibody assay which makes use of HTRF technology is shown in *Figure 1.13* .[55] In the absence of the antigen under surveillance, the donor-labelled antigen binds to the acceptor-labelled antibody and FRET is detected by emission of the acceptor. In the presence of the target antigen, there is competition for the antibody binding site and the extent to which FRET occurs is reduced. By using time-resolved detection of the acceptor emission, the presence and activity of the target antigen can be measured.

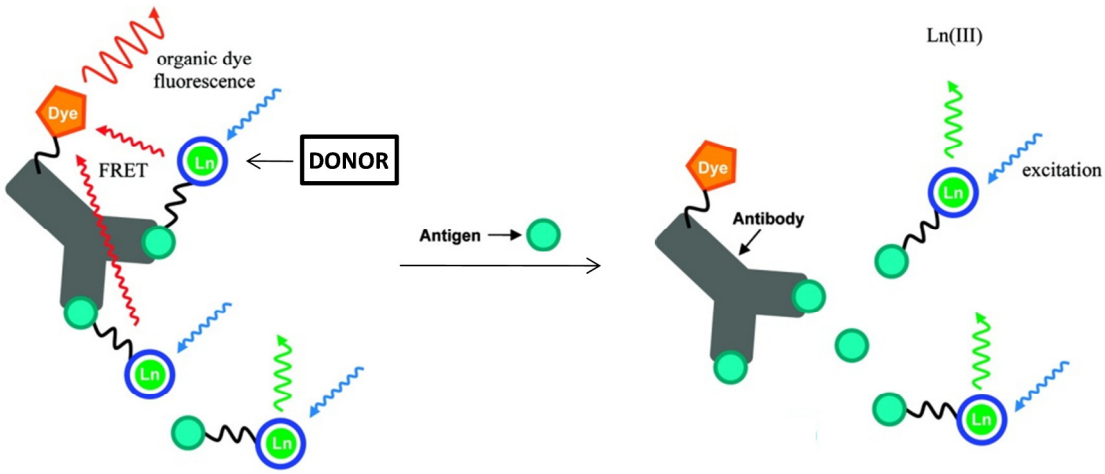

Figure 1.13 A schematic representing the general principle of the homogenous time resolved fluoro- (HTRF) immunoassay. In the presence of the competing antigen, the labeled antigen is displaced and FRET can no longer occur.

As donors, currently the HTRF assay makes use of two compounds discussed in *Section 1.3.4*, $[Eu{\cdot}L^{1.1}]^{3+}$ and $[Tb{\cdot}L^{1.13}]^{-}$.[29, 77] The acceptor pair for $[Eu{\cdot}L^{1.1}]^{3+}$ is an allophycocyanin (APC) dye protein and for $[Tb{\cdot}L^{1.13}]^{-}$, an enhanced green fluorescent protein (EGFP).[78] *Figure 1.14* illustrates the spectral overlap between the donors and their respective acceptors. A feature of each spectrum is that

the spectral overlap of donor emission with acceptor absorption is far from 100 %. In the $[Eu{\cdot}L^{1.1}]^{3+}$ case, only around 25 % of the Eu^{3+} emission overlaps with the APC absorption spectrum. Improving spectral overlap is one of the areas for development, to increase assay efficiency and reduce cost.

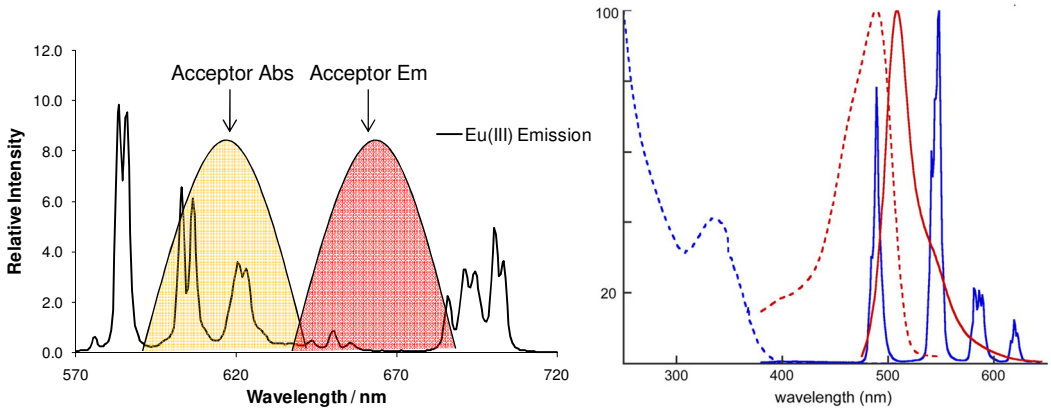

Figure 1.14 Schematics representing the spectral overlap between *left*) the donor emission of $[Eu{\cdot}L^{1.1}]^{3+}$ and an allophycocyanin dye and *right*) the donor emission $[Tb{\cdot}L^{1.13}]^{-}$ (blue solid line) and the acceptor EGFP (absorption – red dashed line, emission – red solid line).

1.5 Aims and Specification

The aim of this project is to design, synthesise and characterise a highly emissive europium complex to act as a donor in the HTRF experiment, described above. The currently used donor, $[Eu{\cdot}L^{1.1}]^{3+}$, was first synthesised in 1987 and, while it serves its purpose, improvements are always sought to increase efficiency and ultimately, reduce cost. Specific areas in which improvements are desired include increasing the spectral overlap integral illustrated in *Figure 1.14* and increasing the overall emission quantum yield, which is 10 % in the presence of 0.4 M potassium fluoride. The specification for a donor complex is as follows:

i) **An emissive europium complex donor** – Design and synthesise a europium complex which absorbs incident light and luminesces with the characteristic europium emission spectrum between 580 and 720 nm.

ii) **Optimise the form of the emission spectrum** – With respect to the spectral overlap integral, maximise the europium emission in the spectral region at which the acceptor absorbs light: that is the 600 – 630 nm region. This is the $\Delta J = 2$ part of the europium emission spectrum. It follows that the Eu emission should be minimised in the other parts of the spectrum. In particular, the emission should be minimised in the spectral region in which the acceptor emits light.

iii) **Select a chromophore with a suitable absorption wavelength** – The absorption wavelength should be above 320 nm to avoid competition for the excitation light source by other fluorophores in the assay.

iv) **Maximise the molar extinction coefficient** – Choose a suitable chromophore which can sensitise Eu^{3+} emission and has a high molar extinction coefficient. From the discussion in *Section 1.3.4*, it is apparent that polyaromatic heterocycles are well suited to this task.

v) **Maximise the quantum yield** – Combine a chromophore which efficiently populates the Eu^{3+} excited state (fast intersystem crossing and appropriate triplet energy level) with a complex whose quenching processes are minimised. To achieve this, the Eu^{3+} centre should be well shielded from external quenchers, including H_2O (i.e. a $q = 0$ complex).

vi) **Design a stable complex in the assay medium** – The Eu^{3+} complex should be kinetically and thermodynamically stable towards dissociation induced by competing ligands, metal ions and other species in the assay medium. From the discussion in *Section 1.3.3*, a multidentate chelating ligand, ideally with charged donor groups, would serve this purpose.

vii) **Water solubility** – The final complex should be soluble in the assay medium, which is a buffered aqueous solution containing proteins, ions and other compounds.

viii) **A conjugation point** – The final complex should have a single functional group, such as a primary amine or a carboxylic acid, which allows coupling to a vector, which is then tagged to the target species (e.g. an antigen, antibody or protein)

The following chapters show the synthesis and characterisation of a number of Eu^{3+} complexes which aim to meet one or more of the specifications above. In *Chapter 2* the number of integral chromophores is varied from one to four with a view to maximising the molar extinction coefficient. *Chapter 3* focuses on increasing the spectral overlap integral and gives a discussion on the factors which affect the form of the Eu^{3+} emission spectrum. In *Chapter 4*, the use of triazacyclononane as the core ligand is introduced, before *Chapter 5* gives information on the final donor complex, which meets the specification given above. *Chapter 6* is devoted to a study into the quenching mechanisms of certain endogenous quenchers.

1.6 References

1. E. N. Harvey, *A History of Luminescence from the Earliest Times until 1900*, The American Philosophical Society, New York, 1957.
2. B. Valeur and M. R. Berberan-Santos, *J. Chem. Educ.*, 2011, **88**, 731-738.
3. E. D. Clarke, *Ann. Philos.*, 1819, 34-36.
4. D. Brewster, *Trans. R. Soc. Edinburgh*, 1934, **12**, 538-545.
5. J. F. W. Herschel, *Philos. Trans.*, 1845, 147-151.
6. G. G. Stokes, *Philos. Trans.*, 1852, **142**, 463-562.
7. B. Valeur, *Fluorescence of Supermolecules, Polymers and Nanosystems*, Springer Verlag, 2008.
8. J. L. Lakowicz, *Principles in Fluorescence Spectroscopy*, 2nd edn., Academic/Plenum Press., New York, 1999.
9. A. Waggoner, *Curr. Opin. Chem. Biol.*, 2006, **10**, 62-66.
10. M. L. Graber, D. C. Dilillo, B. L. Friedman and E. Pastorizamunoz, *Anal. Biochem.*, 1986, **156**, 202-212.
11. A. Minta and R. Y. Tsien, *J. Biol. Chem.*, 1989, **264**, 19449-19457.
12. Y. Urano, M. Kamiya, K. Kanda, T. Ueno, K. Hirose and T. Nagano, *J. Am. Chem. Soc.*, 2005, **127**, 4888-4894.
13. T. Yogo, Y. Urano, Y. Ishitsuka, F. Maniwa and T. Nagano, *J. Am. Chem. Soc.*, 2005, **127**, 12162-12163.
14. E. J. New, D. Parker, D. G. Smith and J. W. Walton, *Curr. Opin. Chem. Biol.*, 2010, **14**, 238-246.
15. J. K. Barton, A. T. Danishefsky and J. M. Goldberg, *J. Am. Chem. Soc.*, 1984, **106**, 2172-2176.
16. U. Neugebauer, Y. Pellegrin, M. Devocelle, R. J. Forster, W. Signac, N. Morand and T. E. Keyes, *Chem. Commun.*, 2008, 5307-5309.
17. R. Bizzarri, M. Serresi, S. Luin and F. Beltram, *Anal. Bioanal. Chem.*, 2009, **393**, 1107-1122.
18. A. P. Alivisatos, K. P. Johnsson, X. G. Peng, T. E. Wilson, C. J. Loweth, M. P. Bruchez and P. G. Schultz, *Nature*, 1996, **382**, 609-611.
19. M. Benezra, O. Penate-Medina, P. B. Zanzonico, D. Schaer, H. Ow, A. Burns, E. DeStanchina, V. Longo, E. Herz, S. Iyer, J. Wolchok, S. M. Larson, U. Wiesner and M. S. Bradbury, *J. Clin. Invest.*, 2011, **121**, 2768-2780.
20. P. Atkins and J. de Paula, *Physical Chemistry*, 4th edn., Oxford University Press, Oxford, 2002.
21. D. Parker, *Coord. Chem. Rev.*, 2000, **205**, 109-130.
22. D. W. Parker, JAG, *Metal Ions in Biological Systems : The Lanthanides and their Interactions with Biosystems*, Chapter 7, 233-280, Wiley, New York, 2003.
23. T. Forster, *Discussions of the Faraday Society*, 1959, 7-17.
24. D. L. Dexter, *J. Chem. Phys.*, 1953, **21**, 836-850.
25. D. Parker, *Chem. Soc. Rev.*, 2004, **33**, 156-165.

26. A. Beeby, I. M. Clarkson, R. S. Dickins, S. Faulkner, D. Parker, L. Royle, A. S. de Sousa, J. A. G. Williams and M. Woods, *J. Chem. Soc. Perkin Trans. 2*, 1999, 493-503.
27. W. P. Cacheris, S. C. Quay and S. M. Rocklage, *Magn. Reson. Imaging*, 1990, **8**, 467-481.
28. P. Caravan, J. J. Ellison, T. J. McMurry and R. B. Lauffer, *Chem. Rev.*, 1999, **99**, 2293-2352.
29. B. Alpha, J. M. Lehn and G. Mathis, *Angew. Chem. Int. Ed.*, 1987, **26**, 266-267.
30. W. P. Cacheris, S. K. Nickle and A. D. Sherry, *Inorg. Chem.*, 1987, **26**, 958-960.
31. T. Moeller and L. C. Thompson, *J. Inorg. Nucl. Chem.*, 1962, **24**, 499-510.
32. J. Pintaske, P. Martirosian, H. Graf, G. Erb, K. P. Lodemann, C. D. Claussen and F. Schick, *Invest. Radiol.*, 2006, **41**, 213-221.
33. M. Oudkerk, P. E. Sijens and E. J. R. Vanbeek, *Invest. Radiol.*, 1995, **30**, 75-78.
34. D. Parker, R. S. Dickins, H. Puschmann, C. Crossland and J. A. K. Howard, *Chem. Rev.*, 2002, **102**, 1977-2010.
35. M. R. Spirlet, J. Rebizant, J. F. Desreux and M. F. Loncin, *Inorg. Chem.*, 1984, **23**, 359-363.
36. C. P. Montgomery, B. S. Murray, E. J. New, R. Pal and D. Parker, *Acc. Chem. Res.*, 2009, **42**, 925-937.
37. L. S. Natrajan, N. M. Khoabane, B. L. Dadds, C. A. Muryn, R. G. Pritchard, S. L. Heath, A. M. Kenwright, I. Kuprov and S. Faulkner, *Inorg. Chem.*, 2010, **49**, 7700-7709.
38. C. Geraldes, M. P. M. Marques and A. D. Sherry, *Inorg. Chim. Acta*, 1987, **139**, 311-313.
39. J. L. Humm, *J. Nucl. Med.*, 1986, **27**, 1490-1497.
40. C. J. Broan, J. P. L. Cox, A. S. Craig, R. Kataky, D. Parker, A. Harrison, A. M. Randall and G. Ferguson, *J. Chem. Soc. Perkin Trans. 2*, 1991, 87-99.
41. G. Nocton, A. Nonat, C. Gateau and M. Mazzanti, *Helv. Chim. Acta*, 2009, **92**, 2257-2273.
42. M. Giraud, E. S. Andreiadis, A. S. Fisyuk, R. Demadrille, J. Pecaut, D. Imbert and M. Mazzanti, *Inorg. Chem.*, 2008, **47**, 3952-3954.
43. A. Nonat, D. Imbert, J. Pécaut, M. Giraud and M. Mazzanti, *Inorg. Chem.*, 2009, **48**, 4207-4218.
44. S. Aime, M. Botta, D. Parker and J. A. G. Williams, *J. Chem. Soc. Dalton Trans.*, 1995, 2259-2266.
45. E. Cole, R. C. B. Copley, J. A. K. Howard, D. Parker, G. Ferguson, J. F. Gallagher, B. Kaitner, A. Harrison and L. Royle, *J. Chem. Soc. Dalton Trans.*, 1994, 1619-1629.
46. S. Aime, P. L. Anelli, M. Botta, F. Fedeli, M. Grandi, P. Paoli and F. Uggeri, *Inorg. Chem.*, 1992, **31**, 2422-2428.
47. J. Notni, P. Hermann, J. Havlickova, J. Kotek, V. Kubicek, J. Plutnar, N. Loktionova, P. J. Riss, F. Roesch and I. Lukes, *Chem. Eur. J.*, 2010, **16**, 7174-7185.
48. T. Vitha, V. Kubicek, J. Kotek, P. Hermann, L. V. Elst, R. N. Muller, I. Lukes and J. A. Peters, *Dalton Trans.*, 2009, 3204-3214.
49. B. Alpha, R. Ballardini, V. Balzani, J. M. Lehn, S. Perathoner and N. Sabbatini, *Photochem. Photobiol.*, 1990, **52**, 299-306.
50. G. Mathis, *Clin. Chem.*, 1993, **39**, 1953-1959.
51. H. R. Murner, E. Chassat, R. P. Thummel and J. C. G. Bunzli, *J. Chem. Soc. Dalton Trans.*, 2000, 2809-2816.

52. R. A. Poole, G. Bobba, M. J. Cann, J. C. Frias, D. Parker and R. D. Peacock, *Org. Biomol. Chem.*, 2005, **3**, 1013-1024.
53. E. J. New and D. Parker, *Org. Biomol. Chem.*, 2009, **7**, 851-855.
54. S. Petoud, S. M. Cohen, J. C. G. Bunzli and K. N. Raymond, *J. Am. Chem. Soc.*, 2003, **125**, 13324-13325.
55. E. G. Moore, A. P. S. Samuel and K. N. Raymond, *Acc. Chem. Res.*, 2009, **42**, 542-552.
56. M. Seitz, M. D. Pluth and K. N. Raymond, *Inorg. Chem.*, 2007, **46**, 351-353.
57. D. Parker, P. K. Senanayake and J. A. G. Williams, *J. Chem. Soc. Perkin Trans. 2*, 1998, 2129-2139.
58. Y. Bretonniere, M. J. Cann, D. Parker and R. Slater, *Org. Biomol. Chem.*, 2004, **2**, 1624-1632.
59. P. Atkinson, K. S. Findlay, F. Kielar, R. Pal, D. Parker, R. A. Poole, H. Puschmann, S. L. Richardson, P. A. Stenson, A. L. Thompson and J. H. Yu, *Org. Biomol. Chem.*, 2006, **4**, 1707-1722.
60. C. P. Montgomery, D. Parker and L. Lamarque, *Chem. Commun.*, 2007, 3841-3843.
61. E. Brunet, O. Juanes, R. Sedano and J. C. Rodriguez-Ubis, *Org. Lett.*, 2002, **4**, 213-216.
62. C. P. Montgomery, E. J. New, L. O. Palsson, D. Parker, A. S. Batsanov and L. Lamarque, *Helv. Chim. Acta*, 2009, **92**, 2186-2213.
63. A. Picot, A. D'Aleo, P. L. Baldeck, A. Grichine, A. Duperray, C. Andraud and O. Maury, *J. Am. Chem. Soc.*, 2008, **130**, 1532-1537.
64. A. Hayek, F. Bolze, J. F. Nicoud, P. L. Baldeck and Y. Mely, *Photochem. Photobiol. Sci.*, 2006, **5**, 102-106.
65. H. Takalo and J. Kankare, *Acta Chem. Scand. B Org. Chem. Biochem.*, 1988, **42**, 373-377.
66. M. Latva, H. Takalo, V. M. Mukkala, C. Matachescu, J. C. RodriguezUbis and J. Kankare, *J. Lumin.*, 1997, **75**, 149-169.
67. J. C. G. Bunzli and C. Piguet, *Chem. Soc. Rev.*, 2005, **34**, 1048-1077.
68. D. Guo, C. Duan, F. Lu, Y. Hasegawa and Q. Meng, *Chem. Commun.*, 2004, 1486-1487.
69. P. Coppo, M. Duati, V. N. Kozhevnikov, J. W. Hofstraat and L. De Cola, *Angew. Chem. Int. Ed.*, 2005, **44**, 1806-1810.
70. W. D. Horrocks, B. Holmquist and B. L. Vallee, *P. Natl. Acad. Sci.*, 1975, **72**, 4764-4768.
71. D. M. Owen, M. A. A. Neil, P. M. W. French and A. I. Magee, *Sem. Cell Dev. Biol.*, 2007, **18**, 591-598.
72. R. G. Kruger, P. Dostal and D. G. McCafferty, *Chem. Commun.*, 2002, 2092-2093.
73. B. Tang, L. Cao, K. Xu, L. Zhuo, J. Ge, Q. Li and L. Yu, *Chem. Eur. J.*, 2008, **14**, 3637-3644.
74. B. N. G. Giepmans, S. R. Adams, M. H. Ellisman and R. Y. Tsien, *Science*, 2006, **312**, 217-224.
75. A. Piljic and C. Schultz, *ACS Chem. Biol.*, 2008, **3**, 156-160.
76. *www.htrf.com, December 2010.*
77. J. Xu, T. M. Corneillie, E. G. Moore, G.-L. Law, N. G. Butlin and K. N. Raymond, *J. Am. Chem. Soc.*, 2011, **133**, 19900-19910.

78. H. E. Rajapakse, N. Gahlaut, S. Mohandessi, D. Yu, J. R. Turner and L. W. Miller, *P. Natl. Acad. Sci. USA*, 2010, **107**, 13582-13587.

2. The 3-Azaxanthone Series

2.1 Introduction

1-Azaxanthone is well established as an excellent sensitising group for europium emission.[1] However, due to the orientation in which the chromophore binds to the metal centre in ligand systems based upon DOTA, a maximum of two azaxanthone moieties per complex is attainable. To increase this value to three, and even four, sensitising groups per complex, the synthesis of a constitutional isomer of 1-azaxanthone was undertaken. The ability of 3-azaxanthone to sensitise Eu^{3+} and its photophysical properties were assessed. This was followed by the incorporation of the sensitiser into a number of model complexes based upon $Eu(DOTA)^-$, in which the number of chromophores was varied from one to four ($[Eu{\cdot}L^1(H_2O)]$ – $[Eu{\cdot}L^4]^{3+}$). As expected, increasing the number of sensitising groups led to an increase in the molar extinction coefficient. Each of the four complexes was fully characterised and their properties are discussed. Comparison of the complex $[Eu{\cdot}L^2(H_2O)]^+$ with the 1-azaxanthone analogue, led to some interesting differences in the behaviour of the complexes with protein. Cell microscopy studies were also carried out with both complexes and showed binding to the DNA of cells undergoing mitosis. As a result of the interesting properties of $[Eu{\cdot}L^2(H_2O)]^+$, the 3-azathiaxanthone analogue was synthesised and a comparative analysis of their behaviour is given.

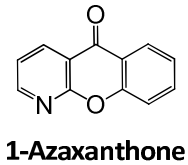

1-Azaxanthone

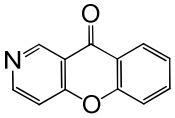

3-Azaxanthone

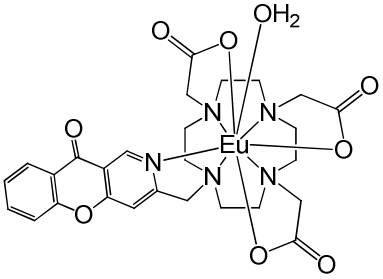

$[EuL^1(H_2O)]$

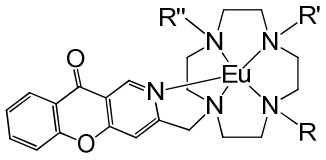

$[EuL^2(H_2O)]^+$: R' = 3-Azaxanthone
R, R'' = $CH_2CO_2^-$

$[EuL^3(H_2O)]^{2+}$: R, R'' = 3-Azaxanthone
R' = $CH_2CO_2^-$

$[EuL^4]^{3+}$: R, R', R'' = 3-Azaxanthone

2.2 Synthetic Aspects

2.2.1 3-Azaxanthone

The synthesis of 1-azaxanthone begins with 2-chloronicotinic acid.[1] To carry out an analogous synthesis to form 3-azaxanthone, 4-chloronicotinic acid is required. While this precursor is commercially available, 4-chloro-6-methylnicotinic acid (***3***) is not. The methyl group in the 6-position is required for subsequent reactions. The first two steps towards the synthesis of ***3*** had been previously published[2] and the conversion of ***2*** to ***3*** was achieved by stirring in neat $POCl_3$ overnight at 100 ºC (*Scheme 2.1*). The removal of excess $POCl_3$ by distillation left the acid chloride of ***3***, which

was converted to the carboxylic acid by addition of water. The product, ***3***, was isolated as a light purple solid.

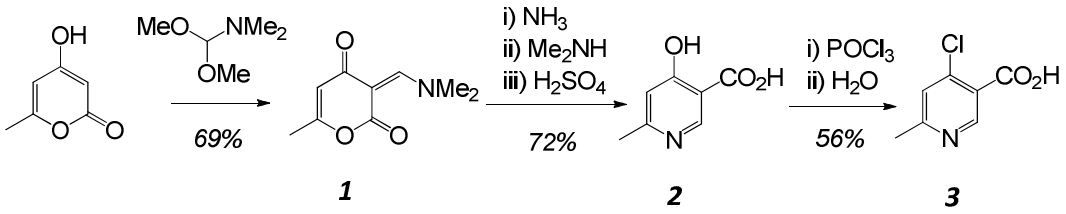

Scheme 2.1

With compound ***3*** in hand, the synthesis of 3-azaxanthone was carried out according to *Scheme 2.2*. Sodium methoxide was produced *in situ* by dissolving Na metal in dry MeOH. 4-Chloro-6-methylnicotinic acid (***3***) and phenol were dissolved in the NaOMe solution. Excess MeOH was removed under reduced pressure to leave a residue which was heated to 180 °C for 2 h. After work up, the product (***4***) was purified by column chromatography. Cyclisation of ***4*** using polyphosphoric acid (PPA) gave 3-azaxanthone (***5***) in a high yield.

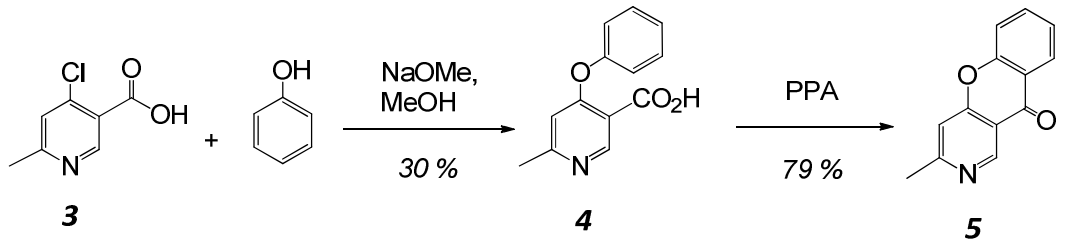

Scheme 2.2

Bromination of the methyl group of ***5*** was attempted using a variety of conditions. Stirring in CCl_4 with N-bromosuccinimide (NBS) and dibenzoyl peroxide at 60 ºC was slow and several additions of NBS were required over a period of 72 hours. The reaction rate was increased upon irradiating the solution with a 100 W tungsten lamp. This is most likely due to the constant initiation of radicals when using the lamp. The heat generated by the lamp also helps the reaction to proceed. As dibromination is possible, the reaction was monitored by ^{1}H-NMR and stopped when an optimal ratio of starting material to monobrominated product to dibrominated product was achieved. The products were separated by column chromatography and the overall yield was increased to 49 % by the conversion of the dibrominated product back to the monobrominated product using $POH(OEt)_2$ and $NH(^iPr)_2$ in THF (*Scheme 2.3*).

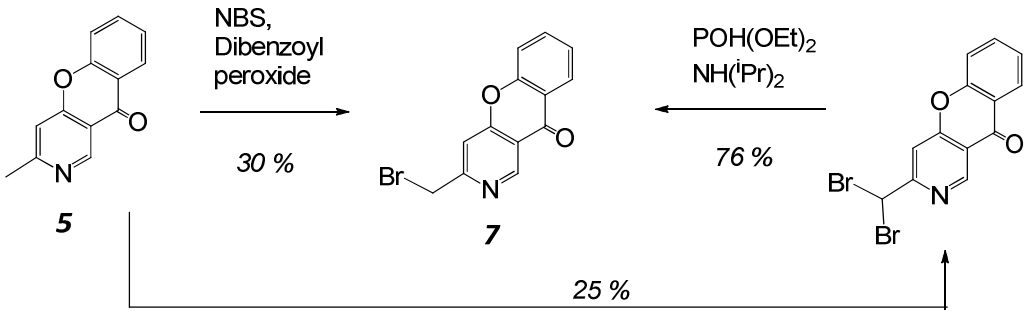

Scheme 2.3

2.2.2 Europium Complexes Containing the 3-Azaxanthone Chromophore

Four europium complexes were synthesised, in which the number of chromophores varies from one to four. The sensitising groups are linked to a 1,4,7,10-tetraazacyclododecane (cyclen) ligand via an N–CH_2–chromophore linkage. The remaining pendant arms are carboxymethyl groups, as in the DOTA complex $[Eu{\cdot}L^{1.3}]^-$. These were chosen as they are known to form kinetically inert lanthanide complexes with good aqueous solubility and europium complexes based on DOTA containing alternative sensitising groups have previously been synthesised,[1] allowing direct comparison.

The first complex synthesised was $[Eu{\cdot}L^1(H_2O)]$ (*Scheme 2.4*). The precursor trimester, DO3A(O^tBu)$_3$, was synthesised by a published procedure in reasonable yield.[3] An S_N2 nucleophilic substitution reaction between the primary bromide, 2-bromomethyl-3-azaxanthone (***7***) , and DO3A(O^tBu)$_3$ afforded ***8*** in excellent yield. The reaction was carried out in a small volume of dry CH_3CN to maximise the rate and extent of reaction; K_2CO_3 was added in stoichiometric amounts to act as a base. Deprotection of the *tert*-butyl ester groups with CF_3CO_2H was followed by complexation in water with $Eu(OAc)_3$. A slight excess of $Eu(OAc)_3$ was used to ensure the complexation went to completion. Excess Eu^{3+} was removed at the end of the reaction by precipitation and syringe filtration of $Eu(OH)_3$ from an aqueous solution at pH 10. High resolution mass spectrometry (HRMS) and reverse phase-high performance liquid chromatography (RP-HPLC) was used to confirm the formation and purity of $[Eu{\cdot}L^1(H_2O)]$.

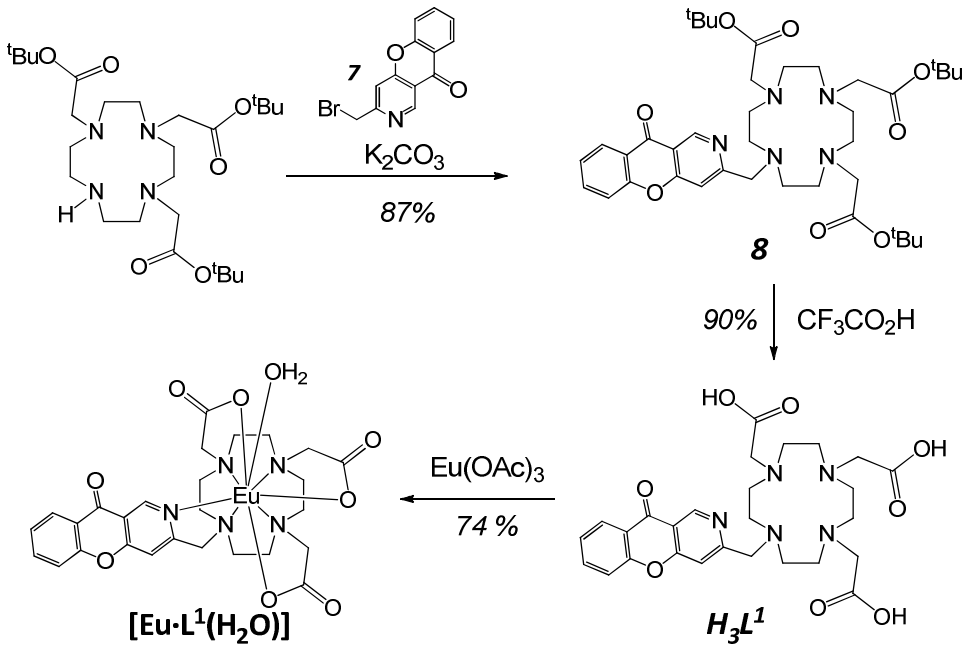

Scheme 2.4

The synthesis of $[Eu{\cdot}L^2(H_2O)]Cl$ was carried out using a similar reaction pathway to that of $[Eu{\cdot}L^1(H_2O)]$, starting from the commercially available, $DO2A(O^tBu)_2$ (*Scheme 2.5*). The resulting complex was isolated as an acetate salt. Small amounts of $(CF_3CO_2)^-$ salts may also have been present, so chloride anion exchange was undertaken, to ensure that each complex had the same counter-ion and that water solubility was maximised. Again, HRMS and RP-HPLC was used to confirm the structure and purity.

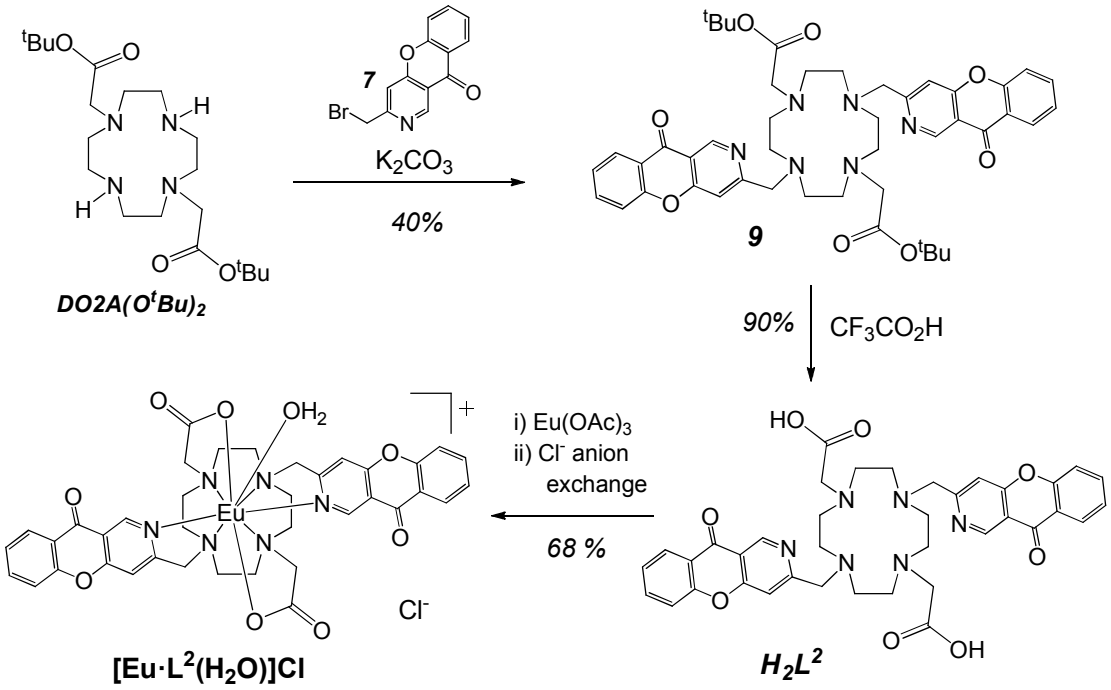

Scheme 2.5

The synthesis of $[Eu{\cdot}L^3(H_2O)]Cl_2$ was achieved via a slightly longer route (*Scheme 2.6*) involving the protection of three of the cyclen nitrogens with *tert*-butoxycarbonyl (BOC) groups. By this method, mono-alkylation using ethyl bromoacetate was achieved in 77 % yield. Selective removal of the BOC groups was possible using CF_3CO_2H, obviating competitive ethyl ester hydrolysis. Alkylation with three equivalents of 2-bromomethyl-3-azaxanthone proceeded cleanly, provided that the intermediate ***11*** had been thoroughly dried over $K_2CO_{3(s)}$ in anhydrous CH_2Cl_2. The hygroscopic nature of ligand ***11*** meant that without drying, hydrolysis of the brominated chromophore to form 2-hydroxymethyl-3-azaxanthone competed with alkylation. Hydrolysis of ***12*** was initially attempted under basic aqueous conditions. However, due to low solubility, alternative conditions were necessary. Hydrolysis of ***12*** was achieved in aqueous HCl (approximately 2 mM). Under reflux, the ligand fully dissolved, due to protonation of the chromophore and cyclen nitrogens. These conditions caused rapid hydrolysis of the ethyl ester, which was confirmed by ^{1}H-NMR. The pH of the solution was adjusted to 5.8 by addition of aqueous NaOH before complexation with $Eu(OAc)_3$. Complexation reactions are typically carried out at pH values above 5, as the carboxylate groups are deprotonated at this pH (pK_a ~ 4.8). Upon complexation, the pH of the solution decreases, due to the expulsion of protons from the cyclen ring. As with $[Eu{\cdot}L^2(H_2O)]^+$, anion exchange was carried out on the final complex, whose synthesis was confirmed by HRMS and RP-HPLC.

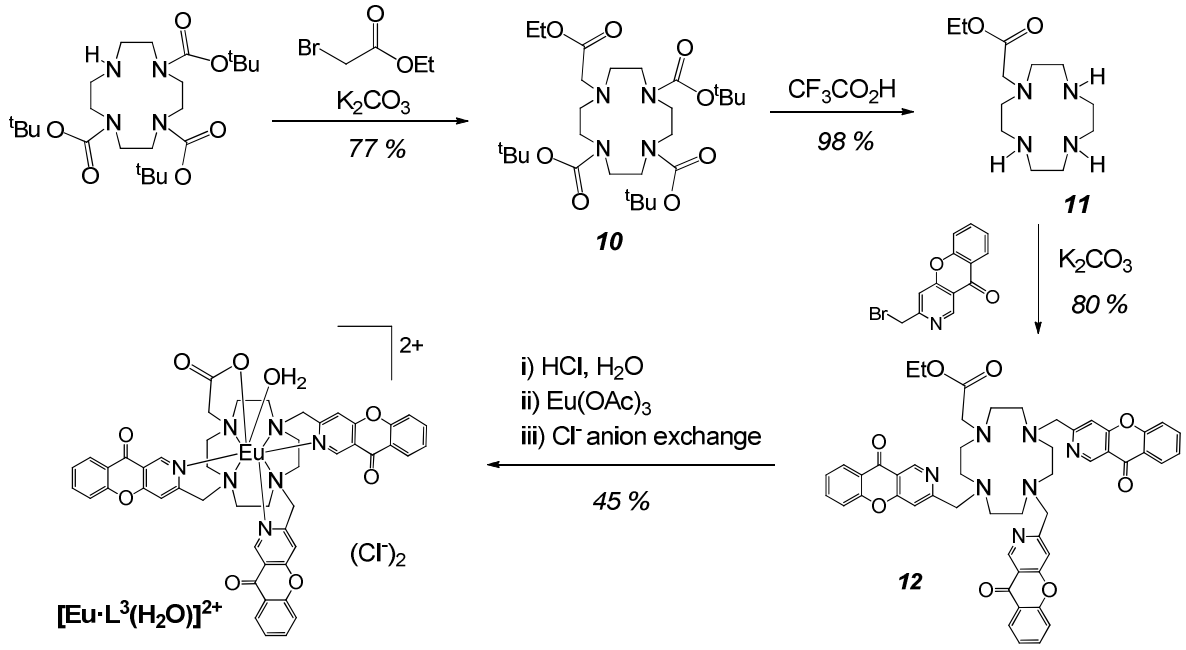

Scheme 2.6

The synthesis of the final complex within the present series, $[Eu{\cdot}L^4]^{3+}$, appeared straightforward but there were concerns about the steric demand of four chromophores and the chemical stability, with respect to metal ion dissociation, of a complex containing eight nitrogen donors. DFT Gaussian simulations of a structurally similar complex were carried out[i] which showed that complex formation should be feasible, as the bulk of the chromophore is directed away from the metal centre, thereby

[i] Calculation by Miss N. Hogg and Dr. I. Kuprov (Durham University)

reducing steric demand at the metal centre (*Figure 2.1*). This prediction was subsequently confirmed by the crystal structure of the tetrapyridyl complex, $[Eu{\cdot}L^{1.4}]^{3+}$, discussed in *Section 1.3.3*.[4]

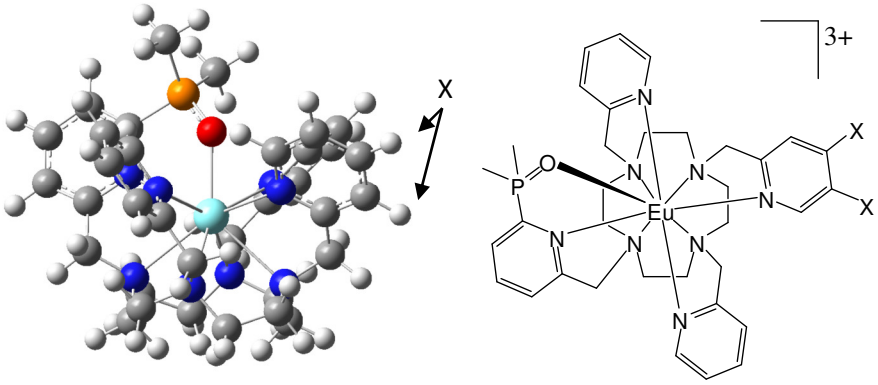

Figure 2.1 *left*) Simulated 3D structure and 2D structure of a europium complex containing 4 pyridyl donating groups. Complexes contain carbon (grey), hydrogen (white), oxygen (red), nitrogen (blue), phosphorus (orange) and a central metal atom (light blue). Note the positions marked X, from which the 3-azaxanthone chromophore extends.

The synthesis of $[Eu{\cdot}L^{4}]^{3+}$ is shown in *Scheme 2.7*. 1,4,7,10-Tetraazacyclododecane was reacted with four equivalents of 2-bromomethyl-3azaxanthone in CH_3CN, using K_2CO_3 as a base. Purification by column chromatography on alumina gave ***L*⁴** in 60 % yield. As ***L*⁴** is a neutral species, complexation was carried out in CH_3CN with $Eu(OTf)_3$. After two days, the solvent was removed under reduced pressure and the residue dissolved in 0.1 mL of MeCN. This solution was dropped into dry $(Et)_2O$, resulting in precipitation of $[Eu{\cdot}L^{4}]^{3+}$ as a triflate salt. Anion exchange to the chloride salt increased the water solubility and allowed the characterisation of the complex in aqueous solution by HRMS and RP-HPLC.

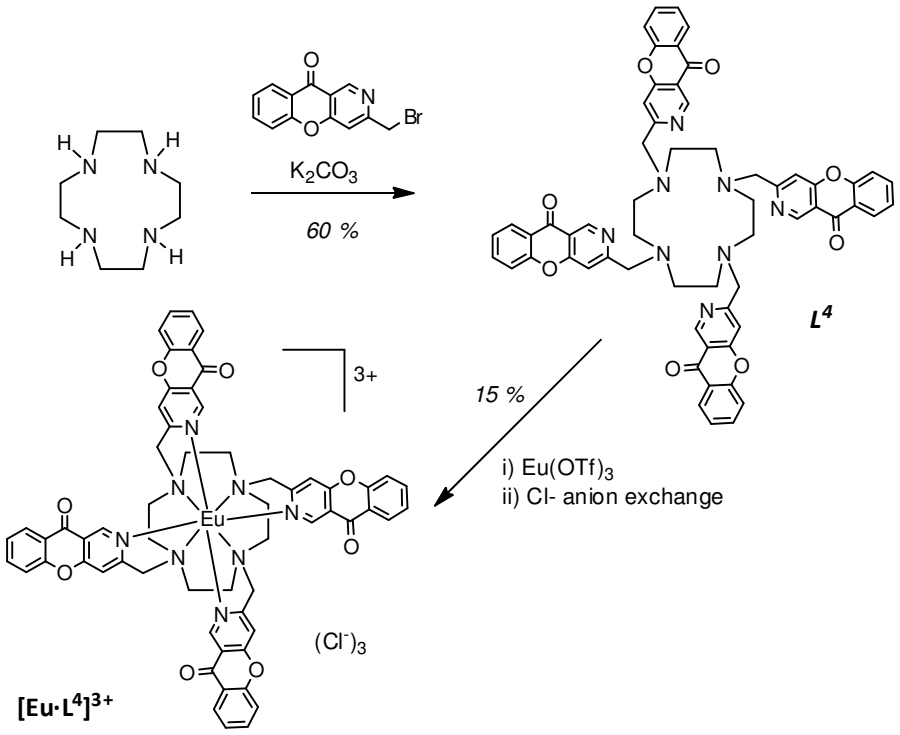

Scheme 2.7

2.2.3 Terbium Complexes Containing the 3-Azaxanthone Chromophore

Two Tb^{3+} complexes were synthesised in the azaxanthone series: $[Tb{\cdot}L^{1}(H_2O)]$ and $[Tb{\cdot}L^{2}(H_2O)]Cl$. Each complex was synthesised from its respective ligand in an analogous manner to the Eu^{3+} counterparts, using $Tb(OAc)_3$ in the place of $Eu(OAc)_3$. The photophysical properties of each Tb^{3+} complex were analysed and are also investigated in the quenching experiments in *Chapter 6*.

2.2.4 Bis(3-azathiaxanthone) Europium Complex

The synthesis of the bis(3-azaxanthone) complex $[Eu{\cdot}L^{2b}(H_2O)]^+$ followed a similar pathway to that of the azaxanthone analogue, $[Eu{\cdot}L^{2}(H_2O)]^+$, with the exception of the first coupling step of the chromophore (*Scheme 2.8*). This reaction takes place in dimethylformamide at 150 °C with K_2CO_3 as the base. Cuprous bromide is also added in catalytic amounts. It is likely that the presence of Cu(I) increases the rate of thiolate addition at the *4*-pyridyl position by the formation of a pyridyl cuprate intermediate. The remaining five steps towards the final complex $[Eu{\cdot}L^{2b}(H_2O)]^+$ were carried out in a similar manner to that of $[Eu{\cdot}L^{2}(H_2O)]^+$ and proceeded smoothly (*Scheme 2.9*).

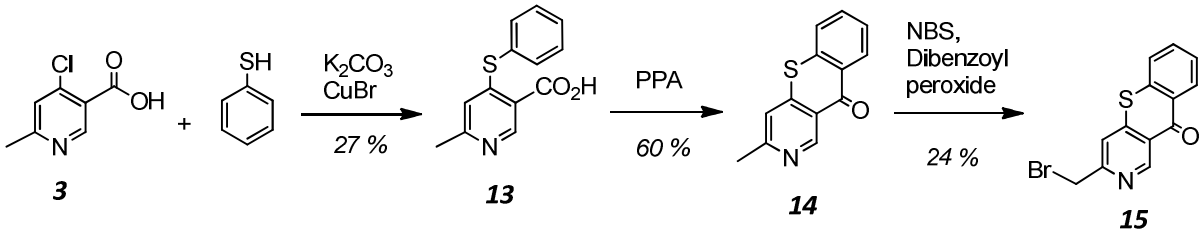

Scheme 2.8

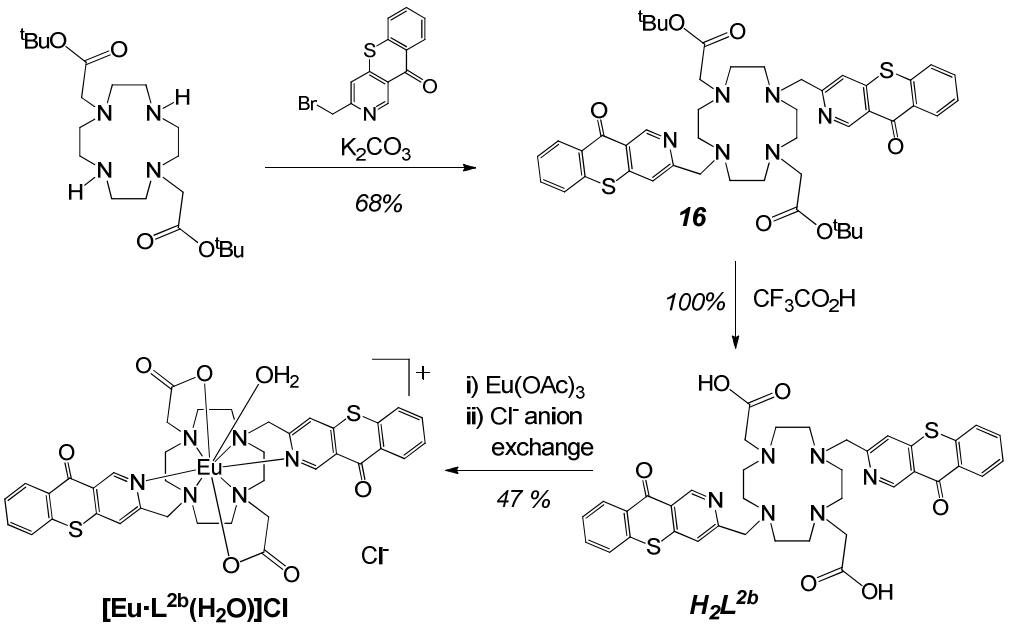

Scheme 2.9

2.3 ^{1}H-NMR Analysis

Proton NMR analysis of each of the complexes $[Eu{\cdot}L^1(H_2O)]$ – $[Eu{\cdot}L^4]Cl_3$ was undertaken in D_2O at 400 MHz and pD 5.8. ^{1}H-NMR allows an assessment of the number of isomeric species in solution and gives information on the local symmetry on the NMR timescale. The neutral complex, $[Eu{\cdot}L^1(H_2O)]$, gave two sets of thirty paramagnetically shifted proton resonances in ratio 5:4 (*Figure 2.2*). These correspond to the square-antiprismatic and twisted square-antiprismatic isomers that have been documented previously in NMR analyses of related derivatives of DO3A.[5, 6] The mono-cationic complex, $[Eu{\cdot}L^2(H_2O)]^+$, gave rise to two sets of 18 proton resonances, in ratio 6:5 (*Figure 2.3*), consistent with the presence of two diastereoisomeric species with C_2-symmetry. The shifts of each set showed a strong correspondence with those observed for $[Eu.L^1(H_2O)]$, in accord with this interpretation. For $[Eu.L^4]^{3+}$, only one set of twelve paramagnetically shifted resonances was observed (*Figure 2.4*), consistent with local C_4-symmetry. Thus, the pyridyl H-6 proton resonated at +12.5 ppm, with the ring ethylene protons observed as a single shifted AA'BB' system, at +30.0, +14.2, -10.9 and -29.1 ppm.

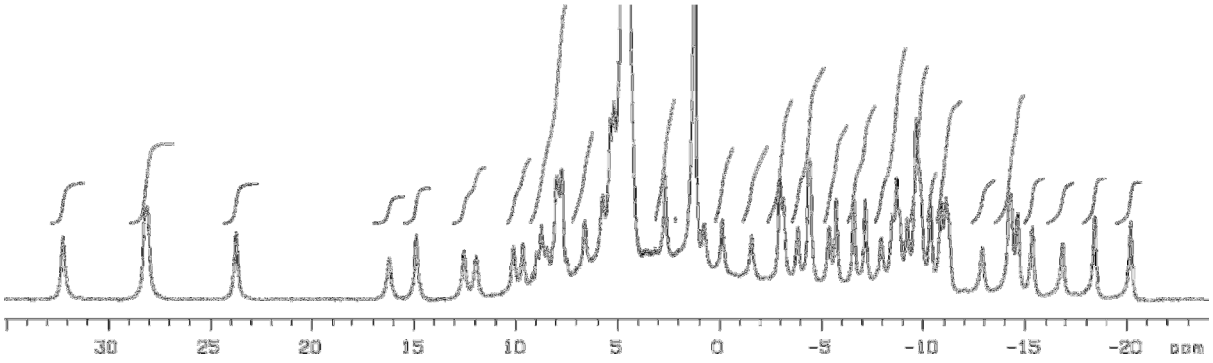

Figure 2.2 ^{1}H-NMR analysis of $[Eu{\cdot}L^1(H_2O)]$ (400 MHz, D_2O, pD 5.8).

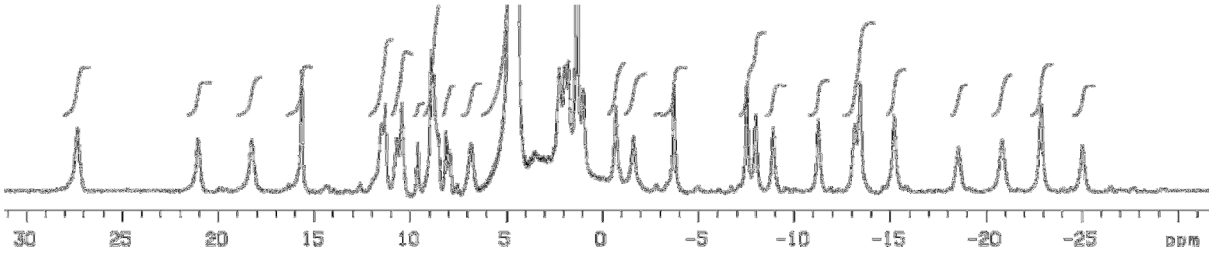

Figure 2.3 ^{1}H-NMR analysis of $[Eu{\cdot}L^2(H_2O)]Cl$ (400 MHz, D_2O, pD 5.8).

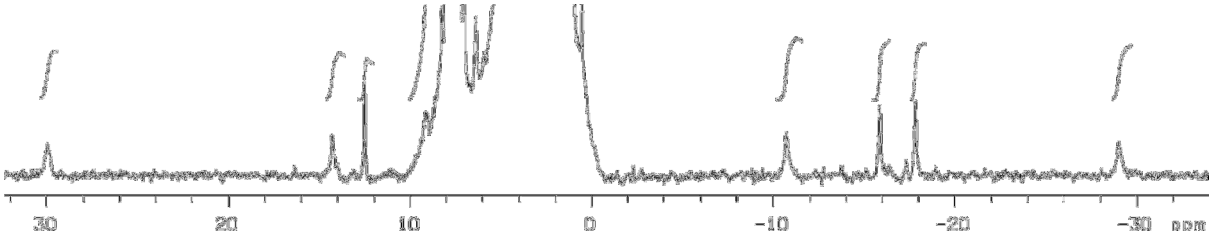

Figure 2.4 ^{1}H-NMR analysis of $[Eu{\cdot}L^4]Cl_3$ (400 MHz, D_2O, pD 5.8).

2.4 Photophysical Studies

2.4.1 2-Methyl-3-Azaxanthone

The absorption spectrum of 2-methyl-3-azaxanthone (***5***) was measured in methanol at 293 K (*Figure 2.5 left*). The longest wavelength absorption maximum is at 324 nm and corresponds to a transition to the singlet excited state with predominantly n-π* character with some degree of π-π* character, as previously observed for 1-azaxanthone.[1] The absorption spectrum was run at a variety of concentrations. A plot of absorbance at 324 nm against concentration allows the determination of the molar extinction coefficient according to the equation,

$$A = \varepsilon cl \qquad [2.1]$$

where A is the absorbance, ε is the molar extinction coefficient, c is the concentration and l is the cell pathlength. The gradient of such a plot is equal to the molar extinction coefficient. From *Figure 2.5 right*, a molar extinction coefficient of 5,600 M^{-1} cm^{-1} was calculated (MeOH, 295 K). This value is similar to the value recorded for 1-azaxanthone (6,900 $M^{-1}cm^{-1}$, λ_{max} = 330 nm, MeOH, 295 K). The similarity between both λ_{max} and ε suggest that the shift in position of N from the 1-position to the 3-position does not greatly affect the photophysical properties of the azaxanthone and that 3-azaxanthone should be as efficient at sensitising lanthanide emission as its parent chromophore.

The fluorescence emission spectrum of 2-methyl-3-azaxanthone was recorded in methanol at 295 K. As with the 1-azaxanthone analogue, the intensity of the emission was exceptionally low, indicating that other processes (non-radiative decay and intersystem crossing) dominate the excited state properties of 2-methyl-3-azaxanthone. This was further indication that the chromophore would be well-suited to sensitisation of Eu^{3+} and Tb^{3+}.

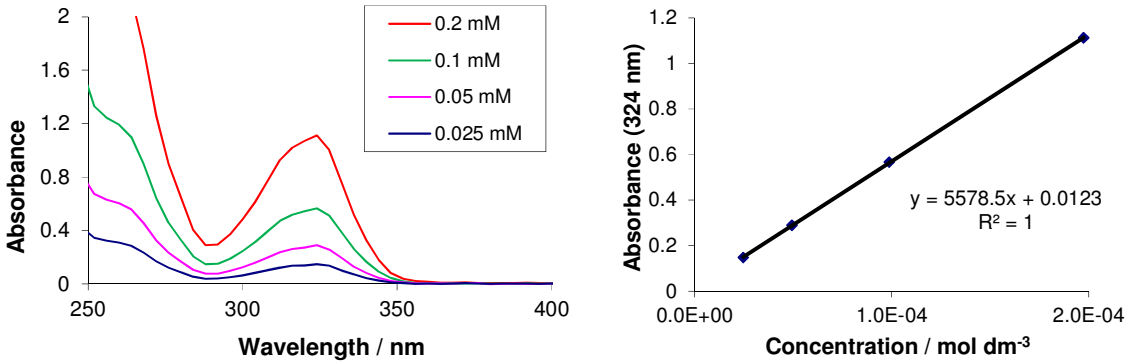

Figure 2.5 *left*) Absorption of 2-methyl-3-azaxanthone at four concentrations (MeOH, 295 K) and *right*) absorbance at λ_{max} as a function of concentration, allow calculation of the molar extinction coefficient.

2.4.2 Europium Complexes Based Upon 2-Methyl-3-Azaxanthone

The photophysical characterisation of the complexes [Eu·L^1(H$_2$O)] – [Eu·L^4]Cl$_3$ was carried out in aqueous solution at pH 5.8 and 295 K (*Table 2.1*). The absorption spectrum of [Eu·L^1(H$_2$O)] in water is shown in *Figure 2.6*. Also shown is the absorption spectrum of 3-azaxanthone in methanol. It is worth noting that the absorption maximum has shifted by 4 nm to longer wavelength. This could be an effect of complexation but is more likely to be a consequence of the change in solvent. A similar red-shift was previously observed for 1-azaxanthone upon moving from a MeOH solution to a MeOH : H$_2$O (2 : 1) mixture.[1] The lowest energy transition for 1-azaxanthone in a less polar medium (MeOH) is n-π* in character. Upon moving to a more polar medium, the contribution of the π-π* excited state, which is similar in energy to the n-π* excited state, to the transition becomes greater and the wavelength maximum shifts slightly to the red. This same principle is likely to account for the shift observed in *Figure 2.6*.

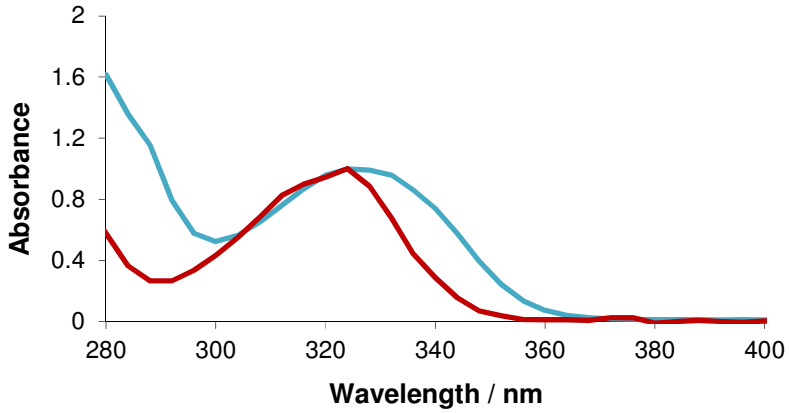

Figure 2.6 Absorption spectra of [Eu·L^1(H$_2$O)] in H$_2$O (*blue*) and 2-methyl-3-azaxanthone in MeOH (*red*), showing a red shift of 4 nm in the maximum absorption wavelength.

Molar extinction coefficients were calculated for each of the four Eu^{3+} complexes (*Table 2.1*). Comparison of the values for [Eu·L^1(H$_2$O)] and 3-azaxanthone, which both contain a single azaxanthone moiety per molecule, show a reduction in molar extinction coefficient upon moving to a more polar solvent. This is, again, consistent with observations noted for 1-azaxanthone in which a reduction in the oscillator strength of the transition due to a change in solvent polarity led to a reduction in molar extinction coefficient. As expected, the molar extinction coefficient approximately doubles upon doubling the number of sensitising groups.

Table 2.1 Photophysical data for Eu^{3+} complexes of $\boldsymbol{L^1}$ – $\boldsymbol{L^4}$. (λ_{ex} = 328 nm, pH 5.8)

Complex	ε / M^{-1} cm^{-1}	$\Phi_{H_2O}^{Eu}$ / %	k_{H_2O} / (ms)$^{-1}$	k_{D_2O} / (ms)$^{-1}$	q
[Eu.L^1(H$_2$O)]	2,500	6.9	1.67	0.51	1.1
[Eu.L^2(H$_2$O)]$^+$	5,800	10	1.70	0.65	1.1
[Eu.L^3(H$_2$O)]$^{2+}$	9,300	5.0	2.00	0.63	1.3
[Eu.L^4]$^{3+}$	15,600	5.4	1.41	0.83	0.4

By measuring the intensity of Eu^{3+} emission as a function of delay time after excitation, the luminescence lifetime of each complex was calculated in H_2O and D_2O (*Table 2.1*). The curves obtained (*Figure 2.7*) were fitted to *Equation 2.2*, to give the rate constant for decay of the lanthanide excited state, *k*. For $[Eu{\cdot}L^1(H_2O)]$, values of 1.67 and 0.51 $(ms)^{-1}$ were found in H_2O and D_2O, respectively. The lifetime of Eu^{3+} emission, τ, is the reciprocal of *k*. For a given complex, the lifetime in D_2O is always longer than in H_2O, due to vibrational quenching by OH oscillators. As discussed in *Section 1.3.2*, values of k_{H2O} and k_{D2O} can be used to calculate the number of inner sphere bound water molecules, *q*. Knowledge of the *q* value is important, as it has consequences upon the emissive quantum yield and allows correlation between the photophysical properties of a complex with the structure and coordination sphere.

$$I = A_0 + A_1 e^{-kt} \qquad [2.2]$$

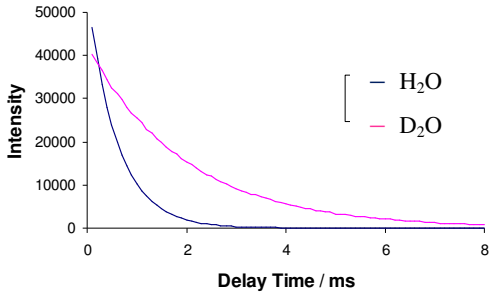

Figure 2.7 Emission decay curves of $[Eu{\cdot}L^1(H_2O)]$ in H_2O and D_2O, allowing calculation of *k* and τ.

From the calculated *q* values, it is clear that for complexes $[Eu{\cdot}L^1(H_2O)]$, $[Eu{\cdot}L^2(H_2O)]^+$ and $[Eu{\cdot}L^3(H_2O)]^{2+}$**,** the average number of bound water molecules at any given time is 1. These values are not exact integers, due to variation in the metal to water bond distance, influence from other nearby X-H oscillators (such as C-H) and second sphere water molecules. A *q* value of 1 suggests that the steric bulk about the europium centre is not too great – there is space for a water molecule to enter the inner sphere. Upon moving to a fourth bound sensitising group ($[Eu{\cdot}L^4]^{3+}$), the steric demand is starting to crowd the inner sphere and the *q* value decreases to 0.4. This value has still not reached zero which suggests that the stability of $[Eu{\cdot}L^4]^{3+}$, from a steric point of view, should be relatively high.

The quantum yield values of the four complexes are in the range 5 – 10 %. These values are comparable to the quantum yields of complexes containing 1-azaxanthone, and indicate that the 3-azaxanthone is able to efficiently populate the Eu^{3+} excited state. The non-zero *q* values for the four complexes are likely to limit the quantum yield. It may have been expected that $[Eu{\cdot}L^4]^{3+}$ would have the highest quantum yield as it has the lowest *q* value. In fact, the quantum yield is much the same as the other complexes. This may well be due to an equilibrium between the $q = 0$ and $q = 1$ $[Eu{\cdot}L^4]^{3+}$ complexes, as seen for the tetra pyridyl complex $[Eu{\cdot}L^{1.4}]^{3+}$ (*Section 1.3.3*).[4] The long lifetime of the Eu^{3+} excited state (0.70 ms) means that the exchange of H_2O on and off the metal centre is not the determining step in the quenching process.

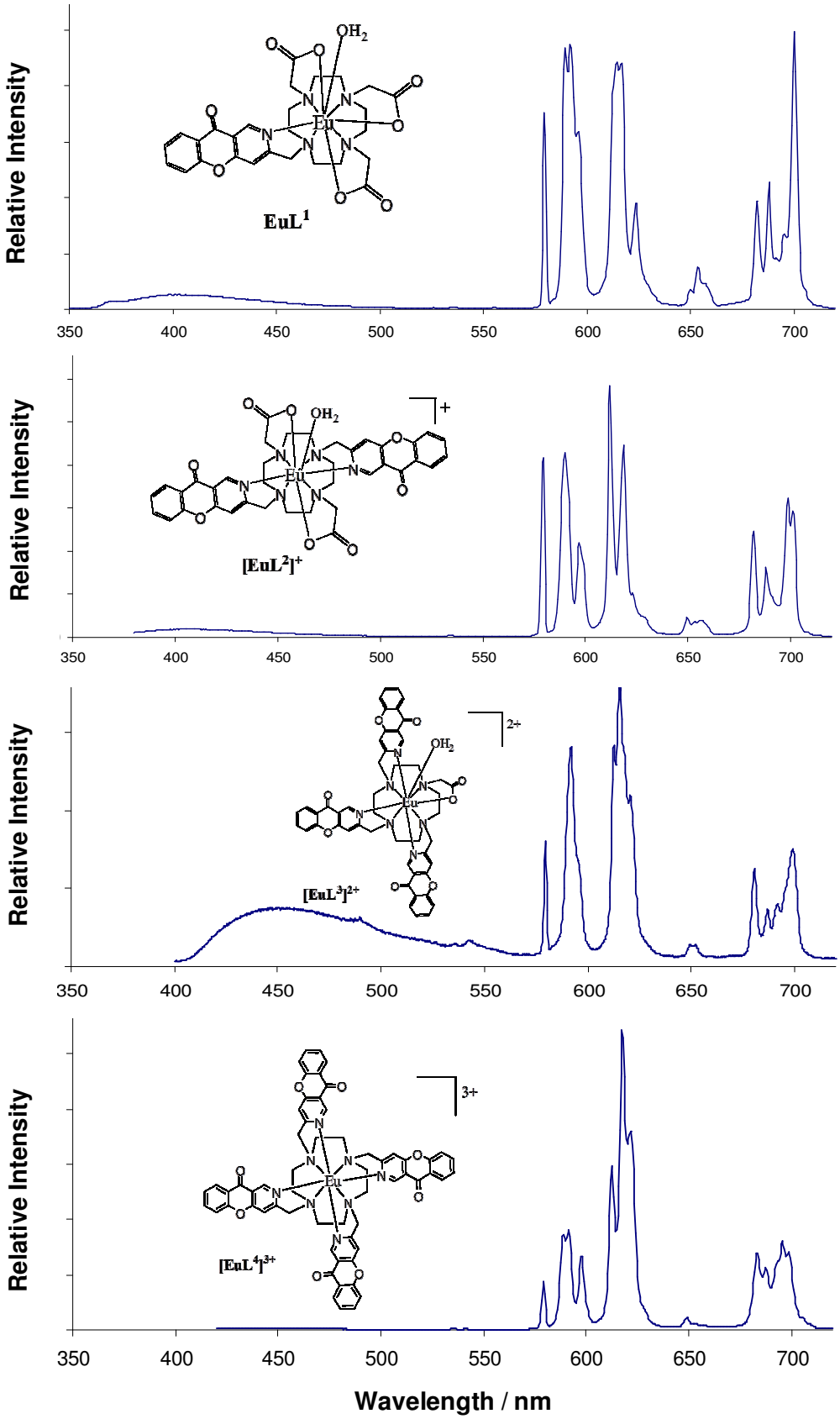

Figure 2.8 Emission spectra of the four europium complexes in water after excitation at 328 nm. Each spectrum was recorded with a complex concentration of 20 μM at pH 5.8 and 293 K.

The emission spectra of the four complexes were recorded after excitation at 328 nm (H_2O, 295 K, *Figure 2.8*). Each spectrum shows the characteristic europium emission containing 5 bands and fine splitting in the $\Delta J = 1$ to $\Delta J = 4$ transitions. Ligand fluorescence can also be observed at 400 nm. The fluorescence is very low for each complex, confirming the hypothesis of a fast rate of intersystem crossing and energy transfer for the 3-azaxanthone sensitiser. The complex with three chromophores, $[Eu{\cdot}L^3(H_2O)]^{2+}$, shows the greatest fluorescence. This may be due to a slight excess of ligand in the sample or even a contaminant which fluoresces to give the unusually large peak at 450 nm. HPLC analysis (*Appendix 1*) shows that a small amount of impurity is present in the sample. Unfortunately, the amount of $[Eu{\cdot}L^3(H_2O)]^{2+}$ was too small to allow further purification.

When analysing europium emission spectra, two features have been shown to determine spectral form. Firstly, the higher the degree of symmetry about the Eu^{3+} centre, the simpler the emission spectrum appears. Secondly, the donating group in the axial position of a square antiprismatic or twisted square antiprismatic complex affects the relative intensity of the $\Delta J = 2$ transition. It is found that hard donors, such as H_2O, lead to a decrease in the relative intensity whereas more polarisable donors lead to an increase. Further details of this aspect are given in *Chapter 3* but, for now, these two empirical observations suffice.

When comparing the emission spectra of $[Eu{\cdot}L^1(H_2O)]$ and $[Eu{\cdot}L^2(H_2O)]^+$, it is apparent that the increased symmetry of $[Eu{\cdot}L^2(H_2O)]^+$ leads to a less complex spectrum. There is more splitting in both the $\Delta J = 1$ and $\Delta J = 2$ bands for $[Eu{\cdot}L^1(H_2O)]$. When looking at $[Eu{\cdot}L^4]^{3+}$, the theory of high symmetry giving a simplified spectrum seems to fall down, as the complex has C_4 symmetry and, yet, it has possibly the most complex spectral form of all. One explanation for this could be that the large size of the complex and the relatively soft donating ability of the nitrogen lone pairs, mean that at any one time many different conformations are adopted. Thermal fluctuations may cause the complex to move away from C_4 symmetry and therefore result in a more complex spectrum.

A correlation between the emission spectra and the q values of the four complexes is observed. A decrease in the number of hard H_2O axial donors leads to an increase in the relative intensity of the $\Delta J = 2$ band. Both $[Eu{\cdot}L^1(H_2O)]$ and $[Eu{\cdot}L^2(H_2O)]^+$ have q value of 1 and this is reflected in a $\Delta J = 2$ band of similar intensity to the less sensitive $\Delta J = 1$ band. A q value of 0.4 was calculated for $[Eu{\cdot}L^4]^{3+}$ and, as a result, the relative intensity of the $\Delta J = 2$ band is greater than that of the other complexes.

One of the aims of the project is to design a complex with a large $\Delta J = 2$ band. Clearly, the absence of water in the capping position is an important factor when designing such a complex. It is likely that the relative intensity would increase even further if a more polarisable group were in the axial position. The absence of a capping H_2O molecule is also likely to increase the overall quantum yield of the complex, as discussed above.

2.4.3 Photoluminescence Stability Assessment

The presence of inner sphere water molecules can lead to a reduction in the Eu^{3+} emission intensity. There are many other processes which can also cause a decrease in emission intensity. A series of experiments was undertaken, with the assistance of workers from CISbioassays, to assess the relative photoluminescence stability of each complex in the presence of a million fold excess of Ca^{2+}, Mg^{2+}, Mn^{2+} or $[EDTA]^{4-}$. Calcium and magnesium were chosen as common dications that can bind competitively to the macrocyclic ligand. Manganese is a dication of comparable size to magnesium, can act as a reductant and also has weak *d* – *d* absorption bands in the visible spectrum, giving it a light pink colour. The $[EDTA]^{4-}$ serves as a competitive ligand for the Eu^{3+} ion. In each case, the complex was present at 10 nM concentration in HEPES buffer at pH 7.4 and the additive (20 μM) was added. Following excitation at 337 nm, the Eu^{3+} emission intensity was measured at 15 min and 18h time-points (*Figure 2.9*). For each complex, the presence of added $CaCl_2$ or $MgCl_2$ did not significantly perturb the Eu^{3+} emission. The effect of added $MnCl_2$ was more significant. $[Eu.L^1(H_2O)]$ showed greater sensitivity to $MnCl_2$ quenching than $[Eu.L^2(H_2O)]^+$. The quenching mechanism must involve a short range encounter between the Eu^{3+} complex and the Mn^{2+} aqua ion. It may be that the cationic $[Eu.L^2(H_2O)]^+$ complex, which is also more sterically bulky than $[Eu.L^1(H_2O)]$, electrostatically and sterically inhibits a close encounter with the Mn^{2+} aqua ion, and therefore is quenched to a lesser extent. The quenching mechanism of Mn^{2+} is not known but is investigated in greater detail in *Chapter 6*.

In terms of stability with respect to trans-complexation by excess $[EDTA]^{4-}$, $[Eu.L^2(H_2O)]^+$ and the sterically hindered complex, $[Eu.L^4]^{3+}$ were the most stable. This is intriguing, as the related tetrapyridyl complex $[Eu.L^{1.4}]^{3+}$ (*Section 1.3.3*) was found to dissociate in the presence of equimolar amounts of DTPA, another competitive multidentate ligand.[4] For each complex examined, the diminution of Eu^{3+} emission after an overnight incubation suggested that no complex completely resisted the exchange process that involves dissociation of Eu^{3+} and competitive re-association with $[EDTA]^{4-}$.

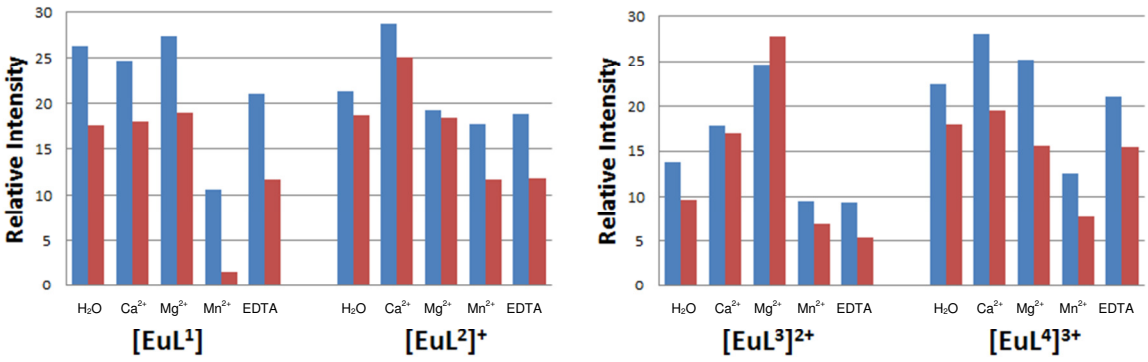

Figure 2.9 Changes in Eu^{3+} emission intensity after 15 min (*blue*) or 18h (*red*) in the presence of the stated additives (10nM complex, 20mM additive, λ_{ex} = 335 nm, λ_{ex} = 620 nm).

2.5 Comparative Studies

2.5.1 Bis(3-Azaxanthone) and Bis(1-Azaxanthone) Europium Complexes

Of the four complexes synthesised, $[Eu{\cdot}L^2(H_2O)]^+$ was found to have the most favourable properties: it has the highest quantum yield and shows the greatest resistance to quenching by $MnCl_2$. As noted in *Section 2.6*, it also exhibits intriguing behaviour in the cellular environment. During the preparation of $[Eu{\cdot}L^2(H_2O)]^+$, an analogous complex $[(1\text{-AX})\text{-}Eu{\cdot}L^2]^+$ was synthesised.[ii] This complex is the constitutional isomer of $[Eu{\cdot}L^2(H_2O)]^+$, incorporating two 1-azaxanthone groups. The behaviour of each complex in the presence of protein (HSA) and DNA was investigated.

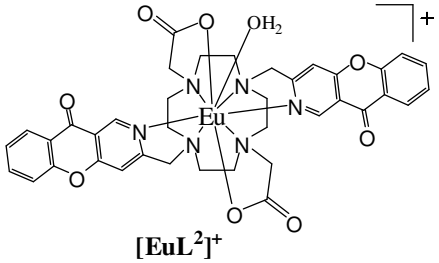

$[EuL^2]^+$

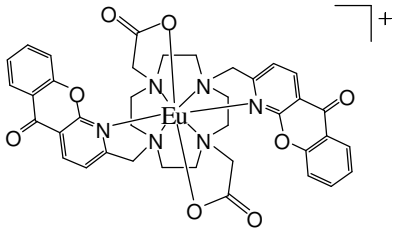

$[(1\text{-AX})\text{-}EuL^2]^+$

Luminescence titrations were carried out for each complex with human serum albumin (HSA). This protein was added in increments from 0 – 700 μM (*Figure 2.10*), to an aqueous solution of the complex (20 μM). A study of the form of the two initial europium emission spectra, prior to HSA addition, shows clearly that the two species have different symmetry about the metal centre. The complexity of the splitting in the $\Delta J = 1$ and $\Delta J = 4$ bands seen in the spectrum of $[(1\text{-AX})\text{-}Eu{\cdot}L^2]^+$ implies a geometry about the europium centre of lower symmetry than that of $[Eu{\cdot}L^2(H_2O)]^+$. To allow binding to the Eu^{3+} centre of each azaxanthone nitrogen lone pair, $[(1\text{-AX})\text{-}Eu{\cdot}L^2]^+$ must adopt a conformation in which the two sensitising groups lean over the top of the complex – a large proportion of the chromophore lies along the principal axis. This increase in steric bulk about the *z* axis is reflected in a *q* value of 0. In contrast, $[Eu{\cdot}L^2(H_2O)]^+$ has a *q* value of 1. The bulk of the two chromophores now lie away from the principal axis, allowing a H_2O molecule to coordinate in the axial position. It is apparent that access to three and four chromophores in this DOTA based system is only possible using the 3-azaxanthone chromophore.

Upon addition of HSA to $[Eu{\cdot}L^2(H_2O)]^+$, the Eu^{3+} centred emission decreased but no change in the form of the spectrum was observed (*Figure 2.10 upper*). This is consistent with many other europium and terbium complexes, for which increasing amounts of protein reduce the emission intensity due to quenching. These mechanisms may include vibrational quenching of the lanthanide excited state by X-H oscillators (e.g. serine O-H, lysine N-H), or involve the sensitiser excited states. In contrast, the behaviour of $[(1\text{-AX})\text{-}Eu{\cdot}L^2]^+$ with serum albumin is quite different. Firstly, upon addition of HSA the form of the europium emission changes – the fine splitting of the $\Delta J = 1$ band goes from three transitions to four, indicative of more than one emissive Eu^{3+} species in solution, and the $\Delta J = 2$ band goes from two transitions to three, suggesting a change in symmetry about the Eu^{3+} centre upon

[ii] Synthesis of $[(1\text{-AX})\text{-}Eu{\cdot}L^2]Cl$ was carried out by Dr. G. –L. Law at Durham University

addition of protein. It seems plausible that increasing amounts of protein serve to displace one of the bound chromophores, which occupy a sterically demanding region in space, leading to a change in geometry about the metal centre and, therefore, a change in the form of the emission spectrum. Secondly, the $\Delta J = 2$ to $\Delta J = 1$ ratio increases in the presence of protein. This suggests that some polarisable group within the protein (perhaps a CO_2^- of a glutamate or aspartate residue) is binding to europium in the previously unoccupied axially position, leading to the observed change. Overall, this comparison shows the greater stability of $[Eu{\cdot}L^2(H_2O)]^+$, containing the 3-azaxanthone group, with respect to steric demand and displacement of the sensitising group by protein.

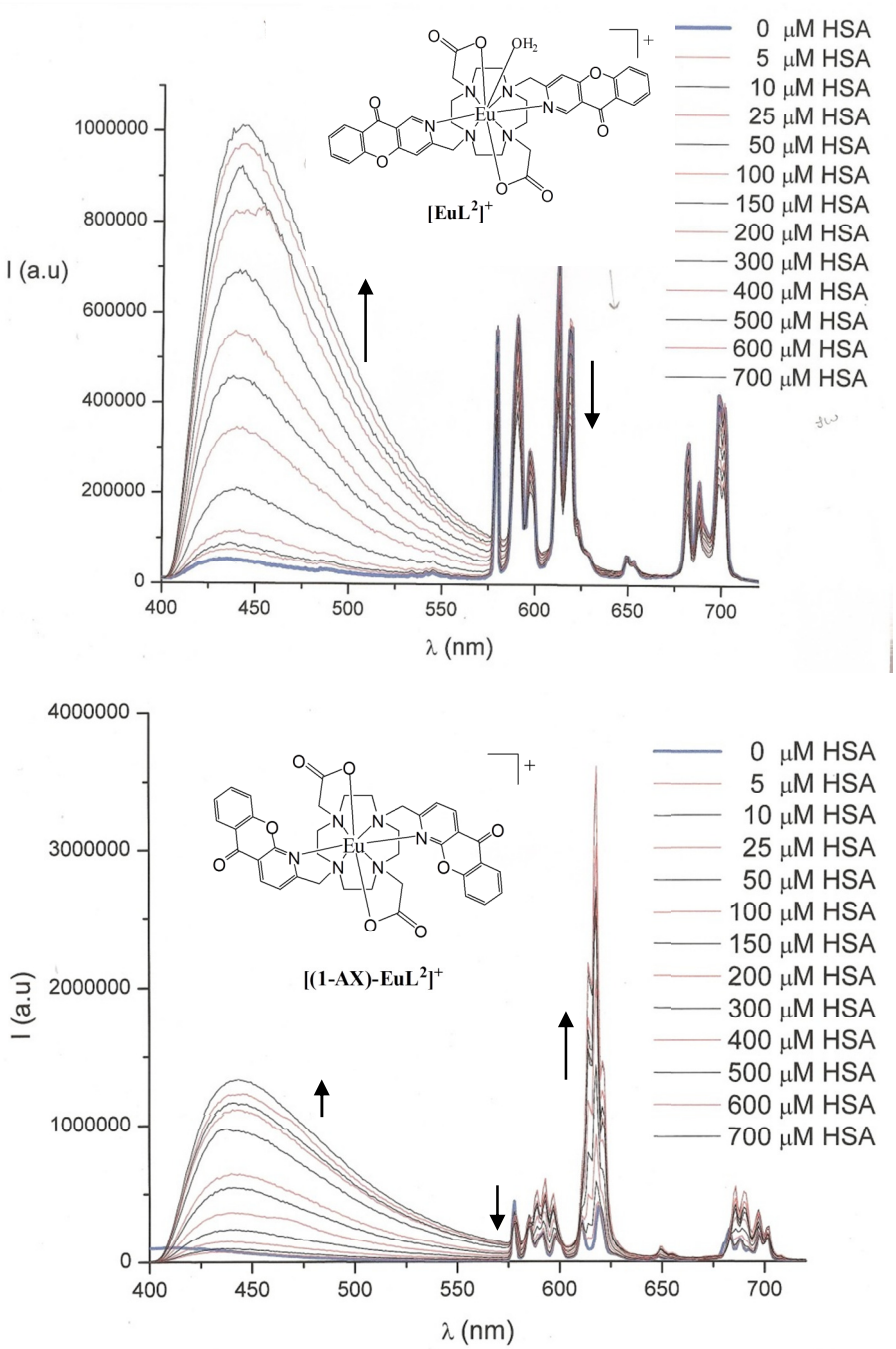

Figure 2.10 Luminescence titrations of $[Eu{\cdot}L^2(H_2O)]^+$ (*upper*) and $[(1\text{-AX})\text{-}Eu{\cdot}L^2]^+$ (*lower*) with an increasing concentration of HSA (complex concentration 20 μM in H_2O, λ_{ex} = 328 nm, pH 7.4, 293 K)

The luminescence lifetime was also measured as a function of added HSA. For $[Eu{\cdot}L^2(H_2O)]^+$, the lifetime was reduced by around 20 %, mirroring the reduction in emission intensity. The isomeric complex, $[(1\text{-AX})\text{-}Eu{\cdot}L^2]^+$, showed an increase in the luminescence lifetime of 50 % at 700 μM, implying that the protein may shield the Eu^{3+} centre, thereby increasing the excited state lifetime. Luminescence titrations with $[Tb{\cdot}L^2(H_2O)]^+$ and $[(1\text{-AX})\text{-}Tb{\cdot}L^2]^+$ gave similar results to the Eu^{3+} complexes. The $[Tb{\cdot}L^2(H_2O)]^+$ excited state was steadily quenched, reflected by a reduction in both lifetime and emission intensity. The lifetime of $[(1\text{-AX})\text{-}Tb{\cdot}L^2]^+$ increased by 65 % whilst the Tb^{3+} emission spectrum, which is less sensitive to its coordination environment, apparently remained unchanged.

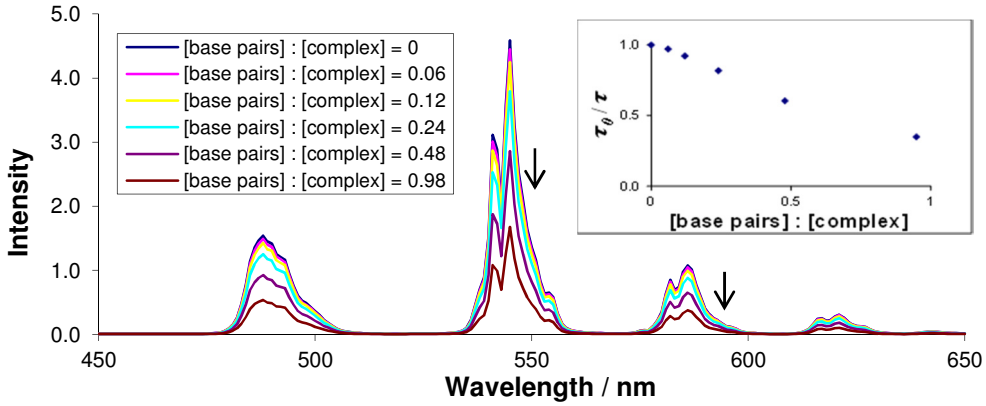

Figure 2.11 Luminescence titration of $[Tb{\cdot}L^2(H_2O)]^+$ with DNA (H_2O, pH 7.4, 295K) and *insert*) Variation in the excited state lifetime as a function of added DNA.

Luminescence titrations with calf thymus DNA (42% CG base pairs) were also carried out with each complex. DNA was added in increments up to a ratio of 4 base pairs per complex. Small decreases (~ 10 %) in the luminescence lifetimes of $[Eu{\cdot}L^2(H_2O)]^+$ and $[(1\text{-AX})\text{-}Eu{\cdot}L^2]^+$ were observed. The forms of the emission spectra were unchanged and the intensities decreased slightly. Addition of DNA to the two Tb^{3+} complexes caused a 50 % reduction in the emission intensity and luminescence lifetime at 1 base pair per complex (*Figure 2.11*). Previous studies examining the behaviour of various lanthanide(III) complexes in the presence of several nucleic acids have revealed charge transfer quenching of lanthanide emission,[7] with Tb complexes much more sensitive to the quenching process. This process may involve exciplex formation between the chromophore and the electron rich C or G bases. Consistent with this idea, addition of poly(dAdT) (DNA without CG base pairs), to either $[Tb{\cdot}L^2]^+$ or $[(1\text{-AX})\text{-}Tb{\cdot}L^2]^+$ led to a 20 % smaller reduction in the intensity of the lanthanide emission than with DNA.

2.5.2 Bis(3-Azathiaxanthone) Europium Complex

The azathiaxanthone complex $[Eu{\cdot}L^{2b}(H_2O)]^+$ was synthesised to investigate the effect of varying O for S upon the behaviour of the complex. It is known that the azathiaxanthones have longer wavelength absorption maxima, making them better suited for biological applications and also have potential use in two photon excitation studies.[8] Despite the longer absorption wavelength, indicative

of a lower singlet excited state energy, the azathiaxanthones possess a smaller singlet-triplet energy gap than the azaxanthones.[1] As a result, azathiaxanthones triplet energies (~24,000 cm^{-1}) are in the range applicable for sensitisation of Eu^{3+}, although Tb^{3+} sensitisation is less efficient.

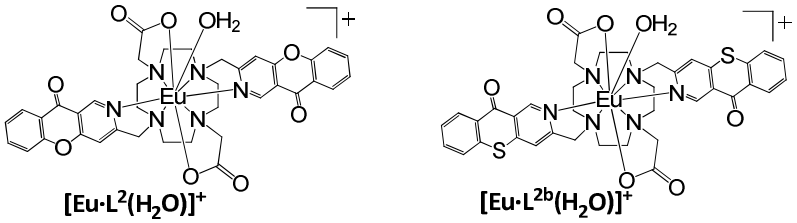

Table 2.2 Photophysical data for $[Eu{\cdot}L^{2}(H_2O)]^+$ and $[Eu{\cdot}L^{2b}(H_2O)]^+$ (H_2O, 295 K unless otherwise stated).

Complex	λ_{abs} / nm	ε / M^{-1} cm^{-1}	$\Phi^{Eu}_{H_2O}$ / %	k_{H_2O} / $(ms)^{-1}$	k_{D_2O} / $(ms)^{-1}$	q
$[Eu.L^{2}(H_2O)]^+$	328	5,800	10	1.70	0.65	1.1
$[Eu.L^{2b}(H_2O)]^+$	368	6,200	8.3	1.76	0.63	1.1

The photophysical properties of $[Eu{\cdot}L^{2b}(H_2O)]^+$ (*Table 2.2*) are very similar to those of $[Eu{\cdot}L^{2}(H_2O)]^+$, with the exception of the absorbance spectral profile. The absorption spectrum of $[Eu{\cdot}L^{2b}]^+$ (*Figure 2.12 insert*) shows two maxima at 310 nm (ε = 12,000 M^{-1} cm^{-1}) and 368 nm (ε = 6,200 M^{-1} cm^{-1}). As with the azaxanthones, these absorption bands are attributed to transitions with dominant n-π* and π-π* character. The emission spectra of $[Eu{\cdot}L^{2b}(H_2O)]^+$ and $[Eu{\cdot}L^{2}(H_2O)]^+$ were measured following excitation at their respective absorption maxima (*Figure 2.12*). The form of the two emission spectra are very similar, indicating that the symmetry and coordination environment about Eu^{3+} is the same in each case. This is also confirmed by the measured q values of 1.1 for each complex. A second observation is the increased fluorescence centred at 440 nm for the azathiaxanthone analogue. The quantum yield for fluorescence is 37 % of the total emission. The significant amount of fluorescence suggests that the intersystem crossing process is less efficient for the azathiaxanthone chromophore than for the azaxanthone chromophore.

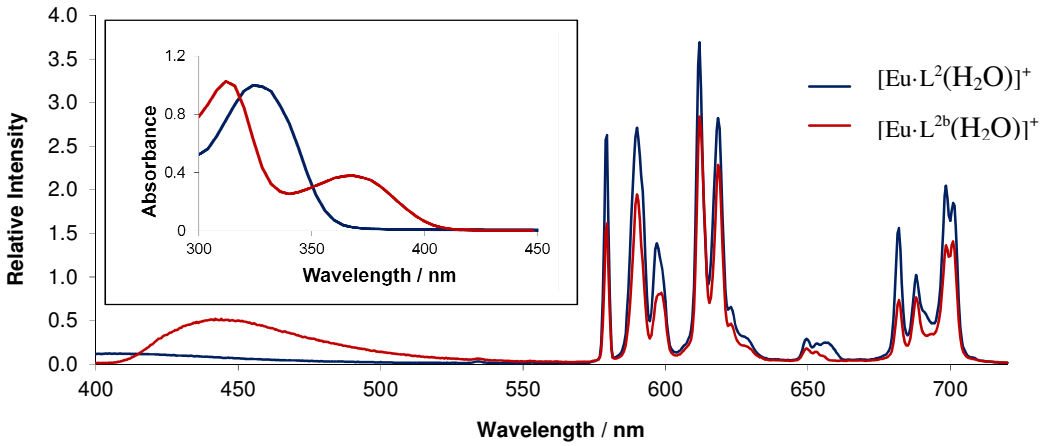

Figure 2.12 Comparison of the absorption (*insert*) and emission spectra of $[Eu{\cdot}L^{2}(H_2O)]^+$ (λ_{ex} = 328 nm) and $[Eu{\cdot}L^{2b}(H_2O)]^+$ (λ_{ex} = 368 nm) (H_2O, pH 5.8, 295 K).

Both protein and DNA titrations were carried out with $[Eu{\cdot}L^{2b}(H_2O)]^+$ in an analogous manner to $[Eu{\cdot}L^{2}(H_2O)]^+$. The results were similar to those of $[Eu{\cdot}L^{2}(H_2O)]^+$. Upon addition of DNA, the Eu^{3+} excited state lifetime fell from 0.57 to 0.47 ms – an 18 % decrease. As with $[Eu{\cdot}L^{2}(H_2O)]^+$, there was no change in the form of the emission spectrum, suggesting no change in the Eu^{3+} coordination environment. It is supposed that quenching by DNA involves the chromophore excited state. The addition of HSA to $[Eu{\cdot}L^{2b}(H_2O)]^+$ led to a reduction in both the excited state lifetime and emission intensity, with no change in the form of the emission.

The general conclusion from the comparison of $[Eu{\cdot}L^{2}(H_2O)]^+$ and $[Eu{\cdot}L^{2b}(H_2O)]^+$ is that varying the sensitising group from an azaxanthone to an azathiaxanthone does not significantly alter the structural or photophysical properties of the Eu^{3+} complex. The advantage of the sulphur containing complex is that the absorption spectrum shifts to a longer wavelength, making it more amenable to cellular studies, where endogenous fluorophores can absorb excitation light of shorter wavelengths.

2.6 Cellular Studies

One potential application of luminescent lanthanide complexes is to report information from within a cellular environment using fluorescence microscopy. The long lived excited state lifetimes and emission spectra in the visible region of the spectrum make them suitable for this purpose. As a result, newly synthesised complexes are often dosed in a number of cell lines to investigate their uptake, localisation and toxicity. Some complexes act as cellular stains while others are designed to report specific changes within the cell. For instance, Eu^{3+} based complexes have been designed which report changes in HCO_3^-,[9] pH and pO_2[10] by a change in the form or intensity of the emission spectrum. For the current series, $[Eu{\cdot}L^{1}(H_2O)]$ – $[Eu{\cdot}L^{4}]^{3+}$, the uptake into cells, the localisation within the cell and the cytotoxicity were all assessed.

2.6.1 Cytotoxicity

An important property of an intracellular complex is its toxicity. The cytotoxicity of a given complex is quantified by its IC_{50} value, which is the concentration of compound required to inhibit cellular activity by 50 %. To calculate the IC_{50} value, NIH-3T3 cells were grown in 96-well plates. After 24 hours, the cells were dosed with complex giving final concentrations over the range 0 – 200 μM. After a further 20 hours incubation, MTT (3-(4,5-dimethylthiazol-2-yl)-2,5-diphenyltetrazolium bromide) was added to each well. This is a compound which is metabolised by mitochondrial dehydrogenase of viable cells to give formazan, a bright purple, insoluble compound. The amount of formazan produced is a measure of the viability of cells after incubation with the complex. After 4 hours incubation with MTT, the amount of formazan was quantified spectrophotometrically upon dissolution in dimethyl sulphoxide. The IC_{50} value is determined as the concentration of complex required to reduce the absorbance to 50 % of that in the untreated, control wells.

Table 2.3 IC_{50} values (± 20 μM) for Eu and Tb complexes calculated using the MTT assay (NIH-3T3 cells).

Complex	IC_{50} / μM
$[Eu{\cdot}L^{1}(H_2O)]$	> 200
$[Tb{\cdot}L^{1}(H_2O)]$	> 200
$[Eu{\cdot}L^{2}(H_2O)]^{+}$	> 200
$[Tb{\cdot}L^{2}(H_2O)]^{+}$	> 200
$[Eu{\cdot}L^{3}(H_2O)]^{2+}$	80
$[Eu{\cdot}L^{4}]^{3+}$	20
$[(1\text{-AX})\text{-}Eu{\cdot}L^{2}]^{+}$	> 200
$[(1\text{-AX})\text{-}Tb{\cdot}L^{2}]^{+}$	> 200
$[Eu{\cdot}L^{2b}(H_2O)]^{+}$	> 200

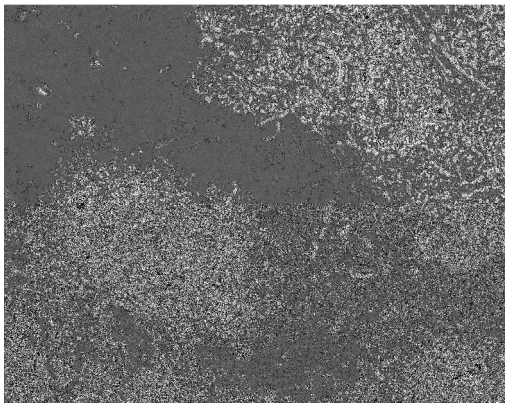

Figure 2.13 Transmission image of NIH-3T3 cells dosed with $[Eu{\cdot}L^{4}]^{3+}$, showing membrane damage.

The results of the cytotoxicity studies (*Table 2.3*) show that increasing the number of sensitising groups, increases the cytotoxicity. Complexes with one and two sensitising groups remain non-cytotoxic up to 200 μM. Varying the Ln^{3+} ion from Eu^{3+} to Tb^{3+} does not appear to alter the toxicity of the complex. The complexes with three and four sensitising groups show higher toxicity. This is likely to be associated with the increase in hydrophobicity of these complexes, leading to rupturing of the phospholipid cell membrane. *Figure 2.13* shows a transmission image of NIH-3T3 cells dosed with $[Eu{\cdot}L^{4}]^{3+}$ (50 μM). The cells have no clear membrane and are leaking cytosol into the medium, consistent with necrotic cell death.

2.6.2 Microscopy Studies

Having established that complexes with one or two sensitising groups were non-cytotoxic up to 200 μM, microscopy studies were undertaken with these complexes to investigate their cellular uptake and localisation profile. The complex $[Eu{\cdot}L^{1}(H_2O)]$ was dosed at 50 μM concentration with NIH-3T3 cells and epifluorescence images were taken at 1, 4 and 24 hour time-points. Using excitation and emission filters, it is possible to selectively excite the Eu^{3+} complex and observe its emission. After a 4 h incubation, Eu^{3+} emission is clearly seen from within the cell (*Figure 2.14*), confirming that the complex is able to permeate the phospholipid membrane and enter the cell.

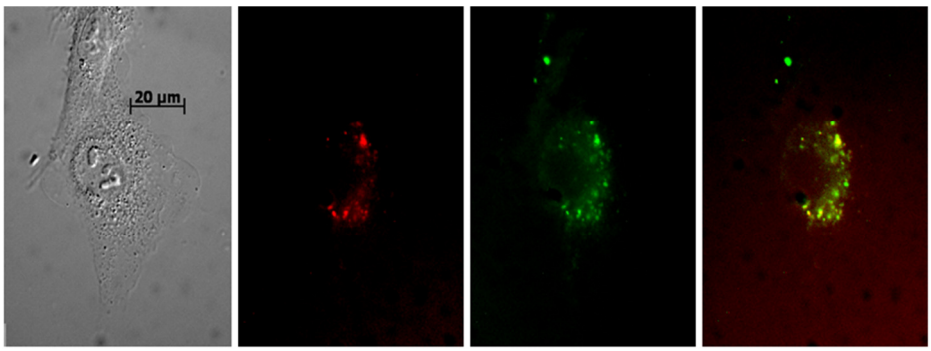

Figure 2.14 Localisation profile of $[Eu{\cdot}L^{1}(H_2O)]$ in NIH-3T3 cells at 4h incubation. From left to right: transmission image, Eu^{3+} emission, LysoTracker emission and a merged image.

The mechanism by which Ln^{3+} complexes containing azaxanthone sensitisers enter cells has been previously investigated.[11] By dosing cells with inhibitors which selectively block certain uptake mechanisms, macropinocytosis was determined as the uptake mechanism, and can be assumed to be the mechanism by which $[Eu{\cdot}L^1(H_2O)]$ enters cells. To establish the localisation profile of $[Eu{\cdot}L^1(H_2O)]$ within the cells, co-localisation studies were performed using commercially available stains. LysoTracker is a dye which selectively stains the lysosomes of cells. By using different filter sets, it is possible to selectively observe $[Eu{\cdot}L^1(H_2O)]$ and LysoTracker emission. *Figure 2.14* clearly shows the co-localisation of the two emissive species, indicating that $[Eu{\cdot}L^1(H_2O)]$ localises in the lysosomes of the cells. The lysosomes are vesicles formed from late endosomes and are responsible for trafficking within the cell, including the removal of waste material. Many Ln^{3+} complexes are visualised within the lysosomes as the cell attempts to remove the foreign material from within the cell.

Lysosomal localisation was observed for $[Eu{\cdot}L^1(H_2O)]$, $[Tb{\cdot}L^1(H_2O)]$, $[Eu{\cdot}L^2(H_2O)]^+$, $[Tb{\cdot}L^2(H_2O)]^+$, $[(1\text{-AX})\text{-}Eu{\cdot}L^2]^+$ and $[(1\text{-AX})\text{-}Tb{\cdot}L^2]^+$ when dosed at 50 μM and visualised by epifluorescence microscopy. Rather different results were found for the complexes $[Tb{\cdot}L^2(H_2O)]^+$ and $[(1\text{-AX})\text{-}Tb{\cdot}L^2]^+$ in HeLa cells, dosed at 0.5 μM and visualised by confocal microscopy.[iii] Confocal microscopy makes use of laser excitation and is able to give images of much higher sensitivity and resolution than epifluorescence microscopy. Under these conditions, the two complexes under surveillance appeared to stain the cell nucleus. This was confirmed by co-localisation studies with Hoechst 33342, a nuclear stain. Furthermore, the staining was selective, with only those cells undergoing mitosis being stained. It is known that during the 'M' phase of mitosis, membrane permeability increases and this may account for this selective staining.[12] For cells at each of the four stages of mitosis (prophase, metaphase, anaphase and telophase) chromosomal DNA could be visualised (*Figure 2.15*). In a separate experiment, a single cell was visualised at various time points as it underwent the early stages of mitosis (*Figure 2.16*). The cell cycle was prematurely stopped before anaphase, possibly due to phototoxicity caused by the excitation light source. These early results of complexes which selectively stain cells undergoing mitosis are unusual and further investigations are required into the mechanism of uptake, trafficking within the cells and the nature of the interaction with the chromatin. The DNA titrations with $[Tb{\cdot}L^2(H_2O)]^+$ and $[(1\text{-AX})\text{-}Tb{\cdot}L^2]^+$ (*Section 2.5.1*) showed that an interaction takes place, leading to a reduction in the Tb^{3+} emission, but suggested that DNA does not change the coordination environment of the Tb^{3+} centre. It is more likely, then, that the binding is via the sensitising group, which is flat and aromatic and may be able to intercalate into major or minor grooves of DNA. Another possibility is that the complexes bind to the protein within the chromatin, which is associated with the compacting of DNA. The protein titration with $[(1\text{-AX})\text{-}Eu{\cdot}L^2]^+$ showed that a specific interaction takes place between the complex and serum albumin, involving the protein directly binding to the Ln^{3+} centre.

[iii] Confocal images taken by Dr. Cornelia Man in Hong Kong University

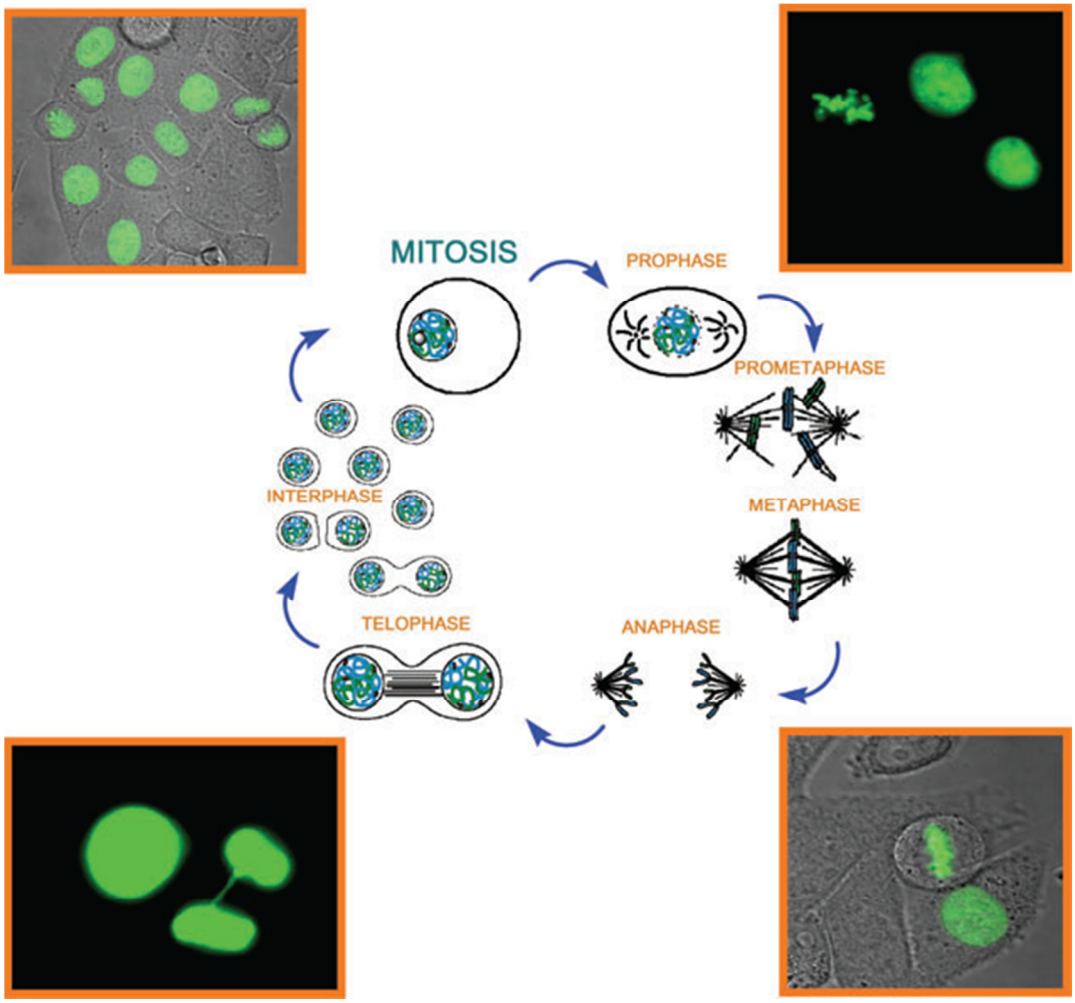

Figure 2.15 Bright field (upper left and lower right) and fluorescence microscopy images of HeLa cells undergoing mitosis, with an illustrative schematic of the cell cycle (0.5 µM, $[(1\text{-AX})\text{-Tb}\cdot L^2]^+$, 3 h , λ_{ex} 355 nm).

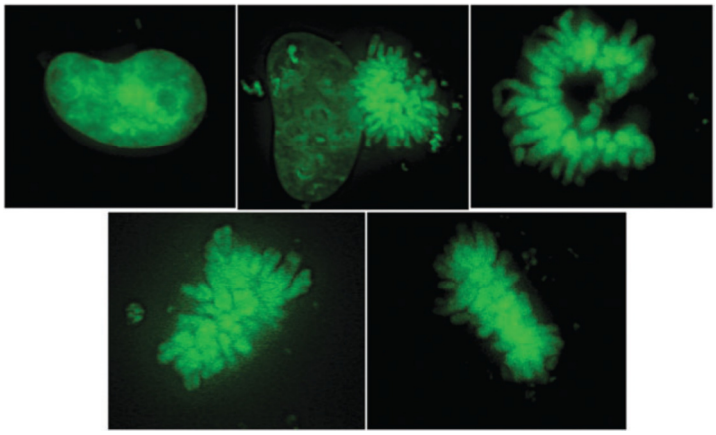

Figure 2.16 Time course (5 min intervals) of fluorescence microscopy images staining chromatin in a cell undergoing division, showing the progression from interphase (top left for comparison) via prophase to prometaphase and metaphase (50 nM $[(1\text{-AX})\text{-Tb}\cdot L^2]^+$, HeLa cell, λ_{ex} 355 nm).

Confocal images were also taken of $[Eu{\cdot}L^{2b}(H_2O)]^+$ in PC3 (human prostate cancer) cells at 50 nM concentration (*Figure 2.17*).[iv] The ability of the azathiaxanthone sensitiser to absorb light at longer wavelengths than the azaxanthone analogue, allowed the use of a 405 nm laser excitation source. As with the complexes $[Tb{\cdot}L^{2}(H_2O)]^+$ and $[(1\text{-AX})\text{-}Tb{\cdot}L^{2}]^+$, $[Eu{\cdot}L^{2b}(H_2O)]^+$ could be visualised within the nucleus of the cell. However, rather than binding to DNA, localisation appears to be in the nucleoli, which contain ribosomes, responsible for protein production within the cell. This hypothesis of $[Eu{\cdot}L^{2b}(H_2O)]^+$ being protein bound is also supported by the non-specific localisation of the complex in the cytosol, which also contains many proteins. It is apparent from these microscopy studies that localisation within the cell is a complex process, which is dependent upon both the cell line and the exact structure of the lanthanide complex and is not easily rationalised.

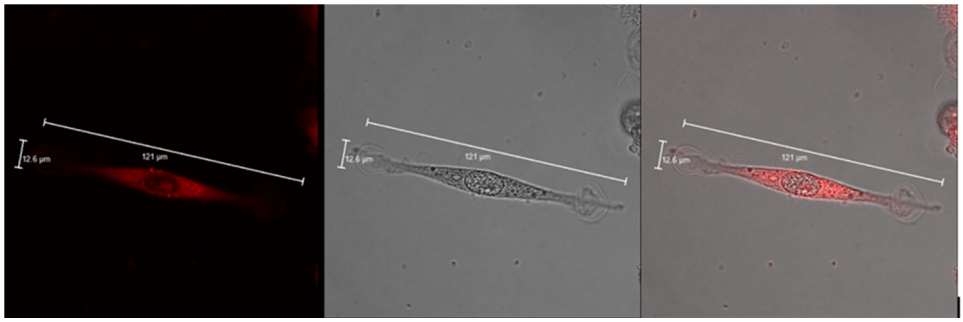

Figure 2.17 Confocal image of $[Eu{\cdot}L^{2b}(H_2O)]^+$ in a PC3 cell line (50 nM, 8 h).

2.7 Conclusions

The initial aim of this study was to investigate whether the 3-azaxanthone chromophore was able to sensitise Eu^{3+} emission and to compare this new chromophore with the 1-azaxanthone constitutional isomer. It was found that altering the position of the N in the chromophore did not significantly alter its photophysical properties. With an extinction coefficient of 2,500 M^{-1} cm^{-1} and a quantum yield of 6.9 %, $[Eu{\cdot}L^{1}(H_2O)]$ is a moderately bright complex upon excitation at 328 nm with typical Eu^{3+} emission between 570 and 720 nm. The advantage of the 3-azaxanthone is the ability to incorporate up to four chromophores per complex, thereby increasing the molar extinction coefficient to 15,000 M^{-1} cm^{-1} for the complex $[Eu{\cdot}L^{4}]^{3+}$, which retains a quantum yield of around 5 %.

The stability of the Eu^{3+} emission was investigated for each complex in the presence of a number of species which could reduce the emission intensity. It was found that the divalent cations Ca^{2+} and Mg^{2+}, which could quench the emission by transmetallation, did not significantly perturb the Eu^{3+} emission. The competitive ligand EDTA showed some ability to extract the Eu^{3+} from its starting ligand, but only after an 18 h incubation time. The species that was able to quench Eu^{3+} emission to the greatest extent was Mn^{2+}. The mechanism of this quenching process is further investigated in *Chapter 6*. The presence of protein and DNA resulted in a decrease in the emission of $[Eu{\cdot}L^{2}(H_2O)]^+$,

[iv] Confocal images taken by Dr. Robert Pal in Durham University

likely due to some non-specific binding. In contrast, the 1-azaxanthone complex $[(1\text{-AX})\text{-Eu}\cdot L^{2}]^{+}$ underwent a change in spectral form, indicative of protein binding directly to the Eu^{3+} centre.

At this stage, a critical assessment of the complexes containing the 3-azaxanthone chromophore is necessary, with respect to their ability to act as donors in the HTRF experiment described in *Section 1.4* and the extent to which these systems meet the specification in *Section 1.5*. The excitation wavelength of this chromophore is suitable to the HTRF application. However, even the complex with the highest molar extinction coefficient ($[Eu\cdot L^{4}]^{3+}$ at 15,000 M^{-1} cm^{-1}) does not exceed that of the currently used tris(bipyridine) complex $[Eu\cdot L^{1.1}]^{3+}$ (18,000 M^{-1} cm^{-1}). The quantum yields are comparable with $[Eu\cdot L^{1.1}]^{3+}$ but show no significant improvement. The stability of each of the complexes in the presence of Mn^{2+}, an ion present in the HTRF assay medium, is also a concern. In terms of the form of the emission spectrum, $[Eu\cdot L^{4}]^{3+}$ has a larger relative $\Delta J = 2$ band, compared to the $[Eu\cdot L^{1.1}]^{3+}$ complex, which would increase spectral overlap with the acceptor moiety in the FRET process. Unfortunately, $[Eu\cdot L^{4}]^{3+}$ is also the complex of lowest aqueous solubility, due to the presence of four aromatic chromophoric groups. Overall, it is apparent that, although the 3-azaxanthone complexes would be applicable to HTRF application, they do not offer any significant advantage over the currently used complex. Other sensitising groups must be investigated which can give large increases in both the molar extinction coefficient and emissive quantum yield, while remaining stable within the assay medium. The form of the emission spectrum must also be improved, which is the subject of the next chapter.

Despite not being further pursued for HTRF applications, the curious behaviour of $[Tb\cdot L^{2}(H_2O)]^{+}$ and $[(1\text{-AX})\text{-Tb}\cdot L^{2}]^{+}$, which selectively stain the DNA of dividing cells, is worth further investigation. Experiments that reveal the nature of the mechanism of cellular uptake and trafficking within the cellular environment are worthy of attention. It is also interesting to find that the azathiaxanthone analogue, $[Eu\cdot L^{2b}(H_2O)]^{+}$, has a different localisation profile. Although a challenging exercise, it may be an area of future study to understand better the processes which determine intracellular localisation with these systems.

2.8 References

1. P. Atkinson, K. S. Findlay, F. Kielar, R. Pal, D. Parker, R. A. Poole, H. Puschmann, S. L. Richardson, P. A. Stenson, A. L. Thompson and J. H. Yu, *Org. Biomol. Chem.*, 2006, **4**, 1707-1722.
2. E. E. Kilbourn and M. C. Seidel, *J. Org. Chem.*, 1972, **37**, 1145-1148.
3. D. A. Moore, *Org. Synth.*, 2008, **85**, 10-11.
4. L. S. Natrajan, N. M. Khoabane, B. L. Dadds, C. A. Muryn, R. G. Pritchard, S. L. Heath, A. M. Kenwright, I. Kuprov and S. Faulkner, *Inorg. Chem.*, 2010, **49**, 7700-7709.
5. P. Caravan, J. J. Ellison, T. J. McMurry and R. B. Lauffer, *Chem. Rev.*, 1999, **99**, 2293-2352.
6. S. Aime, A. S. Batsanov, M. Botta, J. A. K. Howard, M. P. Lowe and D. Parker, *New J. Chem.*, 1999, **23**, 669-670.
7. R. A. Poole, G. Bobba, M. J. Cann, J. C. Frias, D. Parker and R. D. Peacock, *Org. Biomol. Chem.*, 2005, **3**, 1013-1024.
8. L.-O. Palsson, R. Pal, B. S. Murray, D. Parker and A. Beeby, *Dalton Trans.*, 2007, 5726-5734.
9. D. G. Smith, G.-L. Law, B. S. Murray, R. Pal, D. Parker and K.-L. Wong, *Chem. Commun.*, 2011, **47**, 7347-7349.
10. D. Parker, P. K. Senanayake and J. A. G. Williams, *J. Chem. Soc. Perkin Trans. 2*, 1998, 2129-2139.
11. E. J. New, A. Congreve and D. Parker, *Chemical Science*, 2010, **1**, 111-118.
12. A. Khodjakov and C. L. Rieder, *Methods*, 2006, **38**, 2-16.

3. Evaluation of Structural Variation in Monosubstituted DO3A Systems

3.1 Introduction

The 3-azaxanthone series showed that the molar extinction coefficient of an emissive complex could be increased by incorporating multiple chromophores. Within this series however, the form of the Eu^{3+} emission did not meet the specification for a HTRF donor complex defined in *Section 1.5*, which calls for a large $\Delta J = 2$ band, relative to the other emission bands. Enhancing the emission in the $\Delta J = 2$ region (600 – 630 nm) is required to maximise the spectral overlap integral with the designated acceptor moiety, an allophycocyanin dye protein, thereby increasing the FRET efficiency.

Some of the factors which affect the various transitions in the Eu^{3+} spectrum are known. The form of the Eu^{3+} emission spectrum can be assessed as follows: the $\Delta J = 0$ transition is formally forbidden but can gain intensity through J mixing and is sensitive to the symmetry of the complex; the magnetic dipole allowed $\Delta J = 1$ transition is relatively insensitive to the coordination environment and typically consists of two (in C_n symmetry, where $n \neq 1$) or three (lower symmetry complexes) bands; the hypersensitive $\Delta J = 2$ and $\Delta J = 4$ transitions are electric dipole allowed and their intensities are sensitive to the ligand field, particularly the polarisability of the axial donor in a square antiprismatic or twisted square antiprismatic geometry.[1] The sensitivity of the $\Delta J = 2$ band to the polarisability of the axial donor has recently been exploited to probe ratiometrically the concentration of HCO_3^-. This involves displacement of a capping H_2O molecule from a Eu^{3+} complex, causing a 5-fold increase in the relative $\Delta J = 2$ intensity.[2]

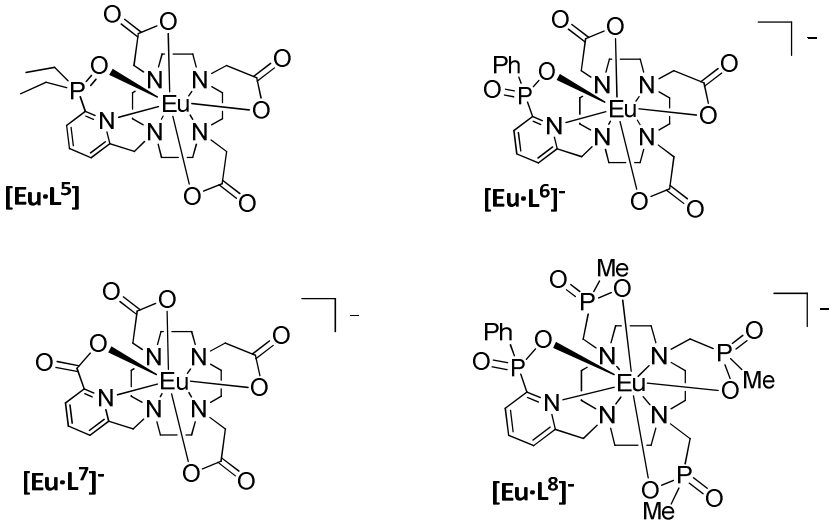

In this chapter, the axial ligand is varied in model [Eu·DO3A] systems, $[Eu{\cdot}L^5]$, $[Eu{\cdot}L^6]^-$ and $[Eu{\cdot}L^7]^-$, to investigate the effect upon the form of the emission spectrum. Having established the moiety that gives the largest $\Delta J = 2$ band, the three carboxylate binding groups are exchanged for methylphosphinate groups ($[Eu{\cdot}L^8]^-$), with a view to enhancing the stability of the emission, with respect to Mn^{2+} quenching.

3.2 Synthetic Aspects

3.2.1 The DO3A Series

The first complex that was synthesised, [Eu·L^5], contains a polarisable phosphonyl group in the axial position of the Eu^{3+} coordination sphere. Synthesis of the phosphonyl moiety was achieved via a one pot, three step process in fairly high yield (*Scheme 3.1*). The commercially available starting material, 2-bromo-6-methylpyridine (***17***) was lithiated with ^{n}BuLi and reacted with chloro-diethyl phosphine before being oxidised to the phosphine oxide by one equivalent of hydrogen peroxide. Purification by column chromatography on silica afforded ***18*** in 70 % overall yield.

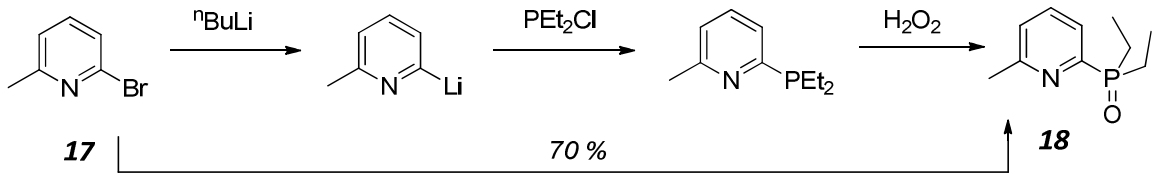

Scheme 3.1

After bromination with N-bromosuccinimide (NBS) and dibenzoyl peroxide, mono-alkylation with the triester DO3A(O^{t}Bu)$_3$ gave the intermediate ***20***. Deprotection of the three *tert*-butoxycarbonyl (BOC) groups of ***20*** with CF_3CO_2H and complexation with Eu(OAc)$_3$ proceeded in high yield (*Scheme 3.2*). The purity of [Eu·L^5] was confirmed by high resolution mass spectrometry (HRMS) and reversed phase-high performance liquid chromatography (RP-HPLC).

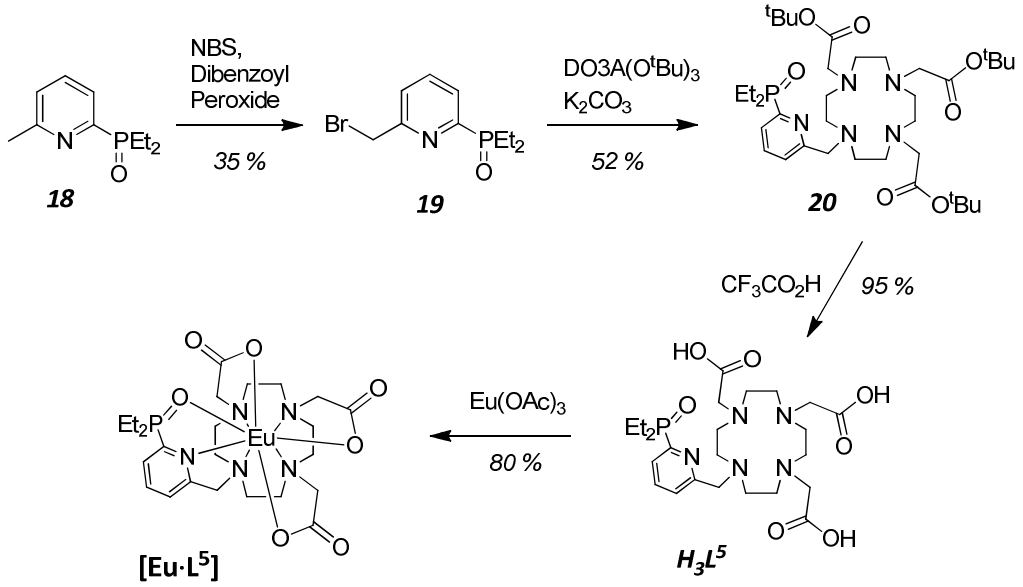

Scheme 3.2

The next synthetic target, $[Eu{\cdot}L^6]^-$, was selected due to the presence of a polarisable phosphinate group in the axial position of the Eu^{3+} coordination sphere. In contrast to $[Eu{\cdot}L^5]$, the axial group is negatively charged, which was expected to increase the stability of the complex and cause a variation in the emissive spectral form. The synthesis of $[Eu{\cdot}L^6]^-$ (*Scheme 3.3*) involved the palladium catalysed cross coupling of 2-bromo-6-methyl pyridine (***17***) with ethyl phenylphosphinate, followed by bromination of the methyl group with NBS and dibenzoyl peroxide. Alkylation with $DO3A(O^tBu)_3$ was followed by deprotection with 6M HCl at 100 °C and complexation with $EuCl_3$, following adjustment of the pH to 5.8. Concentrated HCl was used for deprotection as it cleaves both the three BOC groups and the phosphinate esters. Purification at each step was achieved by column chromatography on silica and the purity of the final complex was confirmed by HRMS and RP-HPLC.

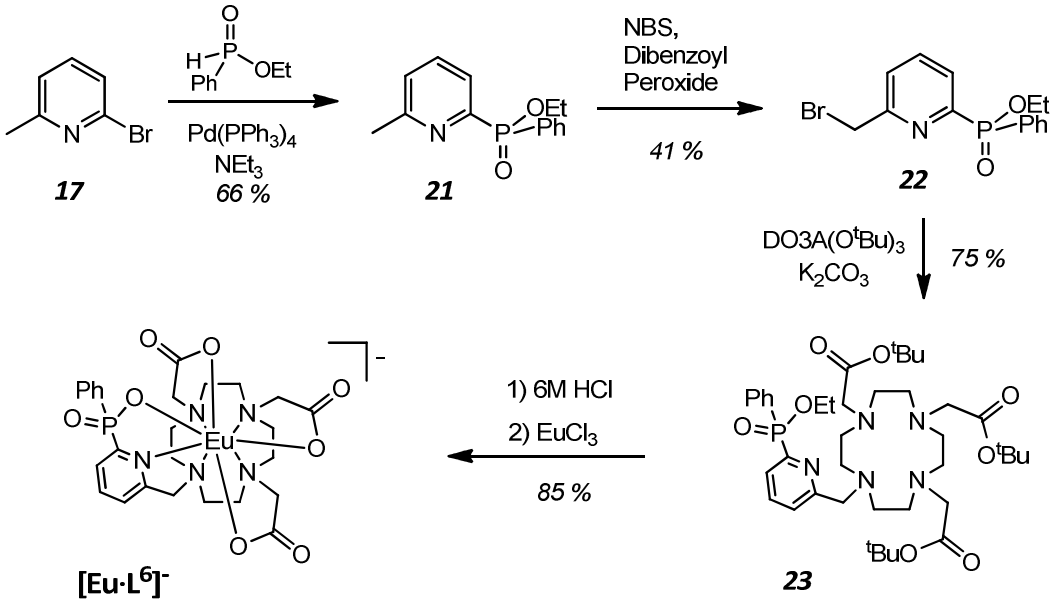

Scheme 3.3

The final complex in the DO3A series is $[Eu{\cdot}L^7]^-$, in which a carboxylate group caps the europium coordination sphere. The picolinate group has been used previously in C_3 symmetric Eu^{3+} complexes (see $[Eu{\cdot}L^{1.6}]$ in *Section 1.3.3*),[3] giving a Eu^{3+} spectrum with a large relative $\Delta J = 2$ band. Bromination of the commercially available material ***24*** using NBS was followed by reaction with $DO3A(O^tBu)_3$ (*Scheme 3.4*). Protecting group removal and complexation with $EuCl_3$ led to the target complex in high yield. Deprotection was achieved in two steps: removal of the O^tBu groups with CF_3CO_2H followed by base hydrolysis with aqueous NaOH (1 M). Both steps were carried out at room temperature. Single step deprotection with 6M HCl at 100 °C (deprotection conditions for $[Eu{\cdot}L^6]^-$) was ruled out due to the possibility of decarboxylation of the acid group in the position alpha to the pyridyl N, as has previously been observed using acidic conditions and high temperatures.[4]

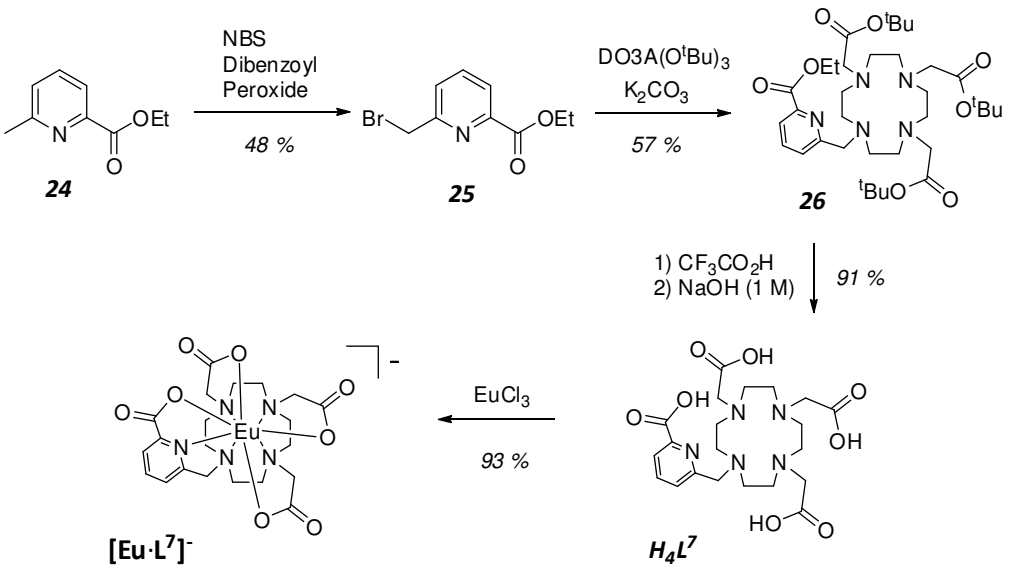

Scheme 3.4

During the course of these studies, Figueroa *et. al.* reported the synthesis and lanthanide coordination chemistry properties of ***L***^{7}.[5] Their work included a DFT calculation for [Gd·L^{7}]$^{-}$, revealing a favoured mono-capped square antiprismatic structure with the carbonyl oxygen occupying the axial site (*Figure 3.1*). In contrast, the related complex [Gd·L^{7b}] exists as two diastereomers in solution in a 2 : 1 ratio.[6] In this complex, the axial donating ligand is a solvent molecule, due to the absence of the pyridyl carboxylate. The reduction in steric demand about the Ln^{3+} centre may be responsible for the presence of the two observed diastereomers.

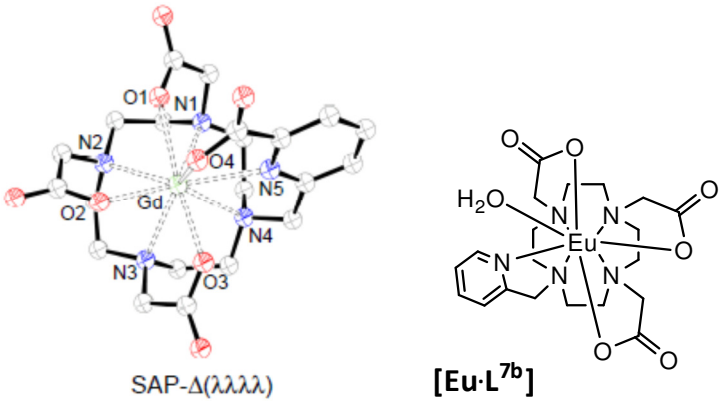

Figure 3.1 Calculated DFT structure of [Gd·L^{7}], showing the carbonyl oxygen (O4) in the axial position of the square antiprismatic geometry.[5]

3.2.2 Methylphosphinate Complex

It was determined that of the three complexes in the DO3A series, $[Eu{\cdot}L^6]^-$ gave the best Eu^{3+} spectral form. In an attempt to improve the stability of this complex, three methyl phosphinate groups were chosen to replace the three carboxylate groups of DO3A. The synthesis of $[Eu{\cdot}L^8]^-$ (*Scheme 3.5*) required mono-substitution of 1,4,7,10-tetraazacyclododecane (cyclen) with the pyridylphenylphosphinate moiety, ***22***. This was achieved using cyclen with three nitrogens protected with BOC groups. After alkylation in MeCN with K_2CO_3, the BOC groups were removed from ***27*** with CF_3CO_2H. Following addition of the three methyl phosphinate groups using $MeP(OEt)_2$ and paraformaldehyde in THF, each phosphinate esters group was hydrolysed in aqueous HCl (6 M). After pH adjustment, complexation was achieved with $EuCl_3$ to give the target complex, $[Eu{\cdot}L^8]^-$.

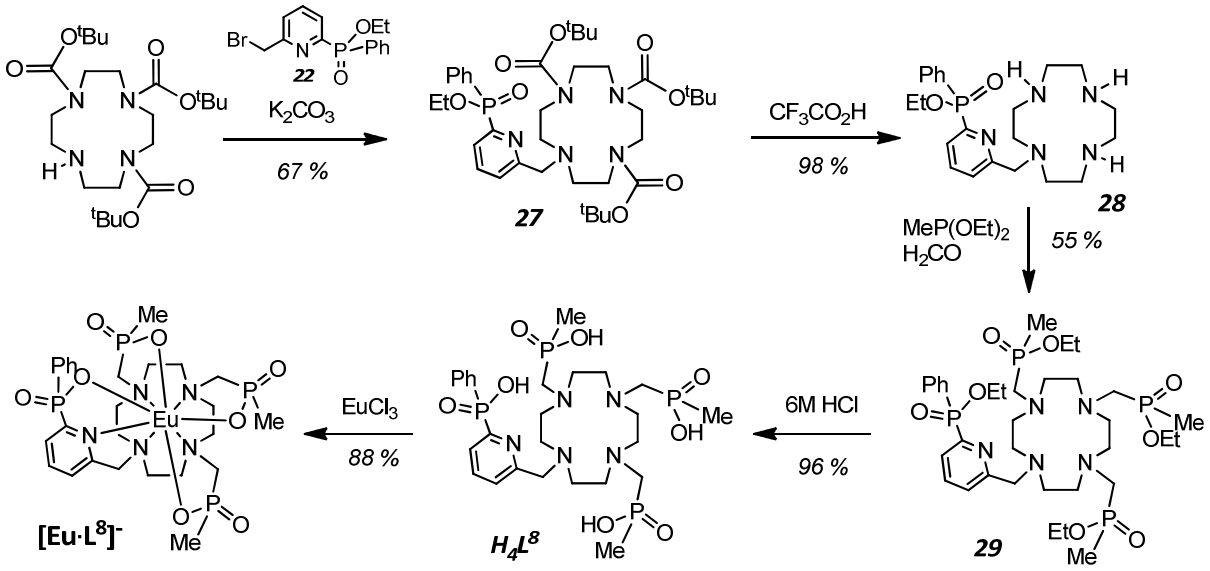

Scheme 3.5

3.3 Photophysical Properties of [Eu·L^5], [Eu·L^6]$^-$ and [Eu·L^7]$^-$

3.3.1 Emission Spectra and Excited State Lifetimes

The absorption spectra of the complexes in the DO3A series each have a maximum absorption wavelengths around 275 nm (*Figure 3.2 inserts*), typical of a pyridyl π-π* transition. An absorption wavelength in this region does not meet the specification in *Section 1.5*. However, the pyridyl moiety can form the basis of a number of chromophores with longer wavelength absorption maxima and therefore serves as a good model at this stage. The pyridyl moiety is also useful, as it is able to populate the europium excited state after excitation at 275 nm, allowing the study of the emission spectra of the various complexes.

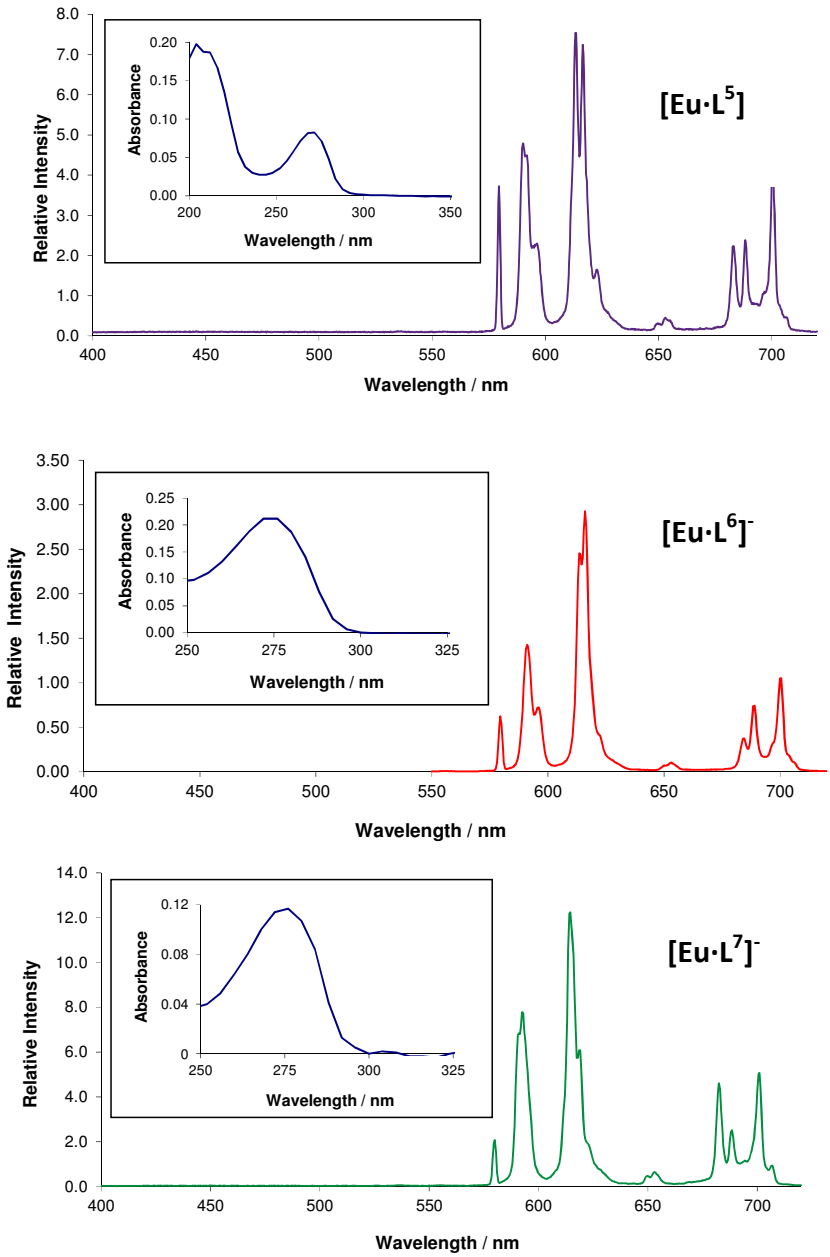

Figure 3.2 Absorption (*insert*) and emission spectra for the three complexes, [Eu·L^5], [Eu·L^6]$^-$ and [Eu·L^7]$^-$. All spectra recorded in H_2O (λ_{ex} = 275 nm, 20 μM, pH 5.8, 295 K).

The Eu^{3+} emission spectra of $[Eu{\cdot}L^5]$, $[Eu{\cdot}L^6]^-$ and $[Eu{\cdot}L^7]^-$ were recorded in H_2O (λ_{ex} = 275 nm, 20 μM, pH 5.8, 295 K) (*Figure 3.2*). No fluorescence is seen in the region 400 – 550 nm, demonstrating the efficiency of Eu^{3+} sensitisation by the pyridyl groups. In each case, it is clear that the $\Delta J = 2$ band is the most intense transition. To allow visual comparison, the three spectra have been overlaid along with that of $[Eu{\cdot}L^{1.1}]^{3+}$, which is the complex currently used as a donor in the HTRF experiment (*Figure 3.3*). The first striking feature is the difference in spectral form between $[Eu{\cdot}L^{1.1}]^{3+}$ and the three new complexes. In particular, the $\Delta J = 2$ band varies from the former, in which two distinct bands appear (605 and 620 nm), to the latter, which each have single emission bands centred at 615 nm. This may be originating from the solvation conditions of the complexes. The $[Eu{\cdot}L^{1.1}]^{3+}$ spectrum was recorded in 0.4 M KF, which is required to expel H_2O from within the tris(bipyridine) cavity, thereby increasing the quantum yield. The new series of complexes are all 9 coordinate $q = 0$ systems and have an advantage over $[Eu{\cdot}L^{1.1}]^{3+}$ in requiring no such additive.

Table 3.1 Photophysical data for the three DO3A complexes and two reference compounds, $[Eu{\cdot}L^1(H_2O)]$ and the tris(bipyridine) complex $[Eu{\cdot}L^{1.1}]^{3+}$. The data for complex $[Eu{\cdot}L^8]^-$ is also shown. All measurements in H_2O (20 μM, pH 5.8, 295 K) [a]Values recorded in 0.4 M KF.

Complex	λ_{ex} / nm	τ (H_2O) / ms	q	Intensity Ratios	
				$\Delta J = 2 / \Delta J = 1$	$\Delta J = 2 / \Delta J = 4$
[a][Eu·L$^{1.1}$]$^{3+}$	303	0.34	0.0	1.40	1.30
[Eu·L^1(H$_2$O)]	328	0.60	1.1	1.13	1.14
[Eu·L^5]	272	1.21	0.0	1.74	1.73
[Eu·L^6]$^-$	272	1.27	0.0	2.14	2.40
[Eu·L^7]$^-$	276	1.14	0.1	1.66	1.62
[Eu·L^8]$^-$	272	0.95	0.0	3.02	5.10

Comparing the emission spectra of the three new complexes (*Figure 3.3*), it is apparent that the species with the highest emission intensity in the $\Delta J = 2$ manifold is $[Eu{\cdot}L^6]^-$. To quantify this observation, integrated intensity ratios $\Delta J = 2 : \Delta J = 1$ and $\Delta J = 2 : \Delta J = 4$ were calculated (*Table 3.1*). The values for the 3-azaxanthone complex $[Eu{\cdot}L^1(H_2O)]$, which is based on the DO3A ligand, have also been included in *Table 3.1*. By comparing the intensity ratios for $[Eu{\cdot}L^1(H_2O)]$ (1.13 and 1.14) with those of $[Eu{\cdot}L^5]$ (1.74 and 1.73) and $[Eu{\cdot}L^7]^-$ (1.66 and 1.62), it can be concluded that exchanging a H_2O molecule in the capping axial position of a twisted square antiprismatic complex for a more polarisable group leads to an increase in the relative intensity of the $\Delta J = 2$ transition. In comparison with $[Eu{\cdot}L^1(H_2O)]$ and $[Eu{\cdot}L^{1.1}]^{3+}$, each of the synthesised complexes have improved intensity ratios, with $[Eu{\cdot}L^6]^-$ showing the highest values of 2.14 and 2.40. Data from *Table 3.1* also show the correlation between the q value and the Eu^{3+} excited state lifetime in water, τ. Those complexes which are $q = 0$ have comparable lifetimes around 1.2 ms, whereas $[Eu{\cdot}L^1(H_2O)]$, which is $q = 1$, has a lifetime of around half this value, due to the vibrational quenching of inner sphere H_2O molecules.

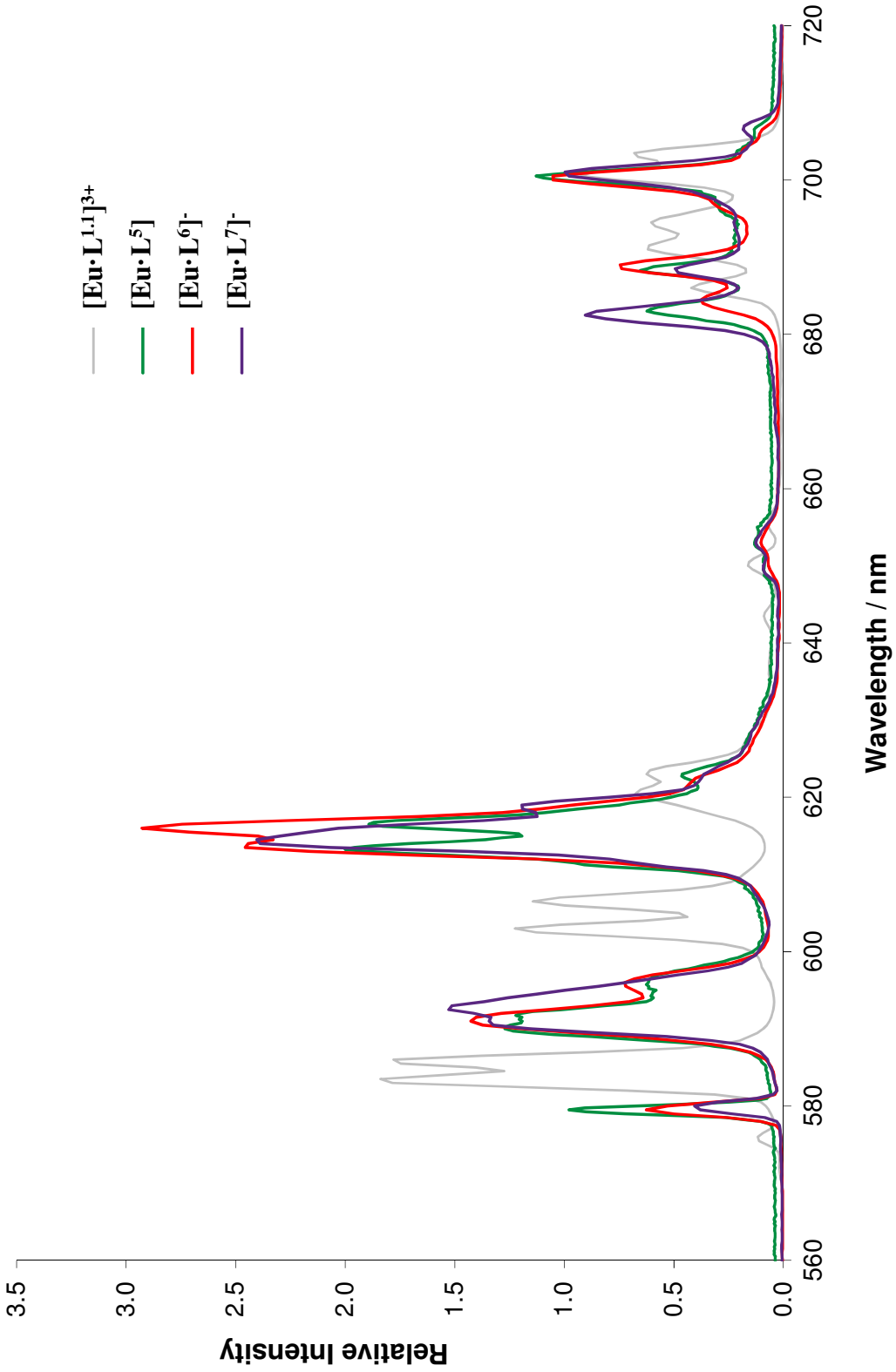

Figure 3.3 Comparison of the emission spectra of [Eu·L^{5}] (*purple*), [Eu·L^{6}]$^{-}$ (*red*) and [Eu·L^{7}]$^{-}$ (*green*). The emission spectrum of the tris(bipyridine) complex [Eu·L$^{1.1}$]$^{3+}$ (*grey*) is also shown. All spectra recorded in H_2O (20 μM complex, pH 5.8, 295 K) except [Eu·L$^{1.1}$]$^{3+}$ which also contains 0.4 M KF. Spectra have been scaled so that the total integrated intensity is equal for each spectrum.

3.3.2 Emission Stability

Another important feature of the current series to consider and compare is the emissive stability of the complexes. This is assessed by measuring the emission intensity at a given wavelength in the presence of the same potential inhibitors used in the stability studies of the 3-azaxanthone complexes in *Section 2.4.3*. Inhibitors include several cations, $EDTA^{4-}$ and two proteins (*Figure 3.4*). From the data, it is apparent that displacement of the Eu^{3+} ion by Ca^{2+} or Mg^{2+} does not occur. In contrast to the 3-azaxanthone complexes, extraction of Eu^{3+} by the competitive ligand $EDTA^{4-}$ is negligible, even after 18 h. This demonstrates the increased kinetic stability of the complexes with 9 coordinate charged ligands compared to, say, the 8 coordinate uncharged ligand in the complex, $[Eu{\cdot}L^4]^{3+}$. As for the 3-azaxanthone complexes, the inhibitor which caused the greatest reduction in emission intensity was Mn^{2+}. In the cases of $[Eu{\cdot}L^6]^-$ and $[Eu{\cdot}L^7]^-$ the emission is completely absent. Displacement of the europium ion seems unlikely and a more rational explanation would be that the emission is quenched at some point along the sensitised emission pathway. Studies reported in *Chapter 6* examine this quenching mechanism in more detail. The two proteins which were tested led to a reduction in the Eu^{3+} emission, and to the same extent with each complex. The most likely explanation is that amino acids containing aromatic moieties (Tyr, Trp, Phe), which have similar absorption spectra to the Eu^{3+} complexes, are absorbing some of the excitation light source, leading to an overall reduction in the number of complexes emitting light. Upon moving to Eu^{3+} complexes with chromophores which absorb light above 300 nm, this effect should no longer be observed.

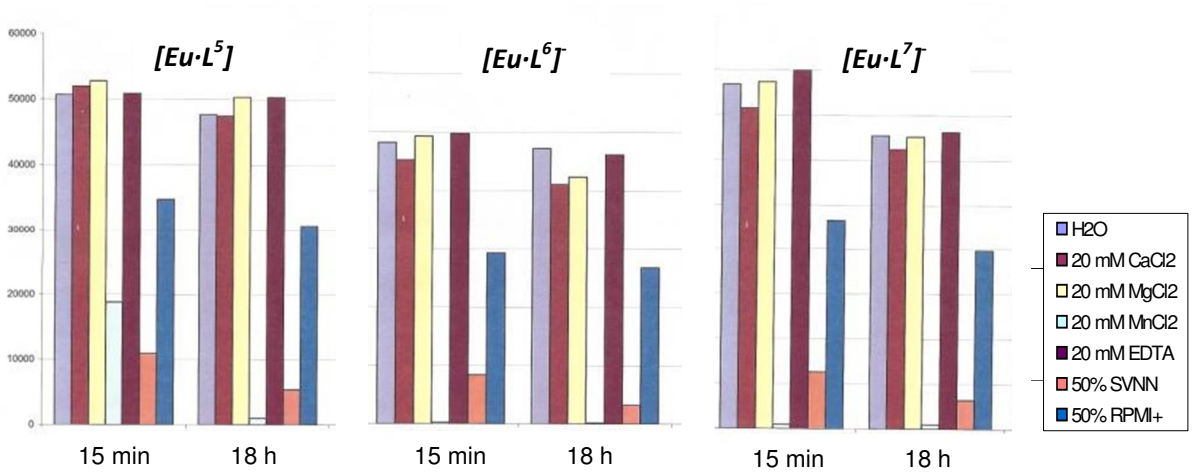

Figure 3.4 Stability data for $[EuL^5]$ (*left*), $[EuL^6]^-$ (*centre*) and $[EuL^7]^-$ (*right*) in HEPES buffer at two time points, 15 min and 18 h (10nM complex, λ_{ex} = 335 nm, λ_{ex} = 620 nm).

3.4 Comparative Analysis with the $[Eu{\cdot}L^8]^-$

3.4.1 Photophysical Properties

From the study of the DO3A series, it was determined that the pyridylphenylphosphinate moiety (***21***) should be used in further complexes, as it leads to the most favourable Eu^{3+} emission spectrum. The complex $[Eu{\cdot}L^6]^-$, however, suffers from severe quenching of emission by Mn^{2+} ions. In an attempt to improve the emissive stability of the complex, $[Eu{\cdot}L^8]^-$ was synthesised. In this system, the three carboxylate groups of the DO3A complex are exchanged for methylphosphinate groups. The advantages of phosphinate groups were discussed in *Section 1.3.3* and include: the formation of complexes with greater stability, due to increased steric bulk about the Ln^{3+} centre; the introduction of stereogenic P centres, which may result in differential interaction with chiral species and the pentavalency of the P centre, leading to an R group (in this case Me) which can be varied to introduce function or variation in properties.

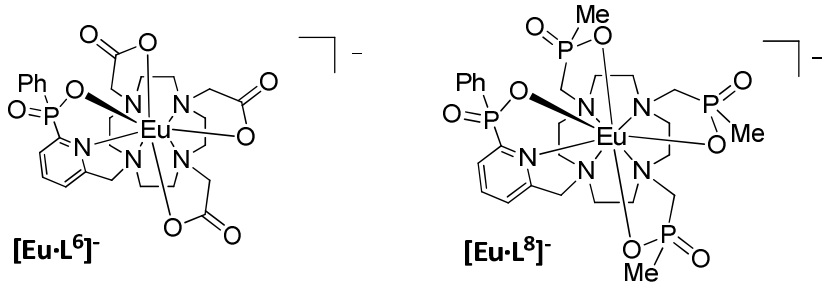

The photophysical data for $[Eu{\cdot}L^8]^-$ were included in *Table 3.1*. As expected, the 9 coordinate complex has no coordinated H_2O and has a luminescence lifetime around 1 ms. The absorption profile is unchanged from the $[Eu{\cdot}L^6]^-$ analogue, with a pyridyl absorption maximum at 272 nm. The main photophysical difference between the two complexes is in their emission spectra (*Figure 3.5*). Firstly, an increase in splitting of the $\Delta J = 2$ band upon moving from the carboxylate to the methylphosphinate coordinating arms is observed. The intensity ratio of the $\Delta J = 2 : \Delta J = 1$ bands also shows a significant increase from 2.14 to 3.02. The $\Delta J = 2 : \Delta J = 4$ ratio has also increased from 2.40 to 5.10. These large improvements in emission spectral form cannot be arising from the polarisability of the axial donor as it is the same in each case. Instead, the change in spectral form must arise from a change in the Eu^{3+} coordination geometry.

DO3A complexes are known to adopt a mono-capped square antiprismatic or twisted square antiprismatic geometry and form two pairs of enantiomeric diastereomers.[6, 7] The added complexity in the $\Delta J = 2$ and $\Delta J = 4$ region of the $[Eu{\cdot}L^8]^-$ spectrum suggest strongly that the symmetry about the Eu^{3+} centre is different. Whilst 9 coordinate systems based upon cyclen-tri(phosphinate) ligands (such as $[Eu{\cdot}L^8]^-$) have not been well characterised, the related tetra(phosphinate) system have been investigated in detail.[8, 9] The tetra(methylphosphinate) and tetra(benzylphosphinate) complexes give rise to a possible 24 isomers based upon being *R* or *S* at each P, the two ring conformations (δδδδ or λλλλ) and the helicity (Δ or Λ). In these systems, one major (> 90 %) diastereomer is present in solution – enantiomers of a twisted square antiprism. The tetra(phenylphosphinate) analogue exists as

a mixture of stereoisomers, as a result of being less sterically demanding. Upon exchanging one of the phosphinate arms in the tetra(methylphosphinate) complex for an alternative group (such as a carboxamide), the number of possible isomers increases to 32 – 16 enantiomeric pairs if the alternative group is achiral.[10] If this group is also chiral, then each isomer becomes diastereomeric. In this situation, the number of isomers in solution increases to 64 – 32 pairs of enantiomers.[11] Despite the many possible isomers, one major species is often observed for tri- and tetra(phosphinate) lanthanide complexes.[10] In accord with this observation, the ^{31}P-NMR spectrum of $[Eu{\cdot}L^{8}]^{-}$, which contains three resonances, suggests that, despite the possible 64 isomeric structures due to the presence of three methyl phosphinate groups and one phenyl phosphinate group, a single major isomer exists in solution.

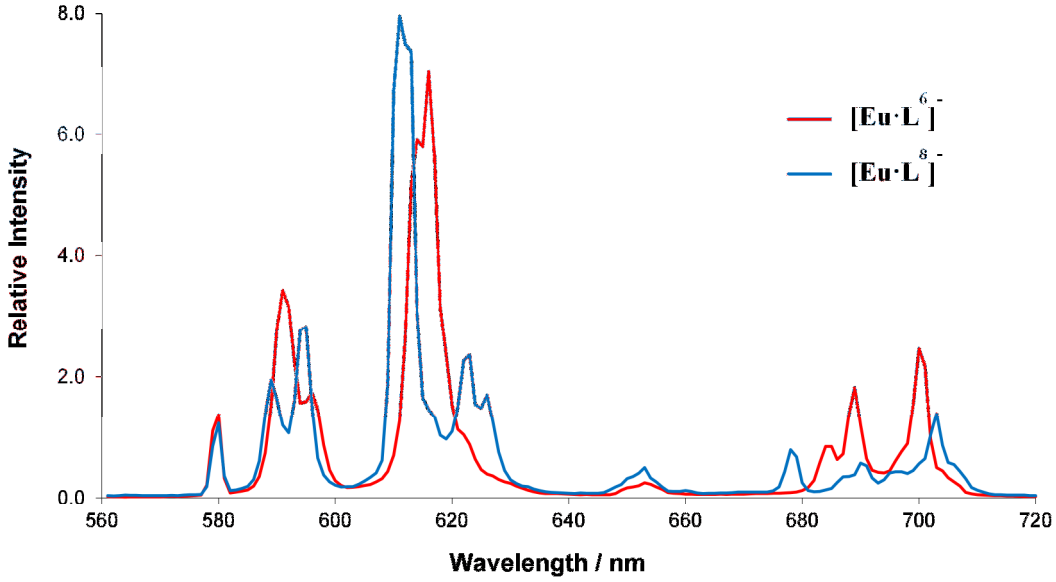

Figure 3.5 Emission spectra of $[Eu{\cdot}L^{6}]^{-}$ (red) and $[Eu{\cdot}L^{8}]^{-}$ (blue) in H_2O (20 μM complex, pH 5.8, 295 K). Spectra have been scaled so that the total integrated intensity is equal for each spectrum.

3.4.2 Emissive Stability

Stability assays were carried out comparing the behaviour of $[Eu{\cdot}L^{6}]^{-}$ and $[Eu{\cdot}L^{8}]^{-}$, in the manner previously described. As expected, the presence of the methylphoshinate groups in place of the carboxylate groups reduces the quenching of emission by Mn^{2+}, due to an increase in the steric bulk about the Eu^{3+} centre (*Figure 3.6*). The emission from $[Eu{\cdot}L^{6}]^{-}$ was entirely quenched by Mn^{2+}, whereas the methylphosphinate analogue remained 50 % emissive, compared to a solution with no inhibitor. This result suggests that the Mn^{2+} quenching process involves some kind of encounter between the Mn^{2+} ion (or $Mn(H_2O)_6^{2+}$ as it is likely exist in solution) and the Eu^{3+} complex, and is dependent upon the proximity of the two species. It can therefore be tentatively proposed that the quenching mechanism involves the Eu^{3+} excited state, rather than an excited state of the sensitising group, which is equally accessible to Mn^{2+} in both the $[Eu{\cdot}L^{6}]^{-}$ and $[Eu{\cdot}L^{8}]^{-}$ complexes. Aside from Mn^{2+}, all other inhibitors added to $[Eu{\cdot}L^{8}]^{-}$ caused the same response as in the assay with $[Eu{\cdot}L^{6}]^{-}$ - only protein led to a reduction in emission, mostly due to competitive absorption.

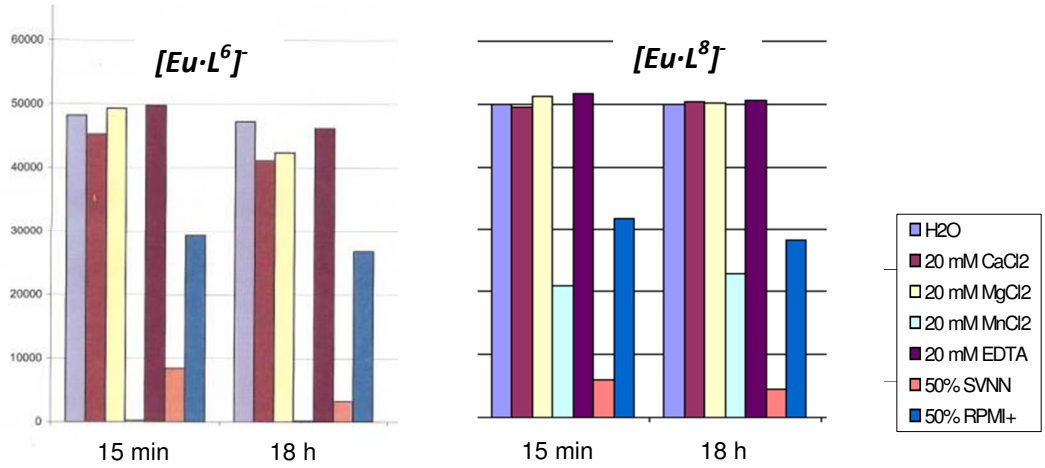

Figure 3.6 Stability data for $[EuL^{6}]^{-}$ (*left*) and $[EuL^{8}]^{-}$ (*right*) in HEPES buffer or at two time points, 15 min and 18 h (10nM complex, λ_{ex} = 335 nm, λ_{ex} = 620 nm).

3.5 Conclusions

This brief study of three Eu^{3+} complexes based upon the DO3A core structure was designed to investigate the effect upon the emission spectrum of varying the axial donating group in the monocapped twisted square antiprismatic geometry. The specification set out in *Section 1.5* calls for a large ΔJ = 2 band to maximise the spectral overlap integral with the absorption spectrum of the designated accepted moiety in the HTRF experiment. The theory that preceded this study was that an increase in the polarisability of the axial donor leads to an increase in the relative intensity of the electric-dipole allowed ΔJ = 2 transition. This was indeed found to be the case, with each of the three complexes displaying a larger ΔJ = 2 band than $[Eu{\cdot}L^{1}(H_2O)]$, which has a water molecule in the axial position.

Of the three new complexes, $[Eu{\cdot}L^{6}]^{-}$ gave the ΔJ = 2 emission band with the highest relative intensity. This complex contains a pyridylphenylphosphinate moiety, with the phosphinate O occupying the axial position in the Eu^{3+} coordination sphere. One of the other benefits of $[Eu{\cdot}L^{6}]^{-}$ is that the phosphinate group is negatively charged and therefore forms a highly kinetically stable complex, which was found to be resistant to dissociation by Ca^{2+}, Mg^{2+} and $EDTA^{4-}$. The presence of protein was found to reduce the observed emission. This is thought to be due to the presence of aromatic chromophores (Phe, Tyr, Trp), which absorb at a similar wavelength to the pyridyl group in $[Eu{\cdot}L^{6}]^{-}$. This pyridyl group could be extended in future complexes to form a sensitising group with a higher absorption wavelength maximum. In the stability assays, as with the 3-azaxanthone complexes in *Chapter 2*, Mn^{2+} was found to be the species leading to the greatest reduction in emission. In the case of $[Eu{\cdot}L^{6}]^{-}$, the emission is completely quenched. Overall, however, the pyridyl phenylphosphinate moiety has led to favourable emissive properties and is worthy of consideration for further development.

With the desire to increase the stability of $[Eu{\cdot}L^6]^-$ towards quenching by Mn^{2+}, the tri(methylphosphinate) complex, $[Eu{\cdot}L^8]^-$ was synthesised. This complex had an increased stability towards Mn^{2+} quenching and also gave an emission spectrum with an even larger $\Delta J = 2$ emission band than $[Eu{\cdot}L^6]^-$. Notwithstanding the improved stability, addition of Mn^{2+} was only found to reduce the emission of $[Eu{\cdot}L^8]^-$ to around 50 % of the value in the absence of Mn^{2+}. To improve the stability further, variation of the alkyl group would be a next logical step. Lanthanide complexes containing benzylphosphinates and phenylphosphinates are known, and may lead to greater resistance to quenching. These complexes were not considered, however, as it was at this stage in the project that the C_3 symmetric complexes based on triazacyclononane were synthesised. These complexes showed a much higher stability towards quenching by Mn^{2+}, and are the subject of the next chapter.

3.6 References

1. D. Parker, *Chem. Soc. Rev.*, 2004, **33**, 156-165.
2. D. G. Smith, G.-L. Law, B. S. Murray, R. Pal, D. Parker and K.-L. Wong, *Chem. Commun.*, 2011, **47**, 7347-7349.
3. G. Nocton, A. Nonat, C. Gateau and M. Mazzanti, *Helv. Chim. Acta*, 2009, **92**, 2257-2273.
4. R. J. Moser and E. V. Brown, *J. Org. Chem.*, 1972, **37**, 3938-3941.
5. M. Regueiro-Figueroa, B. Bensenane, E. Ruscsak, D. Esteban-Gomez, L. J. Charbonniere, G. Tircso, I. Toth, A. de Blas, T. Rodriguez-Blas and C. Platas-Iglesias, *Inorg. Chem.*, 2011, **50**, 4125-4141.
6. S. Aime, A. S. Batsanov, M. Botta, J. A. K. Howard, M. P. Lowe and D. Parker, *New J. Chem.*, 1999, **23**, 669-670.
7. P. Caravan, J. J. Ellison, T. J. McMurry and R. B. Lauffer, *Chem. Rev.*, 1999, **99**, 2293-2352.
8. D. Parker, R. S. Dickins, H. Puschmann, C. Crossland and J. A. K. Howard, *Chem. Rev.*, 2002, **102**, 1977-2010.
9. S. Aime, A. S. Batsanov, M. Botta, J. A. K. Howard, D. Parker, K. Senanayake and G. Williams, *Inorg. Chem.*, 1994, **33**, 4696-4706.
10. S. Aime, M. Botta, D. Parker and J. A. G. Williams, *J. Chem. Soc. Dalton Trans.*, 1995, 2259-2266.
11. S. Aime, M. Botta, R. S. Dickins, C. L. Maupin, D. Parker, J. P. Riehl and J. A. G. Williams, *J. Chem. Soc. Dalton Trans.*, 1998, 881-892.

4. An Isostructural Series of C_3-Symmetric Lanthanide Complexes

4.1 Introduction

The theme of the previous chapter was to investigate the effect of the donor groups in the Eu^{3+} coordination sphere upon the form of the emission spectrum. In accordance with previous reports,[1] it was found that an increase in the polarisability of the axial donor in a capped square antiprismatic geometry led to an increase in the relative intensity of the electric-dipole allowed $\Delta J = 2$ transition. The group which gave the largest relative $\Delta J = 2$ transition was the pyridyl phenylphosphinate group (***21***). Another factor which is believed to influence the form of the europium emission spectrum is the symmetry about the metal ion centre. In general, a high degree of symmetry leads to an emission spectrum with less complexity in the splitting of each manifold. For example, in pure C_2 and C_3 symmetry, the $\Delta J = 1$ manifold has two allowed transitions.[2] In systems with a lower degree of symmetry, this manifold can have up to three transitions. It is also found that complexes in the same symmetry point group have, to a first approximation, the same number of transitions within each manifold.

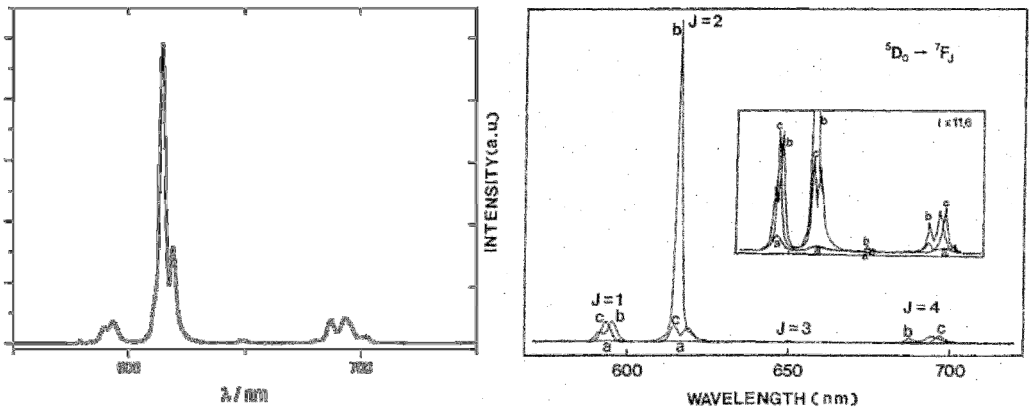

Figure 4.1 Emission spectra of aqueous solutions of *left*) $[Eu\cdot(L^{1.21})_3]^{3-}$ (λ_{ex} = 340 nm),[3] and *right*) a) $Eu(H_2O)_9$, b) $[Eu(DPA)_3]^{3-}$ and c) $[Eu(ODA)_3]^{3-}$ (λ_{ex} = 395 nm in each case).[4]

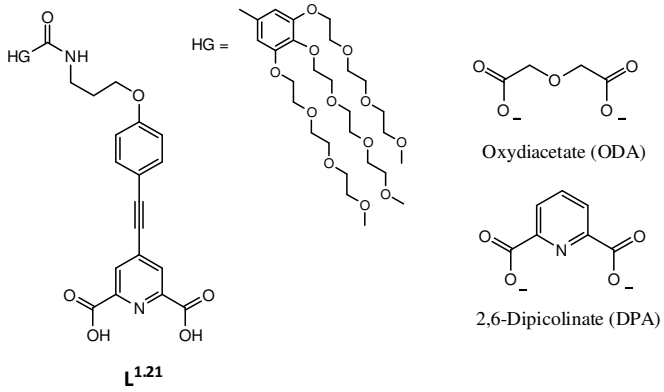

$L^{1.21}$

The dependence of the Eu^{3+} emission spectrum upon the symmetry about the central metal ion is demonstrated by comparison of the emission spectra of $[Eu\cdot(L^{1.21})_3]^{3-}$ (*Figure 4.1 left*) and

$[Eu{\cdot}(DPA)_3]^{3-}$ (*Figure 4.1 right, b*). Both complexes are in the D_3 point group. In each case, the charged oxygen donors form a slightly distorted trigonal prism about the Eu^{3+} centre, with the pyridyl N donor lying in the D_3 horizontal plane, capping each rectangular face.[5] The emission spectra of the structurally related complexes are very similar, with a large relative $\Delta J = 2$ band and very similar emission in the $\Delta J = 1$ region.

The emission spectrum of $[Eu{\cdot}(ODA)_3]^{3-}$ (*Figure 4.1 right c*) shows that symmetry about the Eu^{3+} centre is not the only factor affecting the form of the emission spectrum. This complex is also in the D_3 point groups but the form of the emission spectrum is quite different. The $\Delta J = 2 : \Delta J = 1$ integrated intensity ratio is far less than that of $[Eu(DPA)_3]^{3-}$ (1.3 vs. 4.2) and additional splitting is observed in the $\Delta J = 2$ manifold. In this instance, it is the variation in the polarisability of the donor groups which causes the observed difference in spectral form.

A further example is the complex $[Eu{\cdot}L^{1.6}]$, structurally defined by Mazzanti,[6] which was introduced in *Section1.3.3*. This is a C_3 symmetric complex with a 1,4,7-triazacyclononane macrocycle and three picolinate groups. As with the complexes shown in *Figure 4.1*, the structure is a distorted tricapped trigonal prism and the resulting emission spectrum has a large relative $\Delta J = 2$ transition (*Figure 4.2*).

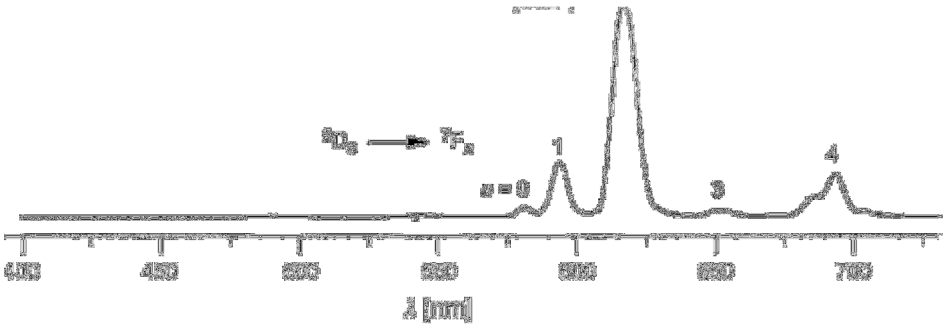

Figure 4.2 Emission spectrum of $[Eu{\cdot}L^{1.6}]$ (H_2O, 295 K, λ_{ex} = 275 nm).[6]

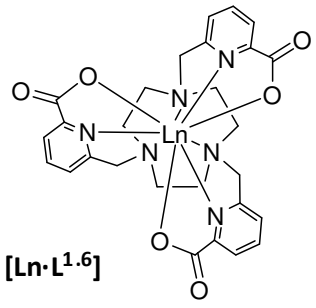

[Ln·L$^{1.6}$]

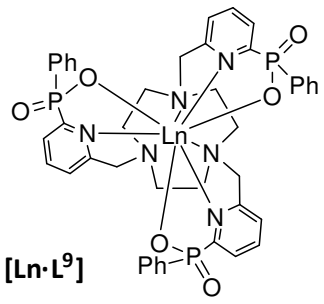

[Ln·L^{9}]

From the examples given above, it is apparent that complexes of D_3 or C_3 symmetry, with pyridyl donating groups lead to emission spectra with large relative $\Delta J = 2$ bands. This is one of the specifications set out in *Section 1.5* and, as a result, the complex $[Eu{\cdot}L^9]$ was a logical next target in the course of this project. In contrast to complexes $[Eu{\cdot}L^1]$ to $[Eu{\cdot}L^8]^-$, the core macrocycle is 1,4,7-triazacyclononane. By incorporating three of the pyridyl phenylphosphinate groups, the overall ligand provides 9 donating groups and forms a structure which should be C_3 symmetric and was anticipated to give a favourable emission spectrum. Having synthesised $[Eu{\cdot}L^9]$, which was found to have some

interesting properties, it was decided that the full lanthanide series from Ce^{3+} to Yb^{3+} should be made. With twelve complexes in hand, any trends which may exist across the series could be investigated. The yttrium complex, [Y·L^9], was also synthesised. The Y ion is triply charged and is of similar size to Ho^{3+} in nine-coordinate systems (104 pm).[7] In contrast to the lanthanides, Y^{3+} is diamagnetic and [Y·L^9] provides a useful complex for comparative NMR studies.

4.2 Synthetic Aspects

The synthesis of each complex in the [Ln·L^9] series was achieved in five steps with an average overall yield of 14 % (*Scheme 4.1*). The first two steps had previously been carried out for the synthesis of [Eu·L^6]$^-$. Three equivalents of the brominated precursor ***22*** were reacted with the free base of 1,4,7-triazacyclononane, which had been liberated from its hydrochloride salt by extraction into CH_2Cl_2, after the salt had been dissolved in aqueous NaOH (1M). The alkylation reaction was carried out in CH_3CN at 50 °C and was monitored by LCMS, which revealed the formation of mono-, di- and tri-substituted products. After 3 hours, the trisubstituted product ***30*** was the major product and was isolated in 62 % yield. If the reaction temperature was increased to 80 °C, the tetra-substituted cationic product was formed. This made separation of ***22*** more challenging, as each compound has a similar R_f value (silica, CH_2Cl_2 : 10 % CH_3OH). Following purification of the ligand ***30***, hydrolysis of the ethyl phosphinate esters with aqueous HCl (6 M) and complexation with $LnCl_3$ were carried out in high yield. Use of LCMS confirmed the consumption of all starting ligand, ***H_3L^9***.

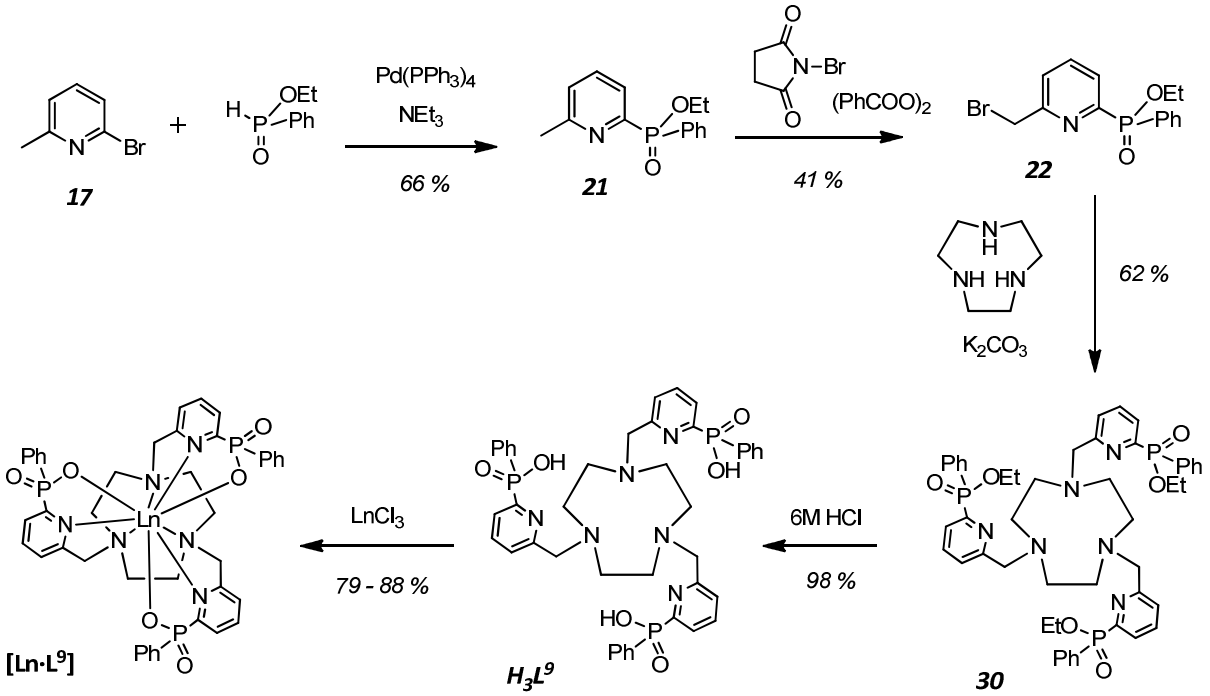

Scheme 4.1

Each complex in the [Ln·L^9] series was purified by short-path column chromatography on silica. Hydrophilic, charged Eu^{3+} complexes are usually too polar to allow purification on silica. The neutral [Ln·L^9] complexes incorporate three hydrophobic phenyl groups, and were mobile on the silica solid phase, using a solution phase comprising CH_2Cl_2, CH_3OH and aqueous ammonia solution (35 % by weight) in a 80 : 20 : 1 ratio. The purity of each complex was confirmed by HRMS and RP-HPLC (a representative trace is shown in *Figure 4.3*).

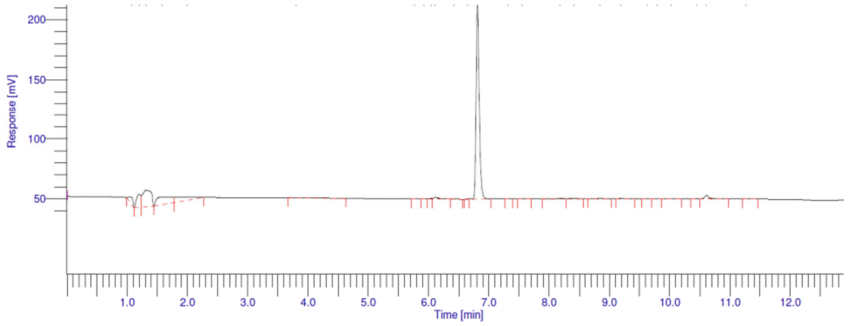

Figure 4.3 A representative RP-HPLC trace of [Ln·L^9], using a gradient elution method (see *Appendix 1*).

4.3 Structure Elucidation

4.3.1 Solid State Structure

The [Ln·L^9] complexes were found to be soluble in CH_3OH but only sparingly soluble in H_2O. As a result, single crystals of each complex were grown by dissolving around 10 mg of complex in CH_3OH (1 mL) and adding H_2O (0.5 mL). Crystals grew within 16 h upon standing at room temperature. The ability to grow single crystals allowed the determination of the solid state structure of [Ln·L^9] by X-ray diffraction methods. Crystals were grown of all thirteen complexes ([Ce·L^9] – [Yb·L^9] and [Y·L^9]). Seven of the structures were solved, including the Ce^{3+} and Yb^{3+} complexes, which have the largest and smallest ionic radii, respectively.

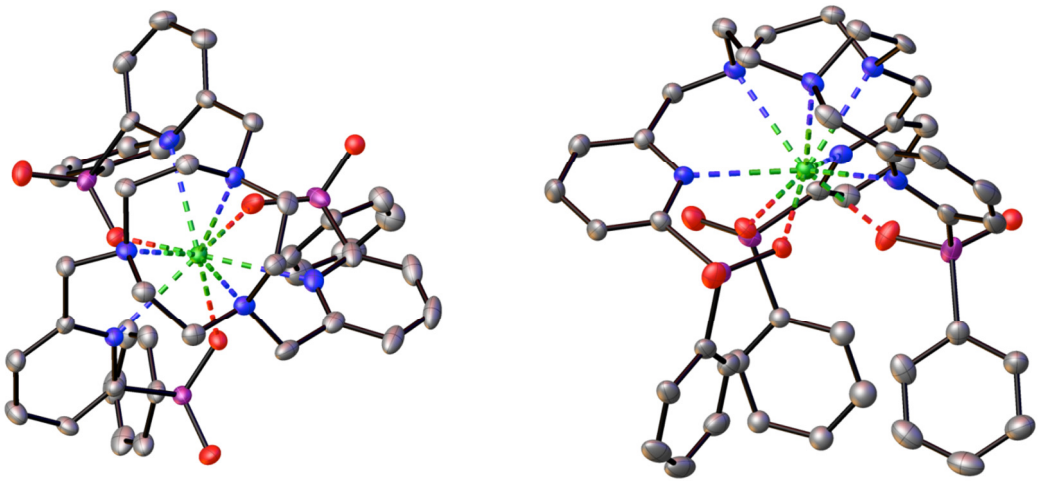

Figure 4.4 Crystal structure of [Eu·L^9] viewed *left*) down the *z* axis, showing the C_3 symmetry and *right*) from the side, showing the three phenyl groups below the plane of the complex. The atoms shown are C (grey), N (blue), O (red), P (purple) and Eu (green).

The first structure solved was [Eu·L^9]. The complex was found to crystallise in the space group $P2_1/n$, with 4 complexes in each monoclinic unit cell. In the solid state, the complex has pseudo-C_3 symmetry, which can be seen by looking down the z axis (*Figure 4.4 left*). The ligand has nine atoms bound to the Eu^{3+} centre in a slightly distorted tricapped trigonal prismatic geometry. The three ring N atoms and the three phosphinate O atoms make up the trigonal prism, with the three pyridyl N atoms capping each rectangular face. The Eu^{3+} ion lies in a plane with the pyridyl nitrogens (*Figure 4.4 right*). All six Eu – N bond distances are similar (average bond distances: Eu – N_{ring} 2.68 Å, Eu – N_{py} 2.66 Å) and the three Eu – O distances are shorter (2.33 Å), reflecting the greater electrostatic attraction between Eu^{3+} and the charged O donors.

The complex exists as a racemic mixture of two enantiomers. The three stereogenic phosphorus centres are either *RRR* or *SSS* (*Figure 4.4 left*). Due to the steric demand of the phosphinate phenyl groups, once the first phosphinate O has bound to the Eu^{3+} centre, rendering the chirality at phosphorus *R* or *S*, the other two must also become *R* or *S*, respectively. In the solid state, there is no evidence for any other diastereomers (*RSR* or *SRS*). For an *R* configuration at P, the average ring N-C-C-N and substituent N-C-C-N_{py} torsion angles are + 47° and - 33°, consistent with a $\delta\delta\delta$ ring conformation and Λ configuration. Hence, the unit cell contains two (*RRR*)-Λ($\delta\delta\delta$) complexes and two of the enantiomeric (*SSS*)-Δ($\lambda\lambda\lambda$) complexes.

Table 4.1 Selected distances (Å) for isostructural [Ln·L^9].

Complex	Ce	Nd	Sm	Eu	Ho	Tm	Yb
Ln - O	2.41	2.38	2.34	2.33	2.29	2.26	2.25
Ln - N(py)	2.73	2.69	2.67	2.66	2.64	2.62	2.62
Ln - N(ring)	2.75	2.71	2.69	2.68	2.65	2.63	2.63
Ln - P	3.62	3.58	3.55	3.54	3.51	3.49	3.48

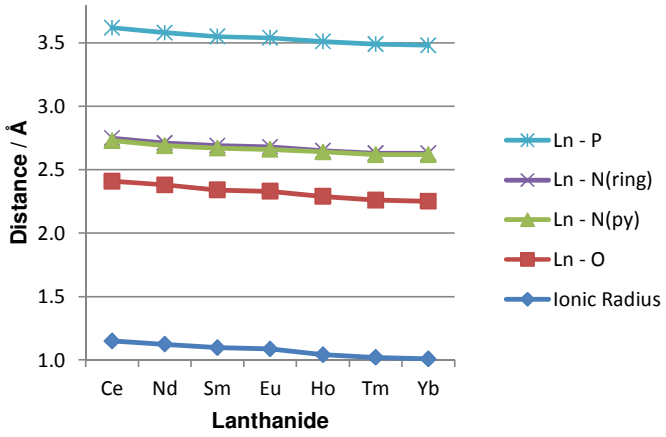

Figure 4.5 Bond distances and ionic radii of the seven isostructural [Ln·L^9] complexes.

The solid state structure of six other complexes in the [Ln·L^9] series were solved. For each structure, the same space group, geometry and stereochemistry was observed to that of [Eu·L^9]. The only variation across the series is the steady decrease in bond lengths between the central lanthanide and the nine coordinating donors (*Figure 4.5* and *Table 4.1*). These decreases follow the lanthanide

contraction, in which the ionic radii of the Ln^{3+} ions decrease,[7] due to an increase in effective nuclear charge felt by the outer *f* electrons. Typically, for series of Ln^{3+} complexes, the change in size of the lanthanide ion across the series enforces a change in geometry or coordination number upon the complex. An example is the series $[Ln{\cdot}L^{1.8}]^-$ (see *Section 1.3.3*).[8] In this series, the tetraphosphinate ligand is 8 coordinate. The lanthanides with larger ionic radii accommodate a solvent H_2O molecule, giving an overall 9 coordinate structure. Complexes beyond $[Eu{\cdot}L^{1.8}]^-$ can no longer accommodate this solvent molecule and are 8 coordinate. The advantage of an isostructural series, such as $[Ln{\cdot}L^9]$, is the ability to observe changes across the series which are dependent solely upon the Ln^{3+} ion, as all other parameters are constant.

4.3.2 Solution State Structure

Determining the solid state structure is informative, but the majority of experiments are carried out in the solution state, and so an appreciation of the solution state structure is very important. The representative RP-HPLC trace (*Figure 4.3*) of $[Ln{\cdot}L^9]$ shows a single peak, which is indicative of a single diastereoisomer in solution. RP-HPLC alone does not provide conclusive evidence for the stereochemistry. NMR is able to provide more information on the species present in solution. The ^{1}H- and ^{31}P-NMR of each complex was measured at 400 MHz (CD_3OD, 295 K). For each complex, the ^{31}P-NMR spectrum shows a single resonance (*Figure 4.6 upper* shows the ^{31}P-NMR spectrum of $[Nd{\cdot}L^9]$). This is consistent with the retention of the *RRR* or *SSS* stereochemistry at phosphorus in solution. Diastereoisomers, such as complexes with *RSR* at phosphorus, would be expected to show more than one resonance in the ^{31}P-NMR spectrum. The ^{1}H-NMR of $[Nd{\cdot}L^9]$ shows a single species with 11 resonance – 8 of these resonances integrate to 3H and 3 resonances integrate to 6H, giving a total of 42H) – and no evidence for any minor species in solution (*Figure 4.6*). The observed resonances indicate that the C_3 symmetry, observed in the solid state, is retained in solution. The four protons in the 1,4,7-triazacyclononane ring are likely those with the largest linewidths (0.73, 2.85, 5.45 and 6.79 ppm), due to their close proximity to the paramagnetic Ln^{3+} ion. The same pattern of resonances integrating to 3H or 6H is observed across the series, with no evidence for the presence of minor species. The conclusion from NMR analysis is that in solution, the complexes $[Ln{\cdot}L^9]$ remain isostructural, and exist as enantiomers of a single stereoisomer, as observed in the solid state.

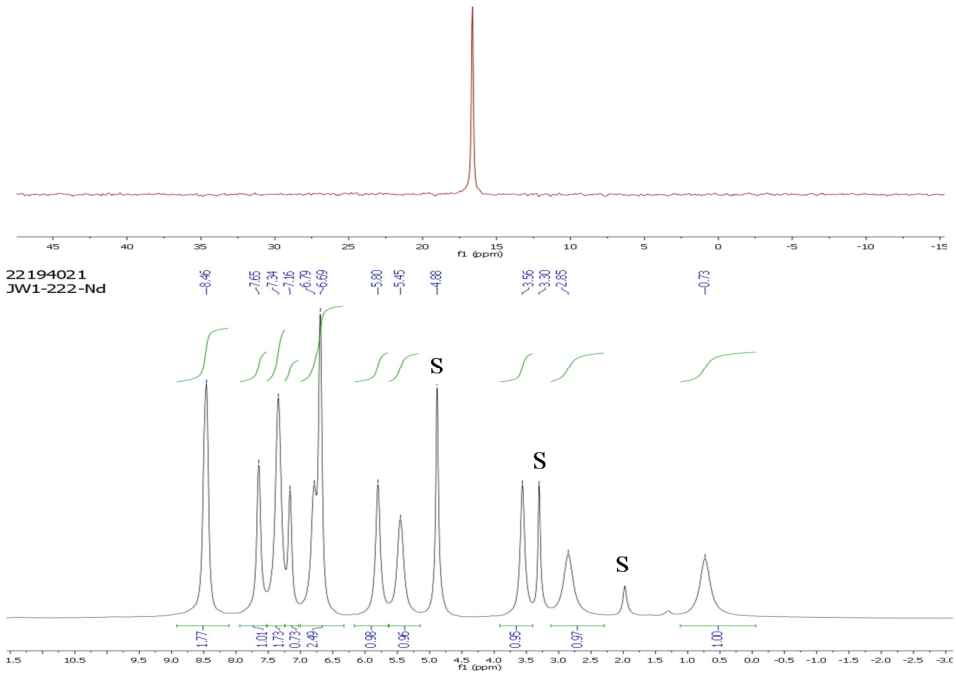

Figure 4.6 ^{1}H-(*lower*) and ^{31}P-(*upper*) NMR spectra for [Nd·L^{9}] (CD_3OD, 400 MHz, 295 K, pD 5.8). Residual solvent peaks are labelled S.

A variable temperature NMR experiment was carried out to investigate whether any change in stereochemistry would take place at higher temperatures. The complexes, [Yb·L^{9}] and [Pr·L^{9}] were chosen to investigate, as the central ions lie at either end of the lanthanide series, and result in complexes with relatively sharp proton resonances, compared to some of the intermediate lanthanides, such as Ho^{3+} and Er^{3+}. The [Yb·L^{9}] proton resonances also occur over a large spectral range, enhancing any changes in shift which may take place.

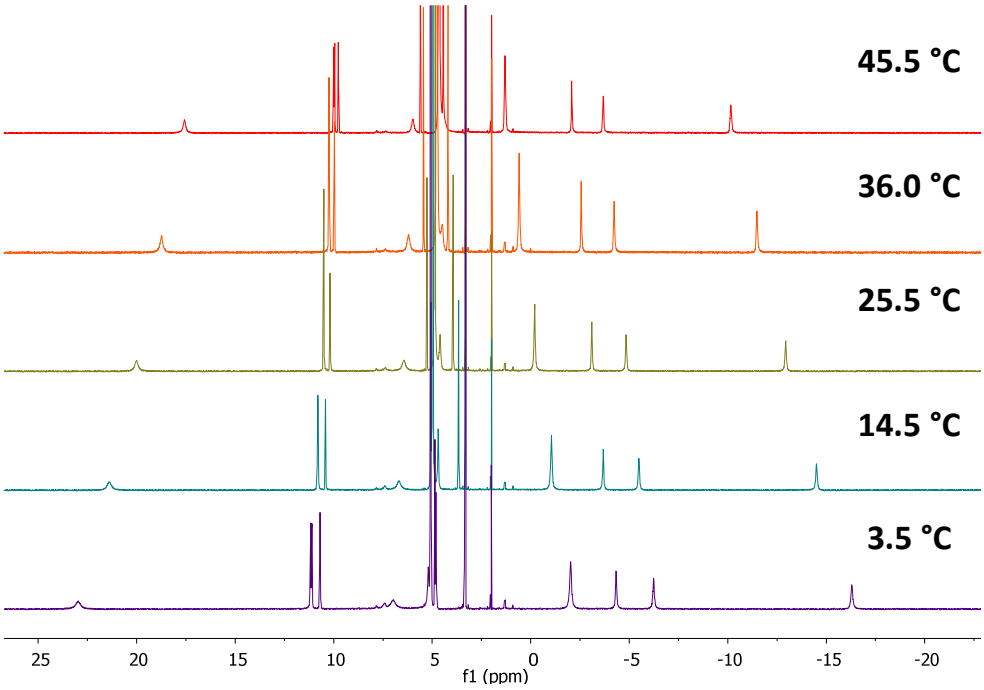

Figure 4.7 Variable temperature ^{1}H-NMR spectrum of [Yb·L^{9}] (CD_3OD, 500 MHz, pD 5.8).

Upon increasing the temperature, the ^{1}H-NMR spectrum of [Y·L^{9}] was found to contract, with the spectral range decreasing from 39 ppm to 27 ppm (*Figure 4.7*). No addition peaks arose, which would indicate the appearance of a minor species. This suggests that the barrier for isomerisation to some other diastereomers is greater than the energy available at 45 °C. Over the chosen temperature range, the ^{31}P-NMR spectrum contained a single peak, which shifted to a slightly higher frequency with increasing temperature. The variations of both the ^{31}P and ^{1}H resonances with T^{-1} and T^{-2} were plotted. It was found that both sets of resonances varied linearly with respect to T^{-2}. This behaviour is normally ascribed to a dominant pseudo-contact (dipolar) contribution to the paramagnetic shift.[9] The P atom is 3.56 Å from the Yb^{3+} centre and so could also be subject to a contact contribution to the observed paramagnetic shift, which would show a T^{-1} dependence.[10] The small changes in ^{31}P shift make the distinction between T^{-1} and T^{-2} dependence difficult to define.

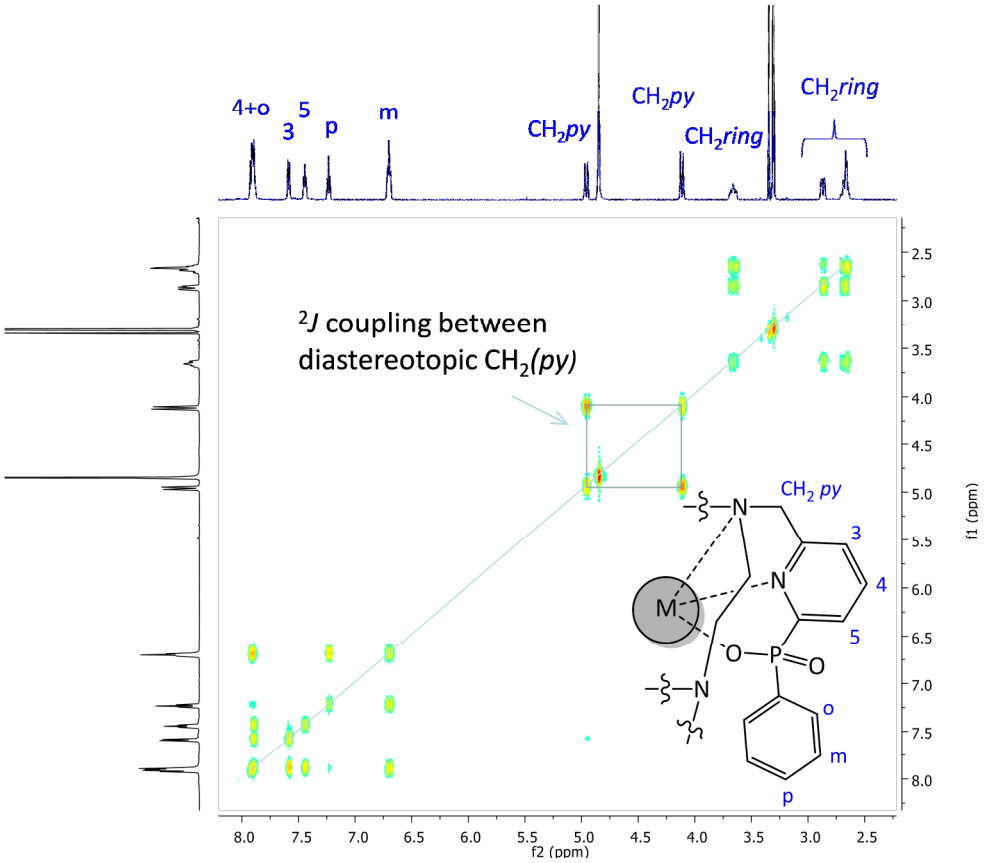

Figure 4.8 ^{1}H-COSY spectrum of [Y·L^{9}] (CD_3OD, 500 MHz, pD 5.8).

4.4 ^{1}H-NMR Assignment

For each complex in the [Ln·L^{9}] series, the ^{1}H-NMR spectrum shows 12 resonances, relating to the 12 distinct proton environments in the C_3 symmetric complexes. The *ortho* and *meta* phenyl protons are equivalent and integrate to 6H, while the remaining 10 resonances integrate to 3H, giving a total of 42H. The spectrum of [Y·L^{9}] shows no line broadening due to the presence of unpaired *f* electrons and is therefore a good point to begin assigning the spectra of [Ln·L^{9}]. In the absence of line broadening, coupling between protons in [Y·L^{9}] can be observed and a ^{1}H-COSY spectrum was measured, to aid assignment (*Figure 4.8*). In the aromatic region of the spectrum there are 6

resonances, which can be fully assigned, using the COSY spectrum and by comparing the splitting patterns to those of the uncomplexed ligand, ***H_3L^9***. The six remaining resonances from the CH_2 groups in the ring and linking the pyridyl moiety to the ring N become diastereotopic upon complexation, due to the rigidity of the complex. Diastereotopic protons couple to one another ($^2J \approx$ -16 Hz) and are clearly identified in the COSY spectrum. The linker CH_2 group can be identified as it also shows weak ^4J coupling to the pyridyl H^3. Of the four magnetically inequivalent ring protons, absolute assignment is made difficult by the overlapping resonances at 2.66 ppm. It is postulated that the proton at 2.87 ppm is an equatorial proton (*Figure 4.9*). Equatorial protons should show ^2J coupling to the axial proton on the same carbon and weaker ^3J coupling to adjacent Hs. Axial Hs will show stronger ^3J coupling to the axial H on the adjacent carbon, according to the Karplus equation.[11] The proton at 2.87 ppm is a doublet with weak coupling to adjacent protons, indicating that it is equatorial. In contrast, the proton at 3.66 ppm has a more complex splitting pattern and is likely to be an axial proton.

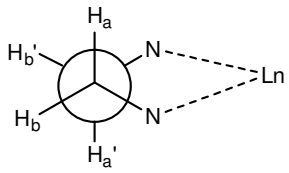

Figure 4.9 Illustration of the ring proton orientations in the [Ln·L^9] series, showing two axial (H_a) and two equatorial (H_b) protons.

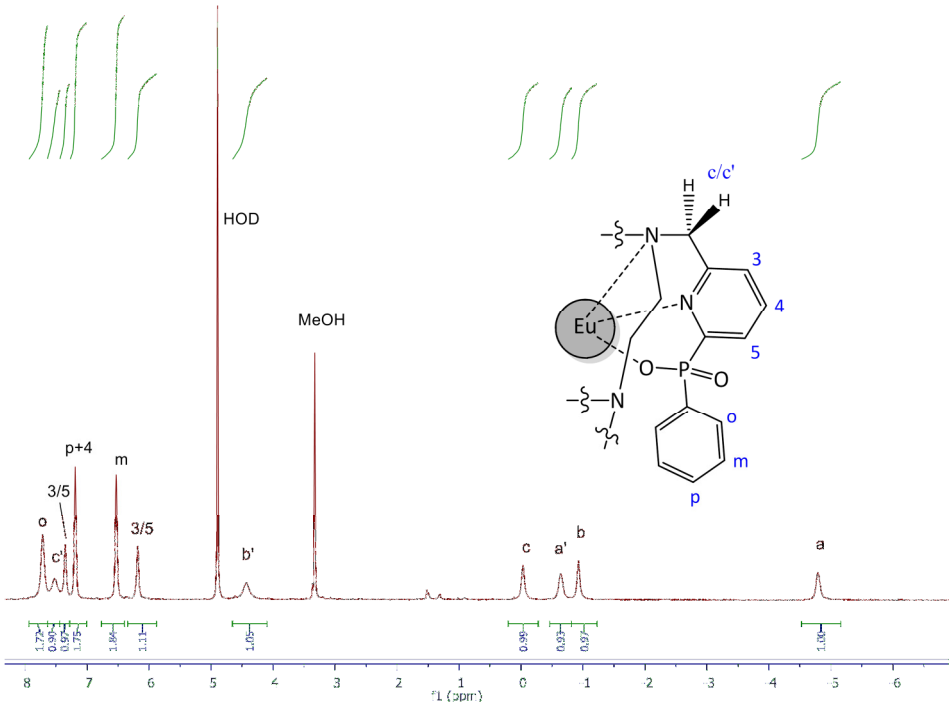

Figure 4.10 ^{1}H-NMR spectrum of [Eu·L^9] (CD_3OD, 400 MHz, pD 5.8); protons denoted *a* and *b* are axial and equatorial ring protons; *c* refers to the diastereotopic CH_2 py protons.

Having assigned the [Y·L^9] spectrum, the ^{1}H-NMR and COSY spectra were measured for the complex [Eu·L^9] (*Figure 4.10*). The europium ion has 6 unpaired *f* electrons, which induce both a paramagnetic shift and line broadening in the ^{1}H-NMR spectrum. The 1,4,7-triazacyclononane ring

protons are closest to the Eu^{3+} centre and show the greatest paramagnetic shift and are also the most line-broadened. These protons are also diastereotopic and show the strongest coupling in the COSY spectrum, allowing their assignment (-4.79, -0.93, -0.64 and 4.52 ppm). The remaining diastereotopic protons (CH_2 linker) are also broadened and show coupling to the pyridyl H^3 proton. Using the COSY spectrum and by comparison with [Y·L[9]], the [Eu·L[9]] spectrum was partially assigned. The [Eu·L[9]] ^{1}H-NMR spectrum was also compared to the assigned spectrum of the tri(picolinate)-triazacyclononane complex, [Eu·L[1.6]], which incorporates three carboxylate groups, in place of the phenyl phosphinate groups of [Eu·L[9]].[6] The two spectra are similar, indicating that the two complexes have similar solution state stereochemistry. The presence of only one series of mutually coupled sets of diastereotopic protons is consistent with a single isomeric structure wherein arm rotation (exchange pyridyl methylene groups) or ring inversion (exchanging axial/equatorial protons) is slow on the NMR timescale.

To further investigate the solution structure of [Ln·L[9]], the ^{13}C-NMR spectrum for [Yb·L[9]] was measured (*Figure 4.11 lower*). Nine C resonances can be seen between 120 – 170 ppm, relating to the aromatic C environments, and three further resonances at 36, 47 and 71 ppm, relating to CH_2 groups. One of these groups is the methylene pyridyl linker, and the remaining two resonances arise from the ring CH_2 groups. The total of twelve resonances confirms the C_3 solution state structure and the presence of two distinct ring CH_2 resonances indicate that the ring is rigid and that $\delta\delta\delta$ – $\lambda\lambda\lambda$ interconversion does not take place on the NMR timescale. To investigate the energy barrier to interconversion, the ^{13}C-NMR spectrum of [Yb·L[9]] was run at 50 °C (*Figure 4.11 upper*). Coalescence of the ring CH_2 resonances was not observed upon heating, showing that the barrier to interconversion is high.

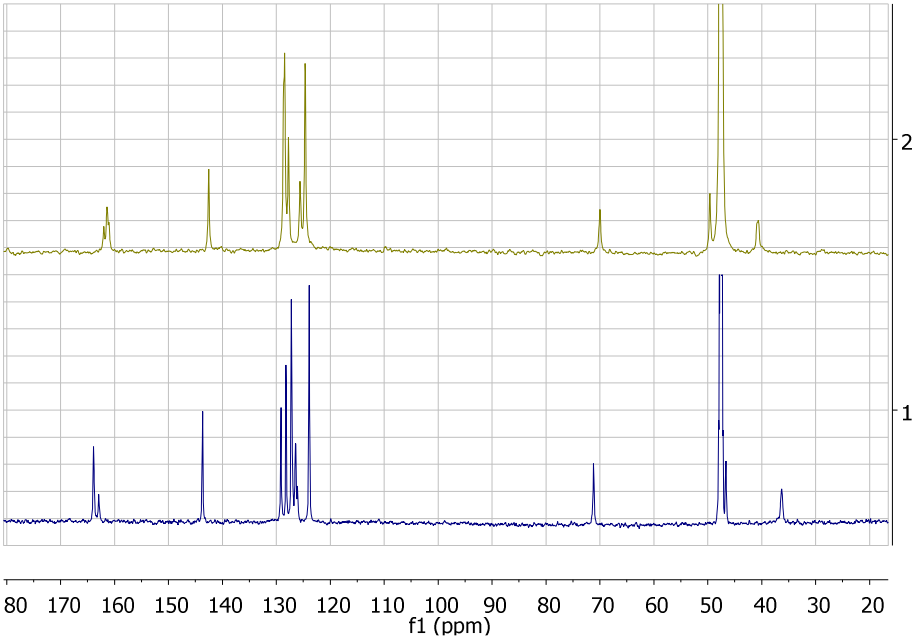

Figure 4.11 ^{13}C-NMR spectrum of [Yb·L[9]] at 22 °C (*lower*) and 50 °C (*upper*, CD_3OD, 400 MHz, pD 5.8)

4.5 Photophysical Properties

4.5.1 Absorption, Emission and Excited State Lifetimes

The motivation behind the synthesis of [Eu·L^9] was to investigate the effect upon the emission spectrum of a change in symmetry about the Eu^{3+} centre, relative to the earlier complexes, [Eu·L^6]$^-$ and [Eu·L^8]$^-$. Within the new [Ln·L^9] series, four of the complexes are emissive in the visible region of the electromagnetic spectrum. The photophysical properties of these complexes were assessed (*Table 4.2*). Each complex has a maximum absorption wavelength at 274 nm with a molar extinction coefficient of around 14,000 M^{-1} cm^{-1}. As previously discussed, a maximum absorption wavelength of 274 nm is too low for biological application but the pyridyl unit can be modified at a later stage into a chromophore that absorbs at longer wavelength. The extinction coefficient is reasonably high, due to the presence of three pyridyl groups. This highlights an advantage of the C_3 symmetric [Ln·L^9] system. Whichever sensitising group is eventually selected, the overall molar extinction coefficient of the complex will be around three times that of a single chromophore. Another property which affects the overall brightness of a complex is the quantum yield. The value for [Eu·L^9] is 9.0 %, which is reasonably high. The [Tb·L^9] has an exceptionally high quantum yield of 50 %. The large difference in these values arises from the overlap between the pyridyl triplet energy and the Ln^{3+} excited states. The pyridyl triplet state lies at around 32,000 cm^{-1},[12] which is close in energy to some of the high lying Tb^{3+} excited states, which can decay to the emissive $^5D_4$ state. Eu^{3+} does not have energy levels in this energy range, and so transfer of energy from the pyridyl group is less efficient. Despite this, the relatively high quantum yields for both complexes suggest the rate of Ln^{3+} excited state quenching is low. This is also reflected in the high emissive lifetimes of both Eu^{3+} and Tb^{3+} emission.

Table 4.2 Photophysical data of the four complexes in the [Ln·L^9] series that emit in the visible region of the spectrum. All data was recorded in H_2O, unless otherwise stated.

Complex	λ_{max} /nm	ε / M^{-1} cm^{-1}	$\tau^{Ln}_{H_2O}$ / *ms*	$\tau^{Ln}_{D_2O}$ / *ms*	*q*	$\Phi^{Ln}_{H_2O}$ / %
[Sm·L^9]	274	14,600	0.03	0.04	0.0	0.7
[Eu·L^9]	274	14,000	1.36	1.54	0.0	9.0
[Tb·L^9]	274	13,800	2.16	2.51	0.0	50
[Dy·L^9]	274	14,400	0.04	0.04	0.0	2.9

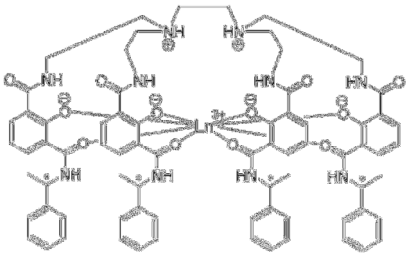

The excited state lifetime and emissive quantum yields of [Sm·L^9] and [Dy·L^9] are significantly lower than the more emissive Eu^{3+} and Tb^{3+} complexes. Having said this, the quantum yield of [Dy·L^9] is

more than twice that of *R*-(+)[Dy·BnMeH22IAM]$^+$, (Φ = 1.3 % in H_2O),[13] one of only a few emissive Dy^{3+} complexes reported.

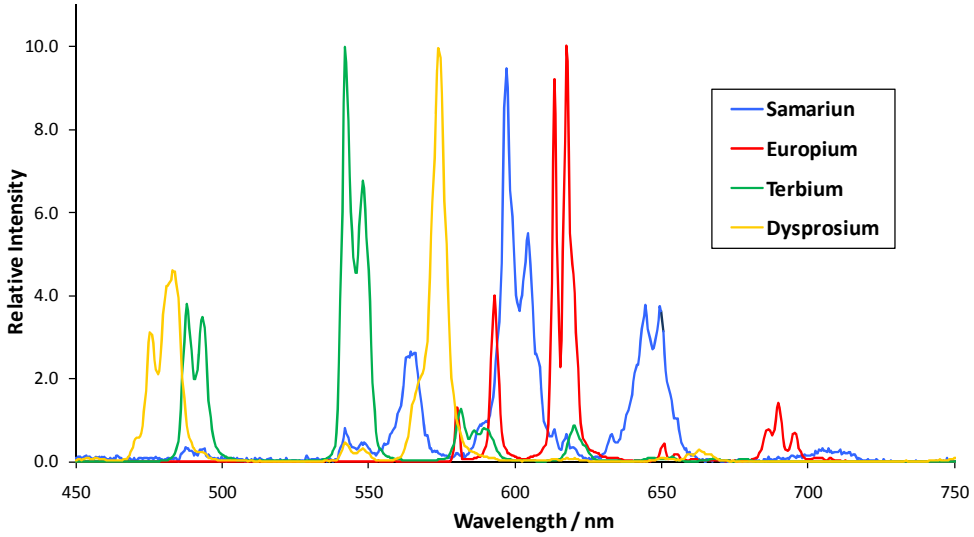

Figure 4.12 Emission spectra of the four emissive complexes in the [Ln·L^9] series (H_2O, λ_{ex} = 274 nm, pH 5.8). Spectra have been scaled so that the maximum intensity is equal in each case.

After excitation at 275 nm, the emission spectra of [Sm·L^9], [Eu·L^9], [Tb·L^9] and [Dy·L^9] were recorded (*Figure 4.12*). Each spectrum contains several bands, due to splitting of the Ln^{3+} ground state energy levels, spanning the entire visible spectrum from 480 nm (Tb^{3+} and Dy^{3+}) to 700 nm (Sm^{3+} and Eu^{3+}). As is typical of emissive lanthanide complexes, emission bands are sharp and show fine splitting. The Eu^{3+} emission spectrum shows some very favourable properties. The C_3 symmetric nature of the complex results in a spectrum with little fine splitting. Within the ΔJ = 1 manifold, there is only one narrow transition. The ΔJ = 2 band has a high relative intensity and is split into two transitions, while emission in the ΔJ = 4 region is weak. The specification outlined in *Section 1.5* calls for a large ΔJ = 2 band relative to the ΔJ = 1 and ΔJ = 4 bands. The spectrum of [Eu·L^9] fits this description very closely.

Table 4.3 Comparison of the integrated intensity ratios of some of the complexes synthesised. All spectra recorded in H_2O (pH 5.8).

Complex	**Intensity Ratios**	
	ΔJ = 2 / ΔJ = 1	*ΔJ = 2 / ΔJ = 4*
[a]**[Eu·L$^{1.1}$]$^{3+}$**	1.40	1.30
[Eu·L^1]	1.13	1.14
[Eu·L^6]$^-$	2.14	2.40
[Eu·L^8]$^-$	3.02	5.10
[Eu·L^9]	4.09	5.09

Comparison of the emission spectrum of [Eu·L^9] with [Eu·L^6]$^-$ illustrates the improvement in the form of the spectrum, with respect to meeting the specification (*Figure 4.13*). The increase in intensity of the ΔJ = 2 region is apparent, along with the reduction in emission in the ΔJ = 1 and ΔJ = 4 region.

The improvement can be quantified by measuring the integrated intensity of the various bands (*Table 4.3*). The results show a 2.9 and 3.9 fold increase for [Eu·L^9] in the $\Delta J = 2 : \Delta J = 1$ and $\Delta J = 2 : \Delta J = 4$ ratios, respectively, relative to the [Eu·L$^{1.1}$]$^{3+}$ complex, currently used in the HTRF experiment. The origin of the favourable [Eu·L^9] spectrum is the combination of polarisable phosphinate donors and the C_3 symmetric geometry about the Eu^{3+} centre.

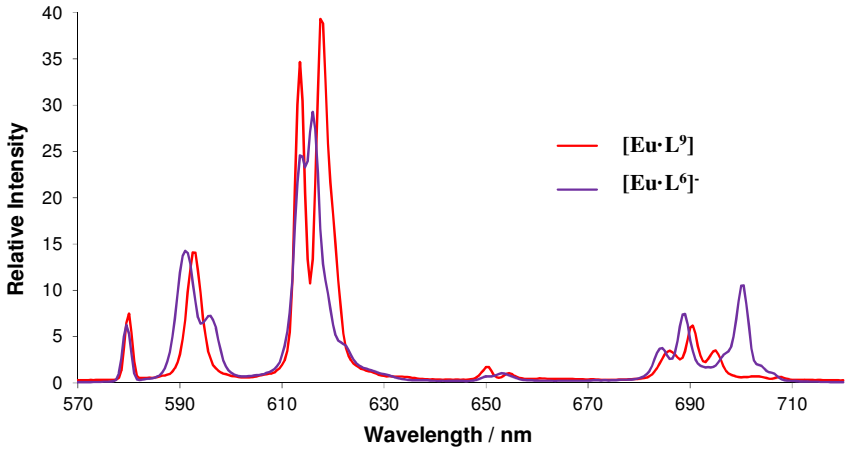

Figure 4.13 Comparison of the emission spectra of [Eu·L^9] and [Eu·L^6]$^-$ (H_2O, λ_{ex} = 274 nm, pH 5.8). Spectra have been scaled so that the total intensity integral is equal in each case.

4.5.2 Emissive Stability Assay

As with the previously synthesised complexes, emissive stability assays were carried out for [Eu·L^9] (*Figure 4.14 left*). As with the earlier complexes, the presence of a million fold excess of Ca^{2+}, Mg^{2+} and $EDTA^{4-}$ did not perturb the Eu^{3+} emission. Encouragingly, Mn^{2+} also caused no reduction in the emission intensity after 15 min and only around 5 % reduction after 18 h. All complexes previously tested had shown some susceptibility to Mn^{2+} quenching, whereas [Eu·L^9] appears to be almost unaffected by Mn^{2+}. One possible explanation for this stability is the shielding of the Eu^{3+} centre by the three phenyl groups below the plane of the complex (*Figure 4.14 right*), reducing the probability of an encounter between an aqua Mn^{2+} species and the Eu^{3+} complex. Further investigations into this effect are reported in *Chapter 6*.

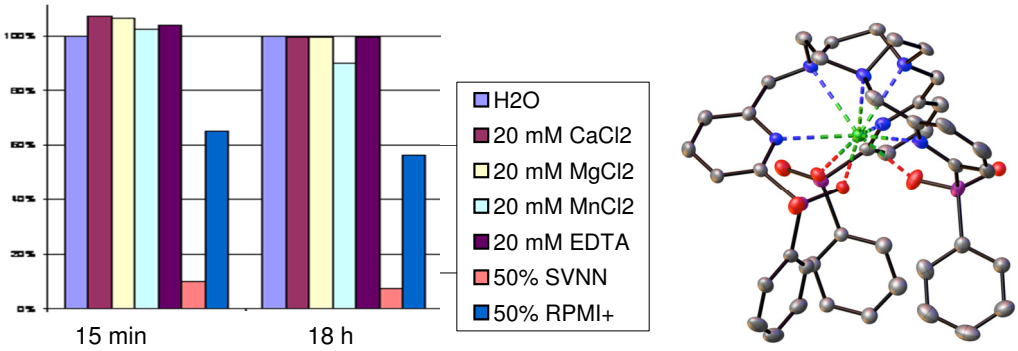

Figure 4.14 *left*) Stability data for [Eu·L^9] in HEPES buffer at two time points, 15 min and 18 h (10nM complex, λ_{ex} = 335 nm, λ_{ex} = 620 nm) and *right*) a side view of the crystal structure of [Eu·L^9], showing the three shielding Ph groups.

4.6 Chiral Analysis

4.6.1 Chiral Resolution

The X-ray crystal structure of [Eu·L^9] revealed the presence of two enantiomers in the solid state. The retention of this stereochemistry in the solution state was confirmed by ^{31}P- and ^{1}H-NMR. The two enantiomers have Λ($\delta\delta\delta$) (*RRR* at P) and Δ($\lambda\lambda\lambda$) (*SSS* at P) stereochemistry. Separation of the enantiomers was achieved by chiral-HPLC, using a CHIRALPAK-IC column. The optimal conditions were found to be an isocratic elution of EtOH : MeOH : $HNEt_2$ (50 : 50 : 0.1) at a flow rate of 1 mL min^{-1} at 15 °C. Under these conditions, the two enantiomers had a Δt_R of 1.6 min (*Figure 4.15*), and could be isolated as pure species. The overall structure of the complex is fairly rigid and the Λ and Δ enantiomers have differential interaction with the chiral stationary phase, leading to the observed difference in retention times. In total, around 1 mg of each enantiomer was isolated from the racemic mixtures of both [Eu·L^9] and [Tb·L^9]. As expected, the choice of lanthanide does not affect the behaviour of the complex on the column. The separated enantiomers were dissolved in refluxing methanol overnight. Under these conditions, no racemisation took place, consistent with the rigidity of the structure, and a high kinetic barrier to racemisation.

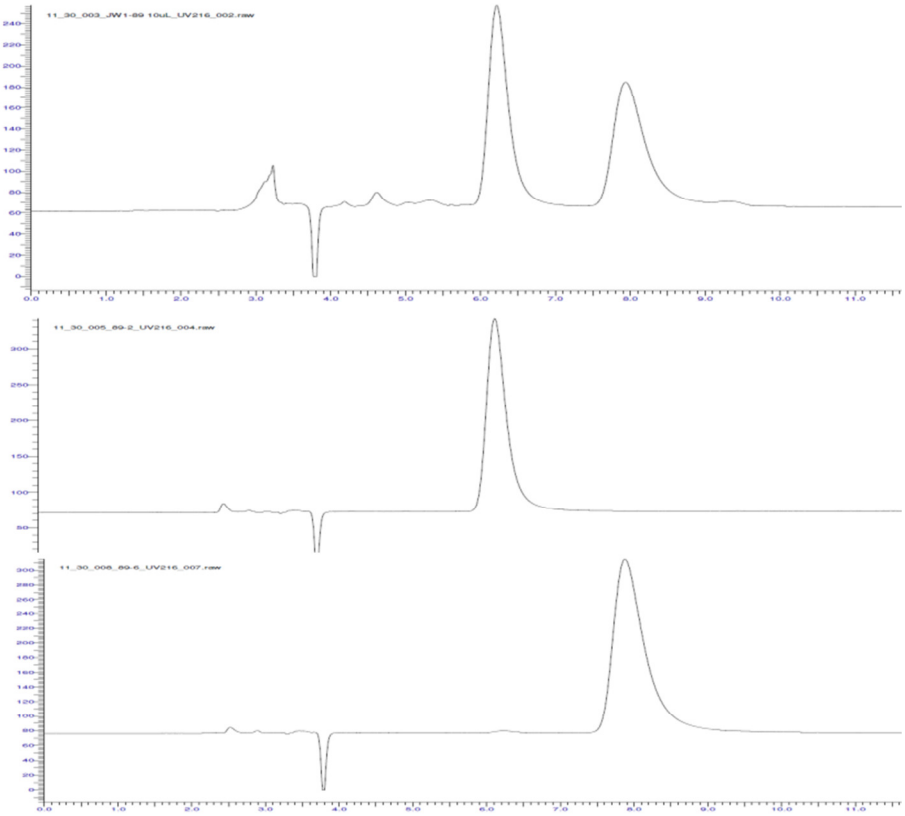

Figure 4.15 Chiral-HPLC traces of *upper*) the racemic mixture and *middle*) and *lower*) the two resolved enantiomers of [Eu·L^9]. Each sample was run on a CHIRALPAK-IC column (ethanol : methanol : diethylamine, 50 : 50 : 0.1 solution phase, isocratic elution, 1 mL min^{-1}, 15 °C).

4.6.2 Chiroptical Properties

Initially the two enantiomers were identified by their retention time upon the chiral column. Enantiomer 1 eluted at 6.2 min, while enantiomer 2 eluted at 8.0 min. With the two enantiomers resolved, chiroptical analysis was carried out. The first measurement undertaken involved measurement of the circular dichroism (CD) spectra. The CD technique measures the differential absorption of left- and right-handed light as a function of wavelength. Enantiomers always have mirror image spectra and the spectra for the two [Tb·L[9]] species are consistent with this definition (*Figure 4.16 left*). The CD spectrum can be used to determine the absolute stereochemistry of the enantiomers. The CD spectrum of enantiomer 2 was compared with a calculated CD spectrum of Δ-[Tb·L[9]] (*Figure 4.16 right*). The calculated spectrum is based upon the application of coupled oscillator model techniques.[14] They make use of the atomic coordinates from the X-ray diffraction crystal structure and NMR data to compute a predicted spectrum. This work was undertaken by Prof. L. DiBari at the University of Pisa. The similarity between the two spectra indicates that enantiomers 2 is the Δ(*λλλ*) (*SSS* at P) enantiomer. Hence, enantiomer 1 is the Λ(*δδδ*) (*RRR* at P) enantiomer. A crystal structure of either enantiomer would confirm this finding. At present, the amount of pure enantiomeric sample required to grow a suitable crystal is not available.

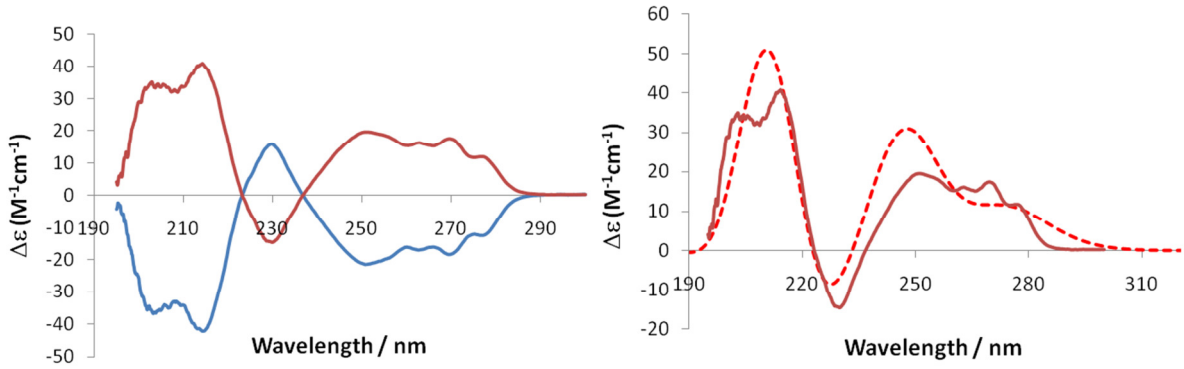

Figure 4.16 *left*) CD spectra for enantiomer 1 (*blue*) and enantiomer 2 (*red*) of [Tb·L[9]] (298 K, CH_3OH, 2.4 mM, 0.02 cm cells) and *right*) comparison of the experimental (*solid line*) and calculated (*dashed line*) CD spectra for Δ-[Tb·L[9]].

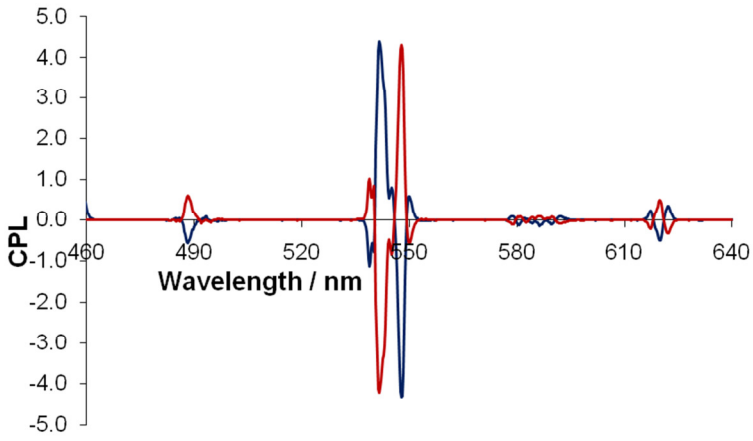

Figure 4.17 Circularly polarised emission spectra for Δ (*red*) and Λ (*blue*) enantiomers of [Tb·L[9]] (1 : 1 aq. CH_3OH, 295 K).

The emission analogue of CD is circularly polarised luminescence (CPL), which measures the differential emission of right- and left-handed circularly polarised light. As with CD, mirror image spectra were measured for the enantiomers of [Tb·L^9] (*Figure 4.17*) and [Eu·L^9] (*Figure 4.18*). The dissymmetry factor, g_{em}, quantifies the CPL, and has a maximum value of 2, according to *Equation 4.1*. Lanthanides are pure spherical emitters, and both [Tb·L^9] and [Eu·L^9] have high g_{em} values, up to 0.4 (*Table 4.4*). The CPL spectra for *SSS*-Δ-[Eu.L^3] exhibited a sign sequence for the transitions in the $\Delta J = 1$ and $\Delta J = 2$ manifolds that was similar to that observed with an enantiopure C_4-symmetric Δ Eu tetra-amide cyclen complex with an N_4O_4 donor set.[15] This is consistent with the absolute configuration assignment made using the CD spectrum.

$$g_{em} = \frac{2(I_L - I_R)}{I_L + I_R} \qquad \textbf{[4.1]}$$

Table 4.4 Emission dissymmetry factors, g_{em}, for [Tb·L^9] and [Eu·L^9] (1 : 1 aq. CH_3OH, 295 K).

	g_{em}(Tb)			g_{em}(Eu)		
λ / nm	*539*	*548*	*620*	*595*	*600*	*708*
Δ	-0.16	-0.32	-0.28	+0.18	+0.33	+0.31
Λ	+0.15	+0.31	+0.28	-0.18	-0.33	-0.31

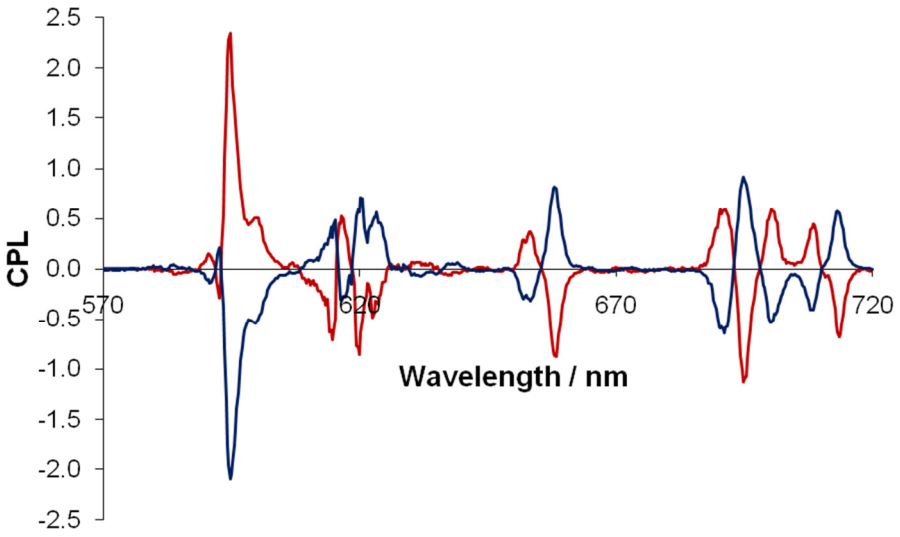

Figure 4.18 Circularly polarised emission spectra for Δ (*red*) and Λ (*blue*) enantiomers of [Eu·L^9] (1 : 1 aq. CH_3OH, 295 K).

The chiroptical properties of [Tb·L^9] and [Eu·L^9] render these complexes highly suitable as the core structures for emissive probes for use in CPL and time-resolved spectroscopic application. For example, it may be possible to observe changes in the CPL from intracellular probes, in response to changes in the chiral cellular environment. To allow intracellular application, the core structure must be modified to allow excitation at wavelengths above 300 nm. This is most easily achieved by further functionalisation of the pyridyl moiety.

4.7 Methylphosphinate Analogue of [Ln·L⁹]

The C_3 symmetric complex, [Eu·L^9], has many favourable properties for the HTRF application. The form of the emission spectrum meets the specification, the excited state lifetime is long, allowing time-gated detection of emission and the presence of three pyridyl units will triple the molar extinction coefficient of whichever chromophore is selected to take its place. One disadvantage of the complex is its low water solubility. An aqueous concentration of up to 100 μM is attainable, based upon absorbance values. However, increasing the aqueous concentration into the mM range is desirable. Within the core structure of [Ln·L^9], three positions can be modified to increase the water solubility (*Figure 4.19*). Position ***1*** is the pyridyl ring, which will be modified at a later stage, to incorporate a Eu^{3+} sensitising group. Position ***2*** is within the core 1,4,7-triazacyclononane ring. Synthetic modifications in this position are known,[16] and would allow addition of a water solubilising group, such as $-(CH_2)_n\text{-}CO_2^-$. The disadvantage of modifying this position is that the C_3 symmetry about the Eu^{3+} centre is perturbed, which may cause a change in the form of the emission spectrum. The final choice is to alter the R group of the phosphinate donor moiety. Exchange of Ph for Me gives [Ln·L^{10}] and should increase the aqueous solubility by reducing the hydrophobicity created by the three Ph groups. The methylphosphinate complex, [Ln·L^{10}], was defined as the next synthetic target.

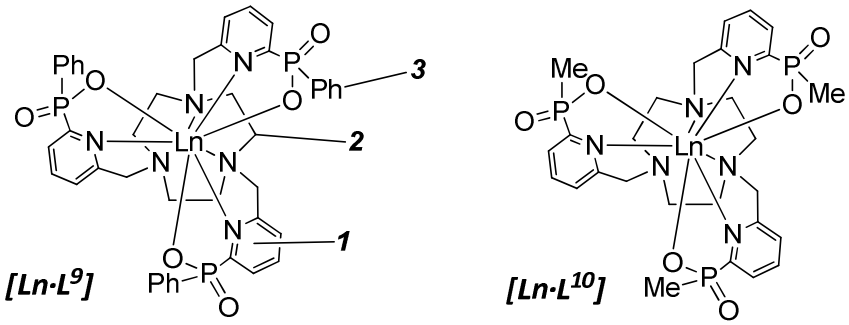

Figure 4.19 [Ln·L^9] positions available for functionalisation

4.7.1 Synthesis of the P-Methylphosphinate Complex

The synthesis of [Eu·L^{10}] would be expected to follow a similar pathway to [Eu·L^9] (*Scheme 4.1*), with the exchange of ethyl phenylphosphinate for ethyl methylphosphinate (***31***). Unfortunately, the starting material, ***31***, is not commercially available. The synthesis of ***31***, was achieved by stirring $MeP(OEt)_2$ with one equivalent of H_2O at room temperature under an atmosphere of argon (*Scheme 4.2*). Under these conditions, ***31*** was generated, along with one equivalent of ethanol. This was confirmed by ^{1}H-NMR.

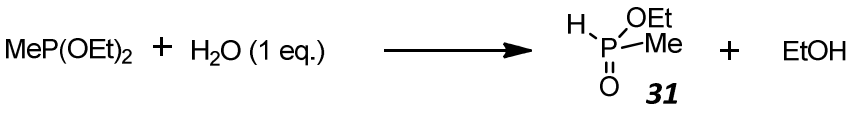

Scheme 4.2

The ethyl methylphosphinate (***31***) / ethanol mixture was used directly in the palladium coupling reaction with 2-bromo-6-methylpyridine. Dry, degassed (freeze-thaw cycle) toluene was added to the solution, which was bubbled with argon for 2 h, prior to the addition of the 2-bromo-6-methylpyridine, NEt_3 and $Pd(PPh_3)_4$. Bubbling of argon through the solution was continuous while the reagents were added, to ensure no atmospheric oxygen, that can poison the Pd(0) catalyst, entered the reaction mixture. After 16 h at 125 °C, the starting materials had been consumed and the product (***32***) was purified by column chromatography on silica.

The remaining steps towards the synthesis of [Eu·L^{10}] are shown in *Scheme 4.3*. The synthesis followed a similar pathway to that of [Eu·L^9], with the exception of the functionalisation of the pyridyl methyl group prior to alkylation. Rather than bromination with NBS and dibenzoyl peroxide, an alternative route was attempted, which was designed to increase the yield and ease of the reaction. The alternative route involves formation of the pyridyl N-oxide ***33***, followed by rearrangement to the pyridyl-$CH_2OC(O)CF_3$, which is hydrolysed *in situ* to the alcohol ***34*** upon addition of anhydrous EtOH. After purification by column chromatography on silica, the alcohol was mesylated with mesyl chloride and NEt_3 in THF. The mesylate ***35*** was then used in the alkylation step with 1,4,7-triazacyclononane. Whilst the overall yield of the pyridyl methyl activation step was reduced (23 % for mesylation vs. 41 % for bromination), the advantage of the mesylation route is the ease of purification at each step, compared to the more challenging separation of the mono-brominated material from the di- and un-brominated products, formed in the NBS reaction. Another advantage is that in the subsequent alkylation step, no evidence for the tetra-substituted product was observed, even at 80 °C in CH_3CN. This is in contrast to the more reactive brominated starting material, which required more stringent control over the reaction conditions to avoid over-alkylation. With the tri-alkylated ligand in hand, hydrolysis and complexation gave [Eu·L^{10}] in high yield. As with the phenylphosphinate analogue, [Eu·L^{10}] was purified by short path column chromatography on silica.

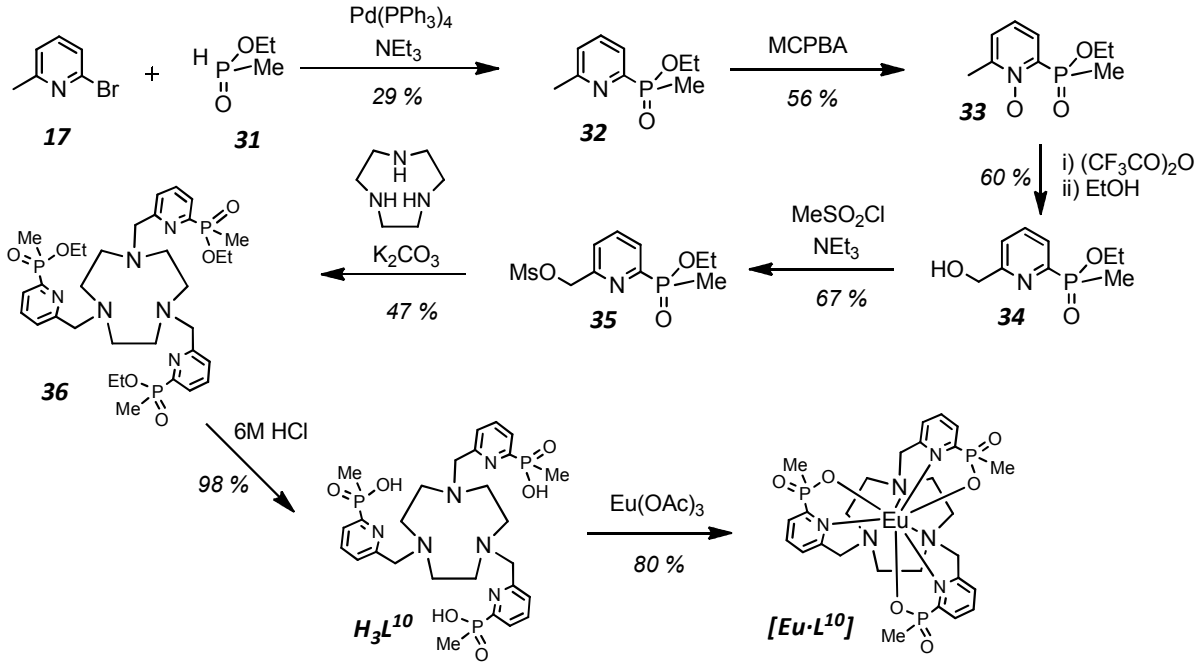

Scheme 4.3

4.7.2 Aqueous Solubility

The methyl phosphinate analogue of [Eu·L^9] was synthesised in order to increase the aqueous solubility of the resultant complex. Solubility of [Eu·L^9] was assessed by measuring the absorbance of a saturated aqueous solution. A limiting concentration of around 100 μM was found. The more hydrophilic complex, [Eu·L^{10}], was found to have a greater aqueous solubility than could be measured by absorbance. Using the extinction coefficient of 8,400 M^{-1} cm^{-1} and a maximum absorbance detection of 3, the complex concentration is > 350 μM, according to the Beer-Lambert equation. An empirical measurement found that 5 mg of [Eu·L^{10}] was soluble in 1 mL of H_2O, giving a concentration of around 6 mM. It can be concluded that, as expected, the methylphosphinate complex has far greater water solubility than the phenylphosphinate analogue.

4.7.3 Structural Analysis

Due to the increased solubility of [Eu·L^{10}] in water, crystals could not be readily grown in the same aqueous methanolic solution used to grow crystals of [Ln·L^9]. Despite this fact, NMR studies could be used to investigate the solution state structure of [Eu·L^{10}]. The ^{31}P-NMR spectrum shows a single resonance consistent with a single major diastereomer in solution. Comparison of the ^{1}H-NMR of [Eu·L^9] and [Eu·L^{10}] reveals that the two complexes have the same structure in solution (*Figure 4.20*). The ^{1}H-NMR spectrum for [Eu·L^{10}] was measured in *d*-methanol to allow comparison with [Eu·L^9]. The spectrum in D_2O has the same form, with small shifts in the ppm values of some of the resonances. In solution, both [Eu·L^9] and [Eu·L^{10}] exist as a single diastereomer, with no evidence for any minor species. The chemical shift values of the ring and pyridyl protons are very similar in each case. Additional Me peaks are seen in the spectrum of [Eu·L^{10}], along with the absence of the phenyl resonances. Overall, it can be reasoned that the two complexes have the same solution state structure, previously determined to be a 9-coordinate, slightly distorted, tricapped trigonal prism, with pseudo-C_3 symmetry.

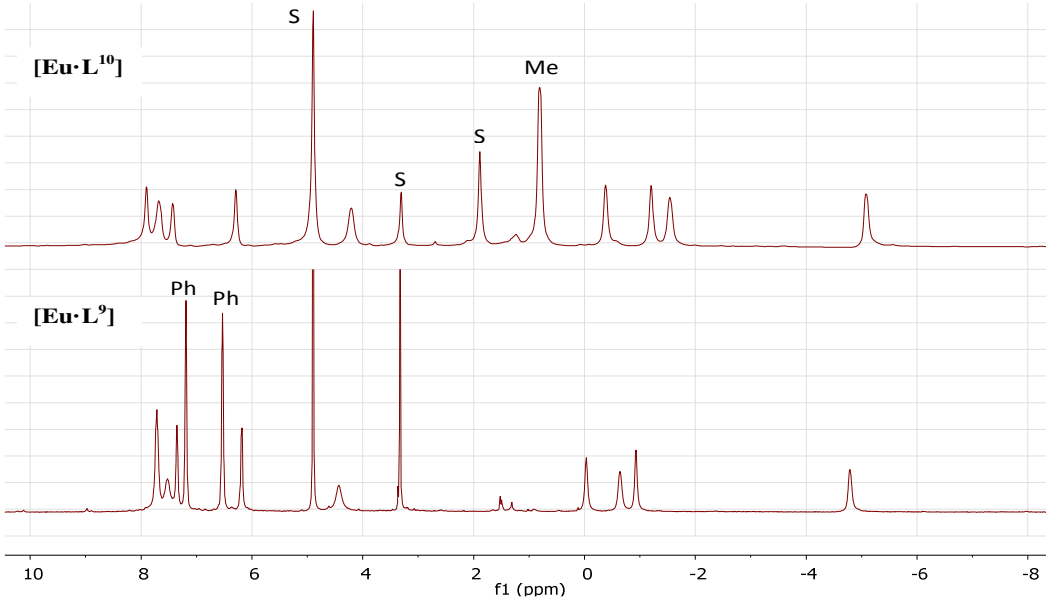

Figure 4.20 ^{1}H-NMR spectra of [Eu·L^{10}] (*upper*) and [Eu·L^9] (*lower*) (CD_3OD, 400 MHz).

4.7.4 Photophysical Properties

Having established that the solution state structure of [Eu·L^{10}] is the same as that of [Eu·L^{9}], the photophysical properties are expected to be somewhat similar. Analysis of [Eu·L^{10}] was carried out under the same conditions as [Eu·L^{9}] (*Table 4.5*). The maximum absorption wavelength and molar extinction coefficient both decrease by a small amount. The emission quantum yield has also dropped slightly. This may be due to a reduction in steric bulk, upon exchanging phenyl groups for methyl groups, allowing quenchers, such as H_2O, greater access to the Eu^{3+} centre. This idea does not hold when looking at the excited state lifetime of [Eu·L^{10}] in H_2O, which is 15 % greater than the value for [Eu·L^{9}]. Overall, the photophysical data are very similar. One of the favourable properties of [Eu·L^{9}] was the form of the emission spectrum. To allow comparison with the spectrum of [Eu·L^{10}], samples were made up with equal absorbance (0.10) and emission spectra were measured (*Figure 4.21*). The lower quantum yield of [Eu·L^{10}] is apparent, by the overall lower emission intensity in each band. The encouraging feature from this comparison is that the two spectra have nearly identical spectral form. This result is entirely predictable, as it is known that [Eu·L^{10}] has the same symmetry and donor set about the Eu^{3+} centre as [Eu·L^{9}]. It can also be concluded from the two spectra that exchanging the phenyl groups for methyl groups does not affect the polarisability of the phosphinate donor, as the integrated intensity ratios of the $\Delta J = n$ bands remain similar.

Table 4.5 Photophysical data for [Eu·L^{9}] and [Eu·L^{10}] measured in H_2O, unless otherwise stated (295 K, pH 5.8/pD 5.4).

Complex	λ_{max} (nm)	ε (M^{-1} cm^{-1})	$\tau^{Ln}_{H_2O}$ / *ms*	$\tau^{Ln}_{D_2O}$ / *ms*	*q*	$\Phi^{Ln}_{H_2O}$ / %	Intensity Ratios	
							ΔJ = 2 / ΔJ = 1	*ΔJ = 2 / ΔJ = 4*
[Eu·L^{9}]	274	14,000	1.36	1.54	0.0	9.0	4.09	5.09
[Eu·L^{10}]	272	8,400	1.56	1.60	0.0	7.2	4.11	5.40

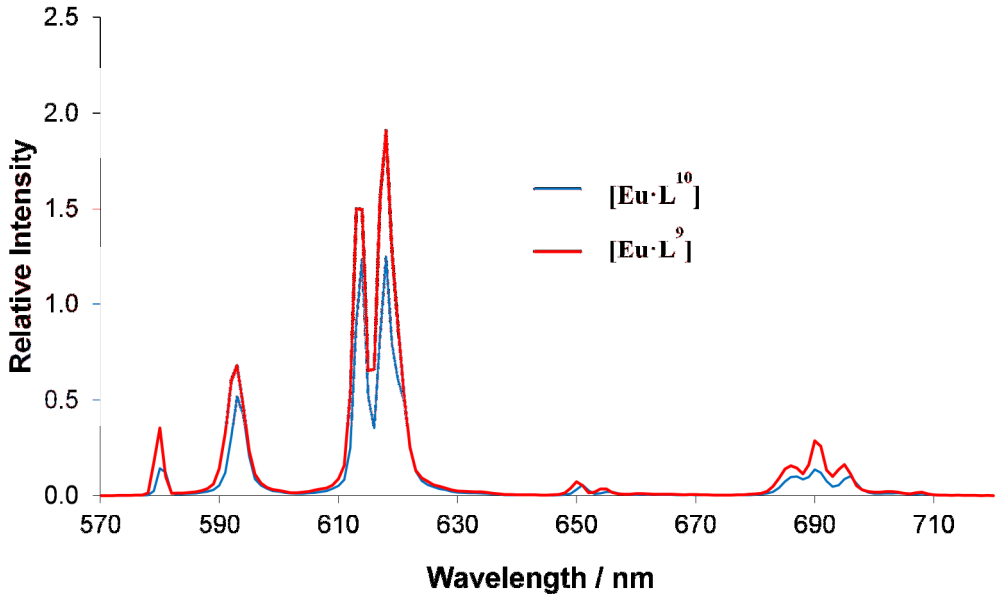

Figure 4.21 Comparison of the emission spectra of [Eu·L^{9}] and [Eu·L^{10}] (H_2O, pH 5.8, λ_{ex} = 274 nm, *A* = 0.10).

4.7.5 The Terbium Complex

To allow comparison of the photophysical data of [Tb·L^9], the methylphosphinate [Tb·L^{10}] was synthesised in an analogous manner to the synthesis of [Eu·L^{10}], with exchange of $Eu(OAc)_3$ for $Tb(OAc)_3$. Data for the two complexes is reported in *Table 4.6*. The change in molar extinction coefficient approximately mirrors the observed changes between [Eu·L^9] and [Eu·L^{10}]. The excited state lifetime and emissive quantum yield both increase slightly upon moving to the methylphosphinate complex. The increase in quantum yield suggests a better overlap between the pyridyl triplet excited state and the Tb^{3+} excited state. The long-lived excited state for each Tb^{3+} complex, reflects the shielded nature of the Ln^{3+} centre, rendering it resistant to quenching processes.

Table 4.6 Photophysical data for [Tb·L^9] and [Tb·L^{10}] measured in H_2O, unless otherwise stated (295 K, pH 5.8/pD 5.4).

Complex	λ_{max} (nm)	ε (M^{-1} cm^{-1})	$\tau^{Ln}_{H_2O}$ / *ms*	$\tau^{Ln}_{D_2O}$ / *ms*	q	$\Phi^{Ln}_{H_2O}$ / %
[Tb·L^9]	274	14,000	2.16	2.51	0.0	50
[Tb·L^{10}]	272	7,400	2.59	2.98	0.0	60

4.8 NMRD Analysis of [Gd·L^9] and [Gd·L^{10}]

Kinetically inert and thermodynamically stable lanthanide complexes are extensively studied for use as contrast agents in magnetic resonance imaging.[17] A potential contrast agent must have a high efficiency in catalysing the water proton relaxation rate.[18, 19] This property is quantified by the relaxivity, which is the increment of the water proton relaxation rate per unit concentration of the contrast agent. The relaxivity depends upon the structural, electronic and dynamic properties of the complex. Complexes of Gd^{3+} are most often studied, as the combination of a high magnetic moment with a long electronic spin relaxation time, leads to high relaxation rates.[20]

The overall relaxivity is determined by the contribution of inner- and outer sphere relaxation mechanisms. The coordinatively saturated complexes, [Gd·L^9] and [Gd·L^{10}], have no inner sphere water molecules and can be described as purely outer sphere contrast agents. The outer sphere mechanism involves the electron – nuclear magnetic dipole coupling, which occurs when the solvent molecules approach the metal complex during their translational diffusion motion.[21] It depends upon the translational diffusion coefficient, D, the electronic relaxation time, τ_S and the distance of closest approach of the water protons to the Gd^{3+} centre, a. The rate of outer sphere relaxivity is also dependent upon the magnetic field.[21] Nuclear magnetic relaxation dispersion (NMRD) profiles show the relaxivity as a function of magnetic field strength and are measured by a fast field-cycling technique developed by Koenig and Brown.[22]

NMRD profiles were measured for [Gd·L[9]] and [Gd·L[10]] by Prof. Botta at the University of Alessandria (*Figure 4.22*). Some of the measured parameters are also shown in *Table 4.7*. The most noticeable difference between the two profiles is the low rate of relaxivity for [Gd·L[9]]. At 20 MHz field strength this value is 0.58 mM^{-1} s^{-1}. A likely explanation for this low value is the nature of the solvation of the complex. To solubilise the complex, a solvent system of H_2O : CH_3OH (9 : 1) was used. The estimated value of *a*, the distance between the Gd^{3+} centre and the nearest water molecule, is 9.9 ± 3.2 Å, suggesting that the complex is surrounded by a shell of methanol molecules, shielding the complex from the approach of water. For the water soluble [Gd·L[10]], a more typical *a* value for outer sphere water of 4.3 ± 0.1 Å was estimated, leading to the higher observed relaxivity. The temperature dependence of the relaxivity was measured for [Gd·L[10]] (*Figure 4.22 right*), and revealed an increase in relaxivity at lower temperatures. As the *a* value should not be affected by temperature, the increase is associated with a change in τ_v and the diffusion coefficient, *D*.

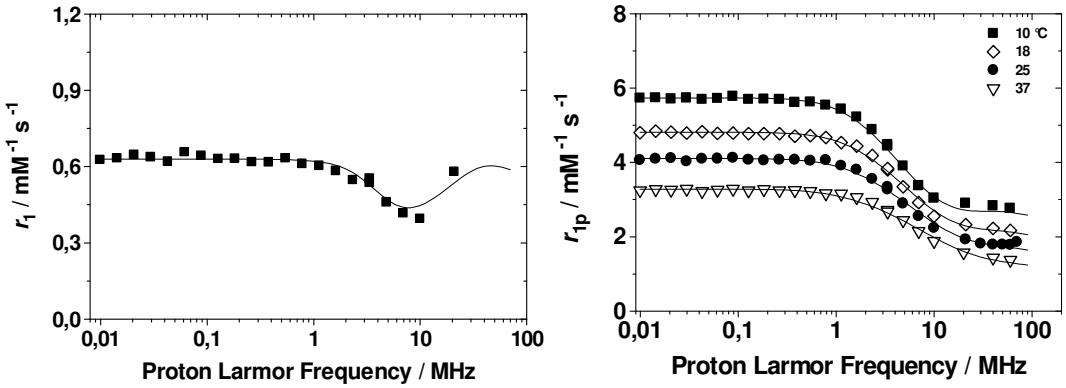

Figure 4.22 NMRD profiles for [Gd·L[9]] (90 : 10, H_2O/CH_3OH, *left*) and [Gd·L[10]] (H_2O) with varying temperature (*right*).

.

Table 4.7 Outer sphere parameters for [Gd·L[9]] and [Gd·L[10]] where r_{1p}^{20} is the relaxivity at 20 MHz, Δ^2 and τ_V are terms which contribute to the electronic relaxation time, *q* is the number of inner sphere water molecules, *a* is the distance between the Gd^{3+} centre and the nearest water molecule and *D* is the diffusion coefficient.

"outer sphere" parameters (25 °C)		
	[Gd·L[10]]	**[Gd·L[9]]**
r_{1p}^{20} (mM^{-1} s^{-1})	1.93	0.58
Δ^2(s^{-2}; $\times10^{19}$)	2.75±0.07	3.16±0.94
τ_V (ps)	10±1	28±4
q	0	0
a (Å)*	4.3±0.1	9.9±3.2
D (cm^2s^{-1};$\times10^5$)*	2.24	2.24

Comparison of the NMRD of [Gd·L^{10}] with the tetra(methylphosphinate) complex (*Figure 4.23*) reveals a similar variation in relaxivity with magnetic field for each complex. The calculated parameters are shown in *Table 4.8*, where the tetra(methylphosphinate) complex is termed [Gd·L$^{1.8}$(Me)]$^-$. Each complex is $q = 0$ but the a value for [Gd·L$^{1.8}$(Me)]$^-$ is slightly shorter, due to the different local hydrophobicity about the Gd^{3+} centre. This parameter, along with the larger Δ^2 value, give [Gd·L$^{1.8}$(Me)]$^-$ an overall higher relaxivity at 20 MHz. Similar analysis with the tetra(benzylphosphinate), [Gd·L$^{1.8}$(Bn)]$^-$, show that although the a value is the same as [Gd·L^{10}], a lower overall relaxivity is measured, that can be tentatively ascribed to the difference in electronic relaxation time (*Figure 4.23 right*).

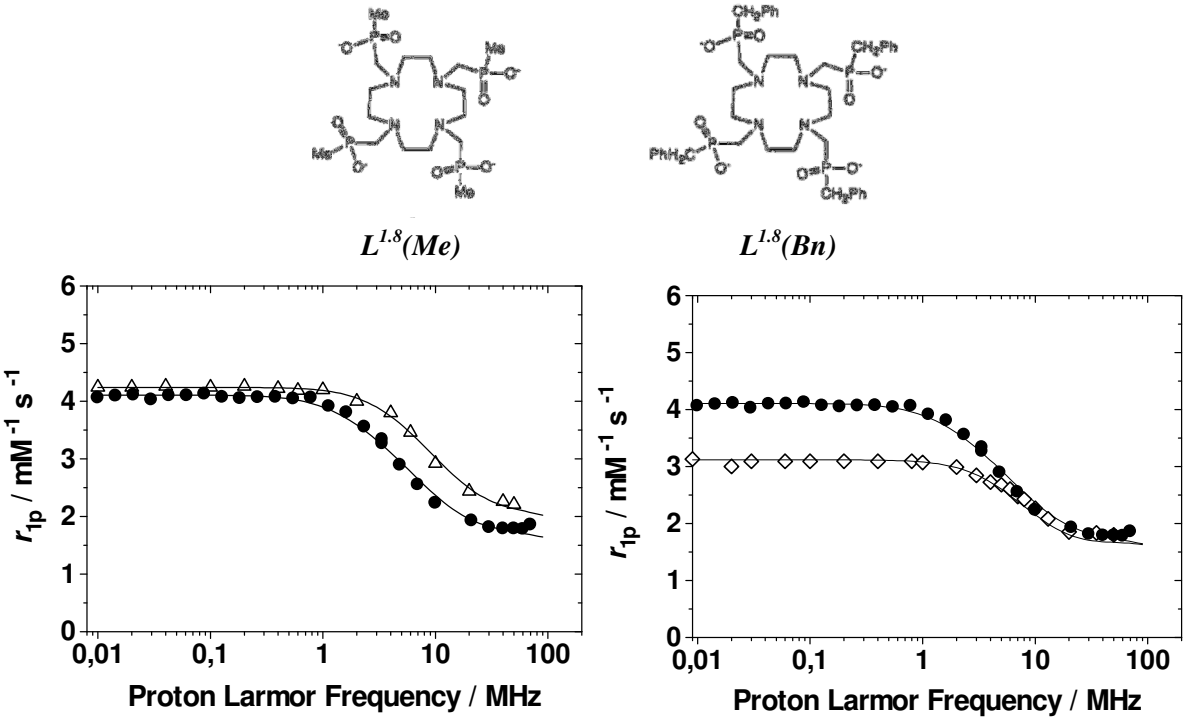

Figure 4.23 Comparison of the NMRD profile of [Gd·L^{10}] (●) with that of [Gd·L$^{1.8}$(Me)]$^-$ (Δ, *left*) and [Gd·L$^{1.8}$(Bn)]$^-$ (◊, *right*).

Table 4.8 Outer sphere parameters for [Gd·L^{10}], [Gd·L$^{1.8}$(Me)]$^-$ and [Gd·L$^{1.8}$(Bn)]$^-$ where r_{1p}^{20} is the relaxivity at 20 MHz, Δ^2 and τ_V are terms which contribute to the electronic relaxation time, q is the number of inner sphere water molecules, a is the distance between the Gd^{3+} centre and the nearest water molecule and D is the diffusion coefficient.

"*outer sphere*" parameters (25 °C)			
	[Gd·L^{10}] (●)	**[Gd·L$^{1.8}$(Me)]$^-$ (Δ)**	**[Gd·L$^{1.8}$(Bn)]$^-$ (◊)**
r_{1p}^{20} ($mM^{-1}\,s^{-1}$)	1.93	2.44	1.85
Δ^2(s^{-2}; ×10^{19})	2.75±0.07	7.1±0.1	7.1±0.1
τ_V (ps)	10±1	10±1	12±1
q*	0	0	0
a (Å)	4.3±0.1	3.6±0.1	4.3
D (cm^2s^{-1};×10^5)*	2.24	2.24	2.24

4.9 Conclusions

The C_3 symmetric complex, [Eu·L^9], was synthesised to investigate the influence of the symmetry about the Eu^{3+} centre on the form of the emission spectrum. It had been established that incorporation of the pyridyl phenylphosphinate moiety (***21***) resulted in a favourable emission spectrum for the DO3A complex, [Eu·L^6]$^-$. By combining three such donor groups in the 1,4,7-triazacyclononane core structure, a ligand with 9 donor groups was synthesised. After complexation with Eu^{3+}, X-ray crystallographic analysis and NMR data confirmed the pseudo-C_3 symmetric nature of the complex. The emission spectrum of [Eu·L^9] was found to meet the specification, outlined in the introduction, exceptionally well. With a large $\Delta J = 2$ band, relative to the $\Delta J = 1$ and $\Delta J = 4$ bands, the form of the emission spectrum is very well suited to maximising the spectral overlap with the allophycocyanin acceptor in the HTRF experiment. The favourable emission spectrum comes from the combination of polarisable donors groups and a high degree of symmetry about the Eu^{3+} centre.

Other favourable photophysical properties of [Eu·L^9] are the long lived Eu^{3+} excited state and the reasonably high quantum yield. These two properties are, in part, due to the shielding of the Eu^{3+} centre by the three phenyl groups, which create steric bulk beneath the plane of the complex. This shielding effect is also thought to be partly responsible for the apparent emission stability of the complex in the presence of Mn^{2+}, a species that has led to a reduction in the emission from each of the earlier complexes examined in this work and by researchers at CISbioassays, over the past decade.

Taking into account all of the encouraging features of [Eu·L^9], it was concluded that the core structure - 1,4,7-triazacyclononane with three pyridyl phosphinate groups – is ideally suited for the HTRF application and meets the specification, regarding emission spectral form and stability. By retaining the core structure and modifying the pyridyl ring, subsequent complexes can be designed which will allow sensitisation of Eu^{3+} emission at a wavelength > 330 nm, without affecting the spectral form or stability. These complexes are the subject of the next chapter.

After the pleasing results from [Eu·L^9], it was decided that the series [Ln·L^9] should be synthesised to investigate any variations across the series. Crystal structures revealed that [Ln·L^9] defined an isostructural series, with a slightly distorted tricapped trigonal prismatic geometry about the Ln^{3+} centre. NMR data showed that this geometry was retained in solution. Isostructural series of lanthanide complexes are rare, and the [Ln·L^9] series will be used in future fundamental NMR studies.

The complexes exist as enantiomers, arising from the chirality at P (*SSS* or *RRR*). The enantiomers have a Δ or Λ configuration, respectively, and were found to interact strongly with the stationary phase of a chiral HPLC column, allowing resolution. With the two enantiomers isolated, CD and CPL analyses were undertaken. Circular dichroism aided the assignment of the two enantiomers, whilst the CPL from the Eu^{3+} and Tb^{3+} complexes was found to have g_{em} values up to 0.4. There is potential for complexes based upon the core structure of [Ln·L^9] to act as chiroptical probes, that can report changes in the chiral cellular environment by a change in CPL.

4.10 References

1. R. S. Dickins, D. Parker, J. I. Bruce and D. J. Tozer, *Dalton Trans.*, 2003, 1264-1271.
2. J. I. Bruce, D. Parker and D. J. Tozer, *Chem. Commun.*, 2001, 2250-2251.
3. A. Picot, A. D'Aleo, P. L. Baldeck, A. Grichine, A. Duperray, C. Andraud and O. Maury, *J. Am. Chem. Soc.*, 2008, **130**, 1532-1537.
4. J.-G. Kim, S.-K. Yoon, Y. Sohn and J.-G. Kang, *J. Alloys Compd.*, 1998, **274**, 1-9.
5. Albertss.J, *Acta Chem. Scand.*, 1970, **24**, 1213-&.
6. G. Nocton, A. Nonat, C. Gateau and M. Mazzanti, *Helv. Chim. Acta*, 2009, **92**, 2257-2273.
7. R. D. Shannon, *Acta Crystallographica Section A*, 1976, **32**, 751-767.
8. S. Aime, M. Botta, D. Parker and J. A. G. Williams, *J. Chem. Soc. Dalton Trans.*, 1995, 2259-2266.
9. J. A. Peters, J. Huskens and D. J. Raber, *Prog. Nucl. Magn. Reson. Spectrosc.*, 1996, **28**, 283-350.
10. A. D. Sherry, P. P. Yang and L. O. Morgan, *J. Am. Chem. Soc.*, 1980, **102**, 5755-5759.
11. P. Atkins and J. de Paula, *Physical Chemistry*, 4th edn., Oxford University Press, Oxford, 2002.
12. K. Enomoto, J. A. LaVerne, S. Seki and S. Tagawa, *J. Phys. Chem. A*, 2006, **110**, 9874-9879.
13. S. Petoud, G. Muller, E. G. Moore, J. Xu, J. Sokolnicki, J. P. Riehl, U. N. Le, S. M. Cohen and K. N. Raymond, *J. Am. Chem. Soc.*, 2007, **129**, 77-83.
14. J. Autschbach, L. Nitsch-Velasquez and M. Rudolph, *Top. Curr. Chem.*, 2011, **298**, 1-98.
15. R. S. Dickins, J. A. K. Howard, C. L. Maupin, J. M. Moloney, D. Parker, J. P. Riehl, G. Siligardi and J. A. G. Williams, *Chem. Eur. J.*, 1999, **5**, 1095-1105.
16. P. G. Graham and D. C. Weatherburn, *Aust. J. Chem.*, 1984, **37**, 2243-2247.
17. P. Caravan, J. J. Ellison, T. J. McMurry and R. B. Lauffer, *Chem. Rev.*, 1999, **99**, 2293-2352.
18. R. B. Lauffer, *Chem. Rev.*, 1987, **87**, 901-927.
19. S. H. Koenig and R. D. Brown, *Prog. Nucl. Magn. Reson. Spectrosc.*, 1990, **22**, 487-567.
20. J. P. Jesson, *NMR of Paramagnetic Molecules*, Academic Press Inc., New York, 1973.
21. S. Aime, A. S. Batsanov, M. Botta, J. A. K. Howard, D. Parker, K. Senanayake and G. Williams, *Inorg. Chem.*, 1994, **33**, 4696-4706.
22. A. D. Sherry, R. D. Brown, C. F. G. Geraldes, S. H. Koenig, K. T. Kuan and M. Spiller, *Inorg. Chem.*, 1989, **28**, 620-622.

5. Emissive Europium Complexes Incorporating Arylalkynylpyridyl Chromophores

5.1 Introduction

As the previous chapters reported, a considerable amount of work was devoted to developing a Eu^{3+} complex with an optimised emission spectral form. The C_3 symmetric complex [Eu·L[9]] comprises a 1,4,7-triazacyclononane macrocycle with three pyridyl phenylphosphinate groups. The emission spectrum of [Eu·L[9]] has a large relative $\Delta J = 2$ band and is very well suited to the desired FRET application. The emission is also stable in the presence of a number of common quenchers and competitors, including Mn^{2+}. At this stage in the project, attention was focussed upon the remaining specification points, outlined in *Chapter 1*. The final target complex must include a chromophore that is able to sensitise Eu^{3+} emission at a wavelength above 300 nm. The complex should have a large molar extinction coefficient and emission quantum yield. Aqueous solubility and a position from which a vector can be conjugated are the final two specification points.

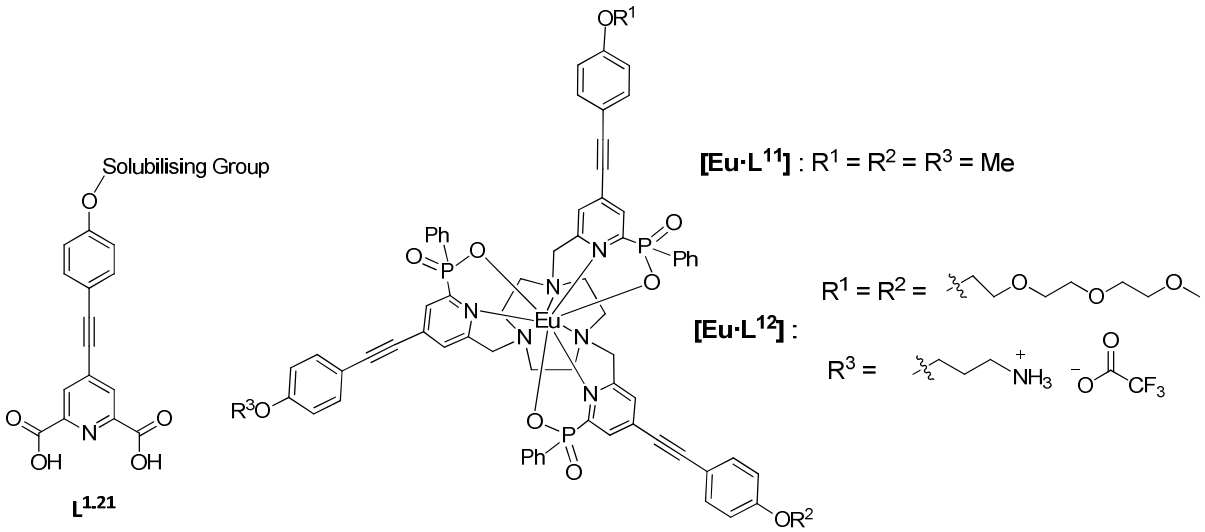

The work in this chapter aims to meet these final points. The core structure of the target complex is the same as that of [Eu·L[9]], so as to retain the favourable emission spectral form and emissive stability. The three pyridyl groups will be modified to form chromophores, whose properties must meet the remaining targets regarding the molar extinction coefficient and quantum yield. One possible chromophore that could be incorporated is the 3-azaxanthone introduced in *Chapter 2*. However, it was concluded that incorporation of this moiety into Eu^{3+} complexes did not show large enough improvements upon the currently used complex, $[Eu\cdot L^{1.1}]^{3+}$. A second option is the pyridylalkynylaryl chromophores, which were discussed in *Section 1.3.4*. Electron rich aryl groups result in internal charge transfer absorption bands with large molar extinction coefficients. The di-carboxylate ligand ***L*[1.21]** was developed during the course of this project by Maury.[1] It is able to sensitise Eu^{3+} emission with excellent photopyhsical properties (λ_{ex} = 332 nm, ε = 25,000 M^{-1} cm^{-1}). Incorporation of alkynylaryl moieties into the 4- position of the pyridyl phenylphosphinate groups of [Eu·L[9]] gives the

complexes [Eu·L[11]] and [Eu·L[12]]. The former is a model complex designed to investigate the photophysical properties of this new chromophore and the latter includes two polyethylene glycol chains to increase aqueous solubility and a primary amine as a point for conjugation. This chapter details the synthesis and characterisation of these complexes. A third complex was also synthesised, $[Eu\cdot L^{13}]^+$, in which only two of the 1,4,7-triazacyclononane nitogens are alkylated with chromophoric moieties. The resultant ligand is 7-coordinate and $[Eu\cdot L^{13}]^+$ has a single bound H_2O molecule in aqueous solution. Addition of various anions and protein cause a change in the form and intensity of the Eu^{3+} emission, as a result of displacement of the labile solvent molecule. This complex is highly emissive and responsive to its environment, and may have potential as an intracellular probe.

5.2 A New Chromophore

5.2.1 Synthetic Aspects

To allow formation of a longer wavelength absorbing chromophore from the pyridyl moiety in [Eu·L[9]], functionalisation in the pyridyl *para* position is required. A halide leaving group (Cl^-, Br^- or I^-) opens up the possibility of transition metal catalysed cross coupling reactions with the alkynylaryl moiety. The first attempt to introduce such functionality was with the phenylphosphinate ***21***. N-oxide formation with MCPBA was followed by nitration with concentrated H_2SO_4 and HNO_3. The intention was to then convert the NO_2 group into a Br group. Two problems arose during the nitration step which made this route unfeasible (*Scheme 5.1*). Firstly, the ethyl phosphinate ester hydrolysed under the reaction conditions and secondly, nitration also took place at the para position in the phenyl group. While the resultant OH group can be re-esterified, using triethyl orthoformate, selective removal of the phenyl NO_2 is less straightforward. As a result, an alternative reaction pathway was sought.

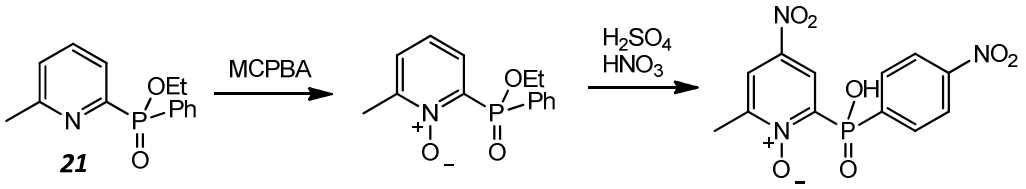

Scheme 5.1

An alternative route was undertaken to functionalise the starting material 2-bromo-6-methylpyridine (***17***). Again, N-oxide formation with MCPBA was followed by nitration (H_2SO_4 / HNO_3, *Scheme 5.2*). The resulting *para*-nitro N-oxide ***38*** was isolated by dropping the reaction mixture into ice, causing a pale yellow precipitate to form. Formation of ***38*** was achieved on a 30 g scale.

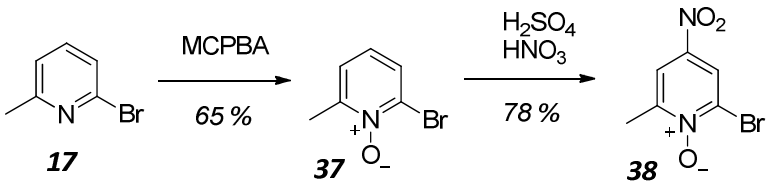

Scheme 5.2

Prior to conversion of the *para*-NO_2 group to Br, the coupling reaction with ethyl phenylphosphinate was undertaken to ensure selective substitution in the pyridyl *ortho* position. Several routes were attempted (*Scheme 5.3*). Firstly, coupling was attempted between the N-oxide intermediate ***38*** and ethyl phenylphosphinate, using $Pd(PPh_3)_4$ as a catalyst. The reaction did not proceed, most likely due to oxidation of the catalyst to Pd(II) by the pyridyl N-oxide. Alternative routes were tried with greater success. Treatment of ***38*** with $Fe_{(s)}$ in AcOH led to the removal of the N-oxide and reduction of NO_2 to NH_2, giving 2-bromo-4-amino-6-methylpyridine. In the absence of the N-oxide, coupling was achieved in a 42 % yield. A second route was also attempted in which the nitro group was left intact and the pyridyl N-oxide was removed using PBr_3 to give 2-bromo-4-nitro-6-methylpyridine (***39***). The coupling reaction was, again, successful affording the *para*-nitro pyridine phosphinate ***40***. The yield of the coupling reaction was comparable for the *para*-NO_2 and *para*-NH_2 reactants.

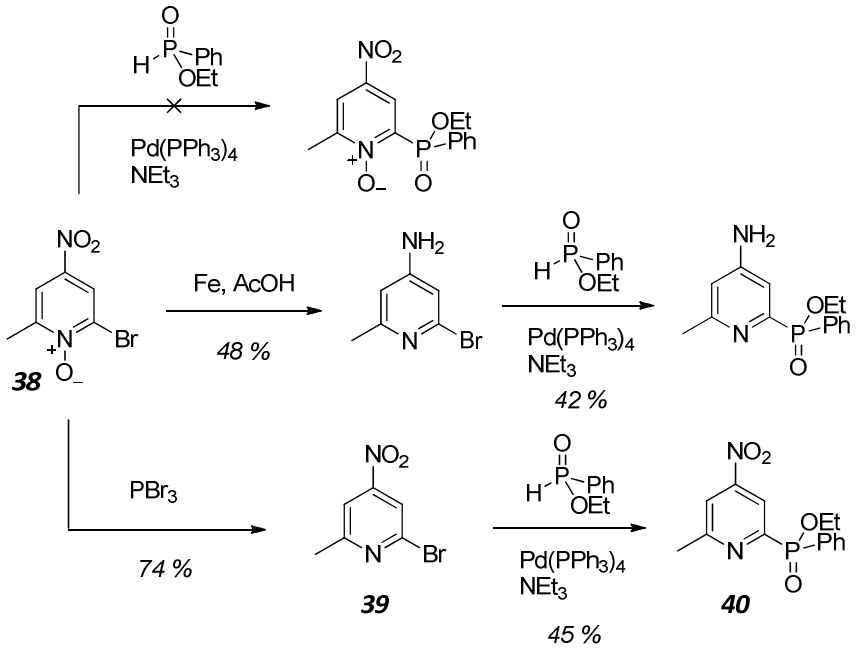

Scheme 5.3

The *para*-NO_2 compound (***40***) was deemed to be the intermediate which could be brominated with greater ease. Conversion of the nitro group to a bromo group was accomplished by stirring ***40*** in neat acetyl bromide (70 °C, 16 h). The resultant reaction mixture was dropped cautiously into ice cold CH_3OH, which converts acetyl bromide to methyl acetate and HBr, which can be removed under reduced pressure. Hydrolysis of the ethyl phosphinate ester is unavoidable under the reaction conditions. Re-esterification was achieved by stirring the phosphinic acid in refluxing triethylorthoformate for 72 hours. The full synthesis is shown in *Scheme 5.4*. Purification of ***42*** was achieved by column chromatography on silica. Upon the initial scale-up of the palladium cross coupling step (***39*** → ***40***) from 100 mg to 2 g scale, the yield was found to be reduced to less than 10 %. The majority of the starting material ***39*** was recovered and it was concluded that degradation of the catalyst was responsible for low yield. It was found that the yield could be increased using a number of simple procedures, prior to reaction. Firstly, starting materials of high purity were used (> 98 %, determined by ^{1}H-NMR). Each starting material was free from solvents such as $CHCl_3$, which

can poison the catalyst. Before carrying out the reaction, the 2-bromo-6-methyl-4-nitropyridine was dissolved in toluene and dried thoroughly under reduced pressure and high vacuum to ensure removal of all such solvents. The catalyst used was fresh $Pd(PPh_3)_4$, stored under an atmosphere of argon. As with all air sensitive cross coupling reactions, the solvent was degassed (freeze-thaw cycle) three times to remove dissolved oxygen, which inactivates the catalyst. After addition of each starting material the solution was degassed once and after addition of all the starting materials the solution was degassed a further three times. Using these procedures, the reaction was successful on a 3 g scale, with a yield, after purification, of 45 %.

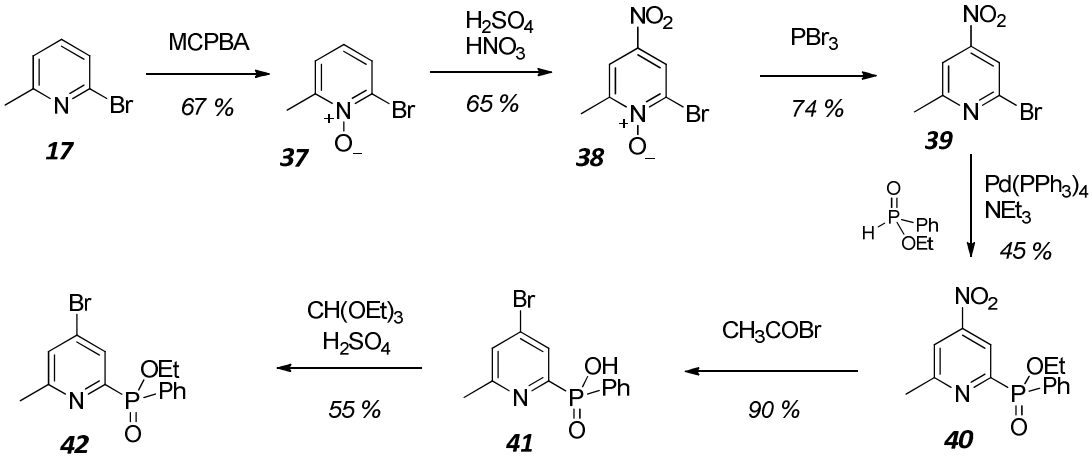

Scheme 5.4

With the *para*-Br group in place, Sonogashira cross coupling was achieved with the commercially available 4-ethynylanisole (*Scheme 5.5*). The general reaction mechanism is believed to involve the oxidative addition of the pyridyl bromide to Pd(0), after dissociation of at least one PPh_3 ligand. The alkyne is activated by coupling to Cu(I) before being transferred to the Pd centre. Reductive elimination of the coupled compound converts Pd(II) back to Pd(0), which goes on to initiate further reactions. The reaction proceeded in high yield, although purification of ***43*** by column chromatography on silica was made slightly more difficult by the presence of $POPh_3$, formed from dissociated PPh_3, as both compounds have similar R_f values (silica, CH_2Cl_2 : 5 % CH_3OH).

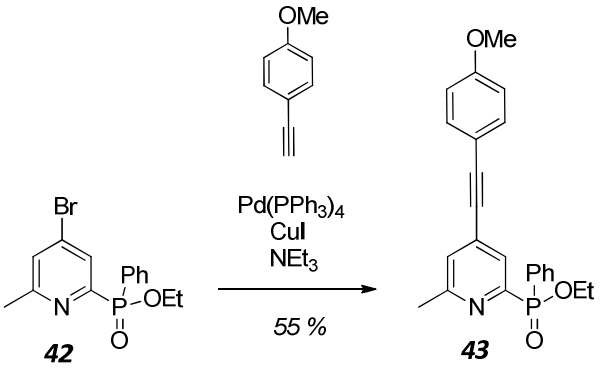

Scheme 5.5

5.2.2 Photophysical Properties

The absorption properties of ***43*** were measured in methanol at 295 K (*Figure 5.1* and *Table 5.1*). The absorption spectrum shows a broad transition centred at 320 nm, assigned as an internal charge transfer (ICT) band from the electron-rich aryl O to the electron deficient pyridyl group. A similar absorption profile is observed for the related compound ***L***$^{1.21}$, which has the same arylalkynylpyridyl core structure.[2] The 3-azaxanthone chromophore, ***5***, has a similar absorption maximum but has a narrower absorption band (*Figure 5.1*), previously ascribed as a π-π* transition with significant n-π* character.[3] The extinction coefficient of ***43*** was found to be 26,500 M^{-1} cm^{-1} at 320 nm. This is around a five-fold increase, relative to the 3-azaxanthone chromophore, and is very encouraging, considering that the final target Eu^{3+} complex will have three chromophores.

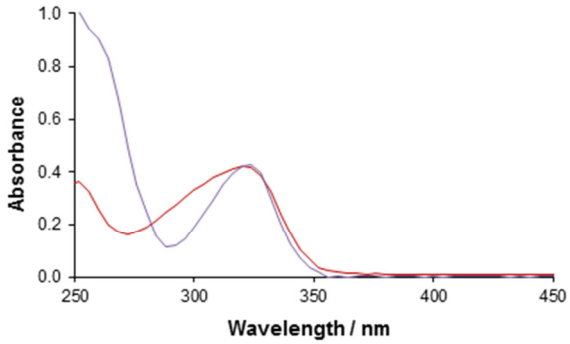

Figure 5.1 Absorption spectra of the chromophore ***43*** (*red*) and 3-azaxanthone ***5*** (*purple*) (MeOH, 295 K).

To assess whether the chromophore ***43*** has the potential to sensitise Eu^{3+} emission, measurement of the triplet energy was undertaken. A suitable sensitiser will have a triplet energy around 2,000 cm^{-1} above the Eu^{3+} excited state (17,200 cm^{-1}), to maximise energy transfer, while minimising back energy transfer. To measure the triplet energy, ***43*** was dissolved in EPA (ether : isopentane : ethanol, 5:5:2; A = 0.1). The solution was cooled to 77 K, using an optical cryostat. The emission spectrum of the resultant glass was measured following excitation at 320 nm (*Figure 5.2*). The highest energy phosphorescence band, centred at 469 nm, was attributed to the 0 – 0 transition from the triplet excited state to the ground state, giving a triplet energy estimation of 21,300 cm^{-1}. Further emission bands can be seen in the spectrum at longer wavelengths which can be assigned to emission from the triplet excited state to higher vibrational energy levels of the ground state. A triplet energy of 21,300 cm^{-1} indicates that the chromophore ***43*** should be capable of sensitising Eu^{3+} emission ($^5D_0$ energy level lies at 17,200 cm^{-1}), providing that the triplet energy does not decrease upon complexation or moving to aqueous conditions.

Table 5.1 Comparative photophysical data for three chromophores: the arylalkynylphenylphosphinate ***43***; the arylalkynyl di-carboxylate ***L***$^{1.21}$ and the 3-azaxanthone ***5***. All values measured in MeOH at 295 K, except E_T values, which are measured in an EPA glass at 77 K.

Chromophore	λ_{max} **/ nm**	ε **/ M^{-1} cm^{-1}**	E_T **/ cm^{-1}**
Alkynyl Phosphinate, *43*	320	26,500	21,300
3-Azaxanthone, *5*	324	5,600	23,700
Alkynyl Carboxylate, ***L*$^{1.21}$**	332	26,200	-

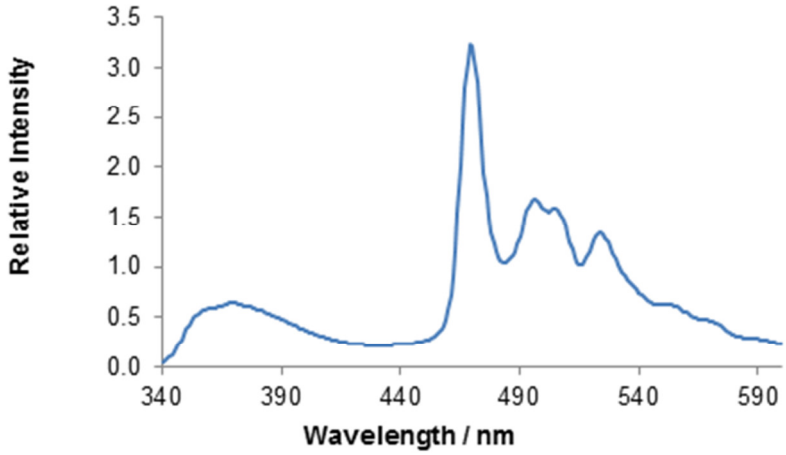

Figure 5.2 Emission spectrum of alkynyl chromophore ***43*** at 77 K (EPA glass, λ_{ex} = 320 nm).

5.3 The Model Complex

5.3.1 Synthetic Aspects

Having established that the chromophore ***43*** has potential as a sensitising group for Eu^{3+} emission, incorporation into a model complex was the next challenge. To allow alkylation with the 1,4,7-triazacyclononane, activation of the methyl group was required. A first attempt at bromination was made using N-bromosuccinimide (NBS) and dibenzoyl peroxide via a radical reaction (*Scheme 5.6 a*). No bromination of the methyl group was observed, even when employing irradiation from a 100 W tungsten lamp, 2 equivalents of NBS and heating at 80 °C. Changes in the ^{1}H-NMR spectrum and TLC showed that the starting material had been consumed. Side reactions, such as radical addition to the alkyne, are likely to account for the unsuccessful reaction. A second attempt involving oxidation of the methyl group to an aldehyde, followed by reduction to an alcohol and subsequent bromination was undertaken using selenium dioxide as the oxidising agent (*Scheme 5.6 b*). This attempt showed no CHO formation. After refluxing in dioxane for 14 h, the starting material was recovered, unchanged.

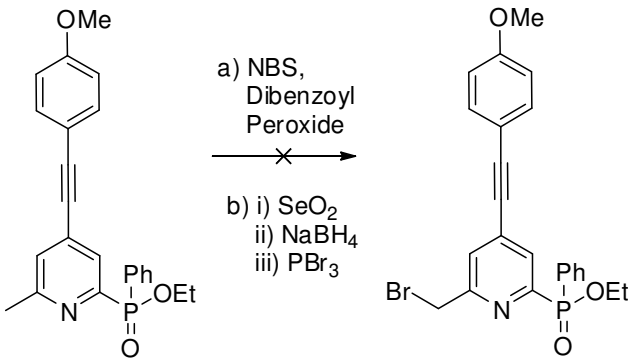

Scheme 5.6

Having found difficultly in activating the methyl group in the presence of the alkyne, an alternative route was devised (*Scheme 5.7*), in which the methyl group is activated prior to the palladium cross coupling reaction. For example, an acetyl group can be converted into a leaving group, using reaction conditions which do not interfere with the C – C triple bond. Acetylation of the methyl group was achieved by stirring the N-oxide ***44*** in acetic anhydride at 120 °C. The reaction mechanism is believed to proceed via the formation of an N-acetate, before rearrangement to the acetate ***45***.[4] With the acetate group in place, the cross coupling reaction proceeded in high yield, in part due to the ease of purification of ***46*** by column chromatography, as its R_f value is less close to that of $POPh_3$ than the previously synthesised alkyne ***43*** (*see Section 5.2.1*). Hydrolysis of the acetate group was achieved in an anhydrous ethanolic solution of NaOEt. Under these conditions, the acetate group is cleaved but the phosphinate ethyl ester is retained. Conversion of the resultant alcohol to a bromide with one equivalent of PBr_3 took place over 1 h at 20 °C.

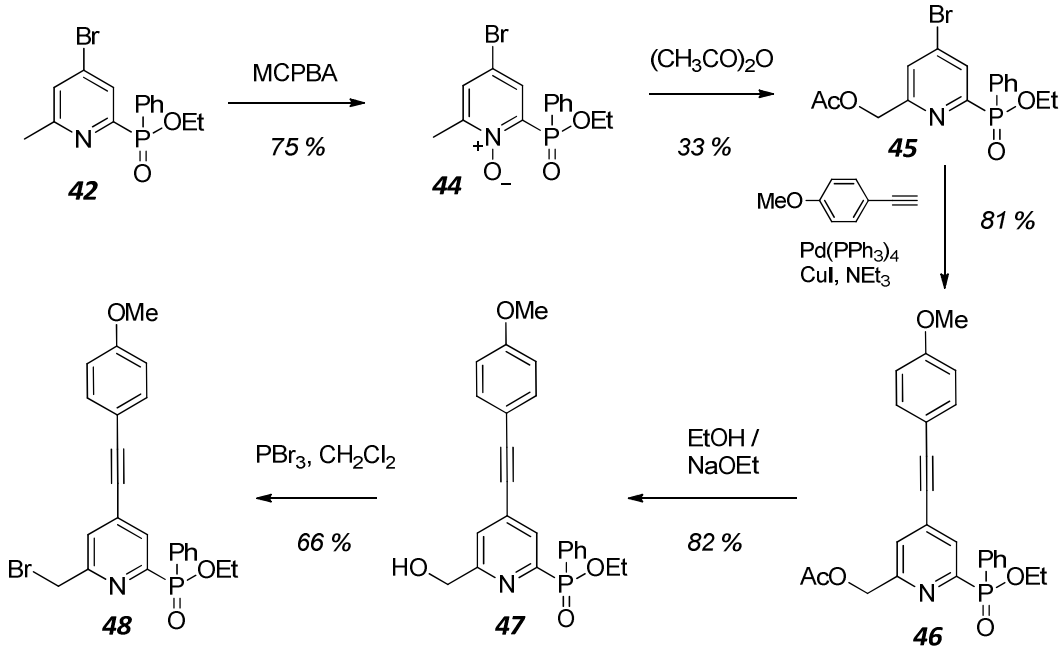

Scheme 5.7

Initially, the hydrolysis step ***46*** → ***47*** was attempted in anhydrous methanolic NaOMe. Under these conditions, the alcohol was formed and the ethyl phosphinate ester was converted to a methyl phosphinate ester. Subsequent reaction to transform the alcohol into a leaving group with PBr_3, PCl_3 and NBS/PPh_3 were all unsuccessful, due to de-methylation of the methyl phosphinate ester. No de-ethylation was observed for the ethyl phosphinate ester ***47***.

Alkylation of 1,4,7-triazacyclononane, with three equivalents of the brominated intermediate ***48***, was followed by hydrolysis of the ethyl phosphinate esters and complexation with $Eu(OAc)_3$ (*Scheme 5.8*). The alkylation step was monitored by LCMS and stopped prior to formation of any tetra-substituted product. Some mono- and di-substituted products were present in the crude reaction mixture, leading to the low observed yield. Purification of ***49*** was achieved by column chromatography on silica. The hydrolysis of ***49*** was carried out on a 10 mg scale with NaOD in deuterated solvents (1 mL), which allowed the reaction to be monitored by ^{1}H-NMR. Once hydrolysis was completed, the pD of the solution was adjusted to 6.2 and complexation with $Eu(OAc)_3$ was carried out. As with the [Ln·L[9]] series, purification of [Eu·L[11]] was possible by short-path column chromatography on silica, using a mobile phase comprising CH_2Cl_2 and CH_3OH (95 : 5, isocratic elution). The product was visualised by TLC as a bright pink/red spot, under irradiation at 365 nm. Identification of [Eu·L[11]] and assessment of purity were carried out by HRMS and RP-HPLC.

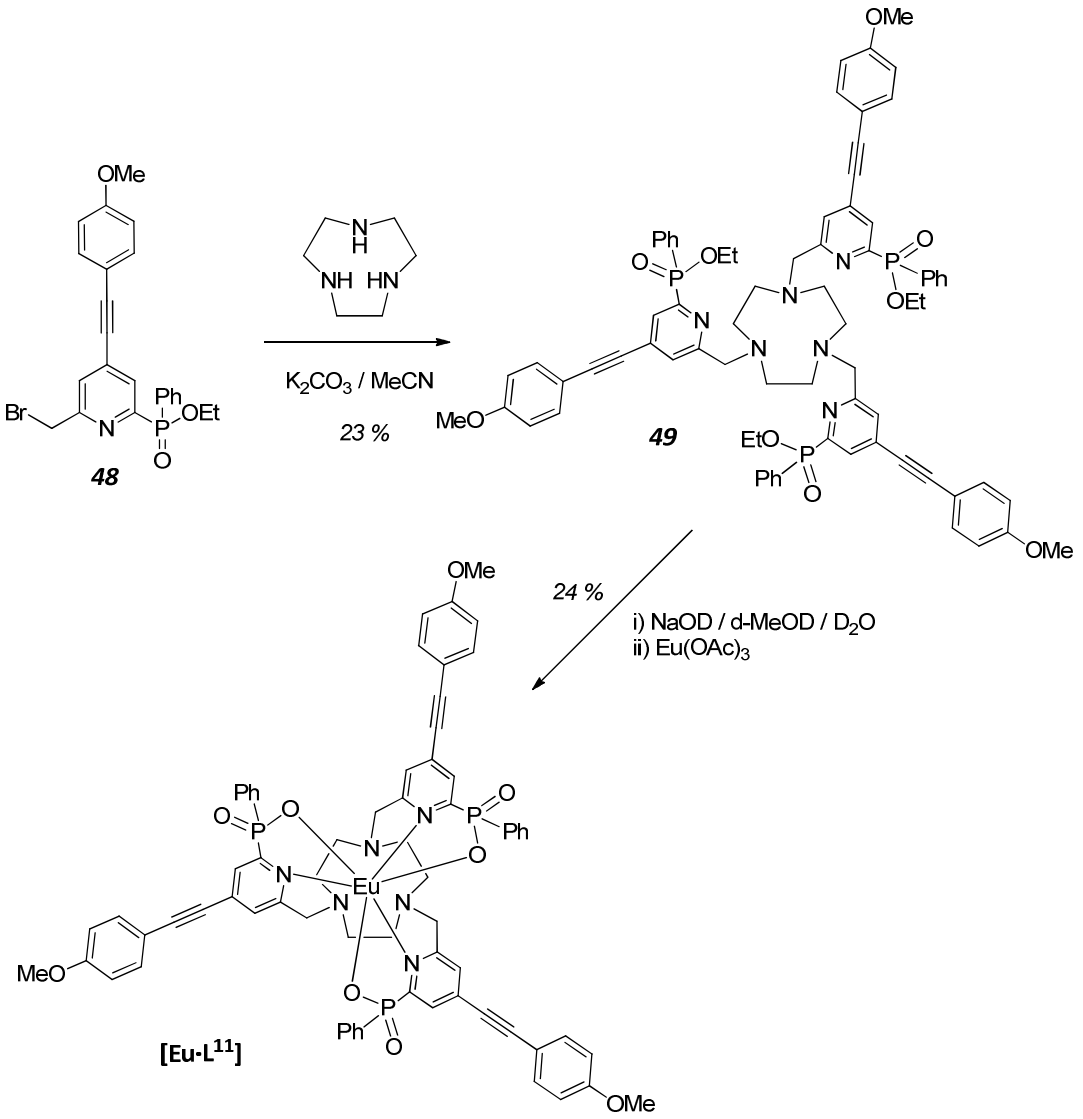

Scheme 5.8

5.3.2 Structural Assignment

Comparison of the ^{1}H-NMR spectrum of [Eu·L^{11}] with the parent complex [Eu·L^{9}] reveals that the solution state stereochemistry of the two complexes is very similar (*Figure 5.3*). The total number of resonances (20 inequivalent Hs) indicates C_3 symmetry. The 6 inequivalent shifted ring proton resonances (4 ring and 2 methylene linker group protons), which are similar in both spectra (7.5 ppm, 4.5 ppm and 4 resonances between 0 and -5 ppm), show that the core structure about the Eu^{3+} centre is unaffected by the additional arylalkynyl groups. Additional aromatic peaks and the resonance due the three equivalent OMe groups (3.8 ppm) are present in the [Eu·L^{11}] spectrum. The conclusion from the ^{1}H-NMR analysis is that the stereochemistry about the Eu^{3+} centre of [Eu·L^{11}] is the same as that of [Eu·L^{9}]: a slightly distorted tricapped trigonal prism, existing as enantiomers of a single diastereomer ((*RRR*)-Λ($\delta\delta\delta$) and (*SSS*)-Δ($\lambda\lambda\lambda$)). The ^{31}P-NMR, which shows a single resonance, confirms the presence of a single diastereomer.

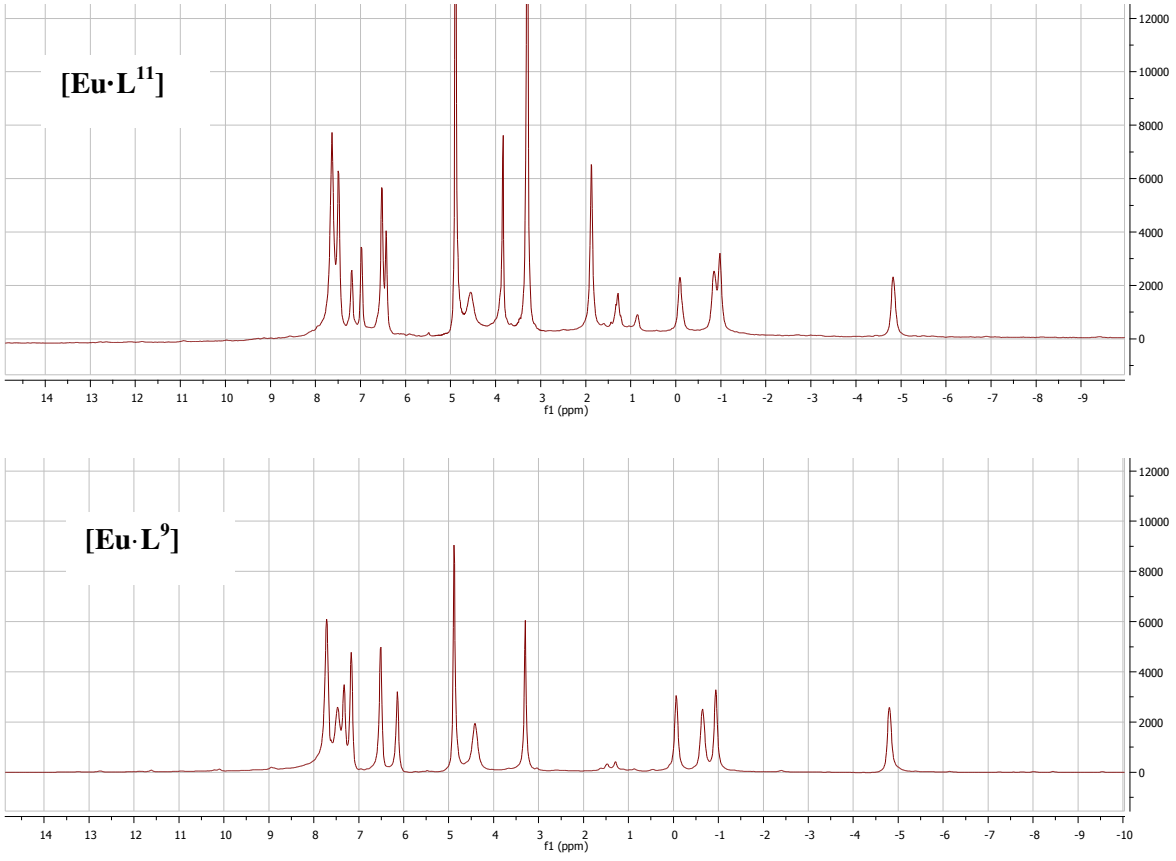

Figure 5.3 ^{1}H-NMR spectra of [Eu·L^{11}] (*upper*) and [EuL^{9}] (*lower*) (d-MeOD, 400 MHz, pD 6.2, 295 K).

Upon standing in a MeOH : H_2O solution (0.5 mL, 2 : 1 *v*/*v*), several single crystals of [Eu·L^{11}] formed, allowing the solid state structure to be investigated by X-ray diffraction. As in the solution state, the pseudo C_3 symmetry about the Eu^{3+} centre is apparent, with the three arylalkynyl groups extending away from the core of the complex (*Figure 5.4*). The angle between the three alkynyl rods shows deviation from 120°, in part due to the presence of disordered solvent molecules in the unit cell. As with the solid state structure of the parent complex [Eu·L^{9}], the new complex [Eu·L^{11}] is a

distorted tricapped trigonal prism, which exists as a single diastereoisomer. The unit cell contains four complexes as two pairs of enantiomers. As was expected, the presence of the three arylalkynyl groups does not alter the core structure of [Eu·L^{11}], relative to the parent complex. Bond lengths for Eu – O, Eu – N_{py} and Eu – N_{ring} and very similar for [Eu·L^{9}] (2.33, 2.66 and 2.68 Å, respectively) and [Eu·L^{11}] (2.32, 2.66 and 2.68 Å, respectively). As the core structure is unchanged, it is anticipated that the favourable photophysical properties of [Eu·L^{9}] will also be retained in the model complex, [Eu·L^{11}].

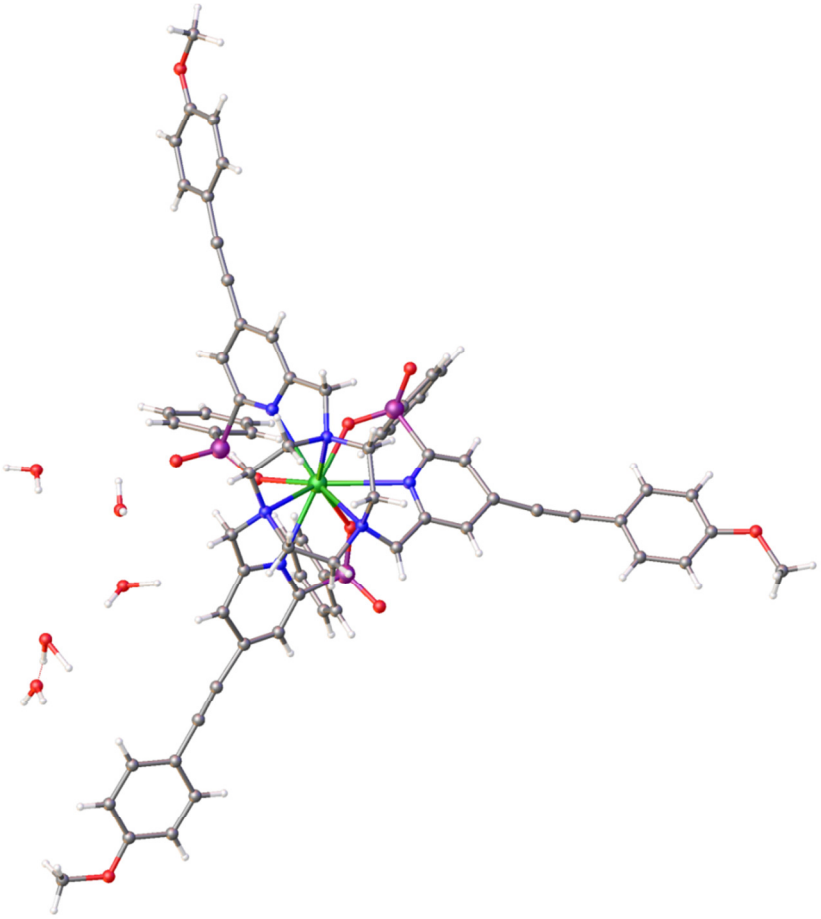

Figure 5.4 Solid state structure of [Eu·L^{11}], assigned by X-ray diffraction studies.

5.3.3 Photophysical Characterisation

The aqueous solubility of [Eu·L^{11}] is very low, due to the combination of three hydrophobic phenyl groups and the arylalkynyl rods. As a result, all photophysical measurements were carried out in methanol. The final target complex must be soluble in water and it is worth noting that, in general, the photophysical properties of emissive complexes are dependent upon the solvent. Despite this, the values of [Eu·L^{11}] in methanol will give some indication of the properties of subsequent water soluble analogues.

The absorption spectrum of [Eu·L^{11}] shows a broad absorption band centred at 332 nm, with a slight shoulder at around 305 nm (*Figure 5.5*). Comparison with the spectrum for the parent methyl-chromophore, ***43*** shows a red shift of 12 nm. As the solvent in the same in each case, this effect must be due to complexation with Eu^{3+}. The absorption is believed to involve an ICT transition with charge

flowing from the aryl oxygen to the pyridyl nitrogen. A possible explanation for the increase in maximum absorption wavelength is that upon complexation, the nitrogen is bound to the positively charged Eu^{3+} centre, stabilising the LUMO, resulting in a decrease in energy of the charge transfer transition. The extinction coefficient of [Eu·L[11]] at 332 nm was found to be 58,000 M^{-1} cm^{-1}. Whilst, this value is not quite three times that of the parent chromophore ***43*** (ε = 26,500 M^{-1} cm^{-1}), it is impressively high and is very encouraging.

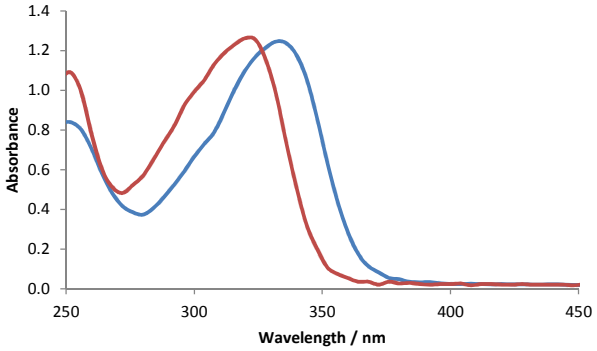

Figure 5.5 Absorption spectra for the alkynyl chromophore ***43*** (*red*) and [Eu·L[11]] (*blue*), which incorporates the same chromophore (MeOH, 295 K).

The emission spectrum for [Eu·L[11]] was measured in methanol, following excitation at 332 nm (*Figure 5.6*). No fluorescence is observed below 500 nm, indicating that the arylalkynylpyridyl chromophore is efficiently populating the Eu^{3+} excited state. The form of the emission spectrum is relatively simple, showing no splitting in the $\Delta J = 1$ band and two predominant bands in the $\Delta J = 2$ manifold. This is indicative of the solution state C_3 symmetry revealed by ^{1}H-NMR analysis. Comparison of [Eu·L[11]] and [Eu·L[9]] shows that the two emission spectra are very similar (*Figure 5.7*). This reinforces the understanding that the symmetry and coordination environment about Eu^{3+} determine the form of the emission spectrum and relative intensity of the various transitions. Upon closer inspection of the two spectra, it is apparent that the presence of the conjugated chromophore leads to a further increase in the relative intensity of the hypersensitive $\Delta J = 2$ transition. The $\Delta J = 2$: $\Delta J = 1$ ratio, which quantifies this effect, has increased from 4.09 for the parent complex to 7.10.

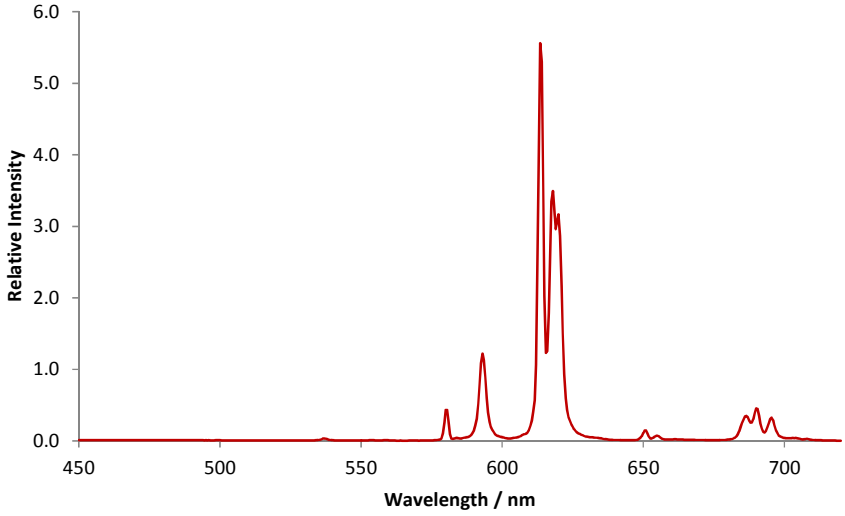

Figure 5.6 Emission spectrum for [Eu·L[11]] (MeOH, λ_{ex} = 332 nm, 295 K).

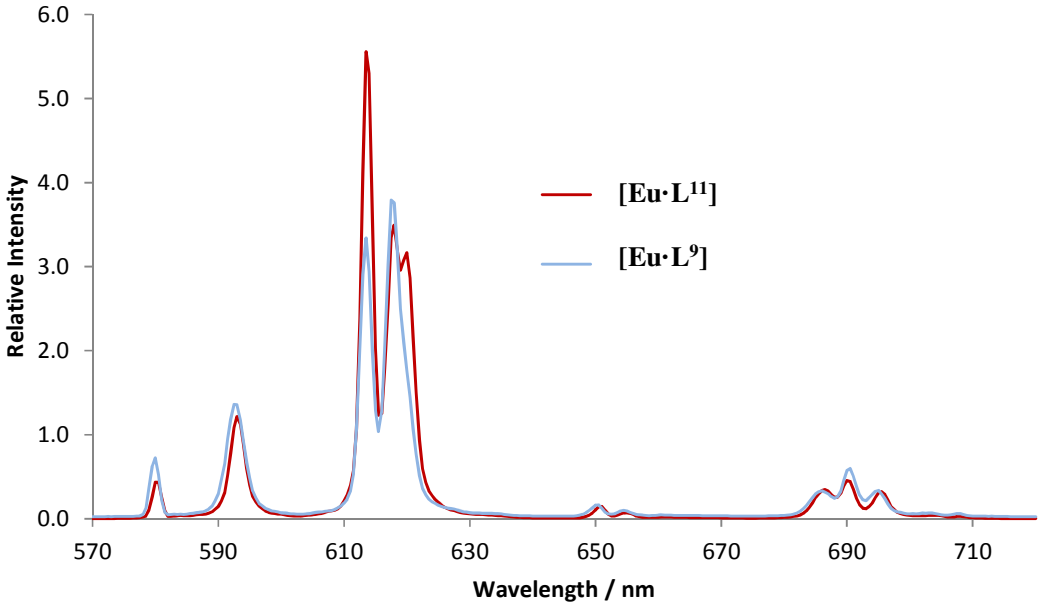

Figure 5.7 Comparison of the emission spectra of [Eu·L[11]] (*red*, λ_{ex} = 332 nm, MeOH, 295 K) and [Eu·L[9]] (*blue*, λ_{ex} = 274 nm, MeOH, 295 K). Spectra have been scaled so that the total integrated emission is the same in each case.

The excellent ability of the arylalkynylpyridyl chromophore to sensitise the Eu^{3+} excited state is clear from the intense emission. The mechanism by which sensitisation occurs has been proposed for the dicarboxylate analogous complex (*Figure 5.8 right*).[2] The proposed mechanism involves transfer of energy from a relaxed charge transfer state to the Eu^{3+} excited state (*Figure 5.8 left*). A similar mechanism is likely to account for the sensitisation by the arylalkynylpyridyl chromophore.

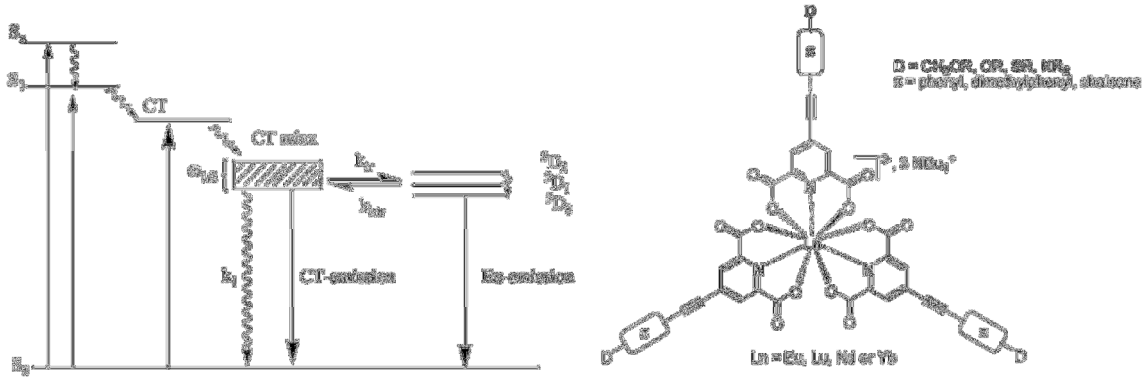

Figure 5.8 Jablonski diagram for the proposed sensitisation mechanism by which Eu^{3+} sensitisation occurs in the complex shown.[2]

Two methods were employed to measure the emission quantum yield of the new complex. Firstly, the quantum yield was measured against standards, including [Eu·L[1]], $[Eu\cdot L^2]^+$ and the tris(bipyridine) complex, $[Eu\cdot L^{1.1}]^{3+}$. The second method utilises an integrating sphere and is a direct measurement of the photons absorbed and photons emitted.[5] In each case a quantum yield of 52 ± 10 % was found. This is an exceptionally high quantum yield for a Eu^{3+} complex in solution and, when combined with the molar extinction coefficient of 58,000 M^{-1} cm^{-1}, the overall brightness (defined as $\varepsilon \times \Phi$) of [Eu·L[11]] is extraordinarily high.

5.3.4 Emissive Stability

Despite the low aqueous solubility of [Eu·L^{11}], it was possible to carry out stability assays, in which the complex concentration is 10 nM in aqueous buffered solution (0.1 M HEPES). For the first time throughout the project the Eu^{3+} emission is not greatly perturbed by any of the additives (*Figure 5.9*). As with the parent complex, Mg^{2+}, Ca^{2+} and $EDTA^{4-}$ did not cause any significant amount of dissociation of [Eu·L^{11}] and Mn^{2+} did not quench the Eu^{3+} emission. In contrast to the parent system, the ability of [Eu·L^{11}] to absorb incident light at 332 nm means that the competitive absorption of light from the two proteins is no longer problematic and more than 80 % of the Eu^{3+} emission is retained in the presence of either protein after 15 min. After 18 h incubation, small decreases in Eu^{3+} emission were observed. Despite this, [Eu·L^{11}] remains the complex with the highest emissive stability synthesised up to this point in the project, and is comparable with the currently used [Eu·L$^{1.1}$]$^{3+}$ tris(bipyridine) complex.

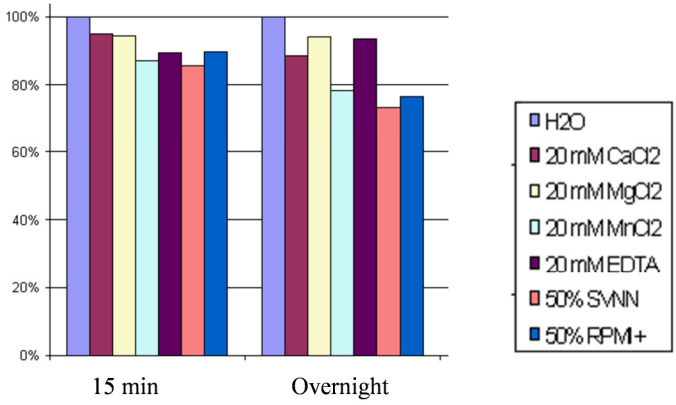

Figure 5.9 Stability data for [Eu·L^{11}] in HEPES buffer (0.1 M) at two time points, 15 min and 18 h (10nM complex, λ_{ex} = 335 nm, λ_{ex} = 620 nm).

5.3.5 The Terbium Analogue

To investigate whether the pyridylalkynylaryl chromophore is able to sensitise Tb^{3+} emission, [Tb·L^{11}] was synthesised by an analogous pathway to [Eu·L^{11}], exchanging $Eu(OAc)_3$ for $Tb(OAc)_3$. Following excitation at 332 nm, the emission spectrum of [Tb·L^{11}] was measured (*Figure 5.10*). An exceptionally weak emission spectrum was found, indicating that the chromophore is not able to efficiently populate the Tb^{3+} excited state. Deoxygenating the sample led to an enhancement in the Tb^{3+} emission, suggesting that back energy is taking place from the Tb^{3+} excited state to the sensitiser excited state, which is susceptible to quenching by molecular oxygen. Comparison of the Tb^{3+} $^5D_4$ excited state (20,400 cm^{-1}) with the sensitiser triplet state (21,300 cm^{-1}), shows that the two states are within the 2,000 cm^{-1} limit, required to avoid back energy transfer. Consequently, this chromophore is not suitable for sensitisation of Tb^{3+} emission. Modifications of the pyridylalkynylaryl chromophore, which lead to an increase in the excited state energy levels, are required to achieve Tb^{3+} sensitisation, and are beyond the scope of this project.

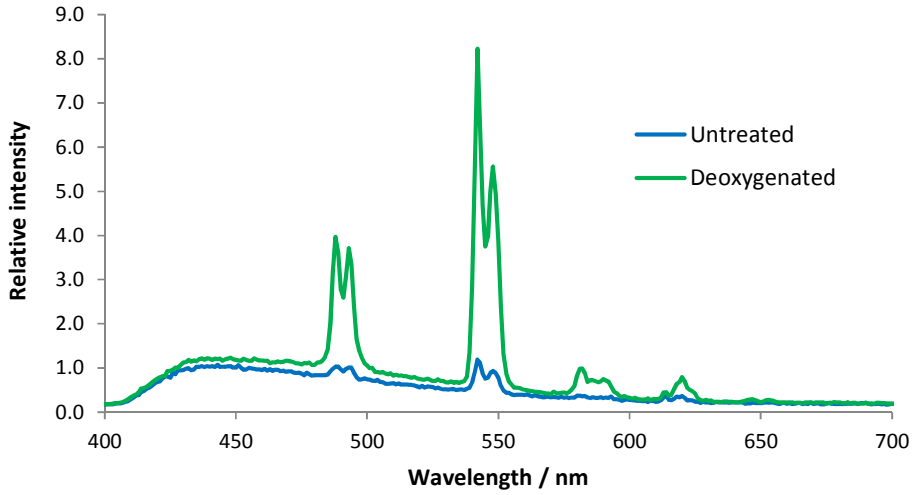

Figure 5.10 Emission spectrum for [Tb·L[11]] prior to (*blue*) and after (*green*) bubbling argon through the solution for 30 s (MeOH, λ_{ex} = 332 nm, 295 K).

The inability of the arylalkynylpyridyl chromophore to sensitise Tb^{3+} gives some indication of which energy levels are involved in the sensitised emission pathway. It is proposed that in the Ln^{3+} complexes, the ICT band, which is broad, has some overlap with the triplet state (*Figure 5.11 left*). The energy of the sensitiser excited states are close to the Tb^{3+} emissive state, allowing back energy transfer, whereas the Eu^{3+} emissive state is lower in energy and back energy transfer does not occur. The 77 K emission spectrum of the arylalkynylpyridyl chromophore, ***43***, and the complex [Gd·L[11]], show the appearance of the broad ICT band (centred at 362 nm) upon complexation, which overlaps with the triplet state at around 469 nm (*Figure 5.11 right*).

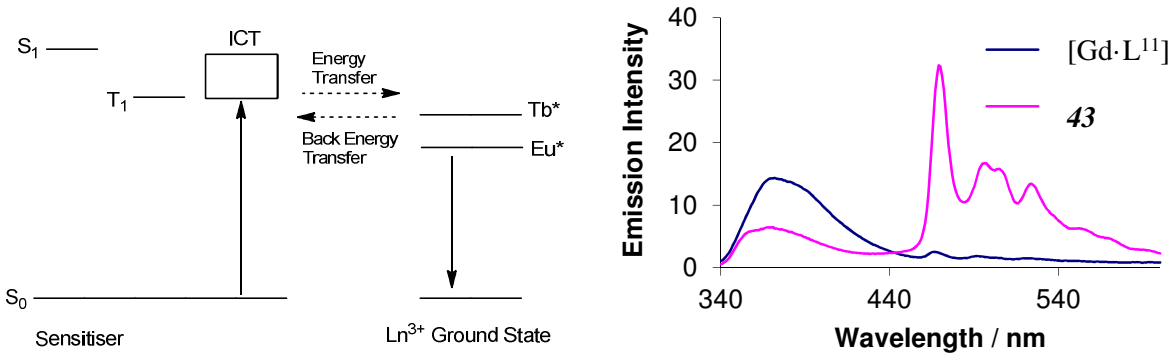

Figure 5.11 *left*) Jablonski diagram showing the proposed sensitised emission pathway and *right*) the 77 K emission spectra of [Gd·L[11]] (*blue*) and the arylalkynylpyridyl chromophore ***43*** in (EPA glass, λ_{ex} = 320 nm).

5.4 The Final Complex

The model complex, [Eu·L^{11}], has excellent photophysical properties, albeit in methanol. It was decided that an analogous complex with greater aqueous solubility would be an ideal candidate to test in the HTRF experiment. One final specification point was to incorporate a group which allows conjugation between the complex and a vector, which can be tagged onto an antigen or antibody. To fulfil these final two criteria, the model complex was modified by the addition of two short polyethylene glycol chains and a primary amine. The design of the final complex positioned these additional groups in the place of the three aryl OMe groups, with the intention of minimally perturbing the photophysical properties of the model complex.

5.4.1 Synthetic Aspects

The synthesis of [Eu·L^{12}] (*Scheme 5.9*) followed a similar reaction pathway to that of [Eu·L^{11}]. Exchanging ethynyl anisole for either the polyethylene glycol (PEG) or $(CH_2)_3$NHBOC containing alkynyl moiety, led to the two brominated intermediates, ***54*** and ***55***. The two trimethylsilyl protected alkynyl moieties were provided by CISbioassays.[6] The cross coupling reaction was carried out in the same manner as for the synthesis of [Eu·L^{11}], with the addition of tetrabutylammonium fluoride (TBAF), which cleaves the Si-C bond, leaving the free alkyne. The synthesis of the PEG containing brominated intermediate ***54*** proceeded smoothly. One step towards the synthesis of the $(CH_2)_3$NHBOC containing analogue, however, was more problematic. The primary amine was protected with a butoxy carbonyl (BOC) group. Under the bromination reaction conditions (***53*** → ***55***), small amounts of HBr were generated. This led to the partial deprotection of the BOC group, resulting in a mixture of the desired product ***55*** and its NH_4Br analogue. Fortunately, the deprotected compound precipitated from solution and it was possible to decant the desired product from the reaction mixture. The NH_3Br salt was then reacted with $(BOC)_2O$ in an attempt to regenerate more of compound ***55***. In total, 13 mg of ***55*** were produced, which was enough to proceed to the final steps.

The final target complex, [Eu·L^{12}], has two PEG containing chromophores and one $(CH_2)_3$NHBOC containing chromophore. To achieve this selectivity, 1,4,7-triazacyclononane (9-N_3) with one nitrogen protected with a BOC group was used (provided by CISbioassays). Alkylation with two equivalents of the PEG containing intermediate ***54***, was followed by removal of the BOC group with CF_3CO_2H and alkylation with intermediate ***55***. Both 9-N_3 containing intermediates were purified by column chromatography on silica. Deprotection of the final ligand ***58*** was carried out over two steps. Firstly, the BOC group was removed to liberate the primary amine as the protonated TFA salt. This was followed by hydrolysis of the three ethyl phosphinate esters. Each deprotection step was monitored by LCMS and, once completed, complexation was carried out using $Eu(OAc)_3$. The final complex, [Eu·L^{12}] was purified by column chromatography on silica with a gradient mobile phase comprising CH_2Cl_2 : CH_3OH : aq. NH_3 solution (90 : 10 : 0→1). The formation and purity of [Eu·L^{12}] was confirmed by HRMS and RP-HPLC.

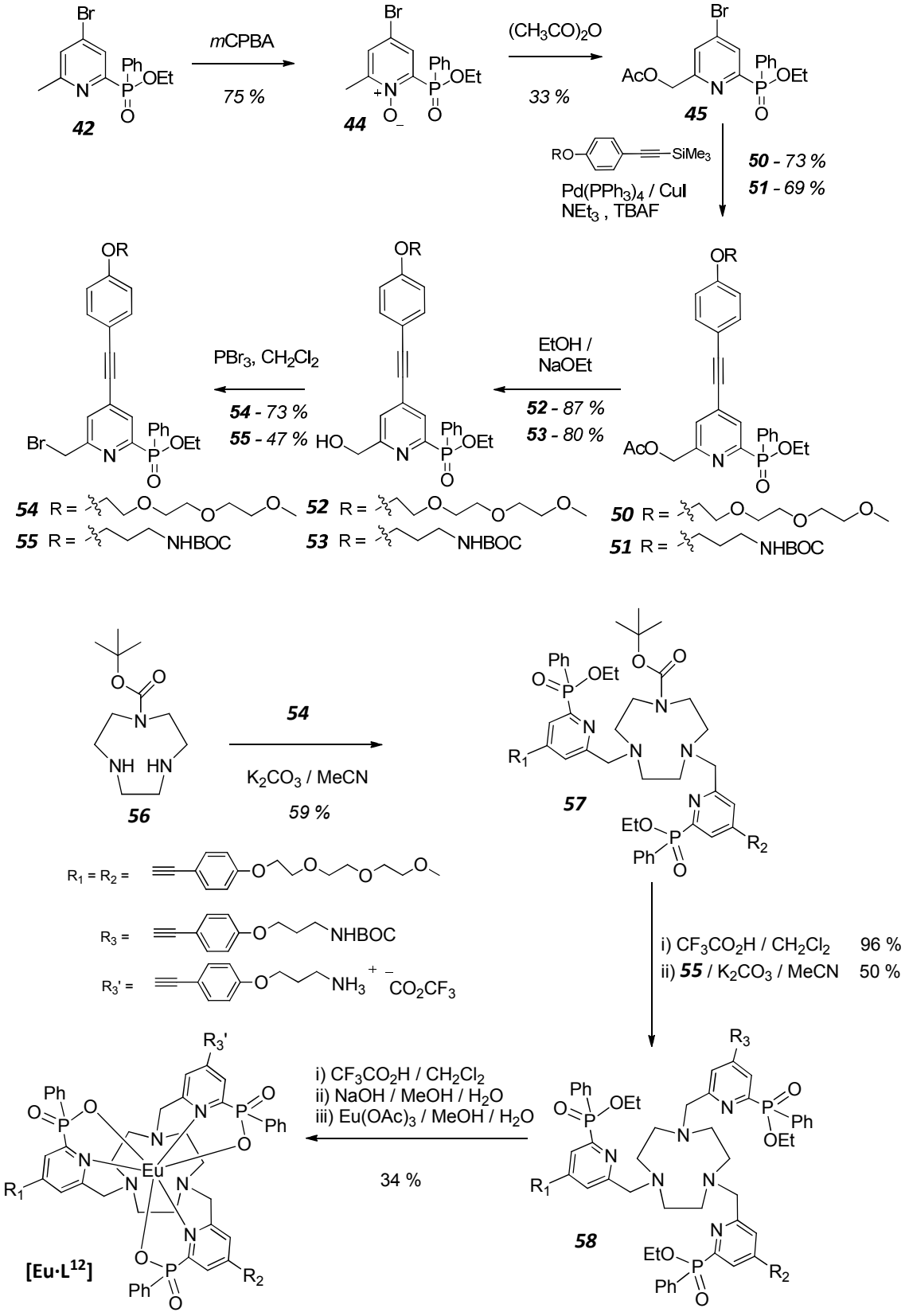
42
mCPBA
75 %
44
(CH3CO)2O
33 %
45
50 - 73 %
51 - 69 %
Pd(PPh3)4 / CuI
NEt3 , TBAF
PBr3, CH2Cl2
54 - 73 %
55 - 47 %
EtOH /
NaOEt
52 - 87 %
53 - 80 %
54 R =
55 R =
52 R =
53 R =
50 R =
51 R =
NHBOC
56
54
K2CO3 / MeCN
59 %
57
R1 = R2 =
R3 =
R3' =
i) CF3CO2H / CH2Cl2 96 %
ii) 55 / K2CO3 / MeCN 50 %
i) CF3CO2H / CH2Cl2
ii) NaOH / MeOH / H2O
iii) Eu(OAc)3 / MeOH / H2O
34 %
58
[Eu·L12]

Scheme 5.9

The low yields of the bromination of intermediate ***53*** with PBr_3 and the N-oxide rearrangement (***44*** → ***45***) led to an optimised route being devised (*Scheme 5.10*).[i] The rearrangement was carried out using $(CF_3CO_2)O$ in place of $(CH_3CO_2)O$. The resultant $CH_2OC(O)CF_3$ intermediate hydrolysed upon addition of H_2O : THF mixture (1 : 1), leaving an alcohol, which was stable under the cross coupling reaction conditions. Rather than using PBr_3, activation of the alcohol was achieved using mesyl chloride, which does not interfere with the BOC protected amine. This alternative route increases the overall yield of the reaction scheme and is recommended for future syntheses.

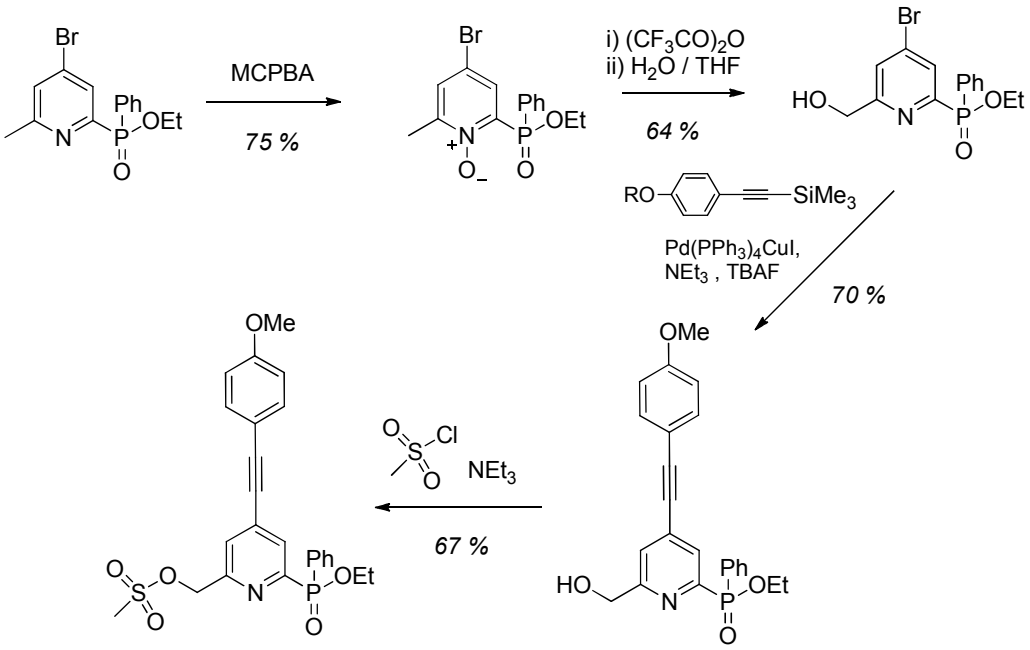

Scheme 5.10

5.4.2 Solubility Assessment

The addition of two PEG groups to the model complex was undertaken to improve the water solubility of the final complex. The linking primary amine was also expected to give [Eu·L^{12}] increased solubility. The presence of these additional groups certainly improved the aqueous solubility, relative to the model complex, [Eu·L^{11}], although not as much as had been hoped. It was found that μM concentrations of [Eu·L^{12}] were achievable but that mM concentrations were not. As a result, assessment of the photophysical properties of [Eu·L^{12}] was carried out in a H_2O : CH_3OH (3 : 1) solvent system. The HTRF experiment is carried out with a concentration of donor complex in the range 10 – 100 nM. The presence of water soluble vector (e.g. antibody, antigen) will also increase the solubility of the final donor moiety. It was concluded that the aqueous solubility of [Eu·L^{12}] was sufficient for the initial testing in the HTRF application, but that increasing solubility will be an area of future research.

[i] Optimisation carried out with the help of CISbioassays

5.4.3 Photophysical Properties

To allow direct comparison, the photophysical properties of the more water soluble complex, [Eu·L^{12}], were carried out in an analogous manner to those of [Eu·L^{11}] (*Table 5.2*). Although expected, the results were very pleasing. Despite the change in solvent system and the additional PEG and $(CH_2)_3NH_3$ groups, the properties of the two complexes are very similar. The molar extinction coefficients and emissive quantum yields are very high, leading to exceptionally bright complexes. The excited state lifetimes are within 0.05 ms and each complex has a *q* value of 0, suggesting that no change in the Eu^{3+} coordination sphere occurs upon addition of the PEG and primary amine appendages. This is confirmed by inspection of two emission spectra, which reveal no distinguishable differences (*Figure 5.12*). It is clear that despite the loss of C_3 symmetry of the complex as a whole, only the groups in close proximity to the Eu^{3+} centre, which retain the C_3 symmetry, influence the form of the emission spectrum.

Table 5.2 Photophysical data for the complexes [Eu·L^{11}], [Eu·L^{12}] and [Eu·L$^{1.1}$]$^{3+}$ (295 K). The solvent systems employed were *a*) CH_3OH, *b*) H_2O, CH_3OH (3 : 1) and *c*) H_2O + 0.4 M KF. Quantum yields ± 10 %.

Complex	λ_{max} / nm	ε / M^{-1} cm^{-1}	Φ (%)	$\Delta J = 2 : \Delta J = 1$ Ratio	*q*	τ / ms
[Eu·L^{11}] *a*	332	58,000	52	7.1	0.0	1.30
[Eu·L^{12}] *b*	332	60,000	54	7.1	0.0	1.25
[Eu·L$^{1.1}$]$^{3+}$ *c*	303	18,000	10	1.4	0.0	1.15

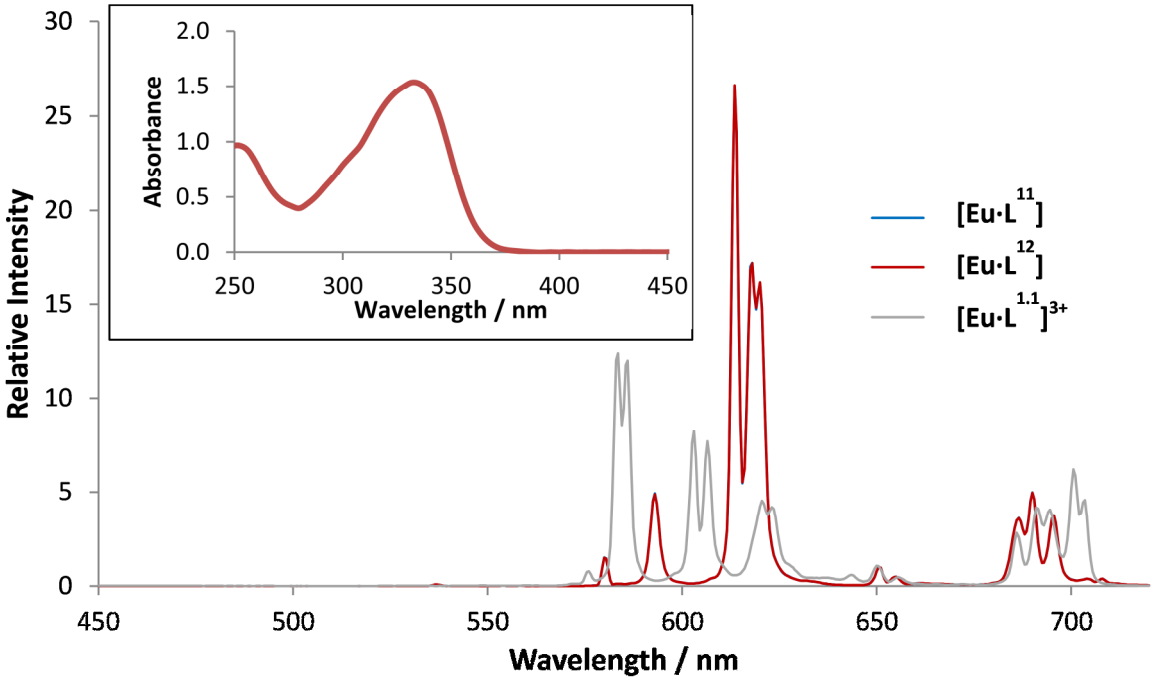

Figure 5.12 Comparison of the emission spectra of [Eu·L^{11}] (CH_3OH, λ_{ex} = 332 nm, 295 K), [Eu·L^{12}] (H_2O : CH_3OH, 1 : 3, λ_{ex} = 332 nm, 295 K) and [Eu·L$^{1.1}$]$^{3+}$ (H_2O, 0.4 M KF, λ_{ex} = 303 nm, 295 K) and *insert*) absorption spectrum for [Eu·L^{12}] (H_2O : CH_3OH, 3 : 1, 295 K).

Having established that [Eu·L^{12}] has the photophysical properties required for the HTRF experiment, it is necessary to compare its properties with the currently used complex, [Eu·L$^{1.1}$]$^{3+}$ (*Table 5.2*). The

combination of a large extinction coefficients, due to three chromophores and a high emissive quantum yield, resulting from an appropriate sensitiser excited state energy and a well shielded Eu^{3+} centre, result in an 18 fold increase in the overall brightness ($\varepsilon \times \Phi$) for [Eu·L^{12}], relative to the tris(bipyridine) complex. This is accompanied by a higher maximum absorption wavelength (*Figure 5.12 insert*) and a 5 fold increase in the integrated intensity $\Delta J = 2 : \Delta J = 1$ ratio (*Figure 5.12*). Overall, [Eu·L^{12}] is superior to the currently used complex, [Eu·$L^{1.1}$]$^{3+}$, and will be taken forward for testing in the HTRF experiment.

5.5 A Responsive System

One of the design specifications of the FRET donor complex, [Eu·L^{12}], was that it should be unresponsive to its environment. This was achieved by shielding the Eu^{3+} centre, so that the presence of added anions, cations or proteins led to no change in the intensity or form of the emission spectrum. Another class of emissive Eu^{3+} complexes exists, in which changes in the emission spectrum report variations in the concentration of specific analytes.[7] Of particular interest is the ability to measure fluctuations in the concentration of intracellular species.[8, 9] A responsive system of this type must meet several important criteria. Firstly, the emission from the probe must show some variation which can be measured in response to the specific analyte. This can include an increase, decrease or change in form of the emission spectrum. The change must be calibrated, so that the analyte concentration can be measured directly from the emission spectrum. One way to achieve calibration is to use ratiometric analysis, which relies upon two or more emissive bands varying at different rates in response to the analyte. The ratio of the two peaks can then be used to measure the concentration of analyte. Using this method, the measurement is independent of the probe concentration, which is usually unknown in cellular applications. The second criterion is that the probe is selective to the specific analyte and unresponsive to other species. Finally, intracellular probes must be non-invasive and may also be required to localise in a specific region or organelle of the cell.[10]

The emission from Eu^{3+} has several transitions, whose form and intensity are dependent upon the symmetry and speciation of the coordination sphere. As a result, Eu^{3+} complexes, whose coordination sphere is unsaturated, have been found to make excellent ratiometric probes. In these systems, exchange of a bound inner sphere solvent molecule by an analyte results in a change in the emission spectrum, which can be used to measure the analyte concentration. As these complexes are typically positively charged, anions, such as citrate, bicarbonate and lactate,[8, 11, 12] are the most commonly probed analytes.

For intracellular applications, it is necessary for an emissive probe to be bright (i.e. a high molar extinction coefficient and emissive quantum yield), to allow detection by fluorescence microscopy. After finding [Eu·L^{12}] to have excellent photophysical properties, a responsive analogue was sought. The complex that was devised, [Eu·$L^{13}(H_2O)$]$^{+}$, incorporates two sensitising groups, resulting in an

unsaturated Eu^{3+} coordination sphere. Luminescence titrations were carried out with a number of anions and protein to investigate the ability of $[Eu{\cdot}L^{13}(H_2O)]^+$ to act as a responsive probe.

5.5.1 Synthetic Aspects

The synthesis of a coordinatively unsaturated analogue of $[Eu{\cdot}L^{12}]$ was straightforward, starting from the previously synthesised intermediate ***57***, which contains a 1,4,7-triazacyclononane ring, incorporating two chromophores with PEG appendages and a BOC group protecting the third ring nitrogen. Removal of the BOC group, by stirring in CF_3CO_2H / CH_2Cl_2 (1 : 1 *v*/*v*), was followed by hydrolysis of the two ethyl phosphinate esters and complexation with $Eu(OAc)_3$ (*Scheme 5.11*). The charged complex was purified by preparative RP-HPLC, as an acetate salt, and HRMS was used to confirm the identity of the complex.

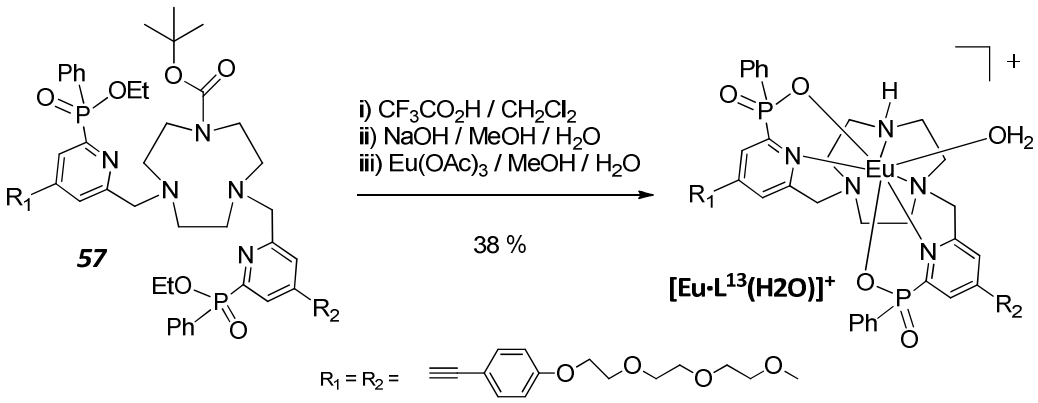

Scheme 5.11

5.5.2 Structural Analysis

To analyse the solution state structure of $[Eu{\cdot}L^{13}(H_2O)]^+$, ^{1}H- and ^{31}P-NMR were employed. Two broad peaks in a 1 : 1 ratio were observed in the ^{31}P-NMR spectrum. These peaks are likely to arise from two diastereoisomers: one being *RR* or *SS* at phosphorus and the other being *RS* or *SR*. In contrast to the sterically congested coordination sphere of $[Eu{\cdot}L^{12}]$, which forces the stereochemistry at P to be *RRR* or *SSS*, the environment around the Eu^{3+} centre of $[Eu{\cdot}L^{13}(H_2O)]^+$ is less crowded, leading to the formation of multiple stereoisomers. A second possible explanation for the two observed shifts in the ^{31}P-NMR spectrum is the presence of the Λ-*SS* and Δ-*SS* (or Λ-*RR* and Δ-*RR*) diastereomers. If this is the case, the two diastereomers must have similar energy as the observed ratio of the two peaks is 1 : 1. The ^{1}H-NMR spectrum is more complex than that of $[Eu{\cdot}L^{12}]$, indicative of multiple species in solution.

From excited state lifetime measurements in D_2O (τ = 0.49 ms) and H_2O (τ = 0.33 ms), an estimated *q* value of 0.9 was found.[13] This is consistent with the less congested Eu^{3+} centre, and implies that $[Eu{\cdot}L^{13}(H_2O)]^+$ will be able to act as a responsive probe. Overall, the Eu^{3+} centre is 8 coordinate, with 7 ligand donors and a single bound H_2O molecule.

5.5.3 Photophysical Properties

Despite the variation in the structure of $[Eu{\cdot}L^{13}(H_2O)]^+$ from the coordinatively saturated $[Eu{\cdot}L^{12}]$, it remains a highly emissive complex (*Table 5.3*). The molar extinction coefficient is around two thirds that of $[Eu{\cdot}L^{12}]$, as a result of having one less chromophore. The quantum yield of 23 ± 10 % is exceptionally high for a q = 1 Eu^{3+} complex and illustrates how efficiently the pyridylalkynylaryl sensitiser is able to populate the emissive state. As expected, the excited state lifetime shows a decrease relative to $[Eu{\cdot}L^{12}]$, due to the presence of an inner sphere water molecule.

Following excitation at 332 nm, the emission spectrum of $[Eu{\cdot}L^{13}(H_2O)]^+$ was measured (*Figure 5.13*). The complexity in the ΔJ = 4 region of the spectrum, suggests the presence of more than one emissive species in solution, likely to be associated with the two diastereoisomers, indicated by the ^{31}P-NMR analysis. As with $[Eu{\cdot}L^{12}]$, the ΔJ = 2 band is the most intense transition, although its relative intensity is less, due to the hard H_2O donor ligand in place of the polarisable phosphinate oxygen.

Table 5.3 Photophysical properties for $[Eu{\cdot}L^{12}]$ and $[Eu{\cdot}L^{13}(H_2O)]^+$ (H_2O : CH_3OH, 3 : 1, 295 K), *a*) quantum yields ± 10 %.

Complex	λ_{max} / nm	ε / M^{-1} cm^{-1}	Φ (%)^a	τ(H_2O : CH_3OH) / ms	τ(D_2O : d-MeOD) / ms	q
$[Eu{\cdot}L^{12}]$	332	60,000	54	1.25	1.76	0.0
$[Eu{\cdot}L^{13}]^+$	332	44,000	23	0.33	0.49	0.9

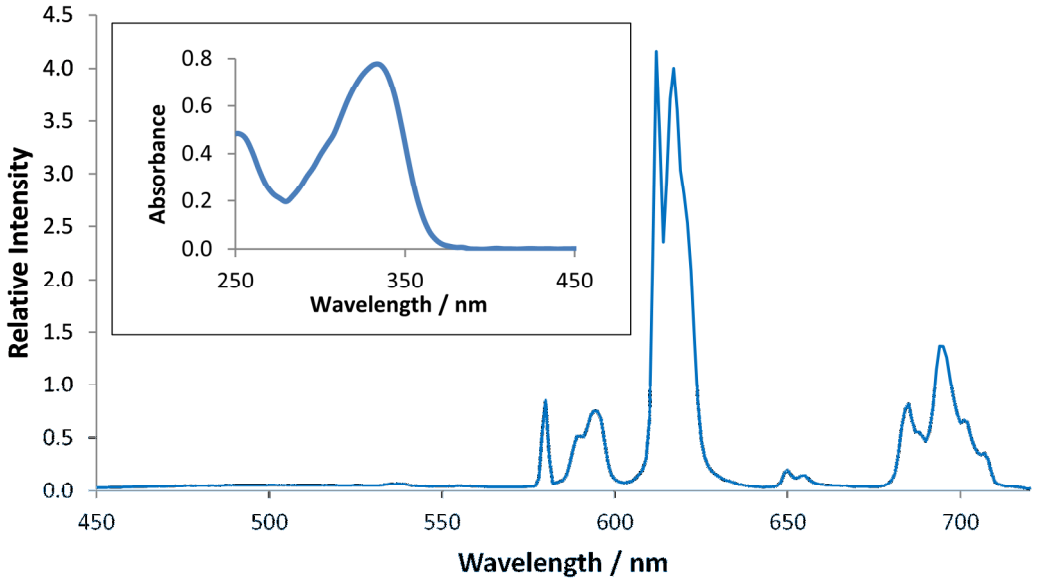

Figure 5.13 Emission and absorption (*insert*) spectra for $[Eu{\cdot}L^{13}(H_2O)]^+$ (H_2O : CH_3OH, 3 : 1, 295 K).

5.5.4 Luminescence Titrations

Prior to commencing luminescence titrations, emission spectra of $[Eu{\cdot}L^{13}(H_2O)]^+$ were recorded in the presence of a 10,000 fold excess of a number of anions and the protein, HSA. The chosen additives were selected on the basis of either being biologically relevant (HSA, bicarbonate, citrate, lactate and phosphate) or being able to give some information on the binding mode of each species. Each limiting spectrum was overlaid with the initial spectrum in the absence of additive (*Figure 5.14*). The first striking feature is that each species causes a change in the form of the emission spectrum, indicative of a change in the Eu^{3+} coordination environment. Upon addition of each anion, an increase in the total intensity of the emission was found. This was accompanied by a change in luminescence lifetime, which was calculated in deuterated and non-deuterated solvents, allowing the determination of q values, which, in each case, were found to be 0.0. Together, these two factors indicate that the added anion displaces the bound H_2O, changing the Eu^{3+} coordination environment and increasing the total emission, due to a reduction in vibrational quenching by H_2O. Only addition of HSA caused a reduction in the observed emission intensity. As with each anion, a change in the Eu^{3+} spectral form was also observed upon addition of HSA. Again, a q value of 0.0 was estimated, suggesting that side chain Glu or Asp residues in the HSA displace the H_2O molecule but also quenches the emission by some other mechanism, perhaps involving the charge transfer quenching of the sensitiser excited states.

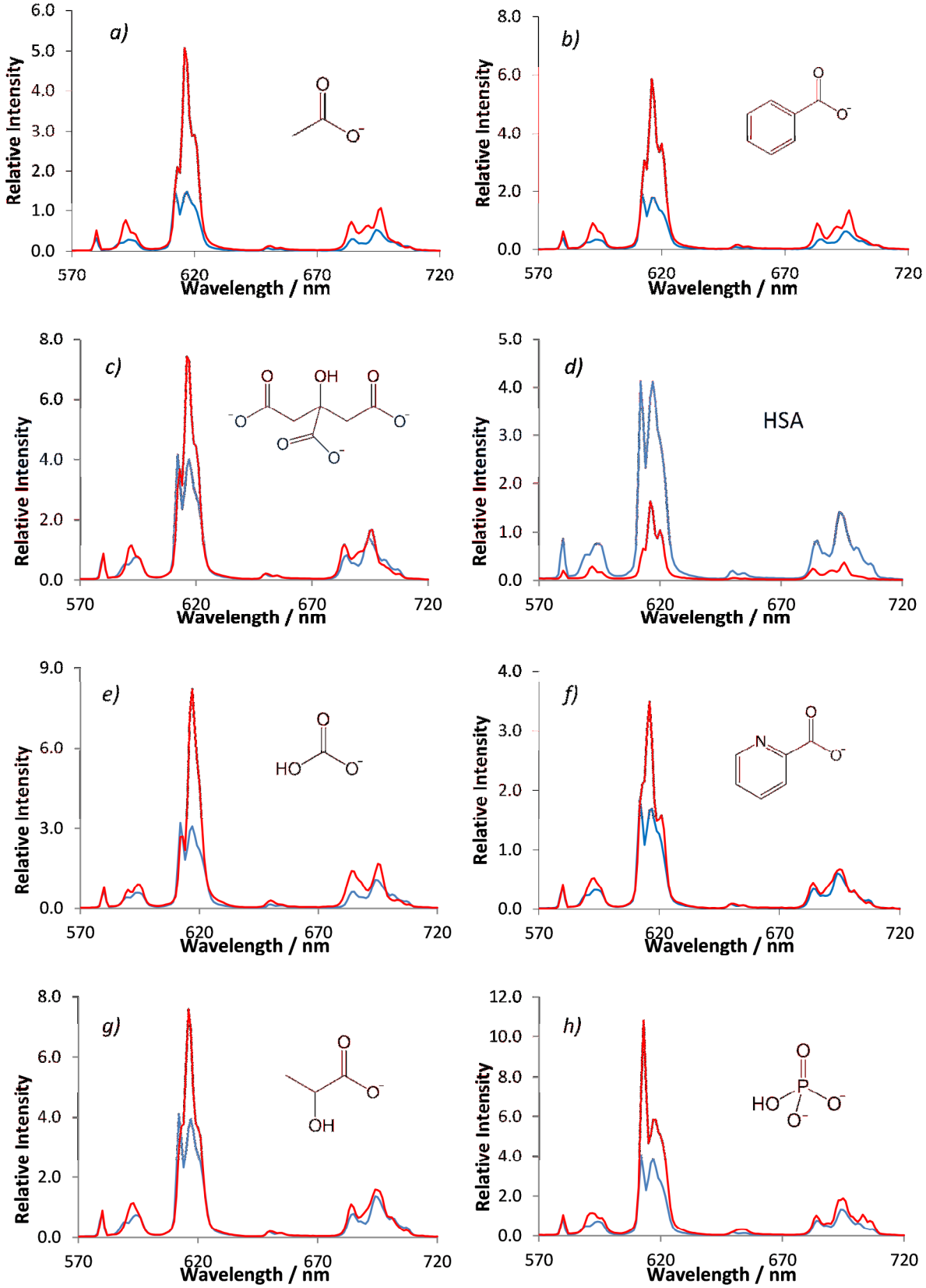

Figure 5.14 Limiting emission spectra for $[Eu{\cdot}L^{13}(H_2O)]^+$ in the presence of an excess of anions or HSA (*red*). The emission spectrum in the absence of additive is also shown (*blue*). Each spectrum was recorded in H_2O : CH_3OH (3 : 1, λ_{ex} = 332 nm, pH 7.4, 295 K). The selected anions are a) acetate, b) benzoate, c) citrate, e) bicarbonate, f) picolinate, g) lactate and h) hydrogen phosphate as their Na^+ salts.

Upon closer inspection of the form of the limiting spectra, it is apparent that four of the spectra are very similar (*Figure 5.15*). Having previously established that the form and intensity of the Eu^{3+} emission spectrum are determined by the symmetry and coordination environment of the central ion, it can be concluded that these four additives must be binding in a consistent manner. Bicarbonate, which is not amongst the four anions in question, has previously been shown to bind in a bidentate manner to unsaturated Ln^{3+} complexes.[7] Acetate, which is a similar size, is also known to bind in this way.[14] The three remaining anions must also be binding via a carboxylate group (*Figure 5.15 insert*), as the similarity in the emission spectra indicates. While this binding mode is expected for benzoate, citrate is usually thought to bind via a 5-membered chelate involving the alcoholic OH and one of the acetate oxygens.[7, 14] It appears that the steric demand about the Eu^{3+} centre may be too great to allow formation of 5-membered chelates. High steric demand about Eu^{3+} is also inferred by the coordination number of 8 in the absence of additive. It is rather intriguing that the $[Eu{\cdot}L^{13}]^+$ emission spectrum in the presence of lactate does not resemble the spectra shown in *Figure 5.15*. Lactate is less sterically bulky than citrate, which may allow the formation of a 5-membered chelate and, therefore, a variation in the emission spectral form. As addition of HSA to $[Eu{\cdot}L^{13}(H_2O)]^+$ results in the same emission spectral form as acetate, it is reasonable to conclude that the protein is binding to Eu^{3+} via a carboxylate, perhaps a glutamate or aspartate residue, as previously observed for Ln^{3+} complexes.[15]

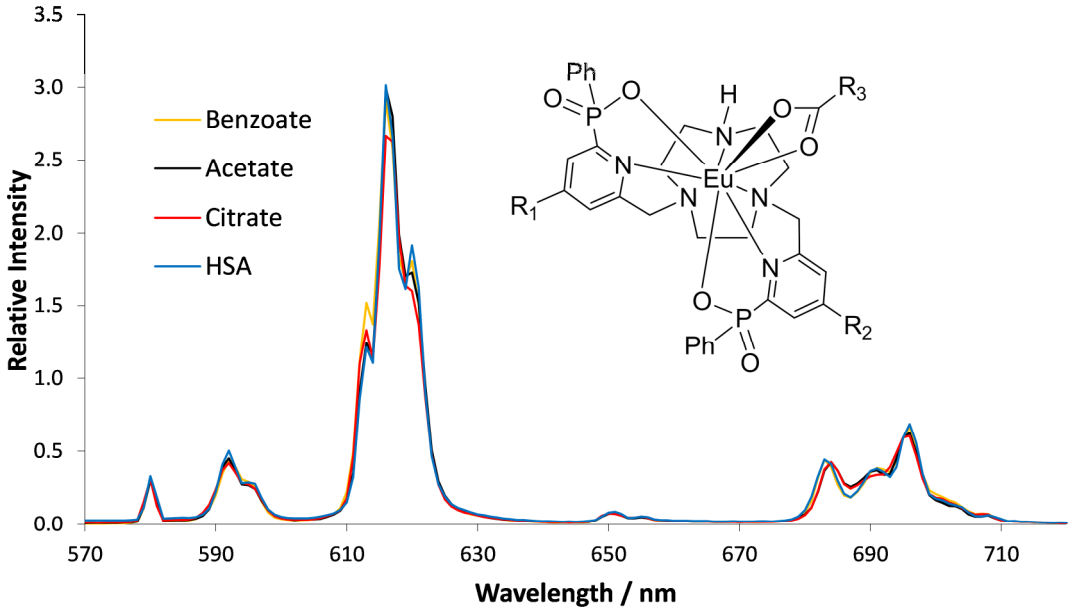

Figure 5.15 Comparison of the limiting emission spectrum for $[Eu{\cdot}L^{13}(H_2O)]^+$ in the presence of excess benzoate, acetate, citrate and HSA (H_2O : CH_3OH, 3 : 1, λ_{ex} = 332 nm, pH 7.4, 295 K). *Insert*) Possible binding mode for the four selected anions (R_1 = R_2 = sensitising groups, R_3 = functional group dependent upon the specific anion).

The limiting emission spectrum of $[Eu{\cdot}L^{13}(H_2O)]^+$ in the presence of the four biologically relevant anions indicated that each species binds to the Eu^{3+} coordination sphere, displacing H_2O. To allow the calculation of binding constants, luminescence titrations were carried out with each anion, starting with bicarbonate. To a sample of $[Eu{\cdot}L^{13}(H_2O)]^+$ in H_2O : CH_3OH (3 : 1, pH 7.4, 10 μM) aqueous $NaHCO_3^-$ (2 mM) was added, initially in 1 μL aliquots. By minimising the volume of anion solution added, the change in $[Eu{\cdot}L^{13}(H_2O)]^+$ concentration was kept to a minimum. Emission spectra were

measured after each addition (*Figure 5.16*). The addition of aq. HCO_3^- led to an increase in the $\Delta J = 2$: $\Delta J = 1$ intensity ratio, which was plotted as a function of the total HCO_3^- concentration (*Figure 5.16 insert*). The resultant curve was fitted to *Equation 8.6* (see Experimental section), which assumes a 1 : 1 binding mode, generating a binding constant, log *K*, for bicarbonate of 3.47. In the same way binding constants for citrate, lactate and phosphate were calculated (*Table 5.4*).

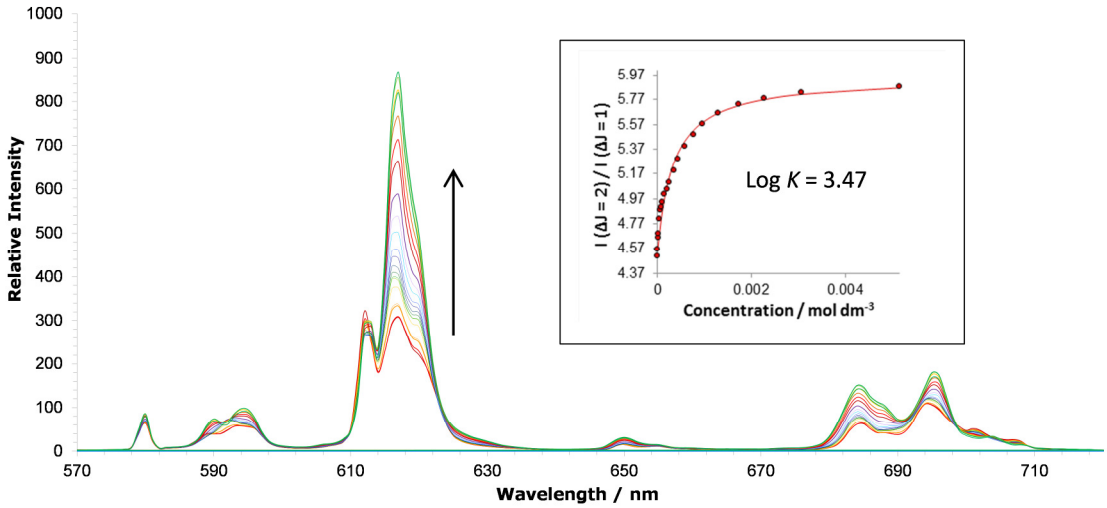

Figure 5.16 Luminescence titration for $[Eu{\cdot}L^{13}(H_2O)]^+$ with added aq. $NaHCO_3$ (2 mM) and *insert*) the integrated intensity ratio of $\Delta J = 2$: $\Delta J = 1$ as a function of $[HCO_3^-]$, allowing the calculation of a binding constant (10 μM complex, H_2O : CH_3OH, 3 : 1, λ_{ex} = 332 nm, pH 7.4, 295 K).

The three carboxy anions all have similar binding constants. The triply charged anion, citrate, is often found to have larger binding constants with Ln^{3+} complexes than the singly charged bicarbonate and lactate, due to greater electrostatic attraction to the Ln^{3+} centre.[7] Citrate is also the largest anion and it appears that in the case of binding to $[Eu{\cdot}L^{13}(H_2O)]^+$, a balance is struck between electrostatic interactions and steric demand, resulting in the similarity in log *K* for the three carboxy anions. The anion with the largest binding constant is hydrogen phosphate, perhaps due the combination of its low steric bulk and being doubly charged, and despite its higher hydration energy in solution.

Table 5.4 Binding constants (± 0.03) for the 1 : 1 binding between $[Eu{\cdot}L^{13}(H_2O)]^+$ and selected anions constant (H_2O : CH_3OH, 3 : 1, pH 7.4, 295 K).

Anion	**Log K**
Bicarbonate	3.47
Citrate	3.54
Lactate	3.51
Hydrogen Phosphate	3.78

A luminescence titration was also carried out with HSA. The protein was added as a solid over the concentration range 0 – 2 mM. The variation in the $\Delta J = 2$: $\Delta J = 1$ intensity ratio, with added HSA revealed two processes taking place (*Figure 5.17*). Initially, the intensity ratio increases and is accompanied by a change in the form of the emission spectrum. This is followed by a decrease in the

intensity ratio but no further change in the form of the spectrum. This result suggests that HSA displaces H_2O from the Eu^{3+} coordination sphere, leading to the change in spectral form, but also quenches the emission, leading to the reduction in both the overall intensity and the intensity ratio at higher HSA concentrations.

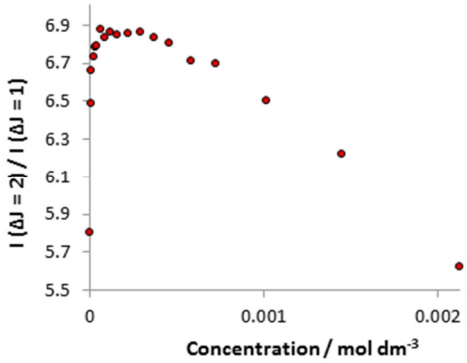

Figure 5.17 Integrated intensity ratio of $\Delta J = 2 : \Delta J = 1$ as a function of [HSA] (10 μM complex, $H_2O : CH_3OH$, 3 : 1, pH 7.4, 295 K).

To investigate the selectivity of $[Eu{\cdot}L^{13}(H_2O)]^+$ to binding a particular anion, the emission spectrum was measured in the presence of a mixture of the four biologically relevant anions, at their estimated extracellular concentrations (*Figure 5.18*). The similarity in the form of the resultant emission spectra and the spectrum in the presence of excess bicarbonate, indicates that in the mixed anion system bicarbonate is bound to the Eu^{3+} centre. This is also suggested by the excited state lifetime, which is 0.45 ms in both the mixed anion and bicarbonate systems. The singly charged bicarbonate anion is the smallest of the four tested anions and the observed selectivity of $[Eu{\cdot}L^{13}(H_2O)]^+$ for bicarbonate is likely to be associated with the steric demand at the Eu^{3+} centre, as previously elucidated.

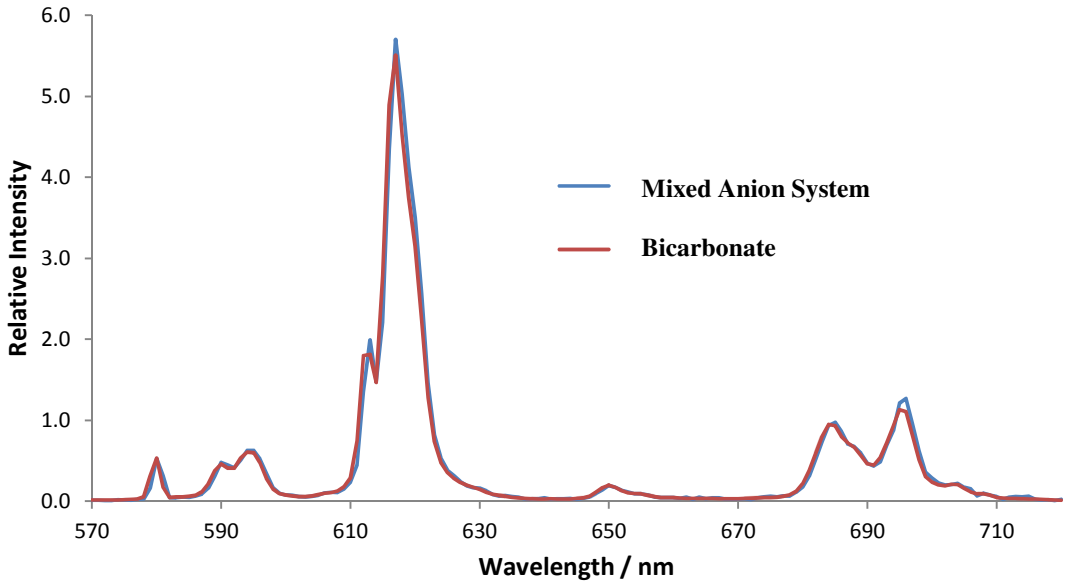

Figure 5.18 Comparison of the $[Eu{\cdot}L^{13}(H_2O)]^+$ emission spectrum in the presence of bicarbonate (*red*) and a mixed anion system (*blue*), comprising sodium salts of bicarbonate (30 mM), citrate (0.13 mM), lactate (2.3mM) and hydrogen phosphate (1.3 mM) (0.1 M NaCl, pH 7.4, 295 K).

5.6 Conclusions

An initial investigation was undertaken to assess the photophysical properties of the pyridylalkynylaryl chromophore. The new chromophore was found to have a maximum absorption wavelength at 320 nm in methanol with a molar extinction coefficient of 26,500 M^{-1} cm^{-1}. By measuring the phosphorescence spectrum at 77 K, a triplet energy of 21,300 cm^{-1} was estimated. It was, therefore, expected that the chromophore would be suitable for sensitisation of Eu^{3+} emission.

Incorporation of the chromophore into a model complex, [Eu·L^{11}], confirmed that population of the Eu^{3+} excited state was readily achieved by the pyridylalkynylaryl moiety. With a quantum yield of 52 % and an overall molar extinction coefficient of 58,000 M^{-1} cm^{-1}, the model complex is exceptionally bright. The coordination sphere about Eu^{3+} is the same for both [Eu·L^{11}] and the parent complex, [Eu·L^{9}], resulting in retention of the favourable emission spectral form.

To increase the aqueous solubility of the model complex, [Eu·L^{12}] was devised, which incorporates two PEG chains along with a primary amine, to allow vector conjugation. The favourable photophysical properties were not changed by these appendages and aqueous solubility was significantly increased. Each of the specification points outlined in the introduction (*Section 1.5*) is met by [Eu·L^{12}] and the properties of this highly emissive complex make it very well suited to act as a FRET donor in the HTRF experiment. In comparison with the currently used donor complex, [Eu·$L^{1.1}$]$^+$, the new system, [Eu·L^{12}], shows an 18 fold increase in brightness and a 5 fold increase in relative emission intensity in the $\Delta J = 2$ manifold, resulting in better spectral overlap with the allophycocyanin acceptor moiety. The emissive stability of [Eu·L^{12}] is high in the assay medium, without the need for 0.4 M KF, which is required to enhance the properties of [Eu·$L^{1.1}$]$^+$. One area for future development is to increase the aqueous solubility of [Eu·L^{12}], which is low and at the workable limit for the HTRF experiment.

Having accomplished the main goal of designing a bright, non-responsive Eu^{3+} complex, attention turned to the synthesis of a responsive system, which would be able to report changes in its local environment through a variation in the intensity and spectral form of the emission. The responsive complex, [Eu·L^{13}(H_2O)]$^+$, contains one fewer sensitising group than [Eu·L^{12}] and has a single inner sphere H_2O donor. Upon addition of several biologically relevant anions, the H_2O molecule is displaced, causing an increase in the intensity and a change in the spectral form of the emission. The spectral form is unique for each anion, although those which bind via a carboxylate group result in similar emission spectra. Binding of bicarbonate, a product of the Krebs cycle in mitochondrial respiration, to [Eu·L^{13}(H_2O)]$^+$ was found to have a log K of 3.47 and was selective over the other anions that were examined, possibly due to the steric demand about the Eu^{3+} centre, leading to preferential binding of the smaller anion. This initial study into the properties of [Eu·L^{13}(H_2O)]$^+$, suggest that it may find application as an intracellular responsive probe. Further experiments that are required to validate the use of this probe include analysis of the selectivity towards bicarbonate in a competitive medium, containing proteins, nucleotides and other biological anions.

The Tb^{3+} analogue of the model complex, [Eu·L^{11}], was synthesised to assess the ability of the pyridylalkynylaryl chromophore to sensitise Tb^{3+} emission. After excitation of the complex at 332 nm, very little Tb^{3+} emission was observed. This is due to thermally induced back energy transfer from the Tb^{3+} excited state to the sensitiser triplet or ICT state, which is quenched by molecular oxygen. By deoxygenating the sample, the emission increased, due to a reduction in this quenching mechanism. While the sensitiser excited state energy is too low to avoid back energy transfer from the Tb^{3+} excited state, it is very well placed to maximise transfer of energy to Eu^{3+}, contributing to the high quantum yields observed for [Eu·L^{11}] and [Eu·L^{12}]. To allow efficient Tb^{3+} sensitisation, the chromophore requires modification, perhaps in the aryl O-R position, to increase to the triplet energy.

5.7 References

1. A. Picot, A. D'Aleo, P. L. Baldeck, A. Grichine, A. Duperray, C. Andraud and O. Maury, *J. Am. Chem. Soc.*, 2008, **130**, 1532-1537.
2. A. D'Aleo, A. Picot, A. Beeby, J. A. G. Williams, B. Le Guennic, C. Andraud and O. Maury, *Inorg. Chem.*, 2008, **47**, 10258-10268.
3. P. Atkinson, K. S. Findlay, F. Kielar, R. Pal, D. Parker, R. A. Poole, H. Puschmann, S. L. Richardson, P. A. Stenson, A. L. Thompson and J. H. Yu, *Org. Biomol. Chem.*, 2006, **4**, 1707-1722.
4. V. Boekelheide and W. J. Linn, *J. Am. Chem. Soc.*, 1954, **76**, 1286-1291.
5. L. Porres, A. Holland, L. O. Palsson, A. P. Monkman, C. Kemp and A. Beeby, *Journal of Fluorescence*, 2006, **16**, 267-272.
6. *www.htrf.com, December 2010*.
7. D. Parker, R. S. Dickins, H. Puschmann, C. Crossland and J. A. K. Howard, *Chem. Rev.*, 2002, **102**, 1977-2010.
8. R. Pal, D. Parker and L. C. Costello, *Org. Biomol. Chem.*, 2009, **7**, 1525-1528.
9. D. Parker, *Chem. Soc. Rev.*, 2004, **33**, 156-165.
10. E. J. New, D. Parker, D. G. Smith and J. W. Walton, *Curr. Opin. Chem. Biol.*, 2010, **14**, 238-246.
11. D. G. Smith, G.-L. Law, B. S. Murray, R. Pal, D. Parker and K.-L. Wong, *Chem. Commun.*, 2011, **47**, 7347-7349.
12. Y. Bretonniere, M. J. Cann, D. Parker and R. Slater, *Org. Biomol. Chem.*, 2004, **2**, 1624-1632.
13. A. Beeby, I. M. Clarkson, R. S. Dickins, S. Faulkner, D. Parker, L. Royle, A. S. de Sousa, J. A. G. Williams and M. Woods, *J. Chem. Soc. Perkin Trans. 2*, 1999, 493-503.
14. R. S. Dickins, S. Aime, A. S. Batsanov, A. Beeby, M. Botta, J. Bruce, J. A. K. Howard, C. S. Love, D. Parker, R. D. Peacock and H. Puschmann, *J. Am. Chem. Soc.*, 2002, **124**, 12697-12705.
15. S. Aime, E. Gianolio, E. Terreno, G. B. Giovenzana, R. Pagliarin, M. Sisti, G. Palmisano, M. Botta, M. P. Lowe and D. Parker, *J. Biol. Inorg. Chem.*, 2000, **5**, 488-497.

6. Investigation into the Quenching of Lanthanide Complexes

6.1 Introduction

6.1.1 Static and Dynamic Quenching

Quenching refers to any process that reduces the overall emissive intensity of a sample, and is divided into two classes. Static quenching involves formation of a non-fluorescent complex between the quencher and the ground state emissive species. Dynamic, or collisional, quenching requires a diffusive encounter between the quencher and the emissive species, during its excited state lifetime. Both quenching processes require molecular contact between the quencher and the emissive species, leading to one application of quenching studies in the determination of the localisation of fluorophores within proteins.[1] If the fluorophores is buried in the interior of a protein, the rate of quenching will be less than if the fluorophore is at the exterior of the protein, where it is more accessible to quenchers.

Static quenching requires the formation of a complex between the quencher and the emissive species. One example is the quenching of the coumarin 120 by uridine.[2] A stacking interaction takes place between the two flat aromatics, leading to a non-fluorescent complex. At higher uridine concentrations, the reduction in coumarin emission is attributed to a combination of static and dynamic quenching.

Dynamic quenching involves an encounter between the quenchers and the excited state emissive species during the lifetime of the excited state, resulting in non-radiative decay to the ground state. Examples of dynamic quenching include electron or charge transfer, energy transfer and triplet state quenching by molecular oxygen. Amines, such as diethylaniline quench the fluorescence from aromatic hydrocarbons, such as anthracene, by formation of an excited state charge transfer complex, while electron rich fluorophores, such as indole, can be quenched by oxidation in the singlet excited state by electron scavengers (e.g. H^+, histidine and Cu^{2+}).[3]

6.1.2 The Stern-Volmer Equation

Dynamic quenching is described by the Stern-Volmer equation,[1]

$$\frac{F_0}{F} = 1 + k_q \tau_0 [Q] = 1 + K_{SV}[Q] \qquad [6.1]$$

where F_0 is fluorescence intensity in the absence of quencher, F is the fluorescence in the presence of the quencher, k_q is the rate constant for the bimolecular quenching process, τ_0 is the excited state lifetime in the absence of quencher and $[Q]$ is the concentration of quencher. The product of k_q and τ_0

is referred to as the Stern-Volmer constant, K_{SV}. Conventionally, the reciprocal constant, K_{SV}^{-1}, is reported. This is the concentration of quencher required to reduce the emissive intensity to 50 % of its original value. For a quenching process between two species occurring via a single mechanism, a plot of F_0 / F versus $[Q]$ gives a straight line with a gradient K_{SV}. For dynamic quenching, τ_0 / τ versus $[Q]$ will also give a straight line with a gradient K_{SV}, hence,

$$\frac{F_0}{F} = \frac{\tau_0}{\tau} = 1 + K_{SV}[Q] \qquad [6.2]$$

In contrast, for static quenching τ_0 / τ is 1 for all $[Q]$. This is because static quenching is a purely ground state phenomenon, and does not affect the excited state properties of the emissive species. In the case of static quenching, the Stern-Volmer equation becomes,

$$\frac{F_0}{F} = 1 + K_S[Q] \qquad [6.3]$$

where K_S is the association constant for complex formation between the quencher and emissive species.

The difference in behaviour of τ_0 / τ with $[Q]$ is one way to differential between static and dynamic quenching. Another method is to measure the temperature dependence upon quenching. For dynamic quenching, increasing the temperature increases the rate of diffusion and therefore, the rate of quenching, whereas the rate of static quenching can be reduced at higher temperatures, due to the dissociation of weak quencher-fluorophore complexes.

Deviation from linearity in the Stern-Volmer plots at higher $[Q]$ occurs for both dynamic and static quenching, due to factors such as inner filter effects and interference from background fluorescence. When carrying out quenching experiments, pH, ionic strength and temperature are kept constant, as they may affect the rate of quenching.

6.1.3 Quenching of Emissive Lanthanide Complexes

Any process that reduces the emissive quantum yield of a lanthanide complex can be thought of as a quenching mechanism. Each of the excited states in the sensitised emission pathway is susceptible to quenching (*Scheme 6.1*). The quenching processes which deactivate the various excited states are an important consideration when designing and analysing emissive lanthanide complexes, particularly those meant for intracellular use, where many endogenous quenchers are present.

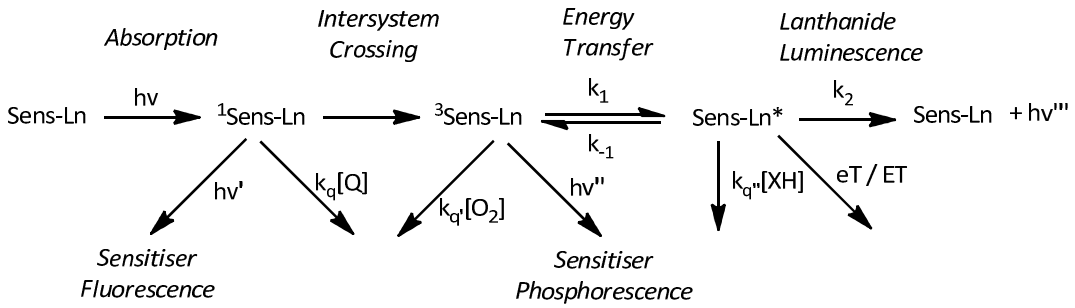

Scheme 6.1

The sensitiser singlet excited state is sensitive to dynamic quenching by electron transfer. This process can be inter- or intramolecular and can be predicted by the Weller equation,[4]

$$\Delta G_{ET} = nF\left([E_{ox} - E_{red}] - E_S - \frac{e^2}{\varepsilon r}\right) J\ mol^{-1} \qquad [6.4]$$

where E_{ox} is the oxidation potential of the donor (e.g. an amine lone pair or an electron rich aromatic group), E_{red} is the reduction potential of the acceptor (e.g. an aryl group or a Ln^{3+} centre), E_s is the singlet excited state energy in eV and e^2 / εr is the attractive energy term related to formation of a radical ion pair (usually less than ca. 0.2 eV). An example of photo-induced electron transfer is the quenching of the phenanthridine sensitiser singlet state (E_{red} = –2.12 V in MeCN, E_S = 3.54 eV, $e^2/\varepsilon r$ = 0.15)[5] by triethylamine (E_{ox} = +1.15 V). According to the Weller equation, ΔG_{ET} = – 30.9 kJ mol^{-1}, and the photo-induced electron transfer is energetically favourable and quenching occurs.[6] Upon protonation of triethylamine, its E_{ox} value increases and quenching is no longer energetically favourable. Europium complexes, incorporating the phenanthridine chromophore have been devised, which act as pH sensors, based upon the turn-on of Eu^{3+} emission at low pH, due to a protonation of phenanthridine and reduction in photo-induced electron transfer quenching.[7]

The sensitiser triplet state is susceptible to dynamic quenching by molecular oxygen.[6] This process is particularly important if the triplet energy level (^{3}*sens*) is close in energy (within 2,000 cm^{-1}) to the Ln^{3+} excited state (Ln*). In this situation, back energy transfer from Ln* to ^{3}*sens* results in a long lived observed triplet state, increasing the probability of quenching by dissolved oxygen. An example of this quenching process was seen for [Tb·L[11]] (*Chapter 5*), in which the pyridylalkynylaryl triplet state was too close in energy to the Tb $^5D_4$ state, resulting in very weak emission. The intensity of emission was increased upon deoxygenating the sample, consistent with the hypothesised quenching mechanism. There are several examples of lanthanide complexes which can report pO_2 by a change in either the intensity of emission of a single emissive complex[8-10] or by the ratiometric analysis of Tb^{3+} and Eu^{3+} emission from complexes based on a common ligand.[11] In the latter case, only the Tb^{3+} complex, whose excited state is higher in energy, is quenched by molecular oxygen, leading to internal calibration of the measurement.

Another mechanism by which the sensitiser triplet state is quenched by intracellular reductants urate, ascorbate and catechol, has recently been elucidated, using transient absorption measurements.[12] In

this study, it was found that the electron-rich quenchers formed excited state complexes (exciplexes) with the electron deficient ^{3}*sens* state of heteroaromatic chromophores. The resulting charge transfer bands were found to be lower in energy than the ^{3}*sens* state. As a result, the rate of back energy transfer from Ln* increased, leading to an overall reduction in emission intensity and luminescence lifetime.

The final state along the sensitised emission pathway that is susceptible to quenching is the lanthanide excited state. We have seen examples of back energy transfer from Ln* to ^{3}*sens*, leading to a reduction in emission. Other quenching processes include electron and energy transfer. Electron transfer to Tb^{3+} is energetically unfavourable (E_{red} = –3.5 V) but formation of Eu^{2+} is feasible, with a strong enough reducing agent (E_{red} = –0.8 to –1.2 V were reported for Eu^{3+} complexes with certain polar octadentate ligands).[6] Energy transfer from Ln* is a more commonly encountered deactivation pathway. Differential transfer of energy to H_2O and D_2O vibrational energy levels is routinely used to determine the q value of Eu^{3+} and Tb^{3+} complex. As the name suggests, energy transfer is also responsible for the FRET process, exploited in the HTRF experiment, for which [Eu·L^{12}] is anticipated to be an excellent donor moiety. As with each of the quenching mechanisms discussed above, energy transfer is highly dependent upon the distance between the quencher and emissive complex. Vibrational quenching (e.g. by H_2O), to a first approximation, has an r^{-6} dependence, as does Förster energy transfer. Dexter energy transfer and electron transfer quenching have an $e^{-\beta r}$ dependence.[13] Other factors, such as dipole orientations and spectral overlap, also affect the efficiency of energy transfer quenching.

6.2 Quenching by Metal Ions

6.2.1 Mn^{2+} Quenching

Throughout this project, emissive stability assays were carried out with each new Eu^{3+} complex, to assess their ability to resist quenching by a number of cations, proteins and the competitive multidentate ligand $EDTA^{4-}$. For the early complexes ([Eu·L^1(H_2O)] – [Eu·L^8]), the quencher which perturbed the Eu^{3+} emission to the greatest extent was Mn^{2+}. In the case of [Eu·L^6] and [Eu·L^7], the emission was completely quenched in the presence of a million fold excess of $MnCl_2$. Upon moving to the C_3 symmetric systems [Eu·L^9] – [Eu·L^{12}], quenching by Mn^{2+} was no longer observed. In an attempt to rationalise these findings, a number of initial quenching experiments were designed to shed light upon the nature of quenching (static or dynamic). Once dynamic quenching had been determined, further experiments were undertaken to assess which excited state along the sensitised emission pathway was being deactivated by Mn^{2+} and the mechanism of quenching.

One process by which Mn^{2+} could potentially quench emission from the Eu^{3+} complexes is transmetallation. This process involves dissociation of Eu^{3+} from its ligand and subsequent complexation with Mn^{2+}, and is dependent upon the thermodynamic stability of the Eu^{3+} and Mn^{2+} complexes and the kinetic stability of the starting Eu^{3+} complex. The ability of each of the synthesised Eu^{3+} complexes to withstand quenching by Mg^{2+} and Ca^{2+} suggests that this process does not take

place, as these ions have the same charge and, in the case of Mg^{2+}, a similar ionic radius to Mn^{2+}. It is also well established that the Ln^{3+} ions form kinetically and thermodynamically stable complexes with octa- and nonadentate ligands, whereas Mn^{2+} favours 6-coordinate octahedral ligands.

To investigate alternative quenching mechanisms, $MnCl_2$ was added to a solution of [Eu·L^1(H_2O)] (H_2O, 100 μM complex, 0.1 M HEPES, 0.1 M NaCl, pH 7.4, 295 K) to give final Mn^{2+} concentrations of 0.1 and 10 mM. Upon addition of Mn^{2+}, both the emission and excited state lifetime of [Eu·L^1] decreased. The ratios F_0 / F and τ_0 / τ were similar, suggesting that dynamic quenching takes place. To better understand which excited state is quenched, the emission spectrum of [Eu·L^1(H_2O)] was recorded at each Mn^{2+} concentration, following excitation of the sensitising group (λ_{ex} = 328 nm, *Figure 6.1 left*) or direct excitation of the Eu^{3+} ion (λ_{ex} = 398 nm, *Figure 6.1 right*). Despite the low signal to noise ratio following direct excitation, it is apparent that the extent of quenching is approximately the same, independent of the mode of excitation. This is indicative of quenching of the lanthanide excited state, rather than one of the sensitiser excited states.

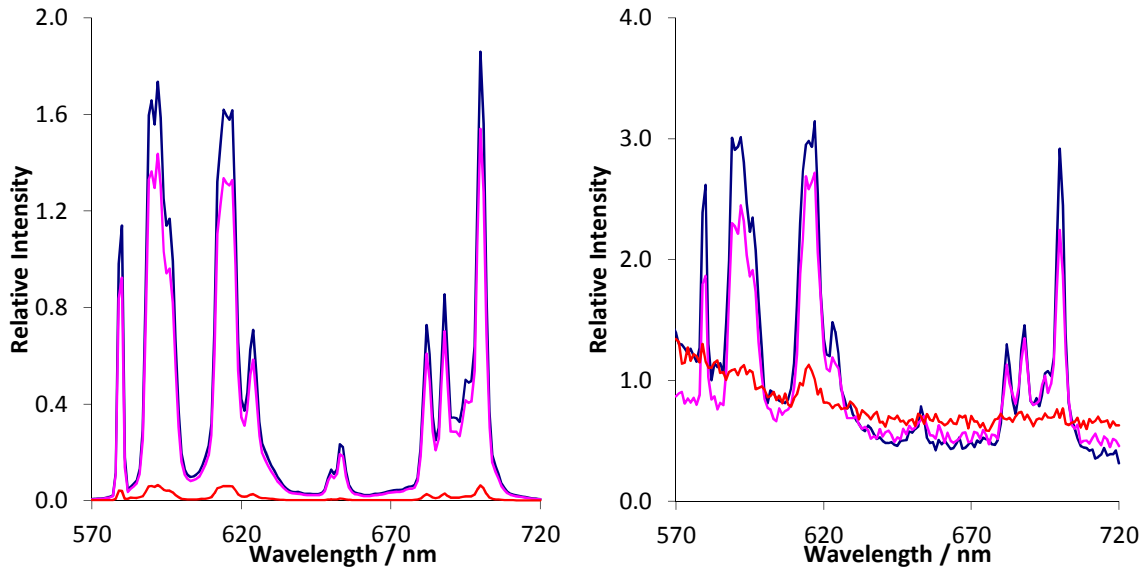

Figure 6.1 Emission spectra for [Eu·L^1(H_2O)] in the presence of 0 mM (*blue*), 0.1 mM (*purple*) and 10 mM (*orange*) $MnCl_2$, following excitation at *left*) 328 nm and *right*) 398 nm (H_2O, 100 μM complex, 0.1 M HEPES, 0.1 M NaCl, pH 7.4, 295 K).

Several empirical observations also support the hypothesis that the Ln* state is quenched by Mn^{2+}. The Eu^{3+} emission intensities of selected complexes were measured in the presence of a million fold excess of $MnCl_2$. The percentage of emission, relative to the intensity of emission prior to Mn^{2+} addition, was recorded for each complex (*Table 6.1*). Comparison of the values for [Eu·L^2(H_2O)]$^+$ and the constitutional isomer [(1-AX)-Eu·L^2]$^+$, show that Mn^{2+} quenching is more efficient for [Eu·L^2(H_2O)]$^+$. Both complexes incorporate azaxanthone chromophores with similar singlet and triplet energies, implying that the quenching mechanism does not involve the sensitiser group. Instead, the quenching mechanism is likely to involve the Ln* state which is more accessible to Mn^{2+} in the case of q = 1 [Eu·L^2(H_2O)]$^+$ than q = 0 [(1-AX)-Eu·L^2]. A second observation that supports this hypothesis is the higher quenching of [Eu·L^6]$^-$ (2 % retention of emission), compared to [Eu·L^9] (96 % retention of emission). Each complex incorporates the same pyridyl phenylphosphinate sensitising

group, suggesting that the greater retention of emission by [Eu·L^9] arises from the shielding of the Eu^{3+} centre by the three phenyl groups below the plane of the C_3 symmetric complex (*Figure 6.2*).

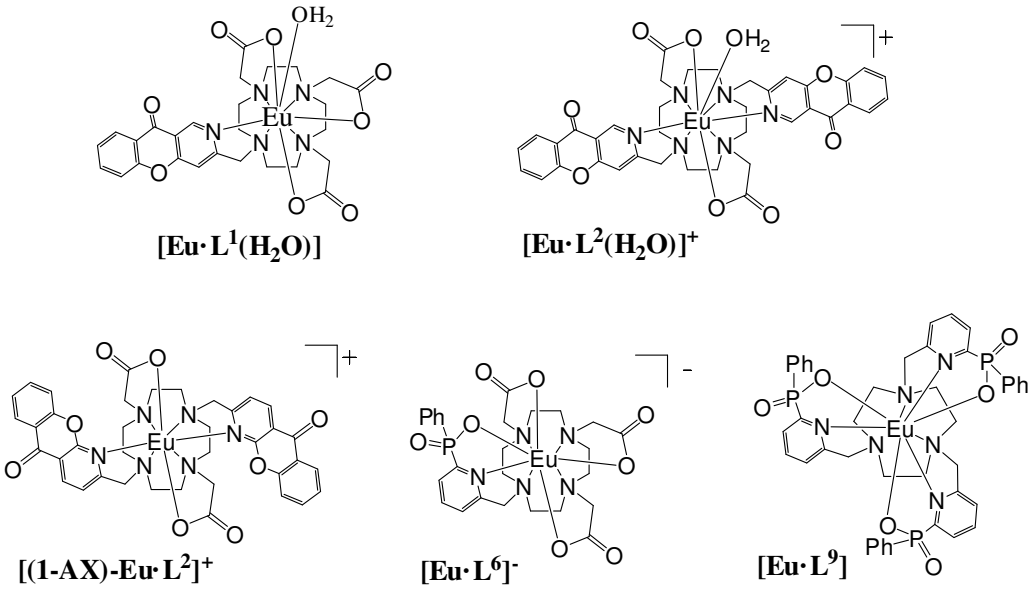

Table 6.1 Comparison of the rate of quenching by Mn^{2+} upon selected Eu^{3+} complexes. The retention of emission is the percentage of emission intensity observed after addition of a million fold excess of $MnCl_2$, relative to the emission intensity in the absence of quencher, and are average values of three independent measurements (± 2 %). All Eu^{3+} complexes 10 nM, except [Eu·L^1], which is 100 μM (H_2O, 0.1 M HEPES, 0.1 M NaCl, pH 7.4, 295 K).

Complex	λ_{ex} / nm	Retention of Emission
[Eu·L^1(H$_2$O)]	328	5 %
[Eu·L^1(H$_2$O)]	398	10 %
[Eu·L^2(H$_2$O)]$^+$	328	59 %
[(1-AX)-Eu·L^2]$^+$	328	88 %
[Eu·L^6]$^-$	275	2 %
[Eu·L^9]	275	96 %

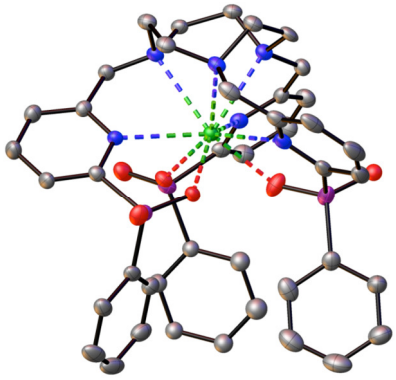

Figure 6.2 Side view of the crystal structure of [Eu·L^9], showing the three shielded nature of the Eu^{3+} centre, reducing its accessibility to quenchers, such as Mn^{2+}.

In a previous study discussed above, it was found that apparent quenching of the Ln* state by urate and ascorbate was, in fact, due to exciplex formation between the electron deficient sensitisers (azaxanthone and tetraazatriphenylene) and the electron-rich quenchers.[12] This led to a lowering in energy of the sensitiser triplet state and an increase in back energy transfer from Ln*. Rather than direct quenching of Ln* itself, quenching was occurring at the sensitiser triplet state. In the case of Mn^{2+}, the quenching must be taking place at the Ln* state, as the difference in quenching between $[Eu{\cdot}L^6]^-$ and $[Eu{\cdot}L^9]$ indicates. Each complex incorporates a pyridyl-based sensitiser, whose triplet energy lies at around 30,000 cm^{-1}. This is more than 12,000 cm^{-1} above the Eu^{3+} excited state, making back energy transfer unrealistic.

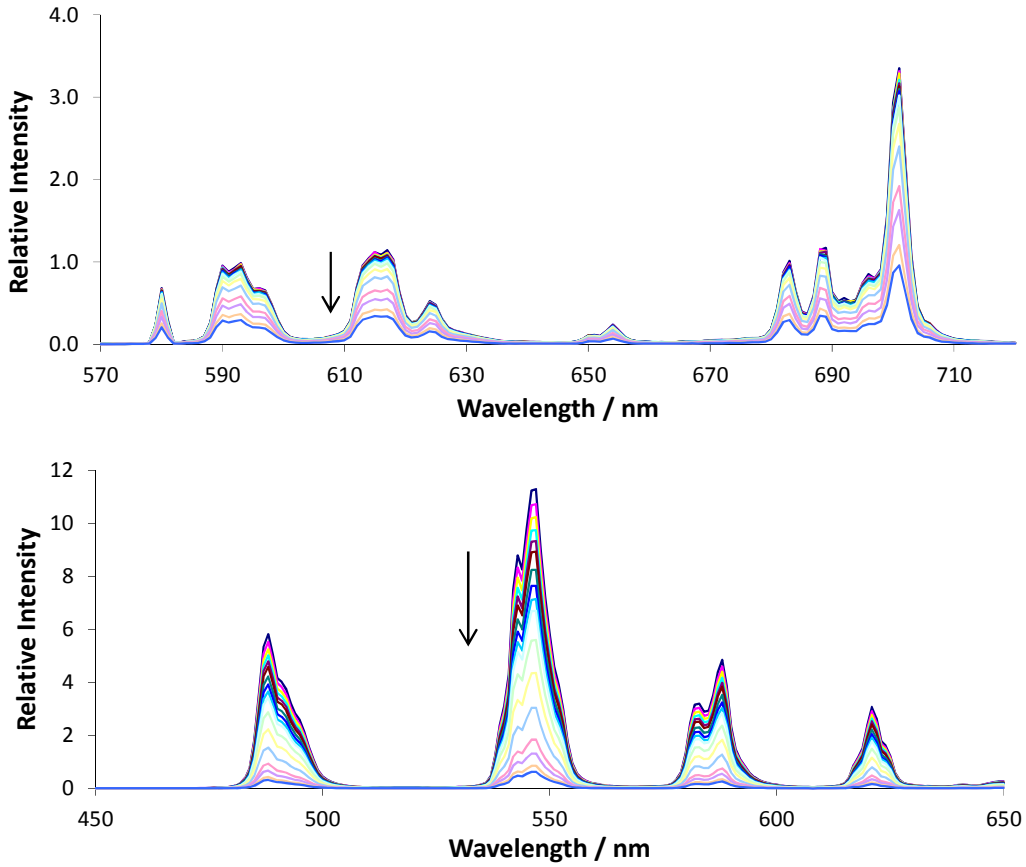

Figure 6.3 Luminescence titrations for $[Eu{\cdot}L^1(H_2O)]$ (*upper*) and $[Tb{\cdot}L^1(H_2O)]$ (*lower*) with increasing concentration of $MnCl_2$ (H_2O, 20 μM complex, 0 – 3 mM $MnCl_2$, 0.1 M HEPES, 0.1 M NaCl, pH 7.4, 295 K).

Having established that Mn^{2+} quenching occurs with the Ln* state, an investigation into the mechanism of quenching was undertaken. Luminescence titration were carried out with $[Eu{\cdot}L^1(H_2O)]$ and $[Tb{\cdot}L^1(H_2O)]$ by measuring the emission spectra in the presence of increasing concentrations of Mn^{2+} (*Figure 6.3*). As expected, the intensity of emission decreases with increasing $[Mn^{2+}]$. To quantify the rate of quenching, Stern-Volmer plots were carried out (*Figure 6.4*). Plotting either F_0 / F or τ_0 / τ against $[Mn^{2+}]$ gave similar slopes, consistent with a dynamic quenching mechanism. From the gradients of the slopes, Stern-Volmer quenching constants, K_{SV}^{-1}, of 1.22 and 0.16 mM were calculated for $[Eu{\cdot}L^1(H_2O)]$ and $[Tb{\cdot}L^1(H_2O)]$, respectively. The plots show no deviation from linearity, consistent with the presence of a single bimolecular quenching process. Stern-Volmer

quenching constants were calculated for three other complexes: the tri(phenylphosphinate) C_3 symmetric complexes, [Eu·L[9]] and [Tb·L[9]], and the methylphosphinate analogue, [Eu·L[10]] (*Table 6.2*). For both the [Ln·L[1](H$_2$O)] and [Ln·L[9]] complexes, the Tb^{3+} species was found to be more susceptible to quenching. This is inconsistent with a quenching mechanism involving electron transfer to the Ln* state, as reduction of Tb^{3+} is highly energetically unfavourable. According to the Weller equation (*Equation 6.4*), even the photo-induced electron transfer from Mn^{2+} to Eu^{3+} is energetically unfavourable, with a ΔG_{ET} = +41.5 kJ mol^{-1} (assuming, $E_{ox}(Mn^{2+})$ = +1.51 V, $E_{red}(Eu^{3+})$ = –1.2 V, E_{Ln*} = +2.13 eV and $e^2/\varepsilon r$ = 0.15). An alternative mechanism is energy transfer, which is highly dependent upon the distance between the donor and acceptor. This would explain the lower K_{SV}^{-1} for [Eu·L[10]], compared to [Eu·L[9]], as the Eu^{3+} centre is less shielded in the methylphosphinate complex, allowing Mn^{2+} greater access to the central Eu^{3+} ion.

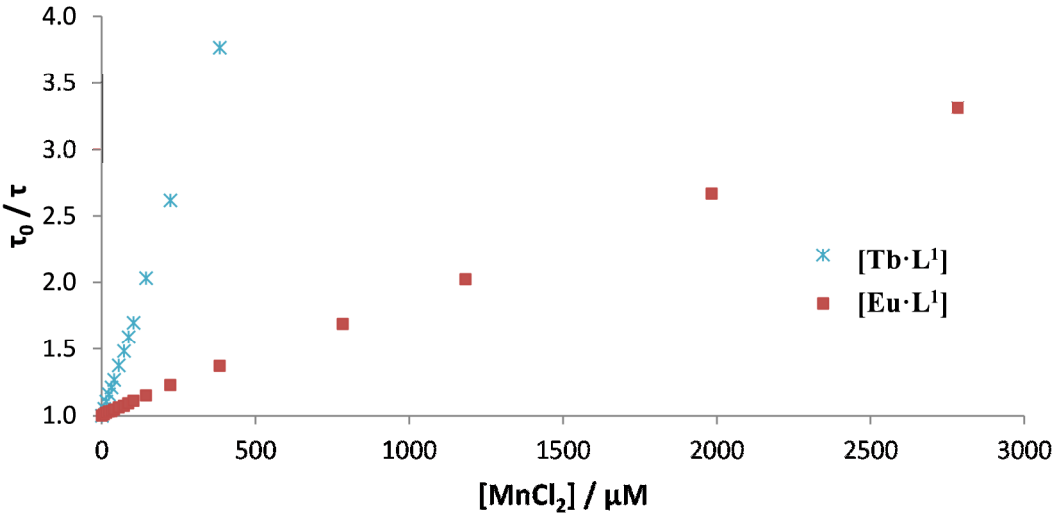

Figure 6.4 Stern-Volmer plots for the quenching of [Eu·L[1](H$_2$O)] and [Tb·L[1](H$_2$O)] by $MnCl_2$ (H$_2$O, 20 μM complex, 0.1 M HEPES, 0.1 M NaCl, pH 7.4, 295 K).

Table 6.2 Stern-Volmer quenching constants for Mn^{2+} quenching of selected Eu^{3+} and Tb^{3+} complexes (H$_2$O, 20 μM complex, 0.1 M HEPES, 0.1 M NaCl, pH 7.4, 295 K).

Complex	K_{SV}^{-1} / mM
[Eu·L[1](H$_2$O)]	1.22
[Tb·L[1](H$_2$O)]	0.16
[Eu·L[9]]	12.3
[Tb·L[9]]	4.00
[Eu·L[10]]	7.69

For energy transfer to occur between Ln* and Mn^{2+}, spectral overlap is required between the donor emission and acceptor absorption spectra. The absorption spectrum of $MnCl_2$ was recorded in water

and was found to have an absorption maximum at 520 nm (*Figure 6.5*). This band arises from a *d – d* transition, which is spin forbidden in the high-spin d^5 Mn^{2+} aqua ion, resulting in a very low molar extinction coefficient (ε = 0.018 M^{-1} cm^{-1}). The emission spectra of [Eu·L^9] and [Tb·L^9] are also shown in *Figure 6.5*, and indicate that spectral overlap exists between both Ln^{3+} emission spectra and the Mn^{2+} absorption spectrum. It is also apparent that the spectral overlap is greatest for Tb^{3+}, which explains the observed lower values of K_{SV}^{-1} for Tb^{3+} complexes of a common ligand. The low molar extinction coefficient of Mn^{2+} may disfavour the hypothesis that energy transfer quenching leads to the observed Mn^{2+} emission. However, as the excited state lifetimes of Ln^{3+} are long-lived (millisecond range), many diffusive encounters can take place between Mn^{2+} ions and Ln*, increasing the probability of energy transfer.

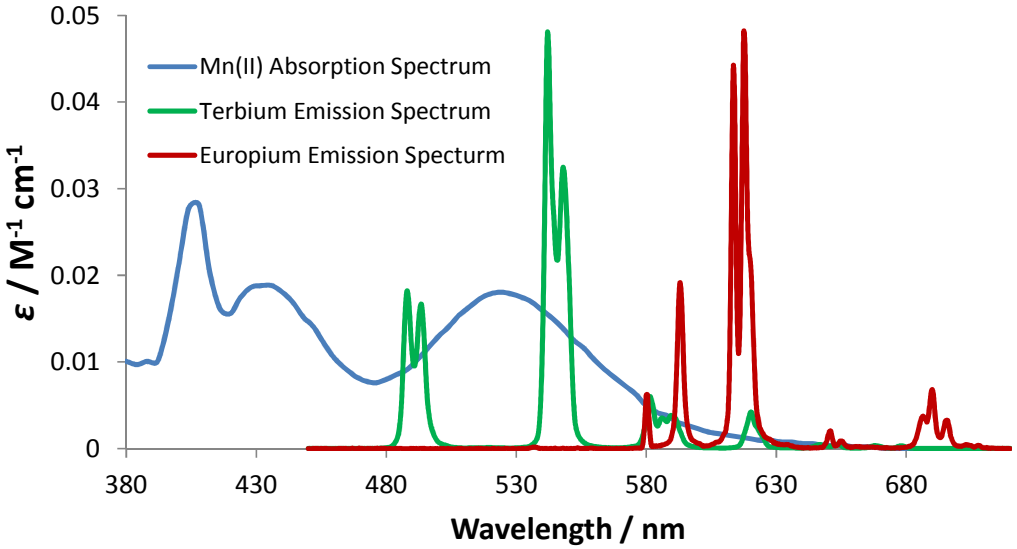

Figure 6.5 Molar extinction coefficient for $MnCl_2$ (*blue*) as a function of wavelength (H_2O, pH 7.4, 295 K). The emission spectra for [Tb·L^9] (*green*) and [Eu·L^9] (*red*) are shown to allow analysis of the spectral overlap integral.

From this brief study of the mechanism of quenching by Mn^{2+} ions, it can be hypothesised that deactivation occurs from the Ln* state, via a mechanism involving energy transfer, during the excited state lifetime of Ln*.

6.2.2 Cu^{2+} Quenching

Parallel quenching studies were carried out with aqueous $CuCl_2$ to investigate any differences in the ability of the two first row transition metals to deactivate the Ln* excited state. Under the same conditions as the Mn^{2+} quenching experiments, Cu^{2+} was found to reduce both the emission intensity and excited state lifetime of [Eu·L^1(H_2O)], [Tb·L^1(H_2O)] and [Eu·L^9]. Stern-Volmer quenching constants were determined and compared with the values measured for Mn^{2+} quenching (*Table 6.3*). In the presence of Cu^{2+}, [Eu·L^1(H_2O)] is quenched to a greater extent than [Tb·L^1(H_2O)]. This is in contrast to the quenching by Mn^{2+}, which showed around 10 fold greater quenching for the Tb^{3+} analogue. A second observation is that the two Eu^{3+} complexes are quenched more efficiently by Cu^{2+}

than Mn^{2+}. There is around a 3 fold increase in quenching for [Eu·L[9]] and a 15 fold increase for the less shielded [Eu·L[1](H$_2$O)].

Table 6.3 Stern-Volmer quenching constants for Cu^{2+} and Mn^{2+} quenching of selected Eu^{3+} and Tb^{3+} complexes (H_2O, 20 μM complex, 0.1 M HEPES, 0.1 M NaCl, pH 7.4, 295 K).

Complex	K_{SV}^{-1} (Cu^{2+}) / mM	K_{SV}^{-1} (Mn^{2+}) / mM
[Eu·L[1](H$_2$O)]	0.08	1.22
[Tb·L[1](H$_2$O)]	0.18	0.16
[Eu·L[9]]	3.78	12.3

To investigate whether these finding are consistent with the proposed energy transfer quenching mechanism, the absorption spectrum of $CuCl_2$ was measured (*Figure 6.6*). A broad *d* – *d* transition, centred at 810 nm is observed. In contrast to the absorption of Mn^{2+}, the d^9 Cu^{2+} transition is spin allowed, resulting in a higher molar extinction coefficient (11 M^{-1} cm^{-1}).[14] The Cu^{2+} absorption band tails into the spectral region of Eu^{3+} emission and, to a lesser extent, Tb^{3+} emission. This would explain to the higher rate of quenching of [Eu·L[1](H$_2$O)], and supports an energy transfer quenching mechanism. Compared to Mn^{2+}, the greater molar extinction coefficient of Cu^{2+} and the better spectral overlap with Eu^{3+} emission, explains the higher rate of quenching by Cu^{2+} of both [Eu·L[1](H$_2$O)] and [Eu·L[9]].

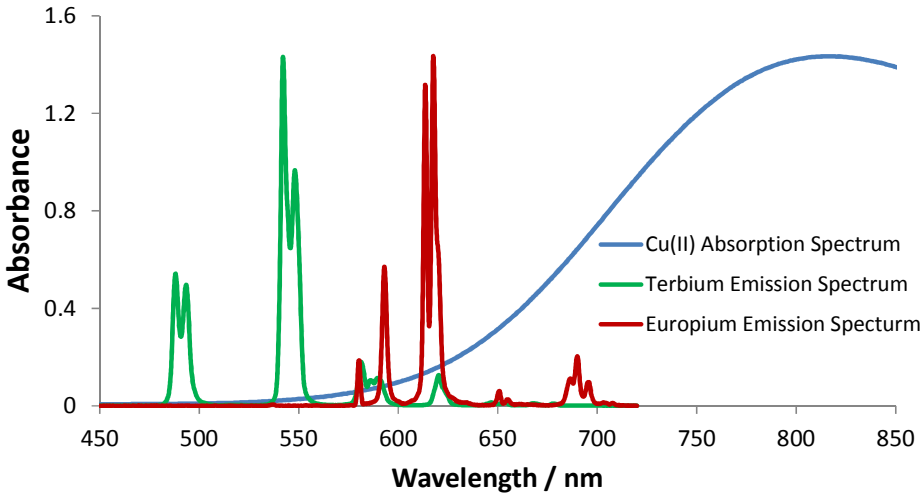

Figure 6.6 Absorption spectrum of $CuCl_2$ (*blue*) as a function of wavelength (H_2O, pH 7.4, 295 K). The emission spectra for [Tb·L[9]] (*green*) and [Eu·L[9]] (*red*) are shown to allow analysis of the spectral overlap integral.

From the preliminary results of the quenching experiments involving several Ln^{3+} complexes and two transition metal ions, the proposed mechanism of quenching is energy transfer from the lanthanide excited state to the transition metal ions, whose *d* – *d* absorption bands show spectral overlap with the Ln^{3+} emission. Consistent with an energy transfer mechanism, which has an r^{-6} dependence, where *r* is the distance between the donor and acceptor, the complex in which the central Eu^{3+} ion is most shielded from the approach of a metal ion, [Eu·L[9]], shows the lowest rate of quenching.

6.3 Quenching by Ascorbate and Urate

Ascorbate and urate are two abundant intracellular antioxidants.[15] Previous reports have commented upon the ability of the two reductants to quench Eu^{3+} and Tb^{3+} emission in complexes that incorporate the electron deficient azaxanthone and tetraazatriphenylene sensitising groups.[16] The mechanism of quenching was shown to involve the formation of an exciplex between the sensitiser triplet excited state and the quencher. To investigate the effect of these quenchers upon $[Eu{\cdot}L^{12}]$ and $[Eu{\cdot}L^{13}(H_2O)]^+$, which incorporate the pyridylalkynylaryl sensitising group, luminescence titrations were carried out.

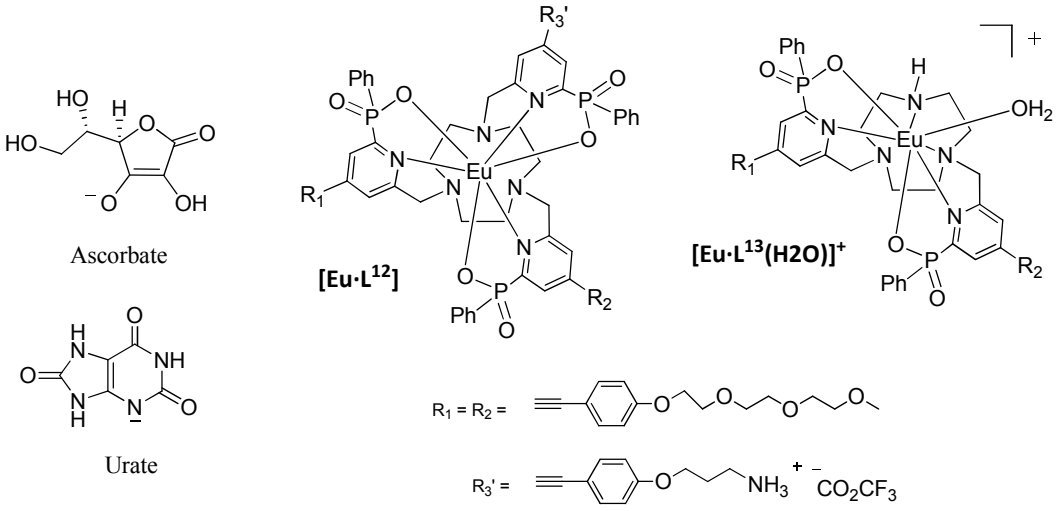

An aqueous solution of ascorbate (50 mM) was added in increments to solutions of $[Eu{\cdot}L^{12}]$ and $[Eu{\cdot}L^{13}(H_2O)]^+$ (H_2O : CH_3OH, 3 : 1, 8 μM complex, 0.1 M HEPES, 0.1 M NaCl, pH 7.4, 295 K), to give final ascorbate concentrations over the range 0 – 10 mM. The emission spectrum and excited state lifetime were measured after each ascorbate addition. Emission spectra and the ascorbate concentrations were corrected for changes in volume upon addition of the ascorbate solution. The two Eu^{3+} complexes were found to have different behaviour in the presence of ascorbate. The coordinatively saturated complex, $[Eu{\cdot}L^{12}]$, showed very little interaction with the intracellular reductant. The form of the emission spectrum remained unchanged throughout the titration, indicating that the Eu^{3+} coordination sphere was not altered by the ascorbate addition (*Figure 6.7 left*). Slight decreases in intensity were due to the change in volume of the sample and, once corrected, no variation in I_0 / I with ascorbate concentration was observed (*Figure 6.8 left*). The excited state lifetime, which is independent of sample concentration, was also unperturbed by ascorbate, with τ_0 / τ remaining around unity throughout the titration (*Figure 6.8 right*).

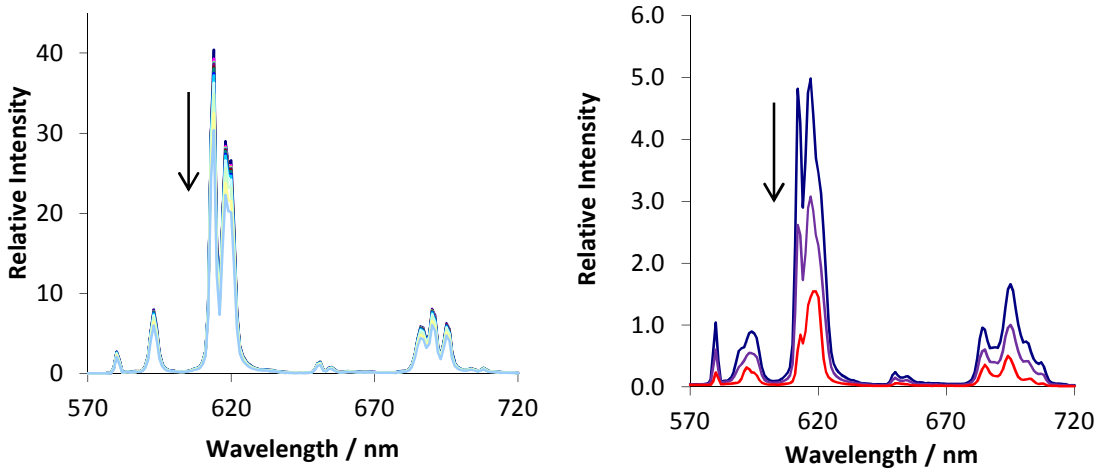

Figure 6.7 Luminescence titrations for [Eu·L[12]] (*left*) and [Eu·L[13](H$_2$O)]$^+$ (*right*) with increasing ascorbate concentrations (H$_2$O : CH$_3$OH, 3 : 1, 8 μM complex, 0 – 10 mM ascorbate, 0.1 M HEPES, 0.1 M NaCl, pH 7.4, 295 K). For [Eu·L[13](H$_2$O)]$^+$, only the emission spectra at 0 (*blue*), 60 (*purple*) and 940 μM (*red*) are shown.

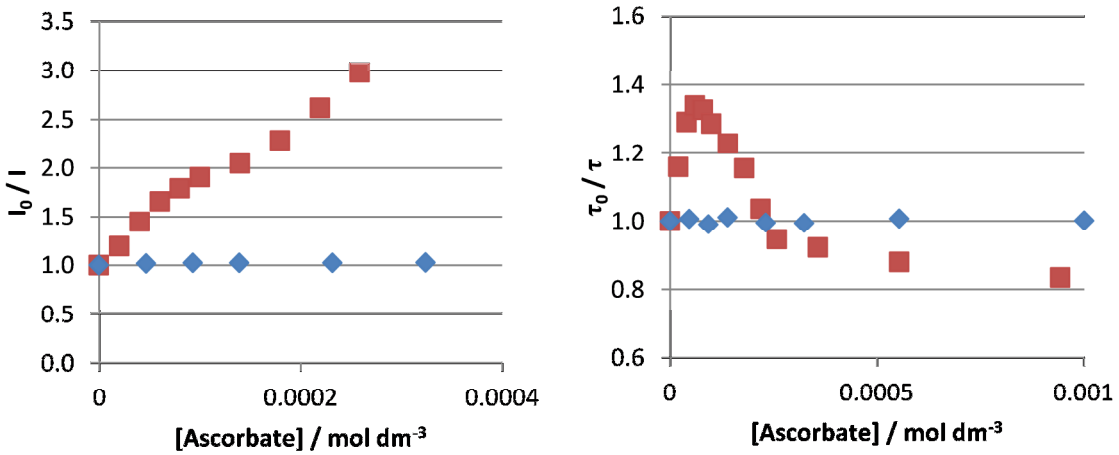

Figure 6.8 Variations in the total integrated emission, I_0 / I (*left*) and excited state lifetime τ_0 / τ (*right*) for [Eu·L[12]] (*blue*) and [Eu·L[13](H$_2$O)]$^+$ (*red*) as a function of added ascorbate.

The coordinatively unsaturated complex, [Eu·L[13](H$_2$O)]$^+$, showed different behaviour in the presence of ascorbate. The overall intensity fell throughout the titration (*Figure 6.7 right*) and a plot of I_0 / I as a function of ascorbate concentration gave an approximately straight line, whose gradient reports an observed Stern-Volmer quenching constant, K_{SV}^{-1}, of 0.14 mM (*Figure 6.8 left*). The excited state lifetime shows unusual behaviour (*Figure 6.8 right*). Initially, the addition of ascorbate led to a decrease in τ, giving a maximum τ_0 / τ of 1.34 at 60 μM. As further additions were made, the excited state lifetime increased and τ_0 / τ fell to a value of 0.83, at the point at which the titration was stopped. To allow interpretation of the change in excited state lifetime with added ascorbate, the emission spectrum of [Eu·L[13](H$_2$O)]$^+$ is shown at three points in the titration: before the ascorbate addition ([ascorbate] = 0 μM) , at the point with the lowest excited state lifetime ([ascorbate] = 60 μm) and after the final ascorbate addition ([ascorbate] = 940 μM). Between 0 – 60 μM, the emission spectrum is unchanged, but between 60 – 940 μM, the spectral form alters slightly, particularly in the hypersensitive ΔJ = 2 band, indicating a change in either the symmetry or the nature of the Eu^{3+} coordination sphere. The relatively small changes in spectral form suggest a change in coordination

environment rather than symmetry, which typically leads to much larger changes in the emission spectrum.

The results of the ascorbate titrations are not easily rationalised. The coordinatively saturated [Eu·L^{12}] appears to show little interaction with ascorbate and no quenching is observed. In contrast, [Eu·L^{13}(H_2O)]$^+$ shows two processes taking place depending upon the concentration of ascorbate. The interaction with [Eu·L^{13}(H_2O)]$^+$ may be related to the positive charge, resulting in a greater Coulombic attraction and a higher probability of encounter with the ascorbate anion. At low concentrations of [Eu·L^{13}(H_2O)]$^+$, a quenching mechanism takes place, leading to the reduction in both emission intensity and lifetime. As the concentration of ascorbate increases beyond 60 μM (7.5 equivalents), the lifetime increases and there is a subtle change in the spectral form of the emission, although the emission intensity continues to fall throughout. The change in emission spectrum suggests that the ascorbate may show a weak binding interaction with the Eu^{3+} centre, which is only apparent at higher concentrations. This is supported by the q value which is initially 1.0, but falls to 0.3 at the end of the titration, suggesting displacement of the bound H_2O by ascorbate. The quenching mechanism, responsible for the initial decrease in τ, must involve either the Eu^{3+} centre or the electron deficient pyridyl moiety, both of which are more accessible to ascorbate in the q = 1 [Eu·L^{13}(H_2O)]$^+$ complex, compared to [Eu·L^{12}].

A hypothesis for the quenching of [Eu·L^{13}(H_2O)]$^+$ by ascorbate involves the initial encounter of the two species, with no displacement of the inner sphere H_2O. Instead, a weak exciplex forms between the electron rich reductant and the electron deficient pyridyl moiety, leading to a lowering and broadening of the sensitiser excited state, causing back energy transfer from the Eu^{3+} excited state. This lowers both the excited state lifetime and emission intensity. This type of exciplex formation was observed between ascorbate and the electron deficient azaxanthone and tetraazatriphenylene sensitisers in previous studies.[12] As the concentration of ascorbate increases, the weak binding interaction with [Eu·L^{13}(H_2O)]$^+$ leads to displacement of the bound H_2O molecule and an increase in excited state lifetime, due to the reduction in vibrational energy transfer quenching. Binding of ascorbate to Eu^{3+} does not alter the symmetry about the metal ion centre, resulting in only small changes in the emission spectrum. For the coordinatively saturated [Eu·L^{12}], the access of ascorbate to both the Eu^{3+} centre and the electron deficient pyridyl group is greatly reduced, leading to no observed quenching of the emission or excited state lifetime.

Luminescence titrations were also carried out with added urate under identical conditions. The addition of urate to samples of [Eu·L^{12}] and [Eu·L^{13}(H_2O)]$^+$ led to similar changes in the observed emission intensity and lifetime, as found with ascorbate. The integrated emission intensity, spectral form and excited state lifetime of [Eu·L^{12}] did not change upon urate addition (*Figure 6.9 left* and *Figure 6.10*). In contrast, a decrease in intensity was observed upon urate addition to [Eu·L^{13}(H_2O)]$^+$ (*Figure 6.9 right* and *Figure 6.10 left*), with an apparent Stern-Volmer quenching constant, K_{SV}^{-1}, of 0.07 mM. Initial decreases in τ were found up to 15 μM urate, before an increase in τ was observed, with τ_0 / τ reaching a maximum value of 0.90 at 280 μM urate (*Figure 6.10 right*). As with the addition of ascorbate, at the end point of the titration a q value of 0.3 was estimated.

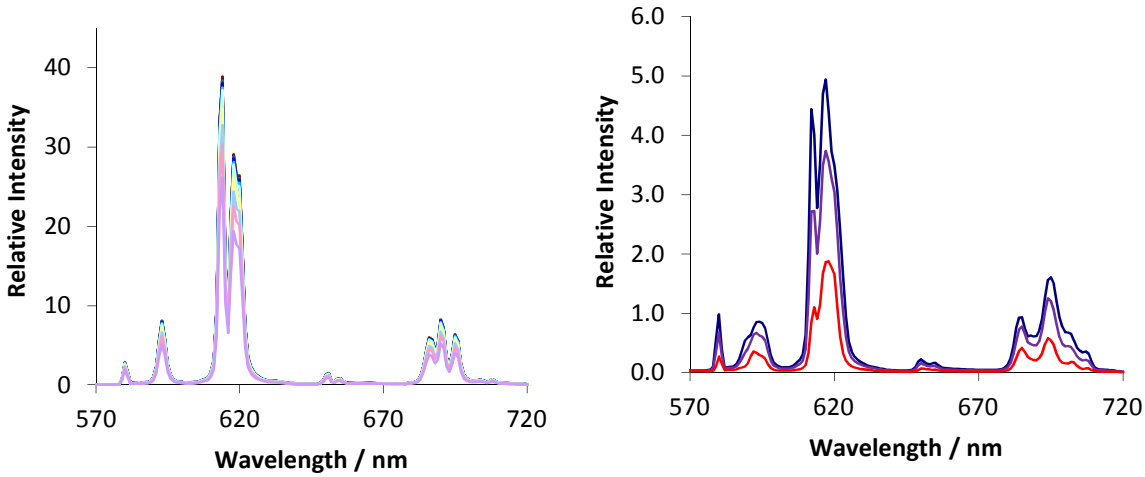

Figure 6.9 Luminescence titrations for [Eu·L^{12}] (*left*) and [Eu·L^{13}(H$_2$O)]$^+$ (*right*) with increasing urate concentrations (H$_2$O : CH$_3$OH, 3 : 1, 8 μM complex, 0 – 300 μM urate, 0.1 M HEPES, 0.1 M NaCl, pH 7.4, 295 K). For [Eu·L^{13}(H$_2$O)]$^+$, only the emission spectra at 0 (*blue*), 15 (*purple*) and 300 μM (*red*) are shown.

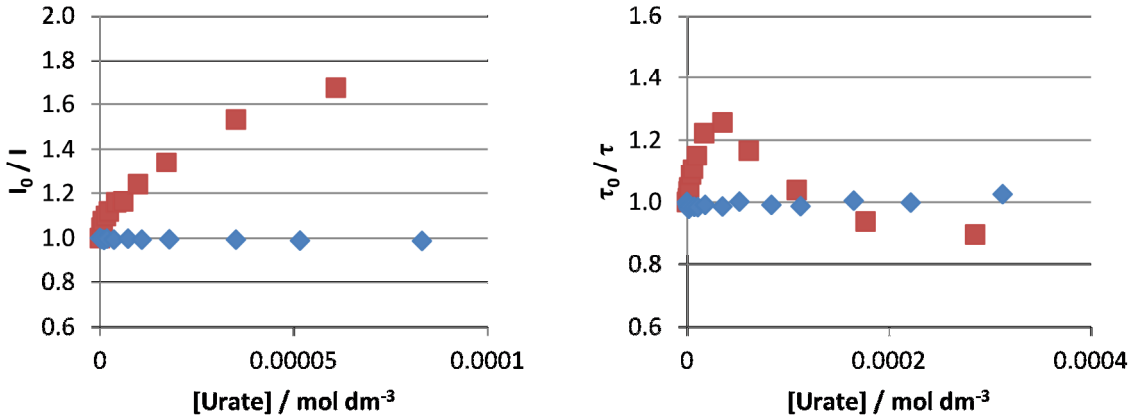

Figure 6.10 Variations in the total integrated emission, I_0 / I (*left*) and excited state lifetime τ_0 / τ (*right*) for [Eu·L^{12}] (*blue*) and [Eu·L^{12}] (*red*) as a function of added urate.

The similarity in the results suggest that both ascorbate and urate quench [Eu·L^{13}(H$_2$O)]$^+$ via the same mechanism. The smaller value of K_{SV}^{-1} for urate was also found in the previous report, which first elucidated the mechanism of quenching,[12] and is further support towards the exciplex formation hypothesis. The similarity in the [Eu·L^{13}(H$_2$O)]$^+$ spectra at the end point of each titration, suggest that the binding mode of the quenchers is similar in each case. Some potential bidentate binding modes of the anions with [Eu·L^{13}(H$_2$O)]$^+$ have been tentatively put forward (*Figure 6.11*), although these are by no means known to be the true structures.

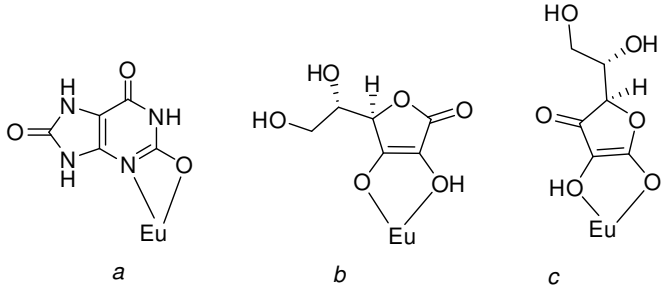

Figure 6.11 Potential binding modes of urate and ascorbate to the Eu^{3+} centre of [Eu·L^{13}]$^+$.

6.4 Conclusions

The quenching of Eu^{3+} and Tb^{3+} emission by Mn^{2+} was shown to be significant for a number of complexes. However, the complexes [Eu·L[9]], [Eu·L[11]] and [Eu·L[12]], which are based upon the 1,4,7-triazacyclononane ligand, with three phenylphosphinate groups, were found to resist Mn^{2+} quenching, in screening assays. To understand the mechanism of quenching, a number of experiments were carried out. Comparison of Mn^{2+} quenching of complexes incorporating the same sensitising group, led to the conclusion that the quenching occurred via the Ln^{3+} excited state. This was supported by the fact that the quenching of Eu^{3+} emission was independent of whether direct excitation or a sensitised emission pathway was employed. Having established that quenching takes place at the Ln^{3+} excited state, the mechanism of quenching was further investigated. An electron transfer process was dismissed, due to the unfavourable free energy changes. Instead, an energy transfer mechanism was proposed in which Mn^{2+} accepts energy from the Ln* state, during the long excited state lifetime. The ability of Mn^{2+} to quench Tb^{3+} emission to a greater extent than Eu^{3+} emission was attributed to the better spectral overlap between the Mn^{2+} absorption and Tb^{3+} emission spectra.

To provide further evidence for the hypothesised quenching mechanism, quenching experiments with aqua Cu^{2+} ions were also carried out. For complexes of a common ligand, it was found that Eu^{3+} emission was quenched to a greater extent than Tb^{3+} emission. This is consistent with an energy transfer mechanism, as the spectral overlap with the Cu^{2+} aqua ion absorption spectrum is greater for Eu^{3+} emission.

An alternative quenching mechanism is hypothesised for the quenching of $[Eu{\cdot}L^{13}(H_2O)]^+$ by ascorbate and urate. At low quencher concentrations, the quencher forms a weak exciplex with the electron deficient pyridyl moiety, leading to quenching of the Eu^{3+} excited state by back energy transfer to the sensitiser excited state. As the quencher concentration increases, a binding process occurs, which displaces the inner sphere H_2O molecule, leading to an increase in the observed excited state lifetime. This hypothesis is supported by a change in the *q* value and the form of the $[Eu{\cdot}L^{13}(H_2O)]^+$ emission spectrum.

6.5 References

1. J. L. Lakowicz, *Principles in Fluorescence Spectroscopy*, 2nd edn., Academic/Plenum Press., New York, 1999.
2. C. A. M. Seidel, A. Schulz and M. H. M. Sauer, *J. Phys. Chem.*, 1996, **100**, 5541-5553.
3. R. F. Steiner and E. P. Kirby, *J. Phys. Chem.*, 1969, **73**, 4130-4135.
4. A. Weller, *Pure Appl. Chem.*, 1968, **16**, 115.
5. S. L. Murov and G. C. Carmichael, *The Handbook of Photochemistry, 2nd ed.*, Dekker, New York, 1999.
6. D. Parker, *Coord. Chem. Rev.*, 2000, **205**, 109-130.
7. D. Parker, P. K. Senanayake and J. A. G. Williams, *J. Chem. Soc. Perkin Trans. 2*, 1998, 2129-2139.
8. T. Gunnlaugsson, D. Parker and J. A. G. Williams, in *Advances in Fluorescence Sensing Technology Iv, Proceedings Of*, ed. J. L. Lakowicz, 1999, vol. 3602, pp. 186-193.
9. G. Bobba, Y. Bretonniere, J. C. Frias and D. Parker, *Org. Biomol. Chem.*, 2003, **1**, 1870-1872.
10. J. C. Frias, G. Bobba, M. J. Cann, C. J. Hutchison and D. Parker, *Org. Biomol. Chem.*, 2003, **1**, 905-907.
11. G.-L. Law, R. Pal, L. O. Palsson, D. Parker and K.-L. Wong, *Chem. Commun.*, 2009, 7321-7323.
12. G. L. Law, D. Parker, S. L. Richardson and K. L. Wong, *Dalton Trans.*, 2009, 8481-8484.
13. N. S. Hush, *Coord. Chem. Rev.*, 1985, **64**, 135-157.
14. J. R. Lalanne, F. Carmona and L. Servant, *Optical Spectroscopies of Electronic Absorption*, World Scientific, 1996.
15. F. Kielar, C. P. Montgomery, E. J. New, D. Parker, R. A. Poole, S. L. Richardson and P. A. Stenson, *Org. Biomol. Chem.*, 2007, **5**, 2975-2982.
16. R. A. Poole, C. P. Montgomery, E. J. New, A. Congreve, D. Parker and M. Bottab, *Org. Biomol. Chem.*, 2007, **5**, 2055-2062.

7. Conclusions and Future Work

7.1 General Conclusions

At the outset of the project, the target was to synthesise a Eu^{3+} complex to act as a FRET donor in the HTRF experiment, using changes in fluorescence to analyse interactions between biological species. The currently used donor, $[Eu{\cdot}L^{1.1}]^{3+}$, serves its purpose well, but improvements are sought, to increase the efficiency of the HTRF assay. To assess the progress made over the past three years, it is worth recapping the original specification, set out at the beginning of the project. The specification was as follows,

i) Design and synthesise an emissive europium complex donor for HTRF application
ii) Optimise the form of the emission spectrum
iii) Select a chromophore with a suitable absorption wavelength
iv) Maximise the molar extinction coefficient and emission quantum yield
v) Design a stable complex in the assay medium
vi) Ensure water solubility
vii) Incorporate a conjugation point

Development went through several stages before a final donor complex was synthesised. Initially, the 3-azaxanthone group was used to sensitise the Eu^{3+} emission, but complexes incorporating this chromophore were found to possess molar extinction coefficients and emission quantum yields that were no higher than $[Eu{\cdot}L^{1.1}]^{3+}$. The change in the form of the Eu^{3+} emission spectrum resulting from variation of the coordinating groups was investigated, and the core ligand structure was varied from 1,4,7,10-tetraazacyclododecane to 1,4,7-triazacyclononane. At each stage of development, improvements were found in the Eu^{3+} emission spectral form and stability in the assay medium.

Using the results from the early stages of the project, a final target complex was designed and synthesised, which met the specification. The emissive complex, $[Eu{\cdot}L^{12}]$, comprises a 1,4,7-triazacyclononane ring with three pyridyl phenylphosphinate groups, providing a 9-coordinate ligand, which saturates the Eu^{3+} coordination sphere. Each of the three pyridyl groups is functionalised in the 4-position with alkynylphenoxy sensitising groups. Extending from two of the sensitising groups are short polyethylene glycol (PEG) chains and from the third, a primary propyl amine.

The properties of the final donor complex fulfil each of the initial specifications set out (*Table 7.1*). The pyridylalkynylphenoxy chromophores are excellent sensitisers for Eu^{3+} emission and absorb light with a maximum absorption wavelength at 332 nm. Using this wavelength of excitation light avoids the excitation of biological fluorophores, such as the aromatic amino acid residues. The molar extinction coefficient of $[Eu{\cdot}L^{12}]$ at 332 nm is very high (60,000 M^{-1} cm^{-1}), as a result of incorporating three chromophores per complex. The chromophore excited state has an energy that is well suited to Eu^{3+} sensitisation, being close enough in energy to maximise energy transfer, while remaining high enough in energy to avoid back energy transfer. This property, along with the shielded nature of the

central Eu^{3+} ion, results in an emission quantum yield of 54 %, which is exceptionally high for a solution state Eu^{3+} complex. The highly shielded nature of the central Eu^{3+} ion, due to the presence of three phenyl groups below the plane of the complex, also gives [Eu·L^{12}] high emission stability in the assay medium. Addition of a series of potential quenchers in a million fold excess led to no reduction in the Eu^{3+} emission. Both the solid and solution state structure of [Eu·L^{12}] were elucidated and revealed a pseudo-C_3 symmetric geometry about the Eu^{3+} centre. Combined with the presence of three polarisable phosphinate donor groups, this led to a highly favourable emission spectrum, with large relative integrated emission intensity in the $\Delta J = 2$ region, giving [Eu·L^{12}] excellent spectral overlap with the designated acceptor moiety in the HTRF experiment. Finally, the presence of the two PEG chains gives [Eu·L^{12}] moderate water solubility and the primary amine allows conjugation in future HTRF experiments.

Table 7.1 Comparison of the properties of the new donor complex, [Eu·L^{12}], and the currently used donor, [Eu·L$^{1.1}$]$^{3+}$. Values for [Eu·L^{12}] measured in H_2O : CH_3OH (3 : 1). Values for [Eu·L$^{1.1}$]$^{3+}$ measured in H_2O (0.4 M KF).

Properties	**[Eu·L^{12}]**	**[Eu·L$^{1.1}$]$^{3+}$**
Maximum Absorption Wavelength, λ_{abs}	332 nm	303 nm
Molar Extinction Coefficient, ε	60,000 M^{-1} cm^{-1}	18,000 M^{-1} cm^{-1}
Emission Quantum Yield, Φ	54 %	10 %
Brightness ($\varepsilon \times \Phi$)	32.4 mM^{-1} cm^{-1}	1.8 mM^{-1} cm^{-1}
$\Delta J = 2$: $\Delta J = 1$ intensity ratio	7.1	1.4
$\Delta J = 2$: $\Delta J = 4$ intensity ratio	3.8	1.3
Aqueous Solubility	Moderate	High
Conjugation Point	✓	✓
Stability in the Assay Medium	High	High

To assess the potential for [Eu·L^{12}] to act as a FRET donor, its properties can be compared to the currently used donor complex (*Table 7.1*). The higher values for the molar extinction coefficient and the emission quantum yield give [Eu·L^{12}] an 18 fold increase in overall brightness ($\varepsilon \times \Phi$). The spectral overlap with the acceptor moiety, which can be quantified by the $\Delta J = 2$: $\Delta J = 1$ ratio, shows a 5 fold increase. Along with these vast improvements upon [Eu·L$^{1.1}$]$^{3+}$, [Eu·L^{12}] is stable in the assay medium, incorporates a conjugation point and has high enough water solubility for the HTRF experiment. Overall, [Eu·L^{12}] is an excellent candidate to act as a FRET donor in the HTRF assays, and commercial development of these systems is underway.

The pyridylalkynylphenoxy chromophore is very well suited to sensitisation of Eu^{3+} emission. As well as the HTRF experiment, many other applications of emissive Eu^{3+} complexes would benefit from the high molar extinction coefficients and emissive quantum yields, which result from incorporation of this chromophore. Indeed, the responsive system, [Eu·L^{13}]$^{+}$, which was shown to bind to a number of anions, leading to large changes in the Eu^{3+} emission spectral form, has excellent photophysical properties (ε = 44,000 M^{-1} cm^{-1} and Φ = 23 %), notwithstanding the presence of an inner sphere water molecule. Competitive anion binding studies found [Eu·L^{13}]$^{+}$ to be selective toward bicarbonate, due to the steric demand at the Eu^{3+} centre. This result demonstrates the ability of complexes

incorporating the chromophore to combine very high brightness with responsiveness, opening up the possibilities of more sensitive optical probes for fluorescence microscopy. In conclusion, the pyridylalkynylphenoxy moiety may define the next generation of chromophores for sensitised europium emission.

An interesting result came out of the investigation into the stereochemistry of the C_3 symmetric series, [Ln·L^9]. In solution, the complexes were found to exist as enantiomers of a single diastereomer. The steric bulk of the three phenylphosphinate groups led to consistent stereochemistry at each phosphorus centre (*RRR* or *SSS*). This, in turn, dictated the conformation of both the 1,4,7-triazacyclononane ring ($\delta\delta\delta$ or $\lambda\lambda\lambda$) and the N_{ring}-C-C-N_{py} (Δ or Λ) torsion angles. The resulting enantiomers were resolved by chiral-HPLC and the absolute stereochemistry was determined by comparison of the theoretical and calculated circular dichroism spectra. Following excitation, intense CPL was measured from the enantiomers of [Eu·L^9] and [Tb·L^9], with g_{em} values up to 0.4. There is a potential application for enantiopure highly luminescent lanthanide complexes in cellular microscopy. If a complex can be prepared with intense CPL and suitable intracellular photophysical properties, it may be able to report changes in the chiral environment within a cell by changes in the CPL emission. Enantiomers of the model complex, [Eu·L^{11}], which has the same core structure as [Eu·L^9], and incorporates the alkynylphenoxy sensitising groups, did not separate under the same chiral-HPLC conditions. If resolution can be achieved, then complexes of this type may find use as intracellular chiroptical probes.

Whilst not applicable to the HTRF application, complexes incorporating azaxanthone and azathiaxanthone chromophores showed some intriguing behaviour in cells. Fluorescence microscopy was used to visualise the complexes in a number of cell lines at a various concentrations. Using a 50 μM complex concentration in the incubation medium, the bis(azaxanthone) complexes, [Ln·L^2]$^+$ and [(1-AX)-Ln·L^2]$^+$, localised in the lysosomes of CHO and NIH-3T3 cell lines. At lower concentrations (50 nM), [Tb·L^2]$^+$ and [(1-AX)-Tb·L^2] were found to localise within cell nuclei. More specifically, the complexes associated with chromatin of cells undergoing mitosis. In contrast, the bis(azathiaxanthone) complex, [Eu·L^{2b}]$^+$, was found to localise within the nucleoli, which are known to be rich in ribosomes. The results suggest the complexes have an affinity for protein, but their behaviour is very curious and not easily rationalised. One thing that is clear is that if the mechanisms for uptake and trafficking of these complexes can be better understood there is huge potential for the use of emissive lanthanide complexes as intracellular probes.

7.2 Future Work

The photophysical properties of [Eu·L[12]] are ideal for the HTRF application. It is hard to envisage significant increases in the molar extinction coefficient or emissive quantum yield without moving to a completely new chromophore and ligand system. One area in which improvement can be made is the aqueous solubility. The rather hydrophobic [Eu·L[12]] has sufficient water solubility for the HTRF experiment but for other applications, such as intracellular fluorescence microscopy, an increase in the solubility is required. To increase the water solubility, while retaining the favourable photophysical properties of [Eu·L[12]], there are two sites which could be modified. These are the phenylphosphinate groups and the terminal groups, which are PEG or propylamine for [Eu·L[12]] (*Figure 7.1*). Initially, the phenyl moiety was selected as the phosphinyl precursor was commercially available. Subsequently, it was found that the phenyl groups play an important role in shielding the Eu^{3+} centre from external quenchers. Exchange of the phenyl groups for more water soluble groups, which also shield the Eu^{3+} centre, could be a great advantage. One example has already been investigated in the transition from [Eu·L[9]] to [Eu·L[10]]. In this case, exchange of phenyl for methyl groups led to a large increase in water solubility, with only a small decrease in the emission stability. A similar exchange in [Eu·L[12]] would be a good first step towards improving solubility. Other water solubilising groups, which could take the place of Ph include $CH_2CH_2CO_2^-$, $CH_2CH_2SO_3^-$ and $PhCO_2^-$.

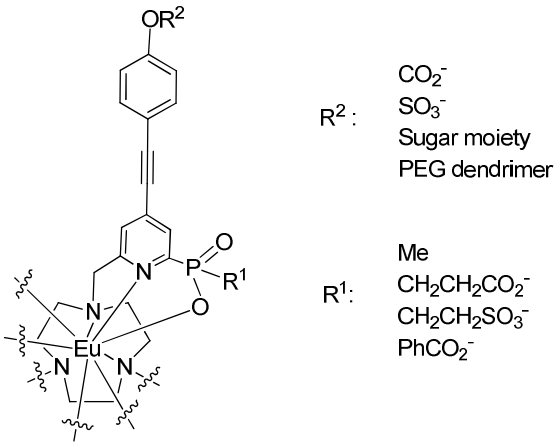

Figure 7.1

The other site available for modification is the terminal alkynylaryl groups (*Figure 7.1* – R^2). Two PEG chains were incorporated into [Eu·L[12]] to increase the water solubility. Whilst some improvement was seen, in comparison to [Eu·L[11]], further improvements could be achieved by incorporating longer chain or dendritic PEG moieties. Alternatively, other water solubilising groups could be investigated, such as SO_3^-, CO_2^- or sugar based moieties. One example of an open chain sugar in this position has already been synthesised, and was found to increase the water solubility to a reasonable extent. To maximise aqueous solubility, modification of both sites on [Eu·L[12]], although synthetically challenging, is probably required.

A second area of future development is to achieve sensitisation of Tb^{3+} emission with pyridylalkynylaryl chromophores. Whilst the chromophore employed in the complexes [Eu·L[11]] and

[Eu·L[12]] are very capable of sensitising Eu^{3+} emission, the analogous [Tb·L[11]] gave very weak emission, following excitation at 332 nm. Measurement of the triplet energy of the pyridylalkynylanisole moiety (***43***) indicated that back energy transfer from the Tb^{3+} long-lived excited state was likely to take place, resulting in the observed weak Tb^{3+} emission. To allow Tb^{3+} sensitisation, a chromophore must be devised, which has a higher triplet energy level. So as to retain the high molar extinction coefficient, the pyridylalkynylphenyl moiety should be retained. Variation of the terminal group is the most reasonable way to raise the triplet energy. To predict which groups will raise the triplet energy is non-trivial. A screening process may be required to investigate the effects of polarity and electron donation or withdrawal of the terminal group upon the triplet energy. It can be predicted that once a triplet energy level of around 22,400 cm^{-1} is achieved, Tb^{3+} sensitisation will be possible.

Another area of future development involves the responsive complexes, such as $[Eu·L^{13}]^+$. This highly emissive complex was found to give large changes in spectral form upon anion binding, and was selective towards bicarbonate. Emissive complexes based upon $[Eu·L^{13}]^+$ which are selective towards other biological anions, such as citrate and lactate, are very desirable. It may be that variation of the Ph groups of $[Eu·L^{13}]^+$ for less sterically demanding groups would relieve steric demand about the Eu^{3+} centre, and lead to greater selectivity towards larger anions. One application for such a probe is in intracellular assays, where fluctuations in the concentration of anions are associated with biological processes. Fluorescence microscopy is the technique used to visualise emissive probes from within cells, and requires that changes in emission are large and spectrally resolved. One technique employed in intracellular anion detection is to combine Eu^{3+} and Tb^{3+} complexes of a common ligand. In these systems, the emission intensity of the Eu^{3+} analogue is more responsive to anion binding, leading to a ratiometric analysis by comparing the Eu^{3+} and Tb^{3+} emission. For this type of ratiometric sensing to be applicable for complexes incorporating the pyridylalkynylaryl chromophore, the two previously discussed improvements, concerning Tb^{3+} sensitisation and aqueous solubility, must be made.

The final area in which future work should be concentrated is in the application of circularly polarised luminescence. While resolution of [Ln·L[9]] was achieved, enantiomers of the extended system [Eu·L[11]] were not isolated. For the proposed application of intracellular chiroptical microscopy, which may reveal changes in the chiral cellular environment by a variation in CPL from emissive complexes, a highly emissive and enantiopure system is required, which can absorb incident light at a wavelength greater than 300 nm. The enantiomers of [Eu·L[12]], or perhaps a more water soluble analogue, would be ideal candidates for this technique. If resolution of [Eu·L[12]] cannot be achieved, one possible alternative would be to resolve an analogue of [Eu·L[9]], say the pyridyl *para*-bromo complex, which could subsequently be functionalised with the alkynylaryl groups. Chiroptical microscopy relies not only upon emissive enantiopure complexes but also the equipment to detect CPL from within cells. Generally, CPL has fairly low intensity and detection from within cells, where quenching processes lead to decreases in emission intensity, is a great challenge, and would require very sensitive detectors. Despite this, a lot of information about cellular processes may be obtained if such a technique were available.

7.3 Final Remarks

Emissive lanthanide complexes are excellent donor moieties for FRET and are routinely exploited in the HTRF immunoassay technology. The development of complexes with high molar extinction coefficients and emissive quantum yields, such as [Eu·L^{12}], leads to improvements in the efficiency of the technique, and ultimately result in a reduction in the cost of each assay.

In the field of fluorescence microscopy, lanthanide complexes are yet to make any commercial impact as intracellular emissive species. The advantages of these systems are the long-lived emission, allowing time-gated detection, and, in the case of europium complexes, the responsiveness of the emission to the coordination environment of the central ion, leading to systems that can probe the cellular environment. To compete with the organic dyes and fluorescent proteins commonly used in fluorescence microscopy, bright and water soluble lanthanide complexes are required, that are resistant to intracellular quenching of emission. The europium complexes described in the latter part of this report, which have quantum yields of up to 50 % and are highly resistant to quenching, due to the shielded lanthanide centre, may well be an important step towards the development of highly emissive lanthanide complexes for fluorescence microscopy.

8. Experimental

8.1 Experimental Procedures

8.1.1 General Procedures

Commercially available reagents were used as received from suppliers. Solvents were laboratory grade and dried using an appropriate drying agent when required. Reactions requiring anhydrous conditions were carried out under an atmosphere of dry argon using Schlenk-line techniques. Where appropriate, solvents were degassed using the freeze-thaw cycle method.

Thin-layer chromatography was carried out on silica plates (Merck 5554) or neutral alumina plates (Merck Art 5550) and visualised under UV (254/365 nm) irradiation or by staining with iodine. Preparative column chromatography was carried out using silica (Merck Silica Gel 60, 230400 mesh) or neutral alumina (Merck Aluminium Oxide 90, activity II-III, 70230 mesh), pre-soaked in ethyl acetate.

pH measurements were carried out at 295 K using a Jenway 3320 pH meter with a Sigma-Aldrich micro-pH combination electrode. Calibration was performed using commercially available buffer solutions at pH = 4.0 ±0.02, pH = 7.00 ±0.02 and pH = 10.00 ±0.02.

NMR spectra (^{1}H, ^{13}C, ^{31}P) were recorded on a Varian VXR-400 spectrometer (^{1}H at 399.97 MHz, ^{13}C at 100.57 MHz, ^{31}P at 161.91 MHz), a Varian Inova-500 spectrometer (^{1}H at 499.78 MHz, ^{13}C at 125.67 MHz) or a Varian VNMRS-700 spectrometer (^{1}H at 699.73 MHz, ^{13}C at 175.95 MHz). Spectra were recorded at 295 K in commercially available deuterated solvents and referenced internally to the residual solvent proton resonances. Variable temperature NMR was carried out using the Varian Inova-500 spectrometer with the assistance of Dr. Alan Kenwright at Durham University.

Both electrospray and high resolution mass spectrometry were performed on a Thermo-Finnigan LTQ FT system using methanol as the carrier solvent.

Melting points were recorded using a Reichart-Köfler block and are uncorrected.

8.1.2 HPLC Analysis

Reverse phase HPLC analysis was performed at 298 K on a Perkin Elmer system, comprising a Perkin Elmer Series 200 pump, Perkin Elmer Series 200 autosampler, Perkin Elmer Series 200 UV/Vis detector and Perkin Elmer Series 200 fluorescence detector. Either a 150 × 4.66 mm 4 micron Phenomenex Synergi 4μ Fusion-RP 80i column or an XBridge C18 10 cm 3.5 μm column was used

with a flow rate of 1 mL / min and run times varying from 15 – 25 min. A solvent system of H_2O (0.1 % HCOOH) / CH_3CN (0.1 % HCOOH) (gradient elution) was used. The UV/Vis and fluorescence detectors were set at appropriate wavelengths according to the species being analysed. Methods and HPLC traces for each complex can be found in *Appendix 1*.

Chiral HPLC was performed at 288 K on the same Perkin Elmer system described above using a CHIRALPAK-IC 4.6 × 250 mm 5 μm column at a flow rate of 1 mL / min and a solvent system of CH_3OH / CH_3CH_2OH / $HNEt_2$ (50 : 50 : 0.1) (isocratic elution).

8.1.3 Optical Techniques

All samples for optical analyses were contained in quartz cuvettes with a path length of 1 cm and a polished base. Measurements were recorded at 295 K unless otherwise stated.

UV/Vis absorbance spectra were measured on a Perkin Elmer Lambda 900 UV/Vis/NIR spectrometer using FL Winlab software. Samples were measured relative to a reference of pure solvent contained in a matched cell.

Emission spectra were measured on a ISA Joblin-Yvon Spex Fluorolog-3 luminescent spectrometer using DataMax v2.20 software. Excitation wavelengths were selected according the specific measurement. An integration time of 0.5 seconds, increment of 0.5 nm and excitation and emission slit widths of 2.5 and 1.5 nm, respectively, were used throughout.

CD spectra were measured by Dr. Lorenzo Di Bari at the University of Pisa.

CPL spectra were recorded on a custom modified Spex Fluoromax-2 spectrometer at the University of Glasgow, with the assistance of Dr. Bob Peacock.

Lifetime measurements were carried out using a Perkin Elmer LS55 luminescence spectrometer. Lanthanide excited state lifetimes were measured by excitation of the sample by a short pulse of light followed by monitoring the integrated intensity of light emitted during a fixed gate time, t_g, after a delay time of t_d. Excitation and emission wavelengths were selected based upon the Ln complex. Measurements were made for at least 30 delay times over a period of three or more lifetimes. A gate time of 0.1 ms was used and the excitation and emission slits were both set to 4 nm. The obtained decay curves were fitted to *Equation 8.1*, using Origin 6.0 software.

$$I = A_0 + A_1 e^{-kt} \qquad [8.1]$$

where: I is the intensity at time t after the excitation pulse; A_0 is the intensity after decay is completed; A_1 is the pre-exponential factor and k is the rate constant for decay of the excited state. The excited state lifetime, τ, is the inverse of the rate constant, k.

The inner sphere hydration number (q) of Eu and Tb complexes were obtained by measuring the excited state lifetime in H_2O and D_2O, following D_2O exchange. The q value was calculated using *Equation 8.2* and *8.3* (see Beeby *et al.* for derivation).[1]

$$q_{Eu} = 1.2\left(k_{H_2O} - k_{D_2O} - 0.25 - 0.075n\right) \quad [8.2]$$

$$q_{Tb} = 5.0\left(k_{H_2O} - k_{D_2O} - 0.06 - 0.010n\right) \quad [8.3]$$

where: q_{Ln} is the inner sphere hydration number; k is the inverse of the excited state lifetime, τ, and n is the number of proximal amide NH oscillators.

Molar extinction coefficients were measured using a Perkin Elmer Lambda 900 UV/Vis/NIR spectrometer. For each sample, a bulk solution was made up by dissolving a known amount of solid (typically 5 mg to ± 0.05 mg accuracy) in a known amount of solvent (typically 10 mL to ± 0.1 μL accuracy). Five solutions of known concentration were then made up by dilution of the bulk solution, with absorbances ranging between 0.05 and 0.5. Molar extinction coefficients were calculated by plotting absorbance as a function of concentration according to *Equation 8.4*.

$$A = \varepsilon c l \quad [8.4]$$

where: A is the absorbance at λ_{max}; ε is the molar extinction coefficient; c is the concentration and l is the pathlength of the cell.

Photoluminescence quantum yield measurements were carried out using a HORIBA Jobin-Yvon Fluorolog 3-22 Tau-3 fluorimeter with a Labsphere Optical Spectralon integrating sphere (diameter 100 mm, reflectance > 99 % over 400 – 1500 nm range) using a method developed by Porrés *et al.*[2] Measurements were performed at 295 K using solutions with absorbances of 0.1 at λ_{max}, contained in a cylindrical quartz cuvette (8 mm diameter) fitted with a Teflon stopper. Quantum yields were also measured by comparison with relevant, known standards (e.g. [Eu·L[11]] was used as a standard for [Eu·L[12]]). For the standards and each of the unknowns, five solutions with absorbances between 0.05 and 0.15 were used. The quantum yield was calculated by plotting the integrated emission as a function of the absorbance for both the known and unknown species according to the *Equation 8.5*.

$$\Phi_x = \Phi_r \cdot \frac{A_r}{A_x} \cdot \frac{E_x}{E_r} \cdot \frac{I_r}{I_x} \cdot \frac{\eta_x^2}{\eta_r^2} \quad [8.5]$$

where: r and x refer to the reference standard and the unknown, respectively; A is the absorbance at λ_{max}; E is the corrected integrated emission intensity; I is the corrected intensity of excitation light and η is the refractive index of the solution.

Triplet energy measurements were carried out using an Oxford Instruments optical cryostat with an ISA Joblin-Yvon Spex Fluorolog-3 luminescent spectrometer. Samples were dissolved in EPA (Et_2O : isopentane : EtOH [2 : 5 : 5 *v*/*v*]) and cooled to 77 K. Triplet energies were calculated by measuring the highest energy phosphorescence emission band, which was attributed to the 0 – 0 transition from the triplet excited state to the ground state.

Binding constants of selected anions and HSA with [Eu·L[13]] were calculated by luminescence titrations. Highly concentrated anion solutions were added so as to minimise increase in sample volume (typically 1 – 50 μL additions to 2500 μL [Eu·L[13]] solution). Each Eu emission spectrum was corrected for dilution. HSA was added as a solid. Apparent binding constants were calculated according to *Equation 8.6*, using Microsoft Excel non-linear iterative curve fitting software.

$$[X] = \frac{\frac{\left(\frac{(F-F_0)}{(F_1-F_0)}\right)}{K} + [Eu]\cdot\left(\frac{(F-F_0)}{(F_1-F_0)}\right) - [Eu]\cdot\left(\frac{(F-F_0)}{(F_1-F_0)}\right)^2}{1-\left(\frac{(F-F_0)}{(F_1-F_0)}\right)} \qquad [8.6]$$

where: *[X]* is the total concentration of anion in the solution; *[Eu]* is the total concentration of the complex; *K* is the binding constant; *F* is the ratio of selected integrals; F_0 is the initial ratio and F_1 is the final ratio.

8.1.4 Cellular Studies and Microscopy

Four cell lines were selected for cellular studies: CHO (Chinese Hamster Ovary), NIH 3T3 (mouse skin fibroblast), HeLa (human endothelial carcinoma cells) and PC3 (human prostate cancer cells). Cells were maintained in exponential growth as monolayers in appropriate media, which were supplemented with 10% foetal bovine serum (FBS) and 1% penicillin and streptomycin. Cells were incubated at 37 °C, 20% average humidity and 5% (v/v) CO_2.

Epifluorescence microscopy images were taken on a Zeiss Axiovert 200M epifluorescence microscope, equipped with an Axiocam CCD camera. Samples were excited using a 340 - 390 nm (90% transmission) bandpass filter. Eu and Tb emission were observed using a 570 nm long-pass filter (85% transmission) and a 490 nm long-pass (LP) filter (85% transmission), respectively.

Cytotoxicity studies were carried out using the MTT assay with the NIH-3T3 cell line.[3] Approximately 1 x 10^4 cells in 100 μL DMEM were seeded into each well of a 96-well plate and allowed to attach overnight. Solutions of complexes were added to triplicate wells to give final concentrations over a 2-log range. After 24 h incubation, MTT 3-(4,5-dimethylthiazol-2-yl)-2,5-diphenyltetrazolium bromide (final concentration 1.0 mM) was added to each well and the plate incubated for a further 4 h. The culture medium was removed, and DMSO (150 μL) was added. The plate was shaken for 20 sec and the absorbance measured immediately at 540 nm in a microplate reader against a blank of DMSO. IC_{50} values were determined as the complex concentration required

to reduce the absorbance to 50% of that in the untreated, control wells, and represent the mean value for data from at least three independent experiments.

8.1.5 X-ray Studies

X-ray diffraction structures were carried out by Dr. Horst Puschmann and Dr. Dmitry Yufit. Single crystal X-ray data for the complexes [Ln·L[9]] were collected at 120 K on a Bruker SMART-CCD 6000 diffractometer (ω-scan, 0.3-0.5° / frame) equipped with an Oxford Cryostream open-flow nitrogen cryostat. The structures were solved by Patterson method and refined by full-matrix least squares on F^2 for all data using SHELXTL[4] and OLEX2[5] software. All non-disordered non-hydrogen atoms were refined with anisotropic displacement parameters. All hydrogen atoms were placed into calculated positions and refined in 'riding'-mode. All structures contain a number of severely disordered solvent molecules. Their contribution to the scattering factors has been taken into account using the MASK procedure of OLEX2 software.

8.2 Synthetic Procedures

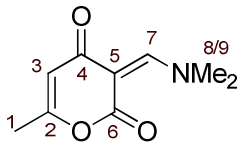

3-(Dimethylaminomethylene)-4-oxo-6-methyl-2-pyrone, 1[6]

To a suspension of 4-hydroxy-6-methyl-2-pyrone (25 g, 0.2 mol) in *p*-dioxane (100 mL) was added N,N-dimethylformamide dimethyl acetal (44 g, 0.37 mol). The resulting solution was stirred at room temperature for 1 h to give a deep red solution containing a yellow precipitate. The mixture was left in the fridge overnight before the precipitate was collected by filtration to yield the *title compound* (25 g, 69 %). A small sample was recrystallized from hot ethanol for characterisation. m.p. 145 - 147 °C (Lit.[6] 152 – 154 °C), δ_H ($CDCl_3$) 8.22 (1H, s, H^3), 5.64 (1H, s, H^7), 3.45 (3H, s, H^8), 3.36 (3H, s, H^9), 2.12 (3H, s, H^1), *m/z* (HRMS$^+$) 182.0821 $[M + H]^+$ ($C_9H_{12}NO_3$ requires 182.0817).

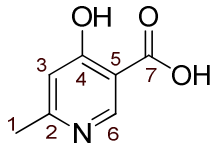

4-Hydroxy-6-methylnicotinic acid, 2[6]

To a solution of 3-(Dimethylaminomethylene)-4-oxo-6-methyl-2-pyrone, ***1*** (6.5 g, 36 mmol) in distilled water (45 mL) was added 35 % ammonia solution (17.8 g, 15.7 mL, 0.37 mol) causing a yellow precipitate to form. After stirring at room temperature for 30 min, 40 % dimethylamine solution was added (4.05 g, 4.55 mL, 36 mmol). The resulting yellow solution was heated at 50 °C for 30 mins before being cooled to room temperature. Upon acidification to pH 5 by addition of sulphuric acid a yellow precipitate formed. The mixture was stirred in an ice bath for 1 h before the precipitate was collected by filtration to yield the *title compound* (4.0 g, 72 %), m.p. 241 - 243 °C (Lit.[6] 267 – 268 °C) , δ_H (D_2O) 8.44 (1H, s, H^6), 6.71 (1H, s, H^3), 2.37 (3H, s, H^1), δ_C (D_2O) 176.5 (C^7), 168.9 (C^4), 154.5 (C^5), 143.0 (C^6), 115.6 (C^3), 114.2 (C^2), 18.5 (C^1), *m/z* (HRMS$^-$) 152.0352 $[M - H]^-$ ($C_7H_6NO_3$ requires 152.0353).

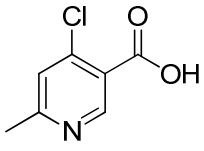

4-Chloro-6-methylnicotinic acid, 3

4-Hydroxy-6-methylnicotinic acid, ***2*** (6.49 g, 38 mmol) was stirred in neat phosphorus oxychloride (50 mL) at 100 °C for 14 h under argon. Excess phosphorus oxychloride was removed by distillation to leave a brown residue. Addition of water (50 mL) afforded a yellow solution containing a light brown precipitate which was collected by filtration to yield the *title compound* (3.65 g, 56%), m.p. 215 - 217 °C, δ_H (D_2O) 8.85 (1H, s, H^6), 7.91 (1H, s, H^3), 2.63 (3H, s, H^1), δ_C (D_2O) 165.3 (C^7), 156.2

(C^4), 152.9 (C^5), 142.8 (C^6), 130.2 (C^3), 129.7 (C^2), 18.9 (C^1), *m/z* (HRMS$^-$) 170.0014 [M – H]$^-$ ($C_7H_6{}^{35}ClNO_2$ requires 170.0014).

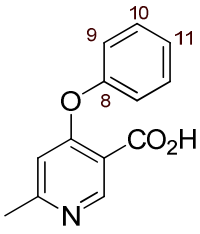

4-Phenoxy-6-methylnicotinic acid, 4

A solution of sodium methoxide was prepared by dissolving sodium metal (1.38 g, 60 mmol) in dry methanol (30 mL). To this solution were added phenol (9.60 g, 100 mmol) and 4-chloro-6-methylnicotinic acid, ***3*** (3.50 g, 20 mmol). The brown solution was stirred at 65 °C for 1 h under argon before the methanol was removed under reduced pressure. The resulting brown residue was stirred at 180 °C for 3 h under argon. The residue was allowed to cool to room temperature before being dissolved in water (20 mL). Excess phenol was removed by extraction with diethyl ether (3 × 25 mL). Acidification of the aqueous layer by addition of acetic acid generated a white precipitate which was collected by filtration to yield the *title compound* (1.5 g, 30 %), m.p. 123-126 °C, δ_H ($CDCl_3$) 8.41 (1H, s, H^6), 7.37 (2H, t, *J* 8.0 Hz, H^{10}), 7.22 (1H, t, *J* 8.0 Hz, H^{11}), 7.04 (2H, d, *J* 8.0 Hz, H^9), 6.61 (1H, s, H^3), 2.28 (3H, s, H^1), δ_C ($CDCl_3$) 170.2 (C^7), 163.7 (C^4), 160.3 (C^5), 154.4 (C^6), 149.7 (C^8), 130.2 (C^3), 125.4 (C^2), 123.2 (C^9), 120.9 (C^{10}), 110.5 (C^{11}), 20.1 (C^1), *m/z* (HRMS$^-$) 228.0665 [M – H]$^-$ ($C_{13}H_{10}NO_3$ requires 228.0666).

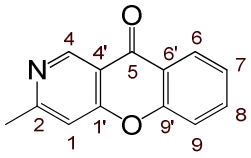

2-Methyl-3-azaxanthone, 5

4-Phenoxy-6-methylnicotinic acid, ***4*** (820 mg, 3.6 mmol) and polyphosphoric acid (50 g) were heated to 120 °C for 14 h under argon. The resulting brown solution was cooled to room temperature and poured into ice water (250 mL). The pH of the yellow solution was adjusted to 7 by addition of KOH pellets. The aqueous solution was then extracted with CH_2Cl_2 (3 × 100 mL). The organic layers were combined, dried over $MgSO_4$, filtered and the solvent was removed under reduced pressure to yield the *title compound* as a pale brown solid (600 mg, 79 %), m.p. 156 - 157 °C, δ_H ($CDCl_3$) 9.32 (1H, s, H^4), 8.24 (1H, d, *J* 8.4 Hz, H^6), 7.69 (1H, dd, *J* 7.0 Hz, 8.4 Hz, H^8), 7.41 (1H, d, *J* 8.4 Hz, H^9), 7.36 (1H, dd, *J* 7.0 Hz, 8.4 Hz, H^7), 7.13 (1H, s, H^1), 2.64 (3H, s, CH_3), δ_C ($CDCl_3$) 176.3 (C^5), 164.5 (C^2), 161.6 ($C^{4'}$), 156.0 ($C^{9'}$), 150.3 (C^4), 135.6 (C^8), 126.8 (C^6), 124.9 (C^7), 123.1 ($C^{6'}$), 118.3 (C^9), 115.8 ($C^{1'}$), 111.2 (C^1), 25.2 (CH_3), *m/z* (HRMS$^+$) 212.0705 [M + H]$^+$ ($C_{13}H_{10}NO_2$ requires 212.0706).

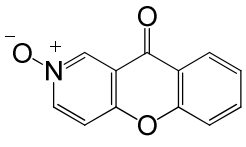

3-(N-oxide)-azaxanthone, 6

3-Azaxanthone (43 mg, 0.22 mmol) was dissolved in $CHCl_3$ (25 mL) and *meta*-chloroperoxybenzoic acid (37 mg, 0.22 mmol) was added. The solution was stirred at 0 °C for 2 h and then, over a further 10 h, allowed to warm to room temperature. The solvent was removed under reduced pressure and the yellow residue was dissolved in CH_2Cl_2 (20 mL). The solution was washed with sodium bicarbonate solution (3 × 20 mL) and the organic layer was dried over $MgSO_4$, filtered and the solvent was removed under reduced pressure to give the *title compound* as a bright yellow solid (42 mg, 90 %), m.p. 225 - 228 °C, δ_H ($CDCl_3$) 9.03 (1H, s, H^4), 8.42 (1H, d, *J* 7.6 Hz, H^2), 8.33 (1H, d, *J* 8.4 Hz, H^6), 7.84 (1H, dd, *J* 7.0 Hz, 8.4 Hz, H^8), 7.55 (1H, d, *J* 8.4 Hz, H^9), 7.50 (1H, dd, *J* 7.0 Hz, 8.4 Hz, H^7), 7.47 (1H, d, *J* 7.6 Hz H^1), δ_C ($CDCl_3$) 172.6 (C^5), 154.8 ($C^{4'}$), 151.3 ($C^{9'}$), 143.6 (C^2), 135.6 (C^4), 135.2 (C^8), 125.9 (C^6), 124.6 (C^7), 120.5 ($C^{6'}$), 118.8 ($C^{1'}$), 117.3 (C^9), 115.4 (C^1), *m/z* ($HRMS^+$) 214.0501 $[M + H]^+$ ($C_{12}H_8O_3N_1$ requires 214.0499).

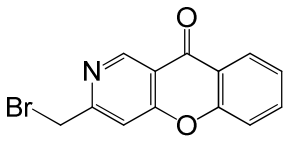

2-Bromomethyl-3-azaxanthone, 7

To a solution of 2-methyl-3-azaxanthone, ***5*** (1.48 g, 7.0 mmol) in carbon tetrachloride (50 mL) was added N-bromo-succinimde (1.87 g, 10.5 mmol) and dibenzoyl peroxide (40 mg, 0.17 mmol). The mixture was stirred and irradiated by a 100 W lamp for 14 h under argon. The reaction was monitored by ^{1}H-NMR and stopped after 14 h. The solvent was removed under reduced pressure and the crude product was dissolved in CH_2Cl_2 (30 mL) and washed with dilute K_2CO_3 solution (30 mL) to remove excess succinimide. The organic layer was dried over $MgSO_4$, filtered and the solvent removed under reduced pressure. Purification by column chromatography on silica (elution: toluene-CH_2Cl_2 1 : 1, MeOH 0 – 2 % using 0.1 % increments) yielded the *title compound* as a yellow solid (620 mg, 30 %), m.p. 177 - 179 °C, δ_H ($CDCl_3$) 9.44 (1H, s, H^4), 8.31 (1H, d, *J* 8.4 Hz, H^6), 7.77 (1H, dd, *J* 7.0 Hz, 8.4 Hz, H^8), 7.53 (1H, s, H^1), 7.52 (1H, d, *J* 8.4 Hz, H^9), 7.44 (1H, dd, *J* 7.0 Hz, 8.4 Hz, H^7), 4.63 (2H, s, CH_2Br), δ_C ($CDCl_3$) 175.9 (C^5), 162.1 (C^2), 161.9 ($C^{4'}$), 156.1 ($C^{9'}$), 150.9 (C^4), 135.9 (C^8), 127.0 (C^6), 125.4 (C^7), 123.2 ($C^{6'}$), 118.4 (C^9), 117.0 ($C^{1'}$), 112.1 (C^1), 33.0 (CH$_2$Br), *m/z* ($HRMS^+$) 291.9785 $[M + H]^+$ ($C_{13}H_9\,^{81}BrNO_2$ requires 291.9791), R_f = 0.57 (silica, toluene-CH_2Cl_2 1 : 1 – MeOH 5 %).

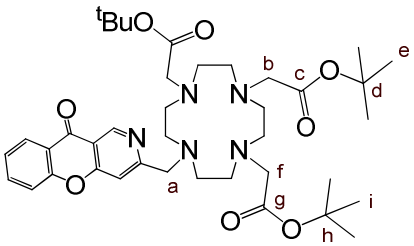

1,4,7-Tris(tert-butoxycarbonyl)-10-[2-methyl-3-azaxanthone]-1,4,7,10-tetraazacyclododecane, 8

1,4,7-Tris(*tert*-butoxycarbonyl)-1,4,7,10-tetraazacyclododecane (120 mg, 0.23 mmol), 2-bromomethyl-3-azaxanthone, ***7*** (67 mg, 0.23 mmol) and K_2CO_3 (16 mg, 0.12 mmol) were stirred in dry CH_3CN (3 mL) at 78 °C for 24 h under argon. The reaction was monitored by TLC to conform that all the brominated starting material had been consumed. The solvent was removed under reduced pressure and the resultant solid was dissolved in CH_2Cl_2 (25 mL) and extracted with water (3 × 25 mL). The organic layer was dried over $MgSO_4$, filtered and the solvent was removed under reduced pressure to give a yellow residue. Purification by column chromatography on silica (CH_2Cl_2 : 0 – 5 % MeOH) gave the *title compound* as a glassy yellow solid (145 mg, 87 %), δ_H ($CDCl_3$) 9.39 (1H, s, H^4), 8.24 (1H, d, *J* 8.4 Hz, H^6), 7.82 (1H, s, H^1), 7.77 (1H, dd, *J* 7.0 Hz, 8.4 Hz, H^8), 7.48 (1H, d, *J* 8.4 Hz, H^9), 7.41 (1H, dd, *J* 7.0 Hz, 8.4 Hz, H^7), 4.76 (2H, s, H^a), 3.63 (2H, s, H^b), 3.49 (4H, s, H^f), 3.42 – 2.86 (16H, m, *cyclen Hs*), 1.41 (9H, s, H^e), 1.38 (18H, s, H^i), δ_C ($CDCl_3$) 176.2 (C^5), 170.3 (C^c), 169.6 (C^g), 161.7 (C^2), 159.8 ($C^{4'}$), 156.1 ($C^{9'}$), 150.5 (C^4), 136.2 (C^8), 126.8 (C^6), 125.4 (C^7), 123.0 ($C^{6'}$), 118.6 (C^9), 117.2 ($C^{1'}$), 114.7 (C^1), 82.4 (C^h), 82.0 (C^d), 56.7 (C^b), 56.5 (C^f) 53.7 (C^a) 52.0 – 48.0 (*cyclen Cs*), 28.4 (C^e), 28.3 (C^i), *m/z* (HRMS$^+$) 724.4281 $[M + H]^+$ ($C_{39}H_{58}N_5O_8$ requires 724.4280); R_f = 0.24 (silica, CH_2Cl_2 : 5 %MeOH).

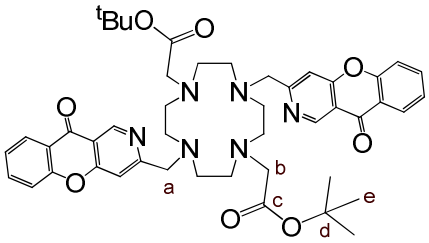

1,7-Bis(tert-butoxycarbonyl)-4,10-bis[2-methyl-3-azaxanthone]-1,4,7,10-tetraazacyclododecane, 9

1,7-Bis(*tert*-butoxycarbonyl)-1,4,7,10-tetraazacyclododecane (75 mg, 0.19 mmol), 2-bromomethyl-3-azaxanthone, ***7*** (108 mg, 0.37 mmol) and K_2CO_3 (26 mg, 0.19 mmol) were stirred in dry CH_3CN (3 mL) at 78 °C for 48 h under argon. The reaction was monitored by TLC to conform that all the brominated starting material had been consumed. The solvent was removed under reduced pressure and the resultant solid was dissolved in CH_2Cl_2 (25 mL) and extracted with water (3 × 25 mL). The organic layer was dried over $MgSO_4$, filtered and the solvent was removed under reduced pressure to give a yellow residue. Purification by column chromatography on silica (CH_2Cl_2 : 0 – 5 % MeOH) gave the *title compound* as a glassy yellow solid (61 mg, 40 %), δ_H ($CDCl_3$) 9.42 (2H, s, H^4), 8.30 (2H, s, H^1), 7.98 (2H, d, *J* 8.4 Hz, H^6), 7.41 (2H, dd, *J* 7.0 Hz, 8.4 Hz, H^8), 7.10 (2H, dd, *J* 7.0 Hz, 8.4

Hz, H^7), 6.62 (2H, d, *J* 8.4 Hz, H^9), 3.94 (4H, s, H^a), 3.25 (4H, s, H^b), 3.00 – 2.80 (16H, m, *cyclen Hs*), 1.40 (18H, s, H^e), δ_C ($CDCl_3$) 176.3 (C^5), 171.1 (C^c), 167.6 (C^2), 162.0 ($C^{4'}$), 155.4 ($C^{9'}$), 150.1 (C^4), 135.2 (C^8), 126.4 (C^6), 124.6 (C^7), 122.6 ($C^{6'}$), 117.7 (C^9), 116.3 ($C^{1'}$), 111.1 (C^1), 81.2 (C^d), 60.5 (C^b), 56.9 (C^a), 55.0 – 52.0 (*cyclen Cs*), 28.4 (C^e), *m/z* (HRMS$^+$) 819.4084 $[M + H]^+$ ($C_{46}H_{55}N_6O_8$ requires 819.4076); R_f = 0.17 (silica, CH_2Cl_2 : 5 %MeOH).

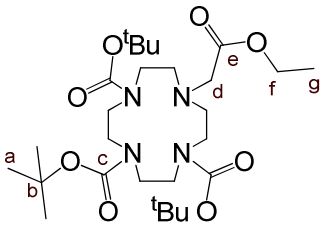

10-(Ethoxycarbonyl)-1,4,7,10-tetraazacyclododecane-1,4,7-tricarboxylic acid tri-tert-butyl ester, 10

1,4,7,10-Tetraazacyclododecane-1,4,7-tricarboxylic acid tri-*tert*-butyl ester (270 mg, 0.572 mmol), ethyl bromoacetate (97 mg, 0.572 mml) and K_2CO_3 (40 mg, 0.3 mmol) were stirred in dry CH_3CN (5 mL) at 78 °C for 36 h under argon. The solvent was removed under reduced pressure and the resultant solid was dissolved in CH_2Cl_2 (25 mL) and extracted with water (3 × 25 mL). The organic layer was dried over $MgSO_4$, filtered and the solvent was removed under reduced pressure. The residue was purified by column chromatography on silica (elution: CH_2Cl_2, MeOH 0 – 1 % using 0.1 % increments) to give the *title compound* as a yellow oil (244 mg, 77%), δ_H ($CDCl_3$) 4.14 (2H, q, *J* 7.2 Hz, H^f), 3.47 (2H, s, H^d), 3.6 – 2.8 (16H, m, *cyclen Hs*), 1.45 (27H, s, H^a), 1.25 (3H, t, *J* 7.2 Hz, H^g), δ_C ($CDCl_3$) 170.6 (C^e), 155.8 (C^c), 79.5 (C^b), 60.3 (C^d), 55.0 (C^f), 53.0 – 47.0 (*cyclen Cs*), 28.7 (C^a), 14.3 (C^g), *m/z* (HRMS$^+$) 559.3698 $[M + H]^+$ ($C_{27}H_{51}N_4O_8$ requires 559.3701), R_f = 0.6 (silica, CH_2Cl_2 – MeOH 5 %).

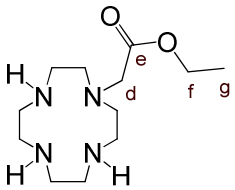

1-(Ethoxycarbonyl)-1,4,7,10-tetraazacyclododecane, 11

10-(Ethoxycarbonyl)-1,4,7,10-tetraazacyclododecane-1,4,7-tricarboxylic acid tri-*tert*-butyl ester, ***10*** (219 mg, 0.39 mmol) was dissolved in CH_2Cl_2 (2 mL) and CF_3CO_2H (2 mL) was added. The mixture was stirred at 20 °C for 12 h under argon. The solvent and excess CF_3CO_2H were removed under reduced pressure and the residue was dissolved in dry CH_2Cl_2 (20 mL). The solution was dried over K_2CO_3 before being filtered and the solvent removed under reduced pressure to yield the *title product* as a yellow oil (98 mg, 98 %), δ_H ($CDCl_3$) 4.21 (2H, q, *J* 7.2 Hz, H^f), 3.54 (2H, s, H^d), 3.3 – 2.8 (16H, m, *cyclen Hs*), 1.28 (3H, t, *J* 7.2 Hz, H^g), δ_C ($CDCl_3$) 174.4 (C^e), 62.8 (C^d), 55.3 (C^f), 50.0 – 43.0 (*cyclen Cs*), 14.4 (C^g), *m/z* (HRMS$^+$) 259. 2129 $[M + H]^+$ ($C_{12}H_{27}N_4O_2$ requires 259.2129).

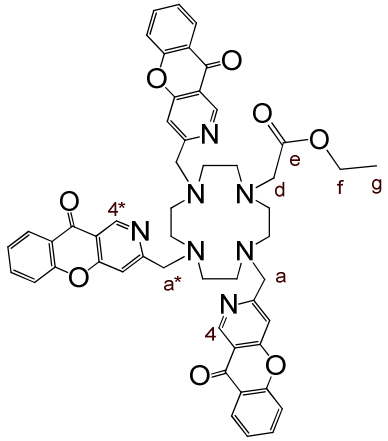

1-(Ethoxycarbonyl)-4,7,10-tris[2-methyl-3-azaxanthone]-1,4,7,10-tetraazacyclododecane, 12

1-(Ethoxycarbonyl)-1,4,7,10-tetraazacyclododecane, ***11*** (16 mg, 0.06 mmol), 2-bromomethyl-3-azaxanthone, ***7*** (70 mg, 0.24 mmol) and K_2CO_3 (25 mg, 0.18 mmol) were dissolved in dry MeCN (3 mL). The solution was stirred at 78 °C for 48 h under argon. The solvent was removed under reduced pressure and the yellow residue was dissolved in CH_2Cl_2 (20 mL). After washing with water (3 × 20 mL), the organic layer was dried over $MgSO_4$, filtered and the solvent was removed under reduced pressure. Purification by column chromatography on alumina (elution: CH_2Cl_2, MeOH 0 – 2 % using 0.1 % increments) gave the *title product* as a yellow oil (43 mg, 80 %), δ_H ($CDCl_3$) 9.38 (2H, s, H^4), 9.34 (1H, s, H^{4*}), 8.19 (1H, d, *J* 8.4 Hz, H^{6*}), 8.13 (2H, d, *J* 8.4 Hz, H^6), 7.75 (2H, dd, *J* 7.0 Hz, 8.4 Hz, H^8), 7.68 (1H, dd, *J* 7.0 Hz, 8.4 Hz, H^{8*}), 7.64 (2H, s, H^1), 7.58 (1H, s, H^{1*}), 7.52 (2H, d, *J* 8.4 Hz, H^9), 7.46 (1H, d, *J* 8.4 Hz, H^{9*}), 7.35 (2H, dd, *J* 7.0 Hz, 8.4 Hz, H^7), 7.27 (1H, dd, *J* 7.0 Hz, 8.4 Hz, H^{7*}), 4.09 (2H, q, *J* 7.2 Hz, H^f), 3.91 (4H, s, H^a), 3.76 (2H, s, H^{a*}), 3.44 (2H, s, H^d), 3.1 – 2.8 (16H, m, *cyclen Hs*), 1.19 (3H, t, *J* 7.2 Hz, H^g), δ_C ($CDCl_3$) 176.1 (C^5), 171.4 (C^e), 170.6 (C^2), 161.8 ($C^{4'}$), 156.1 ($C^{9'}$), 150.3 (C^4), 135.6 (C^8), 126.8 (C^6), 125.0 (C^7), 122.8 ($C^{6'}$), 118.5 (C^9), 116.7 ($C^{1'}$), 112.2 (C^1), 60.7 (C^a), 55.8 (C^d), 55.0 (C^f), 54.0 – 48.0 (*cyclen Cs*), 14.5 (C^g), *m*/*z* (HRMS$^+$) 908.3377 $[M + Na]^+$ ($C_{51}H_{47}O_8N_7Na_1$ requires 908.3378), R_f = 0.40 (alumina, CH_2Cl_2 – MeOH 5 %).

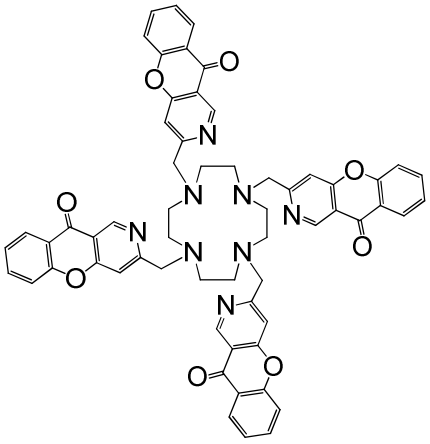

1,4,7,10-Tetra[2-methyl-3-azaxanthone]-1,4,7,10-tetraazacyclododecane, L⁴

1,4,7,10-tetraazacyclododecane (18 mg, 0.10 mmol), 2-bromomethyl-3-azaxanthone, ***7*** (114 mg, 0.40 mmol) and K_2CO_3 (46 mg, 0.34 mmol) were dissolved in dry MeCN (4 mL). The solution was stirred at 78 °C for 72 h under argon. The solvent was removed under reduced pressure and the yellow residue was dissolved in CH_2Cl_2 (20 mL). After washing with water (3 × 20 mL), the organic layer was dried over $MgSO_4$, filtered and the solvent was removed under reduced pressure. Purification by column chromatography on alumina (elution: CH_2Cl_2, MeOH 0 – 1 % using 0.1 % increments) gave the *title product* as a yellow oil (60 mg, 60 %), δ_H ($CDCl_3$) 9.37 (4H, s, H^4), 8.10 (4H, d, *J* 8.4 Hz, H^6), 7.76 (4H, s, H^1), 7.53 (4H, dd, *J* 7.0 Hz, 8.4 Hz, H^8), 7.25 (4H, dd, *J* 7.0 Hz, 8.4 Hz, H^7), 7.08 (4H, d, *J* 8.4 Hz, H^9), 3.87 (8H, s, H^a), 3.00 – 2.80 (16H, m, *cyclen Hs*), *m/z* ($HRMS^+$) 1009.3678 $[M + H]^+$ ($C_{60}H_{49}O_8N_8$ requires 1009.3668), R_f = 0.56 (alumina, CH_2Cl_2 – MeOH 5 %).

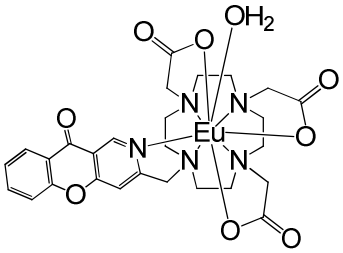

Mono-aqua europium(III) complex of 1,4,7-tris(acetic acid)-10-[2-methyl-3-azaxanthone]-1,4,7,10-tetraazacyclododecane, [Eu·L¹(H₂O)]

1,4,7-Tris(*tert*-butoxycarbonyl)-10-[2-methyl-3-azaxanthone]-1,4,7,10-tetraazacyclododecane, ***8*** (55 mg, 0.10 mmol) was dissolved in CH_2Cl_2 (2 mL) and CF_3CO_2H (2 mL) was added. The mixture was stirred at 22 °C, under argon, for 12 h. Excess CF_3CO_2H and CH_2Cl_2 were removed under reduced pressure and the yellow residue was dissolved in CH_2Cl_2, which was again removed under reduced pressure to ensure the removal of all CF_3CO_2H. Deprotection of the O^{t}Bu groups was confirmed by ^{1}H-NMR, before the residue was dissolved in H_2O – CH_3OH (4 : 1 v/v, 5 mL). Addition of $Eu(OAc)_3$ (48 mg, 0.12 mmol) was followed by adjustment of the pH to 5.8, by the addition of aq. ammonia solution, and the mixture was stirred at 60 °C for 48 h. After allowing the solution to cool to room temperature, the pH was increased to 10 by the addition of aq. ammonia solution. The solution was stirred for 1 h causing excess Eu^{3+} to precipitate as $Eu(OH)_3$, which was removed by syringe filtration. Adjustment of the pH to 5.8 by the addition of CH_3CO_2H, followed by lyophilisation of the solvent,

gave the *title compound* as a yellow solid (52 mg, 74 %), *m/z* (HRMS$^+$) 704.1374 [M + H]$^+$ ($C_{27}H_{31}O_8N_5{}^{151}$Eu requires 704.1366), $\tau_{H_2O} = 0.60$ ms, $\tau_{D_2O} = 1.98$ ms, $\Phi^{em}_{H_2O} = 6.9$ %, t_R (*Method A*) = 8.6 min.

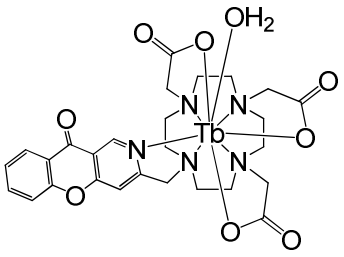

Mono-aqua terbium(III) complex of 1,4,7-tris(acetic acid)-10-[2-methyl-3-azaxanthone]-1,4,7,10-tetraazacyclododecane, [Tb·L¹(H₂O)]

An analogous procedure to that described for the synthesis of [Eu·L^1] was followed using 1,4,7-tris(*tert*-butoxycarbonyl)-10-[2-methyl-3-azaxanthone]-1,4,7,10-tetraazacyclododecane, ***8*** (55 mg, 0.10 mmol) and Tb(OAc)$_3$ (43 mg, 0.011 mmol). The *title compound* was isolated as a yellow solid (49 mg, 72 %), *m/z* (HRMS$^+$) 712.1426 [M + H]$^+$ ($C_{27}H_{31}O_8N_5{}^{159}$Tb requires 712.1421), $\tau_{H_2O} = 1.64$ ms, $\tau_{D_2O} = 2.86$ ms, $\Phi^{em}_{H_2O} = 39$ %, t_R (*Method B*) = 21.0 min.

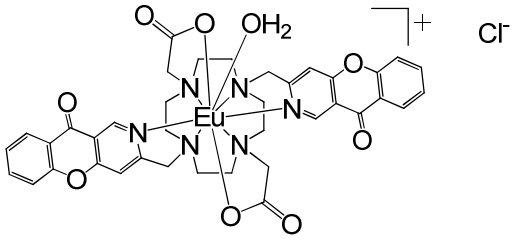

Mono-aqua europium(III) chloride complex of 1,7-bis(acetic acid)-4,10-bis[2-methyl-3-azaxanthone]-1,4,7,10-tetraazacyclododecane, [Eu·L²(H₂O)]Cl

1,7-Bis(*tert*-butoxycarbonyl)-4,10-bis[2-methyl-3-azaxanthone]-1,4,7,10-tetraazacyclododecane, ***9*** (22 mg, 0.031 mmol) was dissolved in CH_2Cl_2 (2 mL) and CF_3CO_2H (2 mL) was added. The mixture was stirred at 22 °C, under argon, for 12 h. Excess CF_3CO_2H and CH_2Cl_2 were removed under reduced pressure and the yellow residue was redissolved in CH_2Cl_2. The solvent was again removed under reduced pressure to ensure the removal of all CF_3CO_2H. Deprotection of the O^{t}Bu groups was confirmed by ^{1}H-NMR before the residue was dissolved in H_2O – CH_3OH (4 : 1 v/v, 4 mL). Addition of Eu(OAc)$_3$ (15 mg, 0.037 mmol) was followed by adjustment of the pH to 5.8, by the addition of aq. ammonia solution, and the mixture was stirred at 60 °C for 48 h. After allowing the solution to cool to room temperature, the pH was raised to 10 by the addition of aq. ammonia solution. The solution was stirred for 1 h causing excess Eu^{3+} to precipitate as $Eu(OH)_3$, which was removed by syringe filtration. Adjustment of the pH to 5.8 by the addition of CH_3CO_2H, followed by lyophilisation of the solvent, gave the product as the acetate salt. The solid was converted to the chloride salt by stirring in H_2O for 1 h with Dowex 1 × 8 200-400 mesh Cl^-, which had been washed successively with 1 M HCl and water. The Dowex was removed by filtration and the solvent lyophilised to yield the *title compound* as

a yellow solid (18 mg, 66 %), *m/z* (HRMS$^+$) 855.1798 [M - Cl]$^+$ ($C_{38}H_{36}O_8N_6{}^{151}Eu$ requires 855.1788), $\tau_{H_2O} = 0.56$ ms, $\tau_{D_2O} = 1.54$ ms, $\Phi^{em}_{H_2O} = 10$ %, t_R (*Method A*) = 8.9 min.

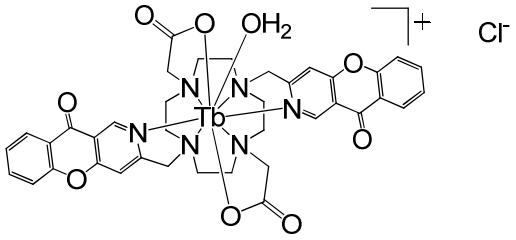

Mono-aqua terbium(III) chloride complex of 1,7-bis(acetic acid)-4,10-bis[2-methyl-3-azaxanthone]-1,4,7,10-tetraazacyclododecane, [Tb·L²(H₂O)]Cl.

An analogous procedure to that described for the synthesis of [Eu·L^2]Cl was followed using 1,7-bis(*tert*-butoxycarbonyl)-4,10-bis[2-methyl-3-azaxanthone]-1,4,7,10-tetraazacyclododecane, ***9*** (22 mg, 0.031 mmol) and $Tb(OAc)_3$ (15 mg, 0.037 mmol). The *title compound* was isolated as a yellow solid (19 mg, 69 %), *m/z* (HRMS$^+$) 863.1853 [M]$^+$ ($C_{38}H_{36}O_8N_6{}^{159}Tb$ requires 863.1843), $\tau_{H_2O} = 1.52$ ms, $\tau_{D_2O} = 2.75$ ms, $\Phi^{em}_{H_2O} = 34$ %, t_R (*MethodA*) = 8.9 min.

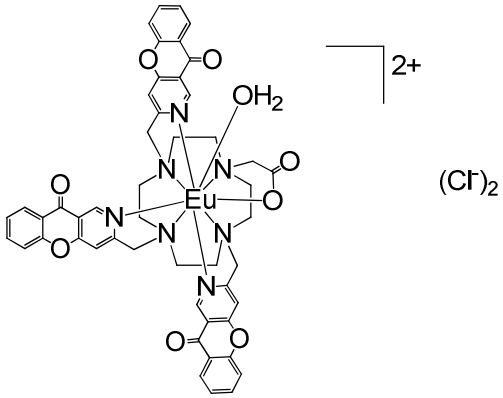

Mono-aqua europium (III) chloride complex of 1-(acetic acid)-4,7,10-tris[2-methyl-3-azaxanthone]-1,4,7,10-tetraazacyclododecane, [Eu·L³(H₂O)]Cl₂

1-(Ethoxycarbonyl)-4,7,10-tris[2-methyl-3-azaxanthone]-1,4,7,10-tetraazacyclododecane, ***12*** (20 mg, 0.023 mmol) was dissolved in 2 mM HCl (4 mL) and the solution was stirred at 100 °C for 2 h. Removal of the OEt protecting group was confirmed by ^{1}H-NMR. The pH was raised to 5.0 using NaOH before $EuCl_3$ (9 mg, 0.028 mmol) was added and the mixture was stirred at 60 °C for 40 h. After allowing the solution to cool to room temperature, the pH was raised to 10 by the addition of aq. NaOH solution. The solution was stirred for 1 h causing excess Eu^{3+} to precipitate as $Eu(OH)_3$, which was removed by syringe filtration. Adjustment of the pH to 5.8 by the addition of HCl, followed by lyophilisation of the solvent, gave the *title compound* as a white solid, (3 mg, 23 %), *m/z* (HRMS$^+$) 503.6147 [M]$^{2+}$ ([$C_{49}H_{42}O_8N_7{}^{151}Eu$]$^{2+}$ requires 503.6141), $\tau_{H_2O} = 0.50$ ms, $\tau_{D_2O} = 1.61$ ms, $\Phi^{em}_{H_2O} = 1.0$ %,t_R (*Method A*) = 8.7 min.

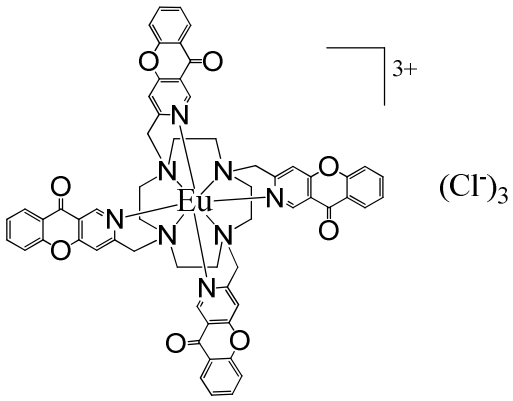

Europium (III) chloride complex of 1,4,7,10-tetra[2-methyl-3-azaxanthone]-1,4,7,10-tetraazacyclododecane, [Eu·L⁴]Cl₃

1,4,7,10-Tetra[2-methyl-3-azaxanthone]-1,4,7,10-tetraazacyclododecane, ***L⁴*** (12 mg, 0.012 mmol) and $Eu(OTf)_3$ (6.5 mg, 0.011 mmol) were dissolved in CH_3CN (3 mL) at 78 °C, under argon, for 40 h. The solvent was removed under reduced pressure and the yellow residue was redissolved in CH_3CN (0.1 mL). This solution was dropped into Et_2O (10 mL) causing immediate precipitation of the product as the triflate salt. The pale yellow solid was converted to the chloride salt by stirring in H_2O for 1 h with Dowex 1 × 8 200-400 mesh Cl^-, which had been washed with 1 M HCl and neutralised with water. The Dowex resin was removed by filtration and the solvent lyophilised to yield the *title compound* as a yellow solid (2 mg, 15 %), *m/z* (HRMS$^+$) 588.1404 $[M - 3Cl + OH]^{2+}$ ($C_{60}H_{49}O_9N_8{}^{151}Eu$ requires 588.1405), $\tau_{H_2O} = 0.71$ ms, $\tau_{D_2O} = 1.20$ ms, $\Phi^{em}_{H_2O} = 5.4$ %, t_R (*Method A*) = 9.5 min.

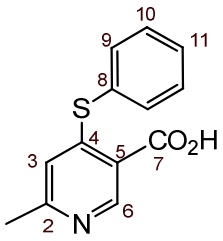

4-Thiophenoxy-6-methylnicotinic acid, 13

4-Chloro-6-methylnicotinic acid, ***3*** (4.6 g, 27 mmol) and thiophenol (3.6 g, 33 mmol) were dissolved in dimethylformamide (50 mL). CuBr (250 mg, 1.7 mmol) and K_2CO_3 (5.4 g, 40 mmol) were added and the mixture was stirred at 150 °C for 16 h under argon. After allowing the brown solution to cool to 23 °C, H_2O (150 mL) was added and excess thiophenol was extracted with Et_2O (3 × 50 mL). The pH was reduced to 4.6 by the addition of AcOH. Upon stirring at 0 °C a pale brown precipitate formed which was collected by filtration to give the *title compound* (1.8 g, 27 %); m.p. 142 – 144 ºC, δ_H ($CDCl_3$) 8.82 (1H, s, H^6), 7.58 (5H, m, $H^{8, 9, 10, 11}$), 6.52 (1H, s, H^3), 2.29 (3H, s, CH_3); δ_C ($CDCl_3$) 166.8 (C^7), 160.0 (C^4), 156.9 (C^5), 154.7 (C^6), 149.6 (C^8), 135.7 (C^3), 130.0 (C^2), 129.2 (C^9), 119.5 (C^{10}), 109.2 (C^{11}), 22.0 (C^1), *m/z* (HRMS$^-$) 244.0436 $[M - H]^-$ ($C_{13}H_{10}O_2NS$ requires 244.0438).

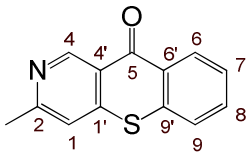

2-Methyl-3-azathiaxanthone, 14

4-Thiophenoxy-6-methylnicotinic acid, ***13*** (1.80 g, 7.35 mmol) and polyphosphoric acid (50 g) were heated to 120 °C for 16 h under argon. The resulting brown solution was cooled to room temperature and poured into ice (250 g). The pH of the yellow solution was adjusted to 7 by addition of KOH pellets. The aqueous solution was then extracted with $CHCl_3$ (3 × 100 mL). The organic layers were combined, dried over $MgSO_4$, filtered and the solvent was removed under reduced pressure to give a brown solid, which was purified by column chromatography on silica (CH_2Cl_2 : 0 – 5 % MeOH in 0.5 % increments) to yield the *title compound* as a pale yellow solid (1.00 g, 60 %), m.p. 174 - 176 °C, δ_H ($CDCl_3$) 9.54 (1H, s, H^4), 8.56 (1H, d, *J* 8.4 Hz, H^6), 7.61 (1H, dd, *J* 7.0 Hz, 8.4 Hz, H^8), 7.52 (1H, d, *J* 8.4 Hz, H^9), 7.49 (1H, dd, *J* 7.0 Hz, 8.4 Hz, H^7), 7.25 (1H, s, H^1), 2.62 (3H, s, C*H*$_3$); δ_C ($CDCl_3$) 179.2 (C^5), 160.3 (C^2), 151.8 (C^4), 146.8 ($C^{4'}$), 136.0 ($C^{9'}$), 132.4 (C^8), 130.5 ($C^{6'}$), 129.7 (C^6), 127.2 (C^7), 126.2 (C^9), 121.9 ($C^{1'}$), 118.5 (C^1), 24.6 (*C*H$_3$), *m/z* (HRMS$^+$) 228.0402 $[M + H]^+$ ($C_{13}H_{10}ONS$ requires 228.0405); R_f = 0.46 (silica, CH_2Cl_2 : 2.5 % MeOH).

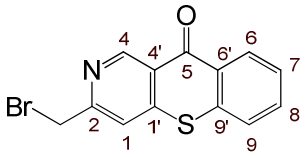

2-Bromomethyl-3-azathiaxanthone, 15

To a solution of 2-methyl-3-azathiaxanthone, ***14*** (500 mg, 2.20 mmol) in carbon tetrachloride (40 mL) was added N-bromo-succinimde (376 mg, 2.20 mmol) and dibenzoyl peroxide (20 mg, 0.08 mmol). The mixture was stirred and irradiated by a 100 W lamp under argon. The reaction was monitored by ^{1}H-NMR and stopped after 14 h. The solvent was removed under reduced pressure and the crude product was dissolved in CH_2Cl_2 (30 mL) and washed with dilute K_2CO_3 solution (30 mL) to remove excess succinimide. The organic layer was dried over $MgSO_4$, filtered and the solvent removed under reduced pressure. Purification by column chromatography on silica (petroleum ether (60 – 80 °C bp) : 0 – 10 % EtOAc in 1 % increments) yielded the *title compound* as a yellow solid (160 mg, 24 %), m.p. 189 - 192 °C, δ_H ($CDCl_3$) 9.59 (1H, s, H^4), 8.58 (1H, d, *J* 8.4 Hz, H^6), 7.66 (1H, dd, *J* 7.0 Hz, 8.4 Hz, H^8), 7.57 (1H, s, H^1), 7.55 (1H, d, *J* 8.4 Hz, H^9), 7.54 (1H, dd, *J* 7.0 Hz, 8.4 Hz, H^7), 4.60 (2H, s, C*H*$_2$Br); δ_C ($CDCl_3$) 178.8 (C^5), 157.8 (C^2), 152.1 (C^4), 147.7 ($C^{4'}$), 135.7 ($C^{9'}$), 133.2 (C^8), 129.7 (C^6), 128.4 ($C^{6'}$), 127.4 (C^7), 126.3 (C^9), 123.1 ($C^{1'}$), 119.2 (C^1), 32.6 (*C*H$_2$Br), *m/z* (HRMS$^+$) 305.9513 $[M + H]^+$ ($C_{13}H_9ONS^{79}Br$ requires 305.9508); R_f = 0.58 (silica, CH_2Cl_2 : MeOH 2 %).

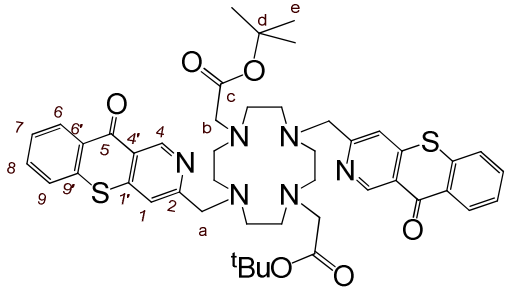

1,7-Bis(tert-butoxycarbonyl)-4,10-bis[2-methyl-3-azathiaxanthone]-1,4,7,10-tetraazacyclododecane, 16

1,7-Bis(*tert*-butoxycarbonyl)-1,4,7,10-tetraazacyclododecane (49 mg, 0.12 mmol), 2-bromomethyl-3-azathiaxanthone, ***15*** (106 mg, 0.35 mmol) and K_2CO_3 (35 mg, 0.34 mmol) were stirred in dry CH_3CN (4 mL) at 78 °C for 18 h under argon. The reaction was monitored by TLC to conform that all the brominated starting material had been consumed. The solvent was removed under reduced pressure and the resultant solid was dissolved in CH_2Cl_2 (25 mL) and extracted with water (3 × 25 mL). The organic layer was dried over $MgSO_4$, filtered and the solvent was removed under reduced pressure. The yellow residue was purified by column chromatography on silica (CH_2Cl_2 : 5 % MeOH) to give the *title compound* as a glassy yellow solid (70 mg, 68 %); δ_H ($CDCl_3$) 9.42 (2H, s, H^4), 8.55 (2H, d, *J* 8.4 Hz, H^6), 7.67 (2H, dd, *J* 7.0 Hz, 8.4 Hz, H^8), 7.60 (2H, dd, *J* 7.0 Hz, 8.4 Hz, H^7), 7.51 (2H, d, *J* 8.4 Hz, H^9), 7.48 (2H, s, H^1), 3.51 (4H, br s, H^a), 3.25 (4H, s, H^b), 3.00 – 2.40 (16H, br m, *cyclen* Hs), 1.38 (18H, s, H^e), δ_C ($CDCl_3$) 178.8 (C^5), 172.5 (C^c) 160.1 (C^2), 151.8 (C^4), 147.4 ($C^{4'}$), 135.6 ($C^{9'}$), 133.2 (C^8), 130.2 ($C^{6'}$), 129.7 (C^6), 127.3 (C^7), 126.4 (C^9), 123.1 ($C^{1'}$), 119.3 (C^1), 82.7 (C^d), 58.6 (C^b), 57.2 (C^a), 51.0 – 49.0 (*cyclen* Cs), 28.1 (C^e), *m/z* (HRMS$^+$) 851.3629 $[M + H]^+$ ($C_{46}H_{55}O_6N_6S_2$ requires 851.3624); R_f = 0.58 (silica, CH_2Cl_2 : MeOH 2 %).

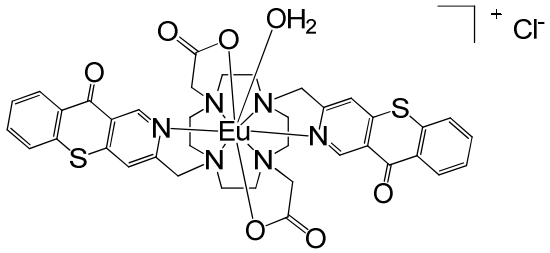

Mono-aqua europium(III) chloride complex of 1,7-bis(acetic acid)-4,10-bis[2-methyl-3-azathiaxanthone]-1,4,7,10-tetraazacyclododecane, [Eu·L^{2b}(H$_2$O)]Cl

1,7-Bis(tert-butoxycarbonyl)-4,10-bis[2-methyl-3-azathiaxanthone]-1,4,7,10-tetraazacyclododecane, ***16*** (41 mg, 0.048 mmol) was dissolved in CH_2Cl_2 (2 mL) and CF_3CO_2H (2 mL) was added. The mixture was stirred at 22 °C under argon for 16 h. Excess CF_3CO_2H and CH_2Cl_2 were removed under reduced pressure and the yellow residue was redissolved in CH_2Cl_2. The solvent was again removed under reduced pressure to ensure the removal of all CF_3CO_2H. Deprotection of the O^{t}Bu groups was confirmed by ^{1}H-NMR before the residue was dissolved in H_2O – CH_3OH (4 : 1 v/v, 4 mL). Addition of $Eu(OAc)_3$ (23 mg, 0.058 mmol) was followed by adjustment of the pH to 5.8, by the addition of aq. ammonia solution, and the mixture was stirred at 60 °C for 18 h. After allowing the solution to cool to room temperature, the pH was raised to 10 by the addition of aq. ammonia solution. The solution was

stirred for 1 h causing excess Eu^{3+} to precipitate as $Eu(OH)_3$, which was removed by syringe filtration. Adjustment of the pH to 5.8 by the addition of CH_3CO_2H, followed by lyophilisation of the solvent, gave the product as the acetate salt. The solid was converted to the chloride salt by stirring in H_2O for 1 h with Dowex 1 × 8 200-400 mesh Cl^-, which had been washed with 1 M HCl and neutralised with water. The Dowex resin was removed by filtration and the solvent lyophilised to yield the *title compound* as a yellow solid (20 mg, 47 %), *m/z* (HRMS$^+$) 887.1329 $[M - Cl]^+$ ($C_{38}H_{36}O_6N_6S_2{}^{151}Eu$ requires 887.1336); $\tau_{H_2O} = 0.56$ ms, $\tau_{D_2O} = 1.57$ ms, $\Phi^{em}_{H_2O} = 5.1$ % t_R (*Method C*) = 6.4 min.

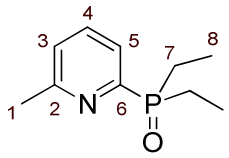

2-(Diethylphosphoryl)-6-methylpyridine, 18

To tetrahydrofuran (20 mL) stirred at -78 °C under argon was added 2.5 M *n*-butyl lithium in hexane (2.9 mL, 7.3 mmol) and 2-bromo-6-methylpyridine, ***17*** (1.75 g, 7.3 mmol). After 1 h, chlorodiethylphosphine (0.90 g, 7.3 mmol) was added and the mixture was left to stir overnight at 23 °C. ^{31}P-NMR was used to confirm coupling of the lithiated pyridine with chlorodiethylphosphine (^{31}P resonance at -11.15 ppm). Oxidation to the phosphorus(V) species was achieved by addition of 34 % H_2O_2 in water (0.22 mL, 7.3 mmol). After stirring at 23 °C for 30 min, the solvent was removed by reduced pressure to give a yellow residue which was purified by column chromatography on silica (CH_2Cl_2 : 0 – 5 % MeOH in 0.2 % increments) yielding the *title product* as a colourless oil (1.0 g, 70 %); δ_H ($CDCl_3$) 7.77 (1H, dd, $^3J_{H\text{-}H}$ 6.0 Hz $^3J_{H\text{-}P}$ 6.0 Hz, H^5), 7.57 (1H, td, $^3J_{H\text{-}H}$ 6.0 Hz $^4J_{H\text{-}P}$ 3.6 Hz, H^4), 7.10 (1H, d, $^3J_{H\text{-}H}$ 6 Hz, H^3), 2.45 (3H, s, H^1), 1.91 (4H, qd, $^3J_{H\text{-}H}$ 7.7 Hz, $^3J_{H\text{-}P}$ 3.5 Hz, H^7), 0.97 (6H, t, $^3J_{H\text{-}H}$ 7.7 Hz, H^8); δ_C ($CDCl_3$) 159.0 (C^2), 154.9 (d, $^1J_{C\text{-}P}$ 119 Hz, C^6), 135.8 (C^4), 125.1 (C^5), 124.7 (C^3), 24.5 (C^1), 20.7 (d, $^1J_{C\text{-}P}$ 96 Hz, C^7), 5.9 (d, $^2J_{C\text{-}P}$ 6 Hz, C^8); δ_P ($CDCl_3$) 49.1; *m/z* (HRMS$^+$) 198.1039 $[M + H]^+$ ($C_{10}H_{17}ONP$ requires 198.1042) ; $R_f = 0.23$ (silica, CH_2Cl_2 : 5 % MeOH).

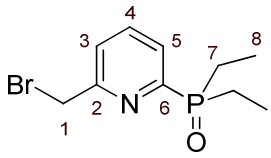

2-(Bromomethyl)-6-(diethylphosphoryl)pyridine, 19

To a solution of 2-(diethylphosphoryl)-6-methylpyridine, ***18*** (210 mg, 1.06 mmol) in carbon tetrachloride (20 mL) was added N-bromo-succinimde (192 mg, 1.06 mmol) and dibenzoyl peroxide (10 mg, 0.4 mmol). The mixture was stirred and irradiated by a 100 W lamp under an argon atmosphere. The reaction was monitored by ^{1}H-NMR and stopped after 16 h. The solvent was removed under reduced pressure and the crude product was dissolved in CH_2Cl_2 (20 mL) and washed with dilute K_2CO_3 solution (20 mL) to remove excess succinimide. The organic layer was dried over $MgSO_4$, filtered and the solvent removed under reduced pressure. Purification by column chromatography on silica (toluene-CH_2Cl_2 1 : 1, MeOH 0 – 2 % using 0.1 % increments) yielded the *title compound* as a yellow oil (102 mg, 35 %); δ_H ($CDCl_3$) 7.96 (1H, dd, $^3J_{H\text{-}H}$ 6.0 Hz $^3J_{H\text{-}P}$ 6.0 Hz,

H^5), 7.87 (1H, td, $^3J_{H\text{-}H}$ 6.0 Hz $^4J_{H\text{-}P}$ 3.6 Hz, H^4), 7.55 (1H, d, $^3J_{H\text{-}H}$ 6 Hz, H^3), 4.56 (2H, s, H^1), 2.08 (4H, qd, $^3J_{H\text{-}H}$ 7.7 Hz, $^3J_{H\text{-}P}$ 3.5 Hz, H^7), 1.15 (6H, t, $^3J_{H\text{-}H}$ 7.7 Hz, H^8); δ_C ($CDCl_3$) 157.8 (C^2), 154.4 (d, $^1J_{C\text{-}P}$ 120 Hz, C^6), 135.3 (C^4), 125.0 (C^5), 124.5 (C^3), 33.4 (C^1), 20.7 (d, $^1J_{C\text{-}P}$ 96 Hz, C^7), 5.9 (d, $^2J_{C\text{-}P}$ 6 Hz, C^8); δ_P ($CDCl_3$) 48.7; *m/z* (HRMS$^+$) 276.0150 $[M + H]^+$ ($C_{10}H_{16}ONP^{79}Br$ requires 276.0153);R_f = 0.44 (silica, CH_2Cl_2 : 5 % MeOH).

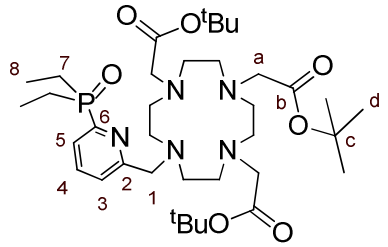

1,4,7-Tris(tert-butoxycarbonyl)-10-[2-(diethylphosphoryl)-6-methylpyridine]-1,4,7,10-tetraazacyclododecane, 20

1,4,7-Tris(*tert*-butoxycarbonyl)-1,4,7,10-tetraazacyclododecane (45 mg, 0.09 mmol), 2-(bromomethyl)-6-(diethylphosphoryl)pyridine, ***19*** (24 mg, 0.09 mmol) and K_2CO_3 (12 mg, 0.09 mmol) were stirred in dry CH_3CN (3 mL) at 78 °C for 24 h under argon. The reaction was monitored by TLC to confirm that all the brominated starting material had been consumed. The solvent was removed under reduced pressure and the resultant residue was dissolved in CH_2Cl_2 (20 mL) and washed with water (3 × 20 mL). The organic layer was dried over $MgSO_4$, filtered and the solvent was removed under reduced pressure. Purification by column chromatography on silica (CH_2Cl_2 : 0 – 5 % MeOH in 0.2 % increments) gave the *title compound* as a glassy colourless solid (33 mg, 52 %); δ_H ($CDCl_3$) 7.88 (1H, m, H^5), 7.87 (1H, m, H^4), 7.62 (1H, m, H^3), 3.20 – 2.85 (8H, br s, $H^{1/a/a'}$), 2.75 – 2.10 (16H, br m, *cyclen* Hs), 2.02 (4H, qd, $^3J_{H\text{-}H}$ 7.7 Hz, $^3J_{H\text{-}P}$ 3.5 Hz, H^7), 1.42 (9H, s, H^d), 1.37 (18H, s, $H^{d'}$), 1.07 (6H, t, $^3J_{H\text{-}H}$ 7.7 Hz, H^8); δ_C ($CDCl_3$) 172.3 (C^b), 172.0 ($C^{b'}$), 158.8 (C^2), 154.8 (d, $^1J_{C\text{-}P}$ 113 Hz, C^6), 137.3 (C^4), 126.0 (C^5), 125.8 (C^3), 82.1 ($C^{c/c'}$), 59.5 (C^a), 56.1 ($C^{a'}$), 56.0 (C^1), 52.0 – 48.0 (*cyclen* Cs), 28.1 (C^d), 28.0 ($C^{d'}$), 21.0 (d, $^1J_{C\text{-}P}$ 69 Hz, C^7), 5.5 (d, $^2J_{C\text{-}P}$ 6 Hz, C^8); δ_P ($CDCl_3$) 44.2; *m/z* (HRMS$^+$) 710.4605 $[M + H]^+$ ($C_{36}H_{65}O_7N_5P$ requires 710.4616) ; R_f = 0.15 (silica, CH_2Cl_2 : 5 % MeOH).

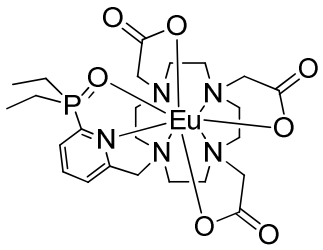

Europium(III) complex of 1,4,7-tris(acetic acid)-10-[2-(diethylphosphoryl)-6-methylpyridine]-1,4,7,10-tetraazacyclododecane, [Eu·L⁵]

1,4,7-Tris(tert-butoxycarbonyl)-10-[2-(diethylphosphoryl)-6-methylpyridine]-1,4,7,10-tetraazacyclododecane, ***20*** (33 mg, 0.046 mmol) was dissolved in CH_2Cl_2 (2 mL) and CF_3CO_2H (1

mL) was added. The mixture was stirred at 22 °C, under argon, for 16 h. Excess CF_3CO_2H and CH_2Cl_2 were removed under reduced pressure and the yellow residue was dissolved in CH_2Cl_2, which was again removed by reduced pressure to ensure the removal of all CF_3CO_2H. Deprotection of the O^{t}Bu groups was confirmed by ^{1}H-NMR, before the residue was dissolved in H_2O – CH_3OH (2 : 1 v/v, 3 mL). Addition of $Eu(OAc)_3$ (19 mg, 0.046 mmol) was followed by adjustment of the pH to 5.8, by the addition of aq. ammonia solution, and the mixture was stirred at 60 °C for 24 h. After allowing the solution to cool to room temperature, the pH was raised to 10 by the addition of aq. ammonia solution. The solution was stirred for 1 h causing excess Eu^{3+} to precipitate as $Eu(OH)_3$, which was removed by syringe filtration. Adjustment of the pH to 5.8 by the addition of CH_3CO_2H, followed by lyophilisation of the solvent, gave the *title compound* as a white solid (24 mg, 74 %); *m/z* (HRMS$^+$) 690.1711 $[M + H]^+$ ($C_{31}H_{38}O_7N_5P^{151}Eu$ requires 690.1707); τ_{H_2O} = 1.21 ms, τ_{D_2O} = 1.85 ms, $\Phi^{em}_{H_2O}$ = 7.5 %; t_R (*Method B*) = 10.3 min.

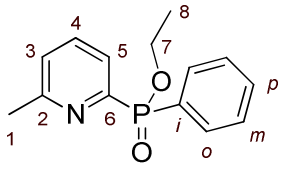

Ethyl (6-methylpyridin-2-yl)(phenyl)phosphinate, 21

2-Bromo-6-methylpyridine, ***17*** (3.0 g, 17.4 mmol), ethyl phenylphosphinate (3.56 g, 20.9 mmol) and triethylamine (10 mL, 71 mmol) were added to dry degassed (freeze-thaw cycle) toluene (30 mL). Tetrakis(triphenylphosphine)palladium(0) (320 mg, 0.27 mmol) was added and the mixture was degassed three times before being stirred at 125 °C for 16 h under argon. The solution was diluted with CH_2Cl_2 (50 mL), washed with HCl (1M, 2 × 60 mL) and water (3 × 60 mL), dried over K_2CO_3, filtered and the solvent removed under reduced pressure to give a dark residue. Purification by column chromatography on silica (CH_2Cl_2 : 0.5 % MeOH) gave the *title compound* as a colourless oil (3.1 g, 66 %); δ_H ($CDCl_3$) 8.01 (2H, dd, $^3J_{H\text{-}H}$ 8.0 Hz $^3J_{H\text{-}P}$ 12.0 Hz, H^o), 7.91 (1H, dd, $^3J_{H\text{-}H}$ 7.0 Hz $^3J_{H\text{-}P}$ 14.0 Hz, H^5), 7.67 (1H, td, $^3J_{H\text{-}H}$ 7.0 Hz $^4J_{H\text{-}P}$ 3.0 Hz, H^4), 7.54 (1H, t, $^3J_{H\text{-}H}$ 8.0 Hz, H^p), 7.48 (2H, td, $^3J_{H\text{-}H}$ 8.0 Hz $^4J_{H\text{-}P}$ 4.0 Hz, H^m), 7.23 (1H, d, $^3J_{H\text{-}H}$ 7.0 Hz, H^3), 4.15 (2H, qd, $^3J_{H\text{-}H}$ 7.0 Hz $^3J_{H\text{-}P}$ 4.5 Hz, H^7), 2.60 (3H, s, H^1), 1.38 (3H, t, $^3J_{H\text{-}H}$ 7.0 Hz, H^8); δ_C ($CDCl_3$) 159.8 (d, $^3J_{C\text{-}P}$ 20 Hz, C^2), 154.0 (d, $^1J_{C\text{-}P}$ 167 Hz, C^6), 135.8 (d, $^3J_{C\text{-}P}$ 10 Hz, C^4), 132.6 (d, $^2J_{C\text{-}P}$ 12 Hz, C^o), 132.5 (d, $^4J_{C\text{-}P}$ 4 Hz, C^p), 130.6 (d, $^1J_{C\text{-}P}$ 136 Hz, C^i), 128.5 (d, $^3J_{C\text{-}P}$ 9 Hz, C^m), 125.8 (d, $^4J_{C\text{-}P}$ 4 Hz, C^3), 125.6 (d, $^2J_{C\text{-}P}$ 22 Hz, C^5), 61.9 (d, $^2J_{C\text{-}P}$ 6 Hz, C^7), 24.9 (C^1), 16.7 (C^8); δ_P ($CDCl_3$) 26.8; *m/z* (HRMS$^+$) 262.0999 $[M + H]^+$ ($C_{14}H_{17}O_2NP$ requires 262.0997); R_f = 0.37 (silica, CH_2Cl_2 : 5 % MeOH).

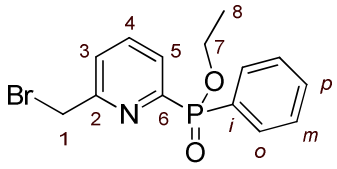

Ethyl [6-(bromomethyl)pyridin-2-yl](phenyl)phosphinate, 22

To a solution of ethyl (6-methylpyridin-2-yl)(phenyl)phosphinate, ***21*** (400 mg, 1.53 mmol) in carbon tetrachloride (25 mL) was added N-bromo-succinimde (327 mg, 1.84 mmol) and dibenzoyl peroxide (20 mg, 0.8 mmol). The mixture was stirred and irradiated by a 100 W lamp under an argon atmosphere. The reaction was monitored by ^{1}H-NMR and stopped after 16 h. The solvent was removed under reduced pressure and the crude product was dissolved in CH_2Cl_2 (20 mL) and washed with dilute K_2CO_3 solution (20 mL) to remove excess succinimide. The organic layer was dried over $MgSO_4$, filtered and the solvent removed under reduced pressure. Purification by column chromatography on silica (CH_2Cl_2, MeOH 0 – 1 % using 0.05 % increments) yielded the *title compound* as a colourless oil (198 mg, 38 %); δ_H ($CDCl_3$) 8.01 (1H, dd, $^{3}J_{H\text{-}H}$ 7.0 Hz $^{3}J_{H\text{-}P}$ 14.0 Hz, H^5), 8.00 (2H, dd, $^{3}J_{H\text{-}H}$ 8.0 Hz $^{3}J_{H\text{-}P}$ 12.0 Hz, H^o), 7.79 (1H, td, $^{3}J_{H\text{-}H}$ 7.0 Hz $^{4}J_{H\text{-}P}$ 3.0 Hz, H^4), 7.53 (1H, t, $^{3}J_{H\text{-}H}$ 8.0 Hz, H^p), 7.52 (1H, d, $^{3}J_{H\text{-}H}$ 7.0 Hz, H^3), 7.46 (2H, td, $^{3}J_{H\text{-}H}$ 8.0 Hz $^{4}J_{H\text{-}P}$ 4.0 Hz, H^m), 4.57 (2H, s, H^1), 4.13 (2H, qd, $^{3}J_{H\text{-}H}$ 7.0 Hz $^{3}J_{H\text{-}P}$ 4.5 Hz, H^7), 1.37 (3H, t, $^{3}J_{H\text{-}H}$ 7.0 Hz, H^8); δ_C ($CDCl_3$) 158.0 (d, $^{3}J_{C\text{-}P}$ 20 Hz, C^2), 154.7 (d, $^{1}J_{C\text{-}P}$ 167 Hz, C^6), 137.3 (d, $^{3}J_{C\text{-}P}$ 10 Hz, C^4), 132.7 (d, $^{2}J_{C\text{-}P}$ 12 Hz, C^o), 132.6 (d, $^{4}J_{C\text{-}P}$ 4 Hz, C^p), 130.2 (d, $^{1}J_{C\text{-}P}$ 136 Hz, C^i), 128.5 (d, $^{3}J_{C\text{-}P}$ 9 Hz, C^m), 127.5 (d, $^{2}J_{C\text{-}P}$ 22 Hz, C^5), 125.8 (d, $^{4}J_{C\text{-}P}$ 4 Hz, C^3), 62.1 (d, $^{2}J_{C\text{-}P}$ 6 Hz, C^7), 33.6 (C^1), 16.7 (C^8); δ_P ($CDCl_3$) 26.0; *m/z* (HRMS$^+$) 340.0122 $[M(^{79}Br) + H]^+$ ($C_{14}H_{16}O_2NP^{79}Br$ requires 340.0102), 342.0098 $[M(^{81}Br) + H]^+$ ($C_{14}H_{16}O_2NP^{81}Br$ requires 342.0088); R_f = 0.57 (silica, CH_2Cl_2 : 5 % MeOH).

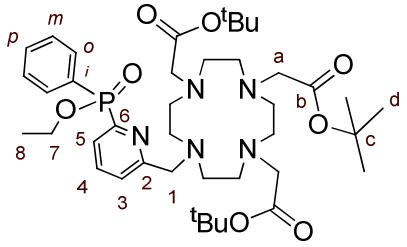

1,4,7-Tris(tert-butoxycarbonyl)-10-[ethyl(6-methylpyridin-2-yl)(phenyl)phosphinate]-1,4,7,10-tetraazacyclododecane, 23

1,4,7-Tris(*tert*-butoxycarbonyl)-1,4,7,10-tetraazacyclododecane (162 mg, 0.30 mmol), ethyl [6-(bromomethyl)pyridin-2-yl](phenyl)phosphinate, ***22*** (107 mg, 0.30 mmol) and K_2CO_3 (42 mg, 0.30 mmol) were stirred in dry CH_3CN (5 mL) at 80 °C for 16 h under argon. The reaction was monitored by TLC to confirm that all the brominated starting material had been consumed. The solvent was removed under reduced pressure and the resultant residue was dissolved in CH_2Cl_2 (30 mL) and washed with water (3 × 30 mL). The organic layer was dried over $MgSO_4$, filtered and the solvent was removed under reduced pressure. Purification by column chromatography on silica (CH_2Cl_2 : 0 – 5 % MeOH in 0.4 % increments) gave the *title compound* as a glassy yellow solid (175 mg, 75 %); δ_H ($CDCl_3$) 7.88 (1H, dd, $^{3}J_{H\text{-}H}$ 7.0 Hz $^{3}J_{H\text{-}P}$ 14.0 Hz, H^5), 7.87 (2H, dd, $^{3}J_{H\text{-}H}$ 8.0 Hz $^{3}J_{H\text{-}P}$ 12.0 Hz, H^o), 7.78 (1H, td, $^{3}J_{H\text{-}H}$ 7.0 Hz $^{4}J_{H\text{-}P}$ 3.0 Hz, H^4), 7.68 (1H, d, $^{3}J_{H\text{-}H}$ 7.0 Hz, H^3), 7.54 (1H, t, $^{3}J_{H\text{-}H}$ 8.0 Hz,

H^{p}), 7.43 (2H, td, $^{3}J_{H\text{-}H}$ 8.0 Hz $^{4}J_{H\text{-}P}$ 4.0 Hz, H^{m}), 4.08 (2H, dqd, $^{2}J_{H\text{-}H}$ -16 Hz $^{3}J_{H\text{-}H}$ 7.0 Hz $^{3}J_{H\text{-}P}$ 4.5 Hz, H^{7}), 3.74 (2H, br s, H^{1}), 3.07 (6H, br s, $H^{a/a'}$), 2.98 – 2.06 (16H, br m, *cyclen* Hs), 1.40 (9H, s, H^{d}), 1.38 (18H, s, $H^{d'}$), 1.35 (3H, t, $^{3}J_{H\text{-}H}$ 7.0 Hz, H^{8}); δ_C ($CDCl_3$) 172.4 (C^{b}), 172.1 ($C^{b'}$), 159.1 (d, $^{3}J_{C\text{-}P}$ 20 Hz, C^{2}), 153.5 (d, $^{1}J_{C\text{-}P}$ 167 Hz, C^{6}), 137.8 (d, $^{3}J_{C\text{-}P}$ 10 Hz, C^{4}), 132.9 (d, $^{4}J_{C\text{-}P}$ 4 Hz, C^{p}), 132.2 (d, $^{2}J_{C\text{-}P}$ 12 Hz, C^{o}), 130.1 (d, $^{1}J_{C\text{-}P}$ 136 Hz, C^{i}), 128.8 (d, $^{3}J_{C\text{-}P}$ 9 Hz, C^{m}), 126.8 (d, $^{4}J_{C\text{-}P}$ 4 Hz, C^{3}), 126.5 (d, $^{2}J_{C\text{-}P}$ 22 Hz, C^{5}), 82.3 ($C^{c/c'}$), 62.1 (d, $^{2}J_{C\text{-}P}$ 6 Hz, C^{7}), 59.3 (C^{a}), 56.4 ($C^{a'}$), 56.0 (C^{1}), 51.2 – 49.3 (*cyclen* Cs), 28.2 (C^{d}), 28.1 ($C^{d'}$), 16.6 (C^{8}); δ_P ($CDCl_3$) 26.8; *m/z* ($HRMS^{+}$) 774.4588 $[M + H]^{+}$ ($C_{40}H_{65}O_8N_5P$ requires 774.4571); R_f = 0.20 (silica, CH_2Cl_2 : 5 % MeOH).

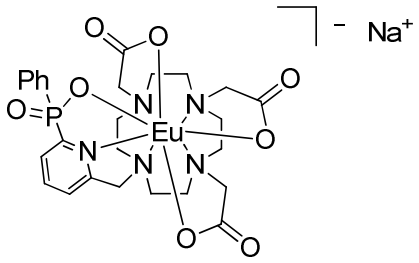

Europium(III) complex of 1,4,7-tris(acetic acid)-10-[ethyl (6-methylpyridin-2-yl)(phenyl)phosphinate]-1,4,7,10-tetraazacyclododecane, Na[Eu·L⁶]

1,4,7-Tris(tert-butoxycarbonyl)-10-[ethyl(6-methylpyridin-2-yl)(phenyl)phosphinate]-1,4,7,10-tetraazacyclododecane, ***23*** (55 mg, 0.070 mmol) was dissolved in HCl (6M, 10 mL) and the solution was stirred at 100 °C for 16 h. The solvent was lyophilised to give a yellow solid. Hydrolysis of the O^{t}Bu and OEt groups was confirmed by ^{1}H- and ^{31}P-NMR (δ_P (D_2O) 13.0). The solid was dissolved in H_2O and the pH of the solution adjusted to 5.8 using aq. ammonia solution. $Eu(OAc)_3$ (29 mg, 0.072 mmol) was added and the solution was stirred at 50 °C for 16 h. After allowing the solution to cool to room temperature, the pH was raised to 10 by the addition of aq. ammonia solution. The solution was stirred for 1 h causing excess Eu^{3+} to precipitate as $Eu(OH)_3$, which was removed by syringe filtration. Adjustment of the pH to 5.8 by the addition of CH_3CO_2H, followed by lyophilisation of the solvent, gave the *title compound* as a white solid (40 mg, 80 %); *m/z* ($HRMS^{-}$) 724.1166 $[M]^{-}$ ($C_{26}H_{32}O_8N_5P^{151}Eu$ requires 724.1187); τ_{H_2O} = 1.27 ms, τ_{D_2O} = 1.92 ms, $\Phi^{em}_{H_2O}$ = 16 %; t_R (*Method B*) = 12.8 min.

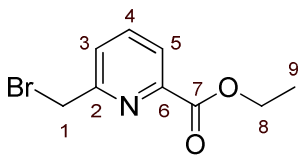

Ethyl 6-(bromomethyl)pyridine-2-carboxylate, 25

To a solution of ethyl 6-methylpridine-2-carboxylate, ***24*** (2.0 g, 12.1 mmol) in carbon tetrachloride (40 mL) was added N-bromo-succinimde (2.2 g, 12.1 mmol) and dibenzoyl peroxide (20 mg, 0.8 mmol). The mixture was stirred and irradiated by a 100 W lamp under an argon atmosphere. The reaction was monitored by ^{1}H-NMR and stopped after 16 h. The solvent was removed under reduced pressure and the crude product was dissolved in CH_2Cl_2 (40 mL) and washed with K_2CO_3 solution

(1.0 M, 40 mL) to remove excess succinimide. The organic layer was dried over $MgSO_4$, filtered and the solvent removed under reduced pressure. Purification by column chromatography on silica (CH_2Cl_2 isocratic elution) yielded the *title compound* as a colourless oil (1.03 g, 35 %); δ_H ($CDCl_3$) 7.97 (1H, d, 8.0 Hz, H^5), 7.79 (1H, t, 8.0 Hz, H^4), 7.61 (1H, d, 8.0 Hz, H^3), 4.58 (2H, s, H^1), 4.43 (2H, q, 6.8 Hz, H^8), 1.37 (3H, t, 6.8 Hz, H^9); δ_C ($CDCl_3$) 164.8 (C^7), 157.3 (C^2), 147.8 (C^6), 138.0 (C^4), 126.9 (C^3), 124.3 (C^5), 62.1 (C^8), 33.2 (C^1), 14.3 (C^9); *m/z* (HRMS$^+$) 243.9977 [M(^{79}Br) + H]$^+$ ($C_9H_{11}O_2N^{79}Br$ requires 243.9973), 245.9957 [M(^{81}Br) + H]$^+$ ($C_9H_{11}O_2N^{81}Br$ requires 245.9953); R_f = 0.51 (silica, CH_2Cl_2 : 2 % MeOH).

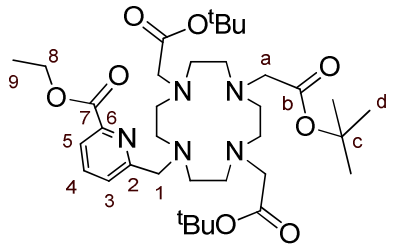

1,4,7-Tris(tert-butoxycarbonyl)-10-[ethyl 6-(bromomethyl)pyridine-2-carboxylate]-1,4,7,10-tetraazacyclododecane, 26

1,4,7-Tris(*tert*-butoxycarbonyl)-1,4,7,10-tetraazacyclododecane (500 mg, 0.97 mmol), ethyl 6-(bromomethyl)pyridine-2-carboxylate, ***25*** (237 mg, 0.97 mmol) and K_2CO_3 (130 mg, 0.97 mmol) were stirred in dry CH_3CN (10 mL) at 80 °C for 20 h under argon. The reaction was monitored by TLC to confirm that all the brominated starting material had been consumed. The solvent was removed under reduced pressure and the resultant residue was dissolved in CH_2Cl_2 (50 mL) and washed with water (3 × 50 mL). The organic layer was dried over $MgSO_4$, filtered and the solvent was removed under reduced pressure. Purification by column chromatography on silica (CH_2Cl_2 : 0 – 5 % MeOH in 0.5 % increments) gave the *title compound* as a glassy yellow solid (526 mg, 57 %); δ_H ($CDCl_3$) 7.98 (1H, d, 8.0 Hz, H^5), 7.91 (1H, t, 8.0 Hz, H^4), 7.55 (1H, d, 8.0 Hz, H^3), 4.33 (2H, q, 6.8 Hz, H^8), 3.60 – 3.20 (8H, br s, $H^{1/a/a'}$), 3.20 – 2.20 (16H, br m, *cyclen* Hs), 1.46 (9H, s, H^d), 1.44 (18H, s, $H^{d'}$), 1.36 (3H, t, 6.8 Hz, H^9); δ_C ($CDCl_3$) 172.0 ($C^{b/b'}$), 164.7 (C^7), 159.2 (C^2), 146.6 (C^6), 138.3 (C^4), 127.1 (C^3), 123.4 (C^5), 82.0 ($C^{c/c'}$), 61.7 (C^8), 59.0 (C^a), 56.1 ($C^{a'}$), 55.7 (C^1), 52.0 – 49.5 (*cyclen* Cs), 28.1 (C^d), 28.0 ($C^{d'}$), 14.3 (C^9); *m/z* (HRMS$^+$) 678.4459 [M + H]$^+$ ($C_{35}H_{60}O_8N_5$ requires 678.4442); R_f = 0.48 (silica, CH_2Cl_2 : 15 % MeOH).

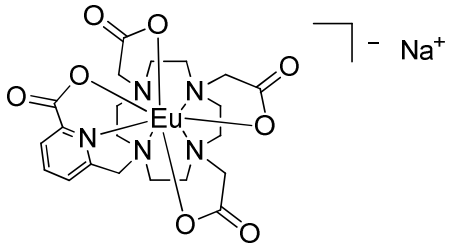

Europium(III) complex of 1,4,7-tris(acetic acid)-10-[ethyl 6-(bromomethyl)pyridine-2-carboxylate]-1,4,7,10-tetraazacyclododecane, Na[Eu·L^7]

1,4,7-Tris(tert-butoxycarbonyl)-10-[ethyl 6-(bromomethyl)pyridine-2-carboxylate]-1,4,7,10-tetraazacyclododecane (100 mg, 0.15 mmol) was dissolved in CH_2Cl_2 (2 mL) and CF_3CO_2H (2 mL)

was added. The mixture was stirred at 22 °C, under argon, for 16 h. Excess CF_3CO_2H and CH_2Cl_2 were removed under reduced pressure and the yellow residue was dissolved in CH_2Cl_2, which was again removed by reduced pressure to ensure the removal of all CF_3CO_2H. Deprotection of the O^{t}Bu groups was confirmed by ^{1}H-NMR. The residue was dissolved in aq. NaOD solution (2 mL, pH 11) and the mixture stirred for 30 min at 22 °C. ^{1}H-NMR was used to confirm that the hydrolysis of the ethyl ester had gone to completion. Adjustment of the pH to 5.8 by the addition of HCl was followed by addition of $EuCl_3$ (52 mg, 0.165 mmol) and the solution was stirred at 60 °C for 40 h. After allowing the solution to cool to room temperature, the pH was raised to 10 by the addition of aq. NaOH solution (1.0 M). The solution was stirred for 1 h causing excess Eu^{3+} to precipitate as $Eu(OH)_3$, which was removed by syringe filtration. Adjustment of the pH to 5.8 by the addition of HCl, followed by lyophilisation of the solvent, gave the *title compound* as a white solid (70 mg, 74 %); *m/z* (HRMS$^-$) 628.1079 $[M]^-$ ($C_{21}H_{27}O_8N_5{}^{151}Eu$ requires 628.1058); τ_{H_2O} = 1.14 ms, τ_{D_2O} = 1.85 ms, $\Phi^{em}_{H_2O}$ = 12 %, t_R (*Method B*) = 4.2 min.

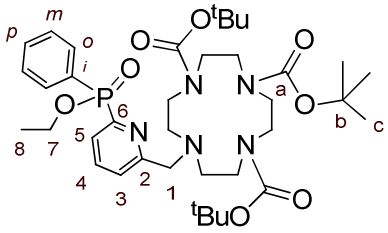

1,4,7-Tri-tert-butyl-10-[ethyl-(6-methylpyridin-2-yl)(phenyl)phosphinate]-1,4,7,10-tetraazacyclododecane-1,4,7-tricarboxylate, 27

1,4,7-Tris(carboxylic acid *tert*-butyl ester)-1,4,7,10-tetraazacyclododecane (169 mg, 0.36 mmol), ethyl [6-(bromomethyl)pyridin-2-yl](phenyl)phosphinate ***22*** (123 mg, 0.36 mmol) and K_2CO_3 (49 mg, 0.36 mmol) were stirred in dry CH_3CN (6 mL) at 80 °C for 16 h under argon. The reaction was monitored by TLC to confirm that all the brominated starting material had been consumed. The solvent was removed under reduced pressure and the resultant residue was dissolved in CH_2Cl_2 (40 mL) and washed with water (3 × 40 mL). The organic layer was dried over $MgSO_4$, filtered and the solvent was removed under reduced pressure. Purification by column chromatography on silica (CH_2Cl_2 : 0 – 3 % MeOH in 0.1 % increments) gave the *title compound* as a white foam solid (156 mg, 67 %); δ_H ($CDCl_3$) 7.97 (1H, dd, $^3J_{H\text{-}H}$ 7.0 Hz $^3J_{H\text{-}P}$ 14.0 Hz, H^5), 7.94 (2H, dd, $^3J_{H\text{-}H}$ 8.0 Hz $^3J_{H\text{-}P}$ 12.0 Hz, H^o), 7.71 (1H, td, $^3J_{H\text{-}H}$ 7.0 Hz $^4J_{H\text{-}P}$ 3.0 Hz, H^4), 7.51 (1H, t, $^3J_{H\text{-}H}$ 8.0 Hz, H^p), 7.44 (2H, td, $^3J_{H\text{-}H}$ 8.0 Hz $^4J_{H\text{-}P}$ 4.0 Hz, H^m), 7.35 (1H, d, $^3J_{H\text{-}H}$ 7.0 Hz, H^3), 4.10 (2H, qd, $^3J_{H\text{-}H}$ 7.0 Hz $^3J_{H\text{-}P}$ 4.5 Hz, H^7), 3.92 (2H, br s, H^1), 3.60 – 2.40 (16H, br m, *cyclen* Hs), 1.46 (9H, s, H^c), 1.41 (18H, s, $H^{c'}$), 1.34 (3H, t, $^3J_{H\text{-}H}$ 7.0 Hz, H^8); δ_C ($CDCl_3$) 172.4 (C^a), 172.1 ($C^{a'}$), 159.3 (d, $^3J_{C\text{-}P}$ 20 Hz, C^2), 155.4 (d, $^1J_{C\text{-}P}$ 167 Hz, C^6), 136.3 (d, $^3J_{C\text{-}P}$ 10 Hz, C^4), 132.7 (d, $^4J_{C\text{-}P}$ 4 Hz, C^p), 132.6 (d, $^2J_{C\text{-}P}$ 12 Hz, C^o), 130.3 (d, $^1J_{C\text{-}P}$ 136 Hz, C^i), 128.5 (d, $^3J_{C\text{-}P}$ 9 Hz, C^m), 128.4 (d, $^4J_{C\text{-}P}$ 4 Hz, C^3), 126.6 (d, $^2J_{C\text{-}P}$ 22 Hz, C^5), 79.6 ($C^{b/b'}$), 61.8 (d, $^2J_{C\text{-}P}$ 6 Hz, C^7), 56.2 (C^1), 52.1 – 46.3 (*cyclen* Cs), 28.7 (C^c), 28.5 ($C^{c'}$), 16.8 (C^8); δ_P ($CDCl_3$) 26.0; *m/z* (HRMS$^+$) 732.4102 $[M + H]^+$ ($C_{37}H_{59}O_8N_5P$ requires 732.4101); R_f = 0.40 (silica, CH_2Cl_2 : 5 % MeOH).

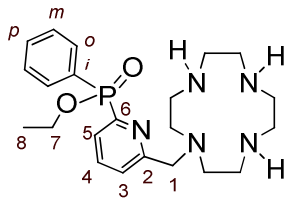

1-[Ethyl-(6-methylpyridin-2-yl)(phenyl)phosphinate]-1,4,7,10-tetraazacyclododecane, 28

1,4,7-Tri-tert-butyl-10-[ethyl(6-methylpyridin-2-yl)(phenyl)phosphinate]-1,4,7,10-tetraazacyclododecane-1,4,7-tricarboxylate, ***27*** (91 mg, 0.14 mmol) was dissolved in CH_2Cl_2 (2 mL). CF_3CO_2H (2 mL) was added and the solution was stirred at 23 °C for 16 h under argon. The solvent and excess CF_3CO_2H were removed under reduced pressure and the yellow residue was redissolved in CH_2Cl_2 (2 mL). The solvent was again removed under reduced pressure. This process was repeated 3 times to ensure the removal of all CF_3CO_2H. No further purification was required and the *title product* was isolated as a yellow glass (59 mg, 98 %); δ_H ($CDCl_3$) 7.77 (1H, td, $^3J_{H\text{-}H}$ 7.0 Hz $^4J_{H\text{-}P}$ 3.0 Hz, H^4), 7.67 (1H, dd, $^3J_{H\text{-}H}$ 7.0 Hz $^3J_{H\text{-}P}$ 14.0 Hz, H^5), 7.65 (2H, dd, $^3J_{H\text{-}H}$ 8.0 Hz $^3J_{H\text{-}P}$ 12.0 Hz, H^o), 7.56 (1H, t, $^3J_{H\text{-}H}$ 8.0 Hz, H^p), 7.47 (2H, td, $^3J_{H\text{-}H}$ 8.0 Hz $^4J_{H\text{-}P}$ 4.0 Hz, H^m), 7.31 (1H, d, $^3J_{H\text{-}H}$ 7.0 Hz, H^3), 4.13 (2H, qd, $^3J_{H\text{-}H}$ 7.0 Hz $^3J_{H\text{-}P}$ 4.5 Hz, H^7), 3.94 (2H, d, $^2J_{H\text{-}H}$ 36 Hz, H^1), 3.60 – 2.80 (16H, br m, *cyclen* Hs), 1.36 (3H, t, $^3J_{H\text{-}H}$ 7.0 Hz, H^8); δ_C ($CDCl_3$) 158.7 (d, $^3J_{C\text{-}P}$ 20 Hz, C^2), 153.4 (d, $^1J_{C\text{-}P}$ 167 Hz, C^6), 137.9 (d, $^3J_{C\text{-}P}$ 10 Hz, C^4), 133.5 (d, $^4J_{C\text{-}P}$ 4 Hz, C^p), 131.5 (d, $^2J_{C\text{-}P}$ 12 Hz, C^o), 129.3 (d, $^3J_{C\text{-}P}$ 9 Hz, C^m), 129.1 (d, $^1J_{C\text{-}P}$ 136 Hz, C^i), 127.1 (d, $^2J_{C\text{-}P}$ 22 Hz, C^5), 126.3 (d, $^4J_{C\text{-}P}$ 4 Hz, C^3), 62.9 (d, $^2J_{C\text{-}P}$ 6 Hz, C^7), 57.0 (C^1), 51.0 – 49.0 (*cyclen* Cs), 16.4 (C^8); δ_P ($CDCl_3$) 28.9; *m/z* (HRMS$^+$) 432.2544 $[M + H]^+$ ($C_{22}H_{35}O_2N_5P$ requires 432.2528).

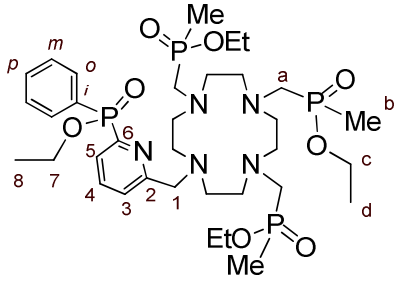

Ethyl-phenyl((6-[(4,7,10-tri([ethoxy(methyl)phosphoryl]methyl)-1,4,7,10-tetraazacyclododecan-1-yl)methyl]pyridin-2-yl))phosphinate, 29

1-[Ethyl (6-methylpyridin-2-yl)(phenyl)phosphinate]-1,4,7,10-tetraazacyclododecane, ***28*** (40 mg, 0.093 mmol) was dissolved in tetrahydrofuran (20 mL) in a flask fitted with a drying tube containing molecular sieves. The solution was heated under reflux for 2 h under argon until a steady flow of solvent through the molecular sieves was established. Paraformaldehyde (12 mg, 0.40 mmol) and diethyl methylphosphonite (57 mg, 0.4 mmol) were added and the mixture was stirred at reflux under argon for a further 18 h. The solution was allowed to cool and excess paraformaldehyde was removed by filtration. The solvent was removed under reduced pressure to give a brown residue which was purified by column chromatography on alumina (CH_2Cl_2 : 0 – 3 % MeOH in 0.1 % increments) to give the *title compound* as a yellow oil (40 mg, 55 %); δ_H ($CDCl_3$) 7.96 (1H, dd, $^3J_{H\text{-}H}$ 7.0 Hz $^3J_{H\text{-}P}$ 14.0 Hz, H^5), 7.95 (2H, dd, $^3J_{H\text{-}H}$ 8.0 Hz $^3J_{H\text{-}P}$ 12.0 Hz, H^o), 7.73 (1H, td, $^3J_{H\text{-}H}$ 7.0 Hz $^4J_{H\text{-}P}$ 3.0 Hz, H^4),

7.60 (1H, d, $^{3}J_{H\text{-}H}$ 7.0 Hz, H^{3}), 7.51 (1H, t, $^{3}J_{H\text{-}H}$ 8.0 Hz, H^{p}), 7.44 (2H, td, $^{3}J_{H\text{-}H}$ 8.0 Hz $^{4}J_{H\text{-}P}$ 4.0 Hz, H^{m}), 4.11 (2H, qd, $^{3}J_{H\text{-}H}$ 7.0 Hz $^{3}J_{H\text{-}P}$ 4.5 Hz, H^{7}), 4.01 (6H, qd, $^{3}J_{H\text{-}H}$ 7.0 Hz $^{3}J_{H\text{-}P}$ 5.6 Hz, H^{c}), 3.12 – 2.86 (8H, br s, $H^{1/a}$), 2.84 – 2.42 (16H, br m, *cyclen* Hs), 1.49 (9H, d, $^{2}J_{H\text{-}P}$ 36 Hz, H^{b}), 1.34 (3H, t, $^{3}J_{H\text{-}H}$ 7.0 Hz, H^{8}), 1.26 (9H, t, 7.0 Hz, H^{d}); δ_C ($CDCl_3$) 155.5 (d, $^{3}J_{C\text{-}P}$ 20 Hz, C^{2}), 150.5 (d, $^{1}J_{C\text{-}P}$ 167 Hz, C^{6}), 136.3 (d, $^{3}J_{C\text{-}P}$ 10 Hz, C^{4}), 132.7 (d, $^{4}J_{C\text{-}P}$ 4 Hz, C^{p}), 132.5 (d, $^{2}J_{C\text{-}P}$ 12 Hz, C^{o}), 130.5 (d, $^{1}J_{C\text{-}P}$ 136 Hz, C^{i}), 128.5 (d, $^{3}J_{C\text{-}P}$ 9 Hz, C^{m}), 126.6 (d, $^{2}J_{C\text{-}P}$ 22 Hz, C^{5}), 125.4 (d, $^{4}J_{C\text{-}P}$ 4 Hz, C^{3}), 61.6 (d, $^{2}J_{C\text{-}P}$ 6 Hz, C^{7}), 60.2 (d, $^{2}J_{C\text{-}P}$ 6 Hz, C^{c}), 55.1 (C^{1}), 55.0 – 52.0 (*cyclen* Cs), 16.7 (C^{d}), 16.5 (C^{8}), 13.6 (d, $^{1}J_{C\text{-}P}$ 94 Hz); δ_P ($CDCl_3$) 53.7 53.5 53.3 (P-Me), 26.8 (P-Ph); *m/z* (HRMS^{+}) 792.3532 $[M + H]^{+}$ ($C_{34}H_{62}O_8N_5P_4$ requires 792.3549); R_f = 0.33 (alumina, CH_2Cl_2 : 5 % MeOH).

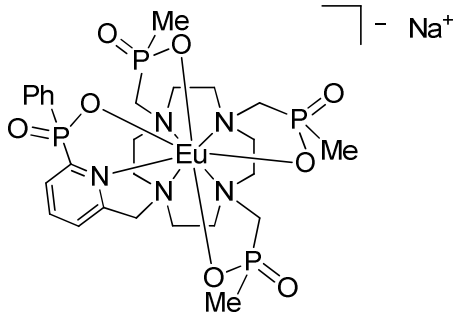

Europium(III) complex of ethyl phenyl((6-[(4,7,10-tri([ethoxy(methyl)phosphoryl]-methyl)-1,4,7,10-tetraazacyclododecan-1-yl)methyl]pyridin-2-yl))phosphinate, Na[Eu·L^{8}]

Ethyl-phenyl((6-[(4,7,10-tri([ethoxy(methyl)phosphoryl]methyl)-1,4,7,10-tetraazacyclododecan-1-yl)methyl]pyridin-2-yl))phosphinate, ***29*** (18 mg, 0.023 mmol) was dissolved in HCl (6M, 5 mL) and the solution was stirred at 100 °C for 16 h. The solvent was lyophilised to give a yellow solid. Hydrolysis of the OEt groups was confirmed by ^{1}H- and ^{31}P-NMR. The solid was dissolved in H_2O and the pH of the solution adjusted to 5.8 using aq. ammonia solution. $Eu(OAc)_3$ (9.2 mg, 0.025 mmol) was added and the solution was stirred at 50 °C for 16 h. After allowing the solution to cool to room temperature, the pH was raised to 10 by the addition of aq. ammonia solution. The solution was stirred for 1 h causing excess Eu^{3+} to precipitate as $Eu(OH)_3$, which was removed by syringe filtration. Adjustment of the pH to 5.8 by the addition of CH_3CO_2H, followed by lyophilisation of the solvent, gave the *title compound* as a white solid (16 mg, 88 %); *m/z* (HRMS^{-}) 826.1129 $[M]^{-}$ ($C_{26}H_{41}O_8N_5P_4{}^{151}$Eu requires 826.1104); τ_{H_2O} = 0.95 ms, τ_{D_2O} = 1.25 ms, $\Phi^{em}_{H_2O}$ = 18 %; t_R (*Method C*) = 11.5 min.

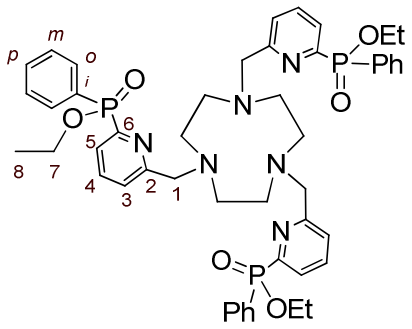

1,4,7-Tri[ethyl-(6-methylpyridin-2-yl)(phenyl)phosphinate]-1,4,7-triazacyclononane, 30

1,4,7-Triazacyclononane (14 mg, 0.11 mmol), ethyl [6-(bromomethyl)pyridin-2-yl](phenyl)phosphinate, ***22*** (130 mg, 0.38 mmol) and K_2CO_3 (51 mg, 0.38 mmol) were stirred in dry CH_3CN (5 mL) at 80 °C for 20 h under argon. The reaction was monitored by TLC to confirm that all the brominated starting material had been consumed. The solvent was removed under reduced pressure and the resultant residue was dissolved in CH_2Cl_2 (30 mL) and washed with water (3 × 30 mL). The organic layer was dried over $MgSO_4$, filtered and the solvent was removed under reduced pressure. Purification by column chromatography on alumina (CH_2Cl_2 : 0 – 2 % MeOH in 0.05 % increments) gave the *title compound* as a glassy yellow solid (60 mg, 62 %); δ_H ($CDCl_3$) 7.96 (3H, dd, $^3J_{H\text{-}H}$ 7.0 Hz $^3J_{H\text{-}P}$ 14.0 Hz, H^5), 7.95 (6H, dd, $^3J_{H\text{-}H}$ 8.0 Hz $^3J_{H\text{-}P}$ 12.0 Hz, H^o), 7.74 (3H, td, $^3J_{H\text{-}H}$ 7.0 Hz $^4J_{H\text{-}P}$ 3.0 Hz, H^4), 7.54 (3H, d, $^3J_{H\text{-}H}$ 7.0 Hz, H^3), 7.47 (3H, t, $^3J_{H\text{-}H}$ 8.0 Hz, H^p), 7.39 (6H, td, $^3J_{H\text{-}H}$ 8.0 Hz $^4J_{H\text{-}P}$ 4.0 Hz, H^m), 4.11 (6H, qd, $^3J_{H\text{-}H}$ 7.0 Hz $^3J_{H\text{-}P}$ 4.5 Hz, H^7), 3.83 (6H, br s, H^1), 2.74 (12H, br s, *ring* Hs), 1.34 (9H, t, $^3J_{H\text{-}H}$ 7.0 Hz, H^8); δ_C ($CDCl_3$) 161.7 (d, $^3J_{C\text{-}P}$ 20 Hz, C^2), 153.9 (d, $^1J_{C\text{-}P}$ 167 Hz, C^6), 136.4 (d, $^3J_{C\text{-}P}$ 10 Hz, C^4), 132.6 (d, $^4J_{C\text{-}P}$ 4 Hz, C^p), 132.5 (d, $^2J_{C\text{-}P}$ 12 Hz, C^o), 130.5 (d, $^1J_{C\text{-}P}$ 136 Hz, C^i), 128.4 (d, $^3J_{C\text{-}P}$ 9 Hz, C^m), 126.6 (d, $^2J_{C\text{-}P}$ 22 Hz, C^5), 125.6 (d, $^4J_{C\text{-}P}$ 4 Hz, C^3), 64.1 (C^1), 61.8 (d, $^2J_{C\text{-}P}$ 6 Hz, C^7), 55.7 (*ring* Cs), 16.7 (C^8); δ_P ($CDCl_3$) 26.7; *m/z* (HRMS$^+$) 907.3661 $[M + H]^+$ ($C_{48}H_{58}O_6N_6P_3$ requires 907.3631); R_f = 0.56 (alumina, CH_2Cl_2 : 5 % MeOH).

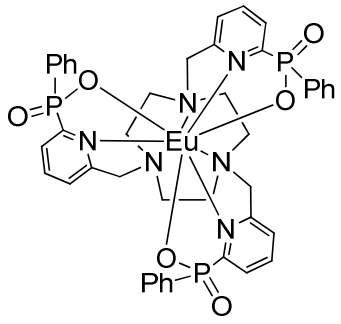

Europium(III) complex of 1,4,7-tri[ethyl (6-methylpyridin-2-yl)(phenyl)phosphinate]-1,4,7-triazacyclononane, [Eu·L^9]

1,4,7-Tri[ethyl (6-methylpyridin-2-yl)(phenyl)phosphinate]-1,4,7-triazacyclononane, ***30*** (38 mg, 0.042 mmol) was dissolved in HCl (6M, 8 mL) and the solution was stirred at 100 °C for 16 h. The solvent was lyophilised to give a yellow solid, ***3***. Hydrolysis of the OEt groups was confirmed by ^{1}H- and ^{31}P-NMR (δ_P ($CDCl_3$) 16.0). The solid was dissolved in H_2O – CH_3OH (1 : 1 v/v, 6 mL) and the pH of the solution adjusted to 5.8 using aq. NaOH solution. $Eu(OAc)_3$ (18 mg, 0.046 mmol) was added and the solution was stirred at 50 °C for 18 h. After allowing the solution to cool to room

temperature, the pH was raised to 10 by the addition of aq. ammonia solution. The solution was stirred for 1 h causing excess Eu^{3+} to precipitate as $Eu(OH)_3$, which was removed by syringe filtration. Adjustment of the pH to 5.8 by the addition of CH_3CO_2H, followed by lyophilisation of the solvent, gave a solid, which was purified by column chromatography (silica, CH_2Cl_2: 20 % CH_3OH: 1 % NH_3) to give the *title compound* as a white solid (32 mg, 82 %); *m/z* (HRMS$^+$) 971.1675 $[M + H]^+$ ($C_{42}H_{43}O_6N_6P_3{}^{151}Eu$ requires 971.1656); δ_P (CD_3OD) +16.6; τ_{H_2O} = 1.36 ms, τ_{D_2O} = 1.54 ms, $\Phi^{em}_{H_2O}$ = 9.0 %, t_R (*Method C*) = 6.8 min. Single crystals of [Eu·L^9] suitable for X-ray diffraction studies were grown by dissolving 10 mg of complex in CH_3OH (1 mL). Addition of H_2O (0.5 mL) led to crystal formation over 16 h. CCDC Ref. 836099.

Cerium(III) complex of 1,4,7-tri[ethyl (6-methylpyridin-2-yl)(phenyl)phosphinate]-1,4,7-triazacyclononane, [Ce·L^9]

An analogous procedure to that described for the synthesis of [Eu·L^9] was followed using 1,4,7-tri[ethyl (6-methylpyridin-2-yl)(phenyl)phosphinate]-1,4,7-triazacyclononane, ***30*** (15 mg, 0.017 mmol) and $Ce(OAc)_3$ (7.0 mg, 0.018 mmol) to give the *title compound* as a white solid (12.2 mg, 77 %); *m/z* (ESI-MS$^+$) 960.3 [M (^{140}Ce) + H]$^+$; δ_P (CD_3OD) +27.8; t_R (*Method C*) = 6.8 min.

Praseodymium(III) complex of 1,4,7-tri[ethyl (6-methylpyridin-2-yl)(phenyl)phosphinate]-1,4,7-triazacyclononane, [Pr·L^9]

An analogous procedure to that described for the synthesis of [Eu·L^9] was followed using 1,4,7-tri[ethyl (6-methylpyridin-2-yl)(phenyl)phosphinate]-1,4,7-triazacyclononane, ***30*** (15 mg, 0.017 mmol) and $Pr(OAc)_3$ (7.0 mg, 0.018 mmol) to give the *title compound* as a white solid (13.3 mg, 84 %); *m/z* (ESI-MS$^+$) 961.3 [M (^{141}Pr) + H]$^+$; δ_P (CD_3OD) +31.3; t_R (*Method C*) = 6.8 min.

Neodymium(III) complex of 1,4,7-tri[ethyl (6-methylpyridin-2-yl)(phenyl)phosphinate]-1,4,7-triazacyclononane, [Nd·L^9]

An analogous procedure to that described for the synthesis of [Eu·L^9] was followed using 1,4,7-tri[ethyl (6-methylpyridin-2-yl)(phenyl)phosphinate]-1,4,7-triazacyclononane, ***30*** (15 mg, 0.017 mmol) and $Nd(OAc)_3$ (7.1 mg, 0.018 mmol) to give the *title compound* as a white solid (12.7 mg, 80 %); *m/z* (ESI-MS$^+$) 964.2 [M (^{144}Nd) + H]$^+$; δ_P (CD_3OD) +21.0; t_R (*Method C*) = 6.8 min, CCDC Ref. 836097.

Samarium(III) complex of 1,4,7-tri[ethyl (6-methylpyridin-2-yl)(phenyl)phosphinate]-1,4,7-triazacyclononane, [Sm·L^9]

An analogous procedure to that described for the synthesis of [Eu·L^9] was followed using 1,4,7-tri[ethyl (6-methylpyridin-2-yl)(phenyl)phosphinate]-1,4,7-triazacyclononane, ***30*** (15 mg, 0.017 mmol) and $Sm(OAc)_3$ (7.2 mg, 0.018 mmol) to give the *title compound* as a white solid (12.5 mg, 78

%); *m/z* (ESI-MS$^+$) 972.2 [M (^{152}Sm) + H]$^+$; δ_P (CD_3OD) +31.4; t_R (*Method C*) = 6.8 min, CCDC Ref. 836098.

Gadolinium(III) complex of 1,4,7-tri[ethyl (6-methylpyridin-2-yl)(phenyl)phosphinate]-1,4,7-triazacyclononane, [Gd·L^9]

An analogous procedure to that described for the synthesis of [Eu·L^9] was followed using 1,4,7-tri[ethyl (6-methylpyridin-2-yl)(phenyl)phosphinate]-1,4,7-triazacyclononane, ***30*** (15 mg, 0.017 mmol) and $Gd(OAc)_3$ (7.3 mg, 0.018 mmol) to give the *title compound* as a white solid (13.0 mg, 81 %); *m/z* (ESI-MS$^+$) 976.2 [M (^{156}Gd) + H]$^+$; t_R (*Method C*) = 6.8 min.

Terbium(III) complex of 1,4,7-tri[ethyl (6-methylpyridin-2-yl)(phenyl)phosphinate]-1,4,7-triazacyclononane, [Tb·L^9]

An analogous procedure to that described for the synthesis of [Eu·L^9] was followed using 1,4,7-tri[ethyl (6-methylpyridin-2-yl)(phenyl)phosphinate]-1,4,7-triazacyclononane, ***30*** (15 mg, 0.017 mmol) and $Tb(OAc)_3$ (7.3 mg, 0.018 mmol) to give the *title compound* as a white solid (12.6 mg, 78 %); *m/z* (ESI-MS$^+$) 979.2 [M (^{159}Tb) + H]$^+$; δ_P (CD_3OD) -35.7; $\tau_{H_2O} = 2.13$ ms, τ_{D_2O} = 2.64 ms, $\Phi^{em}_{H_2O}$ = 60 %, t_R (*Method C*) = 6.8 min.

Dysprosium(III) complex of 1,4,7-tri[ethyl (6-methylpyridin-2-yl)(phenyl)phosphinate]-1,4,7-triazacyclononane, [Dy·L^9]

An analogous procedure to that described for the synthesis of [Eu·L^9] was followed using 1,4,7-tri[ethyl (6-methylpyridin-2-yl)(phenyl)phosphinate]-1,4,7-triazacyclononane, ***30*** (15 mg, 0.017 mmol) and $Dy(OAc)_3$ (7.4 mg, 0.018 mmol) to give the *title compound* as a white solid (13.0 mg, 80 %); *m/z* (ESI-MS$^+$) 984.2 [M (^{164}Dy) + H]$^+$; δ_P (CD_3OD) -13.9; t_R (*Method C*) = 6.8 min.

Holmium(III) complex of 1,4,7-tri[ethyl (6-methylpyridin-2-yl)(phenyl)phosphinate]-1,4,7-triazacyclononane, [Ho·L^9]

An analogous procedure to that described for the synthesis of [Eu·L^9] was followed using 1,4,7-tri[ethyl (6-methylpyridin-2-yl)(phenyl)phosphinate]-1,4,7-triazacyclononane, ***30*** (15 mg, 0.017 mmol) and $Ho(OAc)_3$ (7.4 mg, 0.018 mmol) to give the *title compound* as a white solid (12.7 mg, 78 %); *m/z* (ESI-MS$^+$) 985.3 [M (^{165}Ho) + H]$^+$; δ_P (CD_3OD) -24.6; t_R (*Method C*) = 6.8 min, CCDC Ref. 836100.

Erbium(III) complex of 1,4,7-tri[ethyl (6-methylpyridin-2-yl)(phenyl)phosphinate]-1,4,7-triazacyclononane, [Er·L^9]

An analogous procedure to that described for the synthesis of [Eu·L^9] was followed using 1,4,7-tri[ethyl (6-methylpyridin-2-yl)(phenyl)phosphinate]-1,4,7-triazacyclononane, ***30*** (15 mg, 0.017

mmol) and $Er(OAc)_3$ (7.5 mg, 0.018 mmol) to give the *title compound* as a white solid (14.3 mg, 88 %); *m/z* (ESI-MS$^+$) 988.2 [M (^{168}Er) + H]$^+$; δ_P (CD_3OD) -10.5; t_R (*Method C*) = 6.8 min.

Thulium(III) complex of 1,4,7-tri[ethyl (6-methylpyridin-2-yl)(phenyl)phosphinate]-1,4,7-triazacyclononane, [Tm·L^9]

An analogous procedure to that described for the synthesis of [Eu·L^9] was followed using 1,4,7-tri[ethyl (6-methylpyridin-2-yl)(phenyl)phosphinate]-1,4,7-triazacyclononane, ***30*** (15 mg, 0.017 mmol) and $Tm(OAc)_3$ (7.5 mg, 0.018 mmol) to give the *title compound* as a white solid (12.9 mg, 79 %); *m/z* (ESI-MS$^+$) 989.3 [M (^{169}Tm) + H]$^+$; δ_P (CD_3OD) +8.4; t_R (*Method C*) = 6.8 min, CCDC Ref. 836101.

Ytterbium(III) complex of 1,4,7-tri[ethyl (6-methylpyridin-2-yl)(phenyl)phosphinate]-1,4,7-triazacyclononane, [Yb·L^9]

An analogous procedure to that described for the synthesis of [Eu·L^9] was followed using 1,4,7-tri[ethyl (6-methylpyridin-2-yl)(phenyl)phosphinate]-1,4,7-triazacyclononane, ***30*** (15 mg, 0.017 mmol) and $Yb(OAc)_3$ (7.6 mg, 0.018 mmol) to give the *title compound* as a white solid (13.6 mg, 83 %); *m/z* (ESI-MS$^+$) 994.2 [M (^{174}Yb) + H]$^+$; δ_P (CD_3OD) +17.7; t_R (*Method C*) = 6.8 min.

Yttrium(III) complex of 1,4,7-tri[ethyl (6-methylpyridin-2-yl)(phenyl)phosphinate]-1,4,7-triazacyclononane, [Y·L^9]

An analogous procedure to that described for the synthesis of [Eu·L^9] was followed using 1,4,7-tri[ethyl (6-methylpyridin-2-yl)(phenyl)phosphinate]-1,4,7-triazacyclononane, ***30*** (15 mg, 0.017 mmol) and $Y(OAc)_3$ (6.4 mg, 0.018 mmol) to give the *title compound* as a white solid (13.3 mg, 86 %); *m/z* (ESI-MS$^+$) 908.2 [M (^{89}Y) + H]$^+$; δ_P (CD_3OD) +23.9; t_R (*Method C*) = 6.8 min, CCDC Ref. 836102.

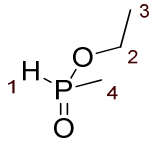

Ethyl methylphosphinate, 31

Neat diethyl methylphosphonite (2 g, 14.7 mmol) was stirred at 0°C and H_2O (264 µL, 14.7 mmol) was added. The mixture was allowed to reach 22 °C over 1 h and stirred for a further 16 h. ^{1}H- and ^{31}P-NMR was used to confirm formation of the *title compound*, which was used *in situ* without further purification. The reaction mixture also contains one equivalent of ethanol as a by-product (100 % conversion by ^{1}H-NMR); δ_H ($CDCl_3$) 7.22 (1H, dq, $^1J_{H\text{-}P}$ 536 $^2J_{H\text{-}H}$ 2.1 Hz, H^1), 4.11 (2H, dqd, $^2J_{H\text{-}H}$ 36 Hz $^3J_{H\text{-}H}$ 7.0 Hz $^3J_{H\text{-}P}$ 4.0 Hz, H^2), 1.54 (3H, dd, $^2J_{H\text{-}P}$ 15.1 Hz $^3J_{H\text{-}H}$ 2.1 Hz, H^4), 1.23 (3H, $^3J_{H\text{-}H}$ 7.0 Hz, H^3); δ_P ($CDCl_3$) +34.5; δ_C ($CDCl_3$) 62.3 (d, $^2J_{C\text{-}P}$ 7 Hz, C^2), 16.1 (C^3), 14.9 (d, $^1J_{C\text{-}P}$ 95 Hz, C^4); *m/z* (HRMS$^+$) 109.0414 [M + H]$^+$ ($C_3H_{10}O_2P$ requires 109.0418).

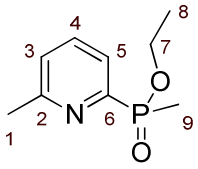

Ethyl (6-methylpyridin-2-yl)(methyl)phosphinate, 32

To neat ethyl methylphospinate, ***31*** (1.59 g, 14.7 mmol), containing one equivalent of ethanol, dry degassed (freeze-thaw cycle) toluene (20 mL), 2-bromo-6-methylpyridine, ***17*** (2.1 g, 12.3 mmol) and triethylamine (6 mL, 43 mmol) were added. Argon was bubbled through the solution for 1 h and tetrakis(triphenylphosphine)palladium(0) (320 mg, 0.27 mmol) was added and the mixture was stirred at 125 °C for 16 h under argon. The resulting solution was decanted from the white ammonium salt precipitate and the solvent removed under reduced pressure. Purification of the yellow oil by column chromatography on silica (silica, CH_2Cl_2 : CH_3OH 0 – 1.6 % in 0.1 % increments) gave the *title compound* as a colourless oil (700 mg, 29 %); δ_H ($CDCl_3$) 7.75 (1H, dd, $^3J_{H\text{-}H}$ 7.0 Hz $^3J_{H\text{-}P}$ 10 Hz, H^5), 7.59 (1H, td, $^3J_{H\text{-}H}$ 7.0 Hz $^4J_{H\text{-}P}$ 4.8 Hz, H^4), 7.16 (1H, d, $^3J_{H\text{-}H}$ 7.0 Hz, H^3), 3.86 (2H, dqd, $^2J_{H\text{-}H}$ 80 Hz $^3J_{H\text{-}H}$ 7.0 Hz $^3J_{H\text{-}P}$ 4.5 Hz, H^7), 2.50 (3H, s, H^1), 1.66 (3H, d, $^2J_{H\text{-}P}$ 15 Hz, H^9), 1.61 (3H, t, $^3J_{H\text{-}H}$ 7.0 Hz, H^8); δ_C ($CDCl_3$) 159.4 (d, $^3J_{C\text{-}P}$ 20 Hz, C^2), 153.7 (d, $^1J_{C\text{-}P}$ 158 Hz, C^6), 136.0 (d, $^3J_{C\text{-}P}$ 10 Hz, C^4), 125.6 (d, $^2J_{C\text{-}P}$ 3 Hz, C^3), 124.6 (d, $^4J_{C\text{-}P}$ 22 Hz, C^5), 60.8 (d, $^2J_{C\text{-}P}$ 6 Hz, C^7), 24.5 (C^1), 16.3 (C^8) 13.3 (d, $^1J_{C\text{-}P}$ 103 Hz, H^9); δ_P ($CDCl_3$) +41.2; *m/z* ($HRMS^+$) 200.0858 $[M + H]^+$ ($C_9H_{14}O_2NP$ requires 200.0862); R_f = 0.25 (silica, CH_2Cl_2 : 5 % MeOH).

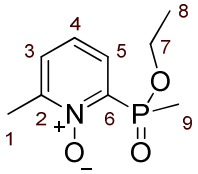

Ethyl methyl(6-methyl-1-oxo-pyridin-2-yl)phosphinate, 33

To a stirred solution of ethyl (6-methylpyridin-2-yl)(methyl)phosphinate, ***32*** (600 mg, 3.0 mmol) in $CHCl_3$ (15 mL) MCPBA (1.04 g, 6.0 mmol) was added. The resulting solution was stirred at 65 °C for 16 h under argon. The reaction was monitored by TLC (silica; CH_2Cl_2 : 5 % CH_3OH, R_f(product) = 0.19, R_f(reactant) = 0.25). The solvent was removed under reduced pressure to give a yellow oil. CH_2Cl_2 (10 mL) was added and the solution decanted from the white benzoic acid precipitate. CH_2Cl_2 was removed under reduced pressure and the resultant yellow oil was purified by column chromatography (silica, CH_2Cl_2 : CH_3OH 0 – 3.2 % in 0.2 % increments) to give the *title* compound as a yellow oil (360 mg, 56 %); δ_H ($CDCl_3$) 7.90 (1H, dd, $^3J_{H\text{-}H}$ 7.0 Hz $^3J_{H\text{-}P}$ 10 Hz, H^5), 7.40 (1H, d, $^3J_{H\text{-}H}$ 7.0 Hz, H^3), 7.26 (1H, td, $^3J_{H\text{-}H}$ 7.0 Hz $^4J_{H\text{-}P}$ 4.8 Hz, H^4), 4.03 (2H, dqd, $^2J_{H\text{-}H}$ 80 Hz $^3J_{H\text{-}H}$ 7.0 Hz $^3J_{H\text{-}P}$ 4.5 Hz, H^7), 2.50 (3H, s, H^1), 1.96 (3H, d, $^2J_{H\text{-}P}$ 15 Hz, H^9), 1.28 0(3H, t, $^3J_{H\text{-}H}$ 7.0 Hz, H^8); δ_C ($CDCl_3$) 149.7 (d, $^3J_{C\text{-}P}$ 20 Hz, C^2), 142.6 (d, $^1J_{C\text{-}P}$ 158 Hz, C^6), 130.4 (d, $^2J_{C\text{-}P}$ 3 Hz, C^3), 124.5 (d, $^4J_{C\text{-}P}$ 22 Hz, C^5), 124.5 (d, $^3J_{C\text{-}P}$ 10 Hz, C^4), 61.7 (d, $^2J_{C\text{-}P}$ 6 Hz, C^7), 17.5 (C^1), 16.3 (C^8) 11.7 (d, $^1J_{C\text{-}P}$ 103 Hz, H^9); δ_P ($CDCl_3$) +34.3; *m/z* ($HRMS^+$) 238.0607 $[M + Na]^+$ ($C_9H_{14}O_3NPNa$ requires 238.0609); R_f = 0.19 (silica, CH_2Cl_2 : 5 % MeOH).

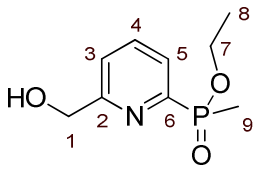

Ethyl [6-(hydroxymethyl)pyridine-2-yl](methyl)phosphinate, 34

Ethyl methyl(6-methyl-1-oxo-pyridin-2-yl)phosphinate, ***33*** (360 mg, 1.67 mmol) was dissolved in $CHCl_3$ (10 mL) and $(CF_3CO)_2O$ (8 mL, 56 mmol) was added. The mixture was stirred at 60 °C and the formation of the trifluoroacetate analogue of the *title compound* was monitored by LC-MS. After 3 h the solution was cooled to 22 °C and the solvent removed under reduced pressure. The residue was dissolved in CH_3CH_2OH (10 mL) and the solution stirred at 60 °C for 3 h. The solvent was removed under reduced pressure to give the crude alcohol which was purified by column chromatography (silica, CH_2Cl_2 : CH_3OH 0 – 2.5 % in 0.25 % increments) to give the *title compound* (220 mg, 60 %); δ_H ($CDCl_3$) 7.91 (1H, dd, $^3J_{H\text{-}H}$ 7.0 Hz $^3J_{H\text{-}P}$ 10 Hz, H^5), 7.80 (1H, td, $^3J_{H\text{-}H}$ 7.0 Hz $^4J_{H\text{-}P}$ 4.8 Hz, H^4), 7.43 (1H, d, $^3J_{H\text{-}H}$ 7.0 Hz, H^3), 4.80 (2H, s, H^1), 3.93 (2H, dqd, $^2J_{H\text{-}H}$ 80 Hz $^3J_{H\text{-}H}$ 7.0 Hz $^3J_{H\text{-}P}$ 4.5 Hz, H^7), 1.75 (3H, d, $^2J_{H\text{-}P}$ 15 Hz, H^9), 1.24 (3H, t, $^3J_{H\text{-}H}$ 7.0 Hz, H^8); δ_C ($CDCl_3$) 160.4 (d, $^3J_{C\text{-}P}$ 20 Hz, C^2), 153.1 (d, $^1J_{C\text{-}P}$ 156 Hz, C^6), 136.8 (d, $^3J_{C\text{-}P}$ 10 Hz, C^4), 126.3 (d, $^4J_{C\text{-}P}$ 22 Hz, C^5), 123.0 (d, $^2J_{C\text{-}P}$ 4 Hz, C^3), 64.1 (C^1), 61.1 (d, $^2J_{C\text{-}P}$ 6 Hz, C^7), 16.4 (C^8) 13.4 (d, $^1J_{C\text{-}P}$ 103 Hz, H^9); δ_P ($CDCl_3$) +40.0; *m/z* (HRMS$^+$) 216.0808 $[M + H]^+$ ($C_9H_{14}O_3NP$ requires 216.0801); R_f = 0.20 (silica, CH_2Cl_2 : 7 % MeOH).

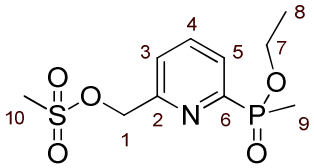

(6-[Ethoxy(methyl)phosphoryl]pyridine-2-yl)methyl methanesulphonate, 35

Ethyl [6-(hydroxymethyl)pyridine-2-yl](methyl)phosphinate, ***34*** (110 mg, 0.51 mmol) was dissolved in anhydrous THF (3 mL) and NEt_3 (213 µL, 1.5 mmol) was added. The mixture was stirred at 5 °C and methanesulfonyl chloride (59 µL, 0.77 mmol) was added. The reaction was monitored by TLC (silica; CH_2Cl_2 : 7 % CH_3OH, R_f(product) = 0.45, R_f(reactant) = 0.20) and stopped after 15 min. The solvent was removed under reduced pressure and the residue dissolved in CH_2Cl_2 (15 mL) and washed with NaCl solution (saturated, 10 mL). The aqueous layer was re-extracted with CH_2Cl_2 (3 × 10 mL) and the organic layers combined, dried over $MgSO_4$ and the solvent removed under reduced pressure to leave the *title compound*, which was used directly in the next step without further purification (100 mg, 67 %); δ_H ($CDCl_3$) 8.07 (1H, dd, $^3J_{H\text{-}H}$ 7.0 Hz $^3J_{H\text{-}P}$ 10 Hz, H^5), 7.92 (1H, td, $^3J_{H\text{-}H}$ 7.0 Hz $^4J_{H\text{-}P}$ 4.8 Hz, H^4), 7.64 (1H, d, $^3J_{H\text{-}H}$ 7.0 Hz, H^3), 5.41 (2H, s, H^1), 4.03 (2H, dqd, $^2J_{H\text{-}H}$ 80 Hz $^3J_{H\text{-}H}$ 7.0 Hz $^3J_{H\text{-}P}$ 4.5 Hz, H^7), 3.15 (3H, s, H^{10}), 1.80 (3H, d, $^2J_{H\text{-}P}$ 15 Hz, H^9), 1.29 (3H, t, $^3J_{H\text{-}H}$ 7.0 Hz, H^8); δ_P ($CDCl_3$) +39.4; *m/z* (HRMS$^+$) 294.2083 $[M + H]^+$ ($C_{10}H_{10}O_5NP$ requires 294.2078); R_f = 0.45 (silica, CH_2Cl_2 : 7 % MeOH).

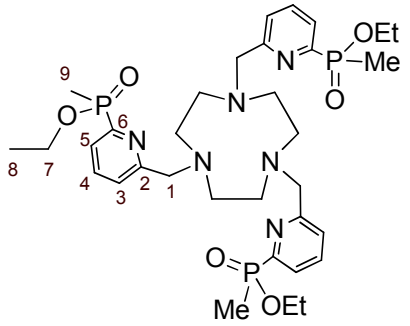

1,4,7-Tri[ethyl-(6-methylpyridin-2-yl)(methyl)phosphinate]-1,4,7-triazacyclononane, 36

1,4,7-Triazacyclononane (15.2 mg, 0.12 mmol), (6-[ethoxy(methyl)phosphoryl]pyridine-2-yl)methyl methanesulphonate, ***35*** (100 mg, 0.34 mmol) and K_2CO_3 (47 mg, 0.34 mmol) were stirred in dry CH_3CN (4 mL) at 60 °C for 3 h under argon. The reaction was monitored by TLC to confirm that all the mesylated starting material had been consumed. The solution was decanted from excess potassium salts and the solvent removed under reduced pressure. Purification by column chromatography on silica (CH_2Cl_2 : 0 – 20 % MeOH in 1 % increments) gave the *title compound* as a colourless oil (40 mg, 47 %); δ_H ($CDCl_3$) 7.89 (3H, dd, $^3J_{H\text{-}H}$ 7.0 Hz $^3J_{H\text{-}P}$ 10 Hz, H^5), 7.75 (3H, td, $^3J_{H\text{-}H}$ 7.0 Hz $^4J_{H\text{-}P}$ 4.8 Hz, H^4), 7.60 (3H, d, $^3J_{H\text{-}H}$ 7.0 Hz, H^3), 3.95 (6H, dqd, $^2J_{H\text{-}H}$ 80 Hz $^3J_{H\text{-}H}$ 7.0 Hz $^3J_{H\text{-}P}$ 4.5 Hz, H^7), 3.90 (6H, br s, H^1), 2.89 (12H, br s, *ring* Hs), 1.72 (9H, d, $^2J_{H\text{-}P}$ 15 Hz, H^9), 1.22 (9H, t, $^3J_{H\text{-}H}$ 7.0 Hz, H^8); δ_C ($CDCl_3$) 157.1 (d, $^3J_{C\text{-}P}$ 20 Hz, C^2), 154.6 (d, $^1J_{C\text{-}P}$ 156 Hz, C^6), 137.1 (d, $^3J_{C\text{-}P}$ 10 Hz, C^4), 126.7 (d, $^4J_{C\text{-}P}$ 20 Hz, C^5), 126.2 (d, $^2J_{C\text{-}P}$ 4 Hz, C^3), 64.1 (C^1), 60.9 (d, $^2J_{C\text{-}P}$ 6 Hz, C^7), 52.7 (*ring* Cs), 16.5 (C^8) 13.5 (d, $^1J_{C\text{-}P}$ 102 Hz, H^9); δ_P ($CDCl_3$) +41.2; *m/z* (HRMS$^+$) 721.4368 $[M + H]^+$ ($C_{33}H_{51}O_6N_6P_3$ requires 721.4361); R_f = 0.05 (silica, CH_2Cl_2 : 10 % MeOH).

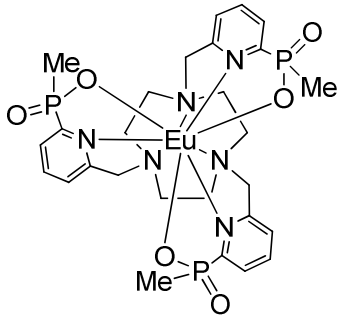

Europium(III) complex of 1,4,7-tri[ethyl (6-methylpyridin-2-yl)(methyl)phosphinate]-1,4,7-triazacyclononane, [Eu·L^{10}]

1,4,7-Tri[ethyl (6-methylpyridin-2-yl)(methyl)phosphinate]-1,4,7-triazacyclononane, ***36*** (10 mg, 0.014 mmol) was dissolved in HCl (6M, 3 mL) and the solution was stirred at 100 °C for 16 h. The solvent was lyophilised to give a white solid. Hydrolysis of the OEt groups was confirmed by ^{1}H- and ^{31}P-NMR (δ_P ($CDCl_3$) +34.5). The solid was dissolved in H_2O – CH_3OH (1 : 1 v/v, 2 mL) and the pH of the solution adjusted to 5.8 using aq. NaOH solution. $Eu(OAc)_3$ (6.7 mg, 0.015 mmol) was added and the solution was stirred at 50 °C for 18 h. After allowing the solution to cool to room temperature, the pH was raised to 10 by the addition of aq. NaOH solution. The solution was stirred for 1 h causing excess Eu^{3+} to precipitate as $Eu(OH)_3$, which was removed by centrifugation. Adjustment of the pH to 5.8 by the addition of HCl, followed by lyophilisation of the solvent, gave the *title compound* as a

white solid containing < 2 % NaCl from pH adjustments (8.8 mg, 80 %); *m/z* (HRMS$^+$) 785.1127 [M + H]$^+$ ($C_{27}H_{36}O_6N_6P_3{}^{151}Eu$ requires 785.1121); δ_P (CD_3OD) +40.1; $\tau_{H_2O} = 1.54$ ms, $\tau_{D_2O} = 1.65$ ms, $\Phi^{em}_{H_2O} = 7.1$ %.

Terbium(III) complex of 1,4,7-tri[ethyl (6-methylpyridin-2-yl)(methyl)phosphinate]-1,4,7-triazacyclononane, [Tb·L^{10}]

An analogous procedure to that described for the synthesis of [Eu·L^{10}] was followed using 1,4,7-tri[ethyl (6-methylpyridin-2-yl)(methyl)phosphinate]-1,4,7-triazacyclononane, ***36*** (10 mg, 0.014 mmol) and $Tb(OAc)_3$ (6.2 mg, 0.015 mmol) to give the *title compound* as a white solid (8.9 mg, 80 %); *m/z* (ESI-MS$^+$) 793.1 [M (^{159}Tb) + H]$^+$; δ_P (CD_3OD) +5.1; $\tau_{H_2O} = 2.59$ ms, $\tau_{D_2O} = 2.98$ ms, $\Phi^{em}_{H_2O} = 61$ %.

Gadolinium(III) complex of 1,4,7-tri[ethyl (6-methylpyridin-2-yl)(methyl)phosphinate]-1,4,7-triazacyclononane, [Gd·L^{10}]

An analogous procedure to that described for the synthesis of [Eu·L^{10}] was followed using 1,4,7-tri[ethyl (6-methylpyridin-2-yl)(methyl)phosphinate]-1,4,7-triazacyclononane, ***36*** (10 mg, 0.014 mmol) and $Gd(OAc)_3$ (6.1 mg, 0.015 mmol) to give the *title compound* as a white solid (8.6 mg, 78 %); *m/z* (ESI-MS$^+$) 790.1 [M (^{156}Gd) + H]$^+$.

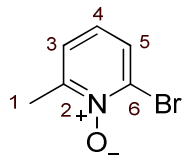

2-Bromo-6-methylpyridine-1-oxide, 37

2-Bromo-6-methylpyridine, ***17*** (20 g, 0.116 mol) was dissolved in $CHCl_3$ (300 mL). MCPBA (40.1 g, 0.232 mol) was added and the solution was stirred at 65 °C under argon for 18 h. The volume of the solution was reduced to 150 mL by removal of the solvent under reduced pressure. The solution was left to stand in the fridge overnight causing precipitation of 3-chlorobenzoic acid, which was removed by filtration. From the remaining filtrate, the solvent was removed under reduced pressure to give a yellow oil, which was dissolved in aq. NaOH solution (1M, 100 mL) and extracted with CH_2Cl_2 (3 × 100 mL). The organic extracts were combined, dried over $MgSO_4$, filtered and the solvent removed under reduced pressure to give the *title compound* as a yellow oil, which cyrstallised upon standing (15 g, 67 %); m.p. 58 – 61 °C; δ_H ($CDCl_3$) 7.55 (1H, dd, *J* 7.9 Hz, 1.6 Hz, H^5), 7.23 (1H, dd, *J* 7.9 Hz, 1.6 Hz, H^3), 7.01 (1H, t, *J* 7.9 Hz, H^4), 2.57 (3H, s, H^1); δ_C ($CDCl_3$) 151.2 (C^2), 133.5 (C^6), 128.7 (C^5), 125.3 (C^3), 125.2 (C^4), 19.3 (C^1); *m/z* (HRMS$^+$) 187.9698 [M + H]$^+$ ($C_6H_7NO^{79}Br$ requires 187.9711); $R_f = 0.16$ (silica, CH_2Cl_2 : 2 % MeOH).

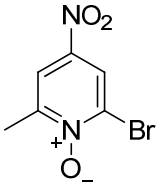

2-Bromo-6-methyl-4-nitropyridine-1-oxide, 38

2-Bromo-6-methylpyridine-1-oxide, ***37*** (15 g, 80 mmol) was dissolved in concentrated H_2SO_4 (98 %, 23 mL, 0.40 mol). The solution was stirred at 0 °C and HNO_3 (70 %, 26 mL, 0.38 mol) was added dropwise. The mixture was heated to 100 °C for 16 h. The yellow solution was dropped onto stirred ice (150 g) causing a pale yellow solid to precipitate. After 1 h the precipitate was filtered and dried under high vacuum to yield the *title compound* (12 g, 65 %); m.p. 138 – 139 °C; δ_H ($CDCl_3$) 8.40 (1H, d, 2.8 Hz, H^5), 8.09 (1H, d, 2.8 Hz, H^3), 2.62 (3H, s, H^1); δ_C ($CDCl_3$) 151.8 (C^2), 140.7 (C^4), 134.0 (C^6), 122.8 (C^5), 118.9 (C^3), 19.6 (C^1); *m/z* (HRMS$^+$) 232.9564 $[M + H]^+$ ($C_6H_6N_2O_3{}^{79}Br$ requires 232.9556); R_f = 0.53 (silica, CH_2Cl_2 : 2 % MeOH).

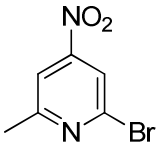

2-Bromo-6-methyl-4-nitropyridine, 39

2-Bromo-6-methyl-4-nitropyridine-1-oxide, ***38*** (5g, 22 mmol) was dissolved in $CHCl_3$ (200 mL) and PBr_3 (6.26 mL, 66 mmol) was added dropwise. The mixture was stirred at 60 °C under argon for 16 h. The solvent was removed under reduced pressure to give a yellow oil. NaOH solution (2 M, 50 mL) was added cautiously and the solution was extracted with CH_2Cl_2 (3 × 100 mL). The organic extracts were combined, dried over $MgSO_4$ and the solvent removed under reduced pressure to give a yellow oil, which was purified by column chromatography on silica (CH_2Cl_2) to yield the *title compound* as a pale yellow oil (3.0 g, 74 %); δ_H ($CDCl_3$) 8.02 (1H, d, 2.8 Hz, H^5), 7.83 (1H, d, 2.8 Hz, H^3), 2.70 (3H, s, H^1); δ_C ($CDCl_3$) 162.9 (C^2), 154.9 (C^4), 142.4 (C^6), 118.4 (C^5), 115.0 (C^3), 24.6 (C^1); *m/z* (HRMS$^+$) 216.9621 $[M + H]^+$ ($C_6H_6N_2O_2{}^{79}Br$ requires 216.9613); R_f = 0.75 (silica, CH_2Cl_2 : 2 % MeOH).

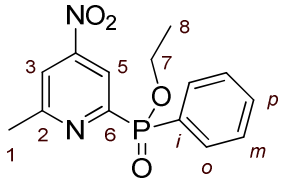

Ethyl (6-methyl-4-nitropyridin-2-yl)(phenyl)phosphinate, 40

2-Bromo-6-methyl-4-nitropyridine, ***39*** (1.01 g, 4.68 mmol), ethyl phenylphosphinate (0.95 g, 5.60 mmol) and triethylamine (2.6 mL, 19.0 mmol) were added to dry degassed (3 × freeze-thaw cycle) toluene (10 mL). Tetrakis(triphenylphosphine)palladium(0) (83 mg, 0.07 mmol) was added and the mixture was degassed three times before being stirred at 125 °C for 16 h under argon. The solution was diluted with CH_2Cl_2 (20 mL), washed with HCl (1M, 2 × 15 mL) and water (3 × 15 mL), dried

over K_2CO_3, filtered and the solvent removed under reduced pressure to give a dark residue. Purification by column chromatography on silica (CH_2Cl_2 : 0.5 % MeOH) gave the *title compound* as a yellow oil (645 mg, 45 %); δ_H ($CDCl_3$) 8.55 (1H, dd, $^3J_{H\text{-}P}$ 5.6 Hz, $^4J_{H\text{-}H}$ 1.4 Hz, H^5), 7.97 (2H, ddd, $^3J_{H\text{-}P}$ 11.2 Hz, $^3J_{H\text{-}H}$ 7.7 Hz, $^4J_{H\text{-}H}$ 1.4 Hz, H^o), 7.90 (1H, d, $^4J_{H\text{-}H}$ 1.4 Hz, H^3), 7.55 (1H, td, $^3J_{H\text{-}H}$ 7.7 Hz, $^4J_{H\text{-}H}$ 1.4 Hz, H^p), 7.46 (2H, td, $^3J_{H\text{-}H}$ 7.7 Hz $^4J_{H\text{-}P}$ 3.5 Hz, H^m), 4.15 (2H, qd, $^3J_{H\text{-}H}$ 7.0 Hz, $^3J_{H\text{-}P}$ 4.2 Hz, H^7), 2.72 (3H, s, H^1), 1.38 (3H, t, $^3J_{H\text{-}H}$ 7.0 Hz, H^8); δ_C ($CDCl_3$) 163.0 (d, $^3J_{C\text{-}P}$ 21 Hz, C^2), 158.1 (d, $^1J_{C\text{-}P}$ 167 Hz, C^6), 154.0 (d, $^3J_{C\text{-}P}$ 13 Hz, C^4), 132.9 (d, $^4J_{C\text{-}P}$ 3 Hz, C^p), 132.5 (d, $^2J_{C\text{-}P}$ 10 Hz, C^o), 129.1 (d, $^1J_{C\text{-}P}$ 140 Hz, C^i), 128.5 (d, $^3J_{C\text{-}P}$ 13 Hz, C^m), 117.6 (d, $^2J_{C\text{-}P}$ 24 Hz, C^5), 117.5 (d, $^4J_{C\text{-}P}$ 3 Hz, C^3), 62.2 (d, $^2J_{C\text{-}P}$ 6 Hz, C^7), 24.9 (C^1), 16.4 (C^8); δ_P ($CDCl_3$) 23.7; *m/z* (HRMS$^+$) 307.0851 $[M + H]^+$ ($C_{14}H_{16}N_2O_4P$ requires 307.0848); R_f = 0.47 (silica, CH_2Cl_2 : 5 % MeOH).

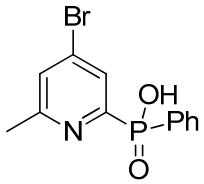

(4-Bromo-6-methylnitropyridin-2-yl)(phenyl)phosphinic acid, 41

Ethyl (6-methyl-4-nitropyridin-2-yl)(phenyl)phosphinate, ***40*** (2.00 g, 6.54 mmol) was dissolved in CH_3COBr (15 mL, 0.2 mol) and the mixture stirred at 70 °C for 16 h under argon. A pale brown precipitate formed. Both precipitate and solution were dropped cautiously into CH_3OH (100 mL) stirred at 0 °C. The solvent was removed under reduced pressure to yield the *title compound* as a pale brown solid (1.81 g, 90 %); δ_H (CD_3OD) 8.33 (1H, dd, $^3J_{H\text{-}P}$ 7.2 Hz, $^4J_{H\text{-}H}$ 2.0 Hz, H^5), 8.23 (1H, d, $^4J_{H\text{-}H}$ 2.0 Hz, H^3), 7.95 (2H, ddd, $^3J_{H\text{-}P}$ 13.2 Hz, $^3J_{H\text{-}H}$ 7.6 Hz, $^4J_{H\text{-}H}$ 1.6 Hz, H^o), 7.63 (1H, td, $^3J_{H\text{-}H}$ 7.6 Hz, $^4J_{H\text{-}H}$ 1.6 Hz, H^p), 7.55 (2H, td, $^3J_{H\text{-}H}$ 7.6 Hz $^4J_{H\text{-}P}$ 3.6 Hz, H^m), 2.77 (3H, s, H^1); δ_C (CD_3OD) 159.4 (d, $^3J_{C\text{-}P}$ 20 Hz, C^2), 151.7 (d, $^1J_{C\text{-}P}$ 160 Hz, C^6), 145.1 (d, $^3J_{C\text{-}P}$ 10 Hz, C^4), 134.8 (d, $^4J_{C\text{-}P}$ 3 Hz, C^p), 133.3 (d, $^2J_{C\text{-}P}$ 10 Hz, C^o), 131.0 (d, $^2J_{C\text{-}P}$ 24 Hz, C^5), 130.6 (d, $^4J_{C\text{-}P}$ 3 Hz, C^3), 130.2 (d, $^1J_{C\text{-}P}$ 140 Hz, C^i), 129.6 (d, $^3J_{C\text{-}P}$ 12 Hz, C^m), 20.4 (C^1); δ_P (CD_3OD) 14.3; *m/z* (HRMS$^-$) 309.9648 $[M - H]^-$ ($C_{12}H_{10}NO_2{}^{79}BrP$ requires 309.9633); R_f = 0.01 (silica, CH_2Cl_2 : 5 % MeOH).

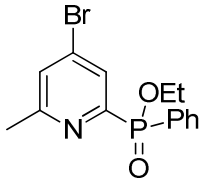

Ethyl (4-bromo-6-methylnitropyridin-2-yl)(phenyl)phosphinate, 42

(4-Bromo-6-methylnitropyridin-2-yl)(phenyl)phosphinic acid, ***41*** (1.80 g, 5.80 mmol) was added to $HC(OCH_2CH_3)_3$ (50 mL) and the mixture stirred at 140 °C for 72 h under argon. The solvent was removed under reduced pressure and the resulting residue was purified by column chromatography on silica (CH_2Cl_2 : 0.5 % MeOH) to yield the *title compound* as a yellow oil (1.08 g, 55 %); δ_H ($CDCl_3$) 8.04 (1H, dd, $^3J_{H\text{-}P}$ 6.3 Hz, $^4J_{H\text{-}H}$ 1.4 Hz, H^5), 7.95 (2H, ddd, $^3J_{H\text{-}P}$ 11.2 Hz, $^3J_{H\text{-}H}$ 7.0 Hz, $^4J_{H\text{-}H}$ 1.4 Hz, H^o), 7.51 (1H, td, $^3J_{H\text{-}H}$ 7.0 Hz, $^4J_{H\text{-}H}$ 1.4 Hz, H^p), 7.43 (2H, td, $^3J_{H\text{-}H}$, 7.0 Hz $^4J_{H\text{-}P}$ 3.5 Hz, H^m), 7.37 (1H, d, $^4J_{H\text{-}H}$ 1.4 Hz, H^3), 4.11 (2H, qd, $^3J_{H\text{-}H}$ 7.0 Hz, $^3J_{H\text{-}P}$ 4.2 Hz, H^7), 2.52 (3H, s, H^1), 1.34 (3H, t,

$^{3}J_{H\text{-}H}$ 7.0 Hz, H^{8}); δ_C ($CDCl_3$) 161.2 (d, $^{3}J_{C\text{-}P}$ 22 Hz, C^{2}), 155.7 (d, $^{1}J_{C\text{-}P}$ 165 Hz, C^{6}), 133.5 (d, $^{3}J_{C\text{-}P}$ 15 Hz, C^{4}), 132.7 (d, $^{4}J_{C\text{-}P}$ 3 Hz, C^{p}), 132.6 (d, $^{2}J_{C\text{-}P}$ 10 Hz, C^{o}), 130.0 (d, $^{1}J_{C\text{-}P}$ 139 Hz, C^{i}), 128.5 (d, $^{4}J_{C\text{-}P}$ 3 Hz, C^{3}), 128.4 (d, $^{2}J_{C\text{-}P}$ 23 Hz, C^{5}), 128.3 (d, $^{3}J_{C\text{-}P}$ 13 Hz, C^{m}), 62.1 (d, $^{2}J_{C\text{-}P}$ 6 Hz, C^{7}), 24.5 (C^{1}), 16.7 (C^{8}); δ_P ($CDCl_3$) 25.5; *m/z* (HRMS$^+$) 340.0102 $[M + H]^+$ ($C_{14}H_{16}NO_2{}^{79}BrP$ requires 340.0102); R_f = 0.56 (silica, CH_2Cl_2 : 5 % MeOH).

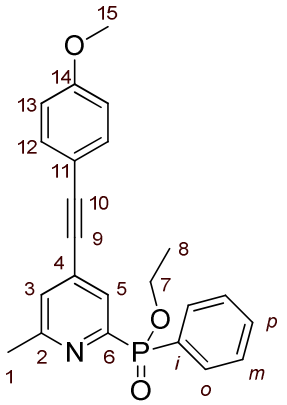

Ethyl (4-[2-(4-methoxyphenyl)ethynyl]-6-methylpyridin-2-yl)(phenyl)phosphinate, 43

Ethyl (4-bromo-6-methylnitropyridin-2-yl)(phenyl)phosphinate, ***42*** (32 mg, 0.094 mmol) was dissolved in dry THF (1 mL) and the solution was degassed (freeze-thaw cycle) three times. 4-Ethynylanisole (19 mg, 0.14 mmol) and NEt_3 (0.5 mL) were added and the solution was degassed once. Tetrakis(triphenylphosphine)palladium(0) (10 mg, 8.7 µmol) and CuI (3.6 mg, 0.019 mmol) were added and the solution was degassed a further three times. The solution was stirred at 65 °C under argon. The reaction was monitored by TLC (silica; CH_2Cl_2 : 2.5 % CH_3OH, R_f(product) = 0.21, R_f(reactant) = 0.26) and stopped after 3 h. The solvent was removed under reduced pressure and the crude material purified by column chromatography (silica, CH_2Cl_2 : CH_3OH 0 – 1.6 % in 0.1 % increments) to give a yellow oil (20 mg, 55 %); δ_H ($CDCl_3$) 8.01 (1H, dd, $^{3}J_{H\text{-}P}$ 6.0 Hz, $^{4}J_{H\text{-}H}$ 1.6 Hz, H^{5}), 7.98 (2H, dd, $^{3}J_{H\text{-}H}$ 8.4 Hz $^{3}J_{H\text{-}P}$ 12.4 Hz, H^{o}), 7.53 (1H, t, $^{3}J_{H\text{-}H}$ 8.4 Hz, H^{p}), 7.47 (2H, d, $^{3}J_{H\text{-}H}$ 8.8 Hz, H^{12}), 7.45 (2H, td, $^{3}J_{H\text{-}H}$ 8.4 Hz $^{4}J_{H\text{-}P}$ 4.2 Hz, H^{m}), 7.28 (1H, d, $^{4}J_{H\text{-}H}$ 1.6 Hz, H^{3}), 6.89 (2H, d, $^{3}J_{H\text{-}H}$ 8.8 Hz, H^{13}), 4.13 (2H, qd, $^{3}J_{H\text{-}H}$ 5.6 Hz $^{3}J_{H\text{-}P}$ 4.8 Hz, H^{7}), 3.84 (3H, s, H^{15}), 2.57 (3H, s, H^{1}), 1.38 (3H, t, $^{3}J_{H\text{-}H}$ 5.6 Hz, H^{8}); δ_C ($CDCl_3$) 160.4 (s, C^{14}), 159.7 (d, $^{3}J_{C\text{-}P}$ 20 Hz, C^{2}), 153.8 (d, $^{1}J_{C\text{-}P}$ 165 Hz, C^{6}), 134.7 (d, $^{2}J_{C\text{-}P}$ 12 Hz, C^{4}), 133.4 (s, C^{12}), 132.4 (d, $^{4}J_{C\text{-}P}$ 5 Hz, C^{p}), 132.2 (d, $^{2}J_{C\text{-}P}$ 10 Hz, C^{o}), 130.2 (d, $^{1}J_{C\text{-}P}$ 139 Hz, C^{i}), 128.2 (d, $^{3}J_{C\text{-}P}$ 22 Hz, C^{5}), 128.1 (d, $^{3}J_{C\text{-}P}$ 12 Hz, C^{m}), 126.8 (d, $^{4}J_{C\text{-}P}$ 3 Hz, C^{3}), 114.1 (s, C^{13}), 114.0 (s, C^{11}), 94.9 (s, C^{10}), 85.3 (d, $^{4}J_{C\text{-}P}$ 2 Hz, C^{9}), 61.7 (d, $^{2}J_{C\text{-}P}$ 6 Hz, C^{7}), 55.2 (s, C^{15}), 27.9 (s, C^{1}), 16.6 (s, C^{8}); δ_P ($CDCl_3$) +26.6; *m/z* (HRMS$^+$) 414.1247 $[M + Na]^+$ ($C_{23}H_{22}O_3NPNa$ requires 414.1235); R_f = 0.21 (silica, CH_2Cl_2 : 2.5 % MeOH).

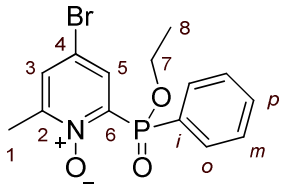

Ethyl (4-bromo-6-methyl-1-oxo-1-pyridin-2-yl)(phenyl)phosphinate, 44

To a stirred solution of ethyl (4-bromo-6-methylnitropyridin-2-yl)(phenyl)phosphinate ***42*** (1.25 g, 3.68 mmol) in $CHCl_3$ (20 mL) was added MCPBA (1.27 g, 7.35 mmol). The resulting solution was stirred at 65 °C overnight (16 h) under argon. The reaction was monitored by TLC (silica; CH_2Cl_2 : 5 % CH_3OH, R_f(product) = 0.28, R_f(reactant) = 0.56). The solvent was removed under reduced pressure to give a yellow oil. This oil was dissolved in CH_2Cl_2 and washed with $NaHCO_3$ solution (0.5 M, 50 mL). The layers were separated and the aqueous layer extracted with CH_2Cl_2 (3 × 30 mL). All organic layers were combined, dried over $MgSO_4$, filtered and the solvent removed under reduced pressure. The resultant yellow oil was purified by column chromatography (silica, CH_2Cl_2 : CH_3OH 0 – 2 % in 0.1 % increments) to give a yellow oil (1.11 g, 75 %); δ_H ($CDCl_3$) 8.05 (1H, dd, $^3J_{H\text{-}P}$ 7.7 Hz, $^4J_{H\text{-}H}$ 2.1 Hz, H^5), 7.98 (2H, dd, $^3J_{H\text{-}H}$ 7.7 Hz $^3J_{H\text{-}P}$ 13.3 Hz, H^o), 7.50 (1H, t, $^3J_{H\text{-}H}$ 7.7 Hz, H^p), 7.44 (1H, d, $^4J_{H\text{-}H}$ 2.1 Hz, H^3), 7.41 (2H, td, $^3J_{H\text{-}H}$ 7.7 Hz $^4J_{H\text{-}P}$ 4.2 Hz, H^m), 4.13 (2H, qd, $^3J_{H\text{-}H}$ 5.6 Hz $^3J_{H\text{-}P}$ 4.9 Hz, H^7), 2.32 (3H, s, H^1), 1.34 (3H, t, $^3J_{H\text{-}H}$ 5.6 Hz, H^8); δ_C ($CDCl_3$) 151.0 (d, $^3J_{C\text{-}P}$ 4 Hz, C^2), 144.2 (d, $^1J_{C\text{-}P}$ 149 Hz, C^6), 133.2 (d, $^2J_{C\text{-}P}$ 11 Hz, C^o), 133.1 (d, $^4J_{C\text{-}P}$ 4 Hz, C^p), 133.0 (d, $^3J_{C\text{-}P}$ 11 Hz, C^5), 132.2 (d, $^4J_{C\text{-}P}$ 4 Hz, C^3), 129.0 (d, $^1J_{C\text{-}P}$ 152 Hz, C^i), 128.4 (d, $^3J_{C\text{-}P}$ 14 Hz, C^m), 117.4 (d, $^2J_{C\text{-}P}$ 12 Hz, C^4), 62.3 (d, $^2J_{C\text{-}P}$ 6 Hz, C^7), 17.5 (C^1), 16.7 (C^8); δ_P ($CDCl_3$) +21.2; *m/z* (HRMS$^+$) 356.0061 $[M + H]^+$ ($C_{14}H_{16}O_3{}^{79}BrNP$ requires 356.0051); R_f = 0.28 (silica, CH_2Cl_2 : 5 % MeOH).

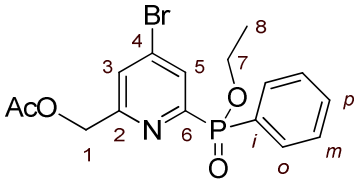

(4-Bromo-6-[ethoxy(phenyl)phosphoryl]pyridine-2-yl)methyl acetate, 45

Ethyl (4-bromo-6-methyl-1-oxo-1-pyridin-2-yl)(phenyl)phosphinate, ***44*** (1.8 g, 5.1 mmol) was dissolved in acetic anhydride (35 mL) and the solution was heated to 120 °C for 3 h with stirring. Reaction progress was monitored by ^{31}P-NMR and TLC (silica, CH_2Cl_2: 5 % CH_3OH, R_f(product) = 0.46, R_f(reactant) = 0.28). The solvent was removed under reduced pressure and the residue purified by column chromatography (silica, CH_2Cl_2 : CH_3OH 0 – 1 % in 0.1 % increments) to give a yellow oil (0.66 g, 33 %); δ_H ($CDCl_3$) 8.16 (1H, dd, $^3J_{H\text{-}P}$ 7.7 Hz, $^4J_{H\text{-}H}$ 2.1 Hz, H^5), 7.93 (2H, dd, $^3J_{H\text{-}H}$ 7.7 Hz $^3J_{H\text{-}P}$ 13.3 Hz, H^o), 7.55 (1H, d, $^4J_{H\text{-}H}$ 2.1 Hz, H^3), 7.51 (1H, t, $^3J_{H\text{-}H}$ 7.7 Hz, H^p), 7.43 (2H, td, $^3J_{H\text{-}H}$ 7.7 Hz $^4J_{H\text{-}P}$ 4.2 Hz, H^m), 5.18 (2H, s, H^1), 4.09 (2H, qd, $^3J_{H\text{-}H}$ 5.6 Hz $^3J_{H\text{-}P}$ 4.9 Hz, H^7), 2.12 (3H, s, H^{OAc}), 1.33 (3H, t, $^3J_{H\text{-}H}$ 5.6 Hz, H^8); δ_C ($CDCl_3$) 170.5 (s, $C^{C=O(OAc)}$), 158.6 (d, $^3J_{C\text{-}P}$ 4 Hz, C^2), 156.0 (d, $^1J_{C\text{-}P}$ 149 Hz, C^6), 134.3 (d, $^2J_{C\text{-}P}$ 25 Hz, C^4), 132.9 (d, $^4J_{C\text{-}P}$ 5 Hz, C^p), 132.7 (d, $^2J_{C\text{-}P}$ 10 Hz, C^o), 130.5 (d, $^3J_{C\text{-}P}$ 23 Hz, C^5), 129.5 (d, $^1J_{C\text{-}P}$ 139 Hz, C^i), 128.6 (d, $^3J_{C\text{-}P}$ 13 Hz, C^m), 126.6 (d, $^4J_{C\text{-}P}$ 3 Hz, C^3), 66.0 (s, C^1), 62.2 (d, $^2J_{C\text{-}P}$ 6 Hz, C^7), 21.0 (s, $C^{Me(OAc)}$), 16.7 (C^8); δ_P ($CDCl_3$) +25.0; *m/z* (HRMS$^+$) 398.0157 $[M + H]^+$ ($C_{16}H_{18}O_4{}^{79}BrNP$ requires 398.0151); R_f = 0.46 (silica, CH_2Cl_2 : 5 % MeOH).

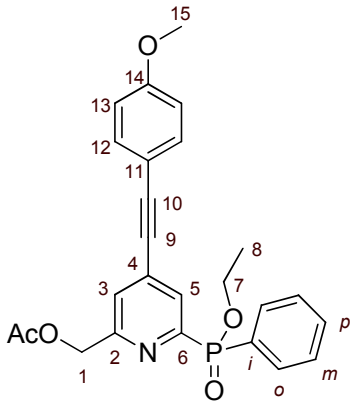

(6-[ethoxy(phenyl)phosphoryl]-4-[2-(4-methoxyphenyl)ethynyl]pyridine-2-yl)methyl acetate, 46

(4-Bromo-6-[ethoxy(phenyl)phosphoryl]pyridine-2-yl)methyl acetate, ***45*** (500 mg, 1.26 mmol) was dissolved in dry THF (10 mL) and the solution was degassed (freeze-thaw cycle) three times. 4-Ethynylanisole (249 mg, 1.89 mmol) and NEt_3 (5 mL) were added and the solution was degassed once. Tetrakis(triphenylphosphine)palladium(0) (145 mg, 0.126 mmol) and CuI (42 mg, 0.252 mmol) were added and the solution was degassed a further three times. The solution was stirred at 60 °C under argon. The reaction was monitored by TLC (silica; CH_2Cl_2 : 5 % CH_3OH, R_f(product) = 0.57, R_f(reactant) = 0.46) and stopped after 4 h. The solvent was removed under reduced pressure. The crude residue was dissolved in CH_2Cl_2 (50 mL) and washed with NH_4Cl (sat. aq. solution, 3 × 40 mL) and NaCl (sat. aq. solution, 1 × 40 mL). The organic layer was dried over $MgSO_4$, filtered and the solvent was removed to give a yellow oil, which was purified by column chromatography (silica, CH_2Cl_2 : CH_3OH 0 – 2.0 % in 0.1 % increments) to give the *title compound* as a yellow oil (400 mg, 81 %); δ_H ($CDCl_3$) 8.09 (1H, dd, $^3J_{H\text{-}P}$ 6.0 Hz, $^4J_{H\text{-}H}$ 1.6 Hz, H^5), 7.98 (2H, dd, $^3J_{H\text{-}H}$ 8.4 Hz $^3J_{H\text{-}P}$ 12.4 Hz, H^o), 7.54 (1H, t, $^3J_{H\text{-}H}$ 8.4 Hz, H^p), 7.49 (2H, d, $^3J_{H\text{-}H}$ 8.8 Hz, H^{12}), 7.47 (2H, td, $^3J_{H\text{-}H}$ 8.4 Hz $^4J_{H\text{-}P}$ 4.2 Hz, H^m), 7.26 (1H, d, $^4J_{H\text{-}H}$ 1.6 Hz, H^3), 6.90 (2H, d, $^3J_{H\text{-}H}$ 8.8 Hz, H^{13}), 5.24 (2H, s, H^1), 4.13 (2H, qd, $^3J_{H\text{-}H}$ 5.6 Hz $^3J_{H\text{-}P}$ 4.8 Hz, H^7), 3.84 (3H, s, H^{15}), 2.16 (3H, s, H^{OAc}), 1.38 (3H, t, $^3J_{H\text{-}H}$ 5.6 Hz, H^8); δ_C ($CDCl_3$) 170.5 (s, $C^{C=O(OAc)}$), 160.6 (s, C^{14}), 157.1 (d, $^3J_{C\text{-}P}$ 20 Hz, C^2), 154.4 (d, $^1J_{C\text{-}P}$ 165 Hz, C^6), 133.7 (s, C^{12}), 133.2 (d, $^2J_{C\text{-}P}$ 12 Hz, C^4), 132.5 (d, $^4J_{C\text{-}P}$ 5 Hz, C^p), 132.4 (d, $^2J_{C\text{-}P}$ 10 Hz, C^o), 130.3 (d, $^1J_{C\text{-}P}$ 139 Hz, C^i), 129.1 (d, $^3J_{C\text{-}P}$ 22 Hz, C^5), 128.8 (d, $^3J_{C\text{-}P}$ 12 Hz, C^m), 124.4 (d, $^4J_{C\text{-}P}$ 3 Hz, C^3), 114.3 (s, C^{13}), 113.7 (s, C^{11}), 96.0 (s, C^{10}), 85.3 (d, $^4J_{C\text{-}P}$ 2 Hz, C^9), 66.3 (s, C^1), 61.9 (d, $^2J_{C\text{-}P}$ 6 Hz, C^7), 55.4 (C^{15}), 20.9 (s, $C^{Me(OAc)}$), 16.5 (C^8); δ_P ($CDCl_3$) +26.1; *m/z* (HRMS$^+$) 472.1303 $[M + Na]^+$ ($C_{25}H_{24}O_5NPNa$ requires 472.1290); R_f = 0.57 (silica, CH_2Cl_2 : 5 % MeOH).

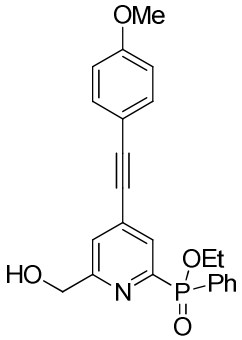

Ethyl (6-(hydroxymethyl)-4-[2-(4-methoxyphenyl)ethynyl]pyridin-2-yl)(phenyl)phosphinate, 47

(6-[Ethoxy(phenyl)phosphoryl]-4-[2-(4-methoxyphenyl)ethynyl]pyridine-2-yl)methyl acetate, ***46*** (350 mg, 0.78 mmol) was dissolved in anhydrous CH_3CH_2OH (12 mL). A catalytic amount of sodium metal (~5 mg) was added and the solution was stirred at 40 °C under argon. The reaction was monitored by TLC (silica; CH_2Cl_2 : 5 % CH_3OH, R_f(product) = 0.28, R_f(reactant) = 0.57) and stopped after 40 min. To the crude reaction mixture CH_2Cl_2 (100 mL) was added and sodium salts were removed by washing with H_2O (1 × 25 mL). The aqueous layer was re-extracted with CH_2Cl_2 (3 × 20 mL). The organic layers were combined, dried over $MgSO_4$, filtered and the solvent was removed under reduced pressure. The crude residue was purified by column chromatography (silica, CH_2Cl_2 : CH_3OH 0 – 3.0 % in 0.2 % increments) to give a colourless oil (200 mg, 82 %); δ_H ($CDCl_3$) 8.01 (1H, dd, $^3J_{H\text{-}P}$ 6.0 Hz, $^4J_{H\text{-}H}$ 1.6 Hz, H^5), 7.93 (2H, dd, $^3J_{H\text{-}H}$ 8.4 Hz $^3J_{H\text{-}P}$ 12.4 Hz, H^o), 7.51 (1H, t, $^3J_{H\text{-}H}$ 8.4 Hz, H^p), 7.45 (1H, d, $^4J_{H\text{-}H}$ 1.6 Hz, H^3), 7.44 (2H, d, $^3J_{H\text{-}H}$ 8.8 Hz, H^{12}), 7.43 (2H, td, $^3J_{H\text{-}H}$ 8.4 Hz $^4J_{H\text{-}P}$ 4.2 Hz, H^m), 6.87 (2H, d, $^3J_{H\text{-}H}$ 8.8 Hz, H^{13}), 4.75 (2H, s, H^1), 4.12 (2H, qd, $^3J_{H\text{-}H}$ 5.6 Hz $^3J_{H\text{-}P}$ 4.8 Hz, H^7), 3.80 (3H, s, H^{15}), 1.35 (3H, t, $^3J_{H\text{-}H}$ 5.6 Hz, H^8); δ_C ($CDCl_3$) 161.4 (d, $^3J_{C\text{-}P}$ 20 Hz, C^2), 160.8 (s, C^{14}), 153.4 (d, $^1J_{C\text{-}P}$ 165 Hz, C^6), 133.9 (s, C^{12}), 133.2 (d, $^2J_{C\text{-}P}$ 12 Hz, C^4), 132.8 (d, $^4J_{C\text{-}P}$ 5 Hz, C^p), 132.4 (d, $^2J_{C\text{-}P}$ 10 Hz, C^o), 129.8 (d, $^1J_{C\text{-}P}$ 140 Hz, C^i), 128.7 (d, $^3J_{C\text{-}P}$ 12 Hz, C^m), 128.4 (d, $^3J_{C\text{-}P}$ 22 Hz, C^5), 124.1 (d, $^4J_{C\text{-}P}$ 3 Hz, C^3), 114.5 (s, C^{13}), 114.0 (s, C^{11}), 96.1 (s, C^{10}), 85.6 (d, $^4J_{C\text{-}P}$ 2 Hz, C^9), 64.3 (s, C^1), 62.0 (d, $^2J_{C\text{-}P}$ 6 Hz, C^7), 55.6 (C^{15}), 16.7 (C^8); δ_P ($CDCl_3$) +25.6; *m/z* (HRMS$^+$) 408.1382 $[M + H]^+$ ($C_{23}H_{23}O_4NP$ requires 408.1365); R_f = 0.28 (silica, CH_2Cl_2 : 5 % MeOH).

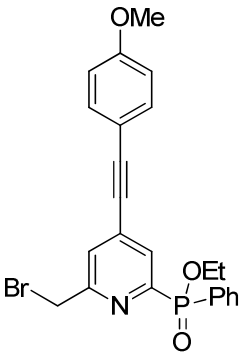

Ethyl-[6-(bromomethyl)-4-[2-(4-methoxyphenyl)ethynyl]pyridin-2-yl](phenyl)phosphinate, 48

Ethyl-(6-(hydroxymethyl)-4-[2-(4-methoxyphenyl)ethynyl]pyridin-2-yl)(phenyl)phosphinate, ***47*** (143 mg, 0.35 mmol) was dissolved in dry CH_2Cl_2 (4 mL) and the solution was stirred at 0 °C under argon.

PBr_3 (50 µL, 0.53 mmol) was added and the solution was stirred for a further 1 h at 0 °C. The reaction mixture was allowed to warm to room temperature and monitored by TLC (silica; CH_2Cl_2 : 5 % CH_3OH, R_f(product) = 0.69, R_f(reactant) = 0.28). After 1 h at 20 °C CH_2Cl_2 (50 mL) was added and the solution was washed with aq. $NaHCO_3$ solution (1M, 25 mL). The aqueous layer was re-extracted with CH_2Cl_2 (3 × 20 mL). The organic layers were combined, dried over $MgSO_4$ and the solvent was removed under reduced pressure. The crude residue was purified by column chromatography (silica, CH_2Cl_2 : CH_3OH 0 – 0.5 % in 0.1 % increments) to give a pale yellow oil (110 mg, 66 %); δ_H ($CDCl_3$) 8.05 (1H, dd, $^3J_{H\text{-}P}$ 6.0 Hz, $^4J_{H\text{-}H}$ 1.6 Hz, H^5), 8.00 (2H, dd, $^3J_{H\text{-}H}$ 8.4 Hz $^3J_{H\text{-}P}$ 12.4 Hz, H^o), 7.56 (1H, d, $^4J_{H\text{-}H}$ 1.6 Hz, H^3), 7.50 (1H, t, $^3J_{H\text{-}H}$ 8.4 Hz, H^p), 7.47 (2H, d, $^3J_{H\text{-}H}$ 8.8 Hz, H^{12}), 7.46 (2H, td, $^3J_{H\text{-}H}$ 8.4 Hz $^4J_{H\text{-}P}$ 4.2 Hz, H^m), 6.87 (2H, d, $^3J_{H\text{-}H}$ 8.8 Hz, H^{13}), 4.52 (2H, s, H^1), 4.13 (2H, qd, $^3J_{H\text{-}H}$ 5.6 Hz $^3J_{H\text{-}P}$ 4.8 Hz, H^7), 3.80 (3H, s, H^{15}), 1.36 (3H, t, $^3J_{H\text{-}H}$ 5.6 Hz, H^8); δ_C ($CDCl_3$) 160.9 (s, C^{14}), 158.1 (d, $^3J_{C\text{-}P}$ 20 Hz, C^2), 154.8 (d, $^1J_{C\text{-}P}$ 165 Hz, C^6), 133.9 (s, C^{12}), 133.6 (d, $^2J_{C\text{-}P}$ 12 Hz, C^4), 132.7 (d, $^4J_{C\text{-}P}$ 5 Hz, C^p), 132.5 (d, $^2J_{C\text{-}P}$ 10 Hz, C^o), 130.3 (d, $^1J_{C\text{-}P}$ 140 Hz, C^i), 128.8 (d, $^3J_{C\text{-}P}$ 12 Hz, C^m), 128.7 (d, $^3J_{C\text{-}P}$ 22 Hz, C^5), 126.8 (d, $^4J_{C\text{-}P}$ 3 Hz, C^3), 114.5 (s, C^{13}), 113.9 (s, C^{11}), 96.5 (s, C^{10}), 85.1 (d, $^4J_{C\text{-}P}$ 2 Hz, C^9), 62.2 (d, $^2J_{C\text{-}P}$ 6 Hz, C^7), 55.6 (C^{15}), 33.3 (s, C^1), 16.7 (C^8); δ_P ($CDCl_3$) +25.8; *m/z* (HRMS$^+$) 492.0341 $[M + Na]^+$ ($C_{23}H_{21}O_3NP^{79}BrNa$ requires 492.0340); R_f = 0.69 (silica, CH_2Cl_2 : 5 % MeOH).

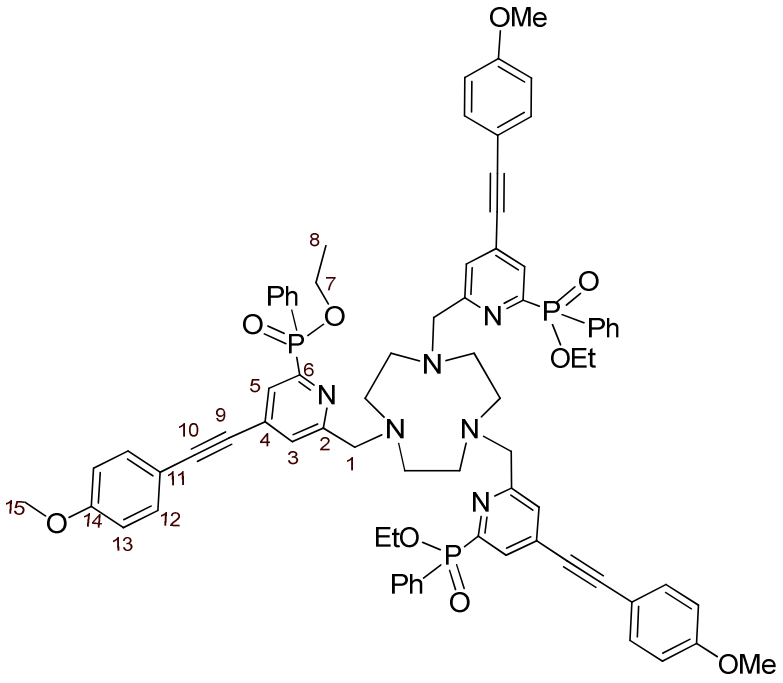

Tri-ethyl phenylphosphinate ester of L¹¹, 49

1,4,7-Triazacyclononane (10 mg, 0.078 mmol) and ethyl-[6-(bromomethyl)-4-[2-(4-methoxyphenyl)ethynyl]pyridin-2-yl](phenyl)phosphinate, ***48*** (110 mg, 0.234 mmol) were dissolved in anhydrous CH_3CN (5 mL) and K_2CO_3 (32 mg, 0.234 mmol) was added. The mixture was stirred under argon at 78 °C and monitored by TLC (silica; CH_2Cl_2 : 10 % CH_3OH, R_f(product) = 0.06, R_f(reactant ***48***) = 0.85). After 16 h the reaction was cooled and the solution decanted from excess potassium salts. The solvent was removed under reduced pressure and the crude material purified by column chromatography (silica, CH_2Cl_2 : CH_3OH 0 – 30 % in 1 % increments) to give the *title product* as a yellow oil (23 mg, 23 %): δ_H ($CDCl_3$) 8.03 (3H, dd, $^3J_{H\text{-}P}$ 6.0 Hz, H^5), 7.94 (6H, dd, $^3J_{H\text{-}P}$

12.4 Hz, $^{3}J_{H\text{-}H}$ 6.8 Hz, H^{o}), 7.58 (3H, s, H^{3}), 7.45 (6H, d, $^{3}J_{H\text{-}H}$ 8.8 Hz, H^{12}), 7.42 (3H, t, $^{3}J_{H\text{-}H}$ 6.8 Hz, H^{p}), 7.37 (6H, td, $^{3}J_{H\text{-}H}$, 6.8 Hz $^{4}J_{H\text{-}P}$ 3.6 Hz, H^{m}), 6.87 (6H, d, $^{3}J_{H\text{-}H}$ 8.8 Hz, H^{13}), 4.10 (6H, qd, $^{3}J_{H\text{-}H}$ 7.2 Hz, $^{3}J_{H\text{-}P}$ 4.2 Hz, H^{7}), 3.83 (6H, s, H^{1}), 3.82 (9H, s, H^{15}), 2.74 (12H, br s, ring Hs), 1.33 (9H, t, $^{3}J_{H\text{-}H}$ 7.2 Hz, H^{8}); δ_P ($CDCl_3$) +26.6; *m/z* (HRMS$^+$) 1297.486 $[M + H]^+$ ($C_{75}H_{76}O_9N_6P_3$ requires 1297.488); R_f = 0.06 (silica, CH_2Cl_2 : 10 % MeOH).

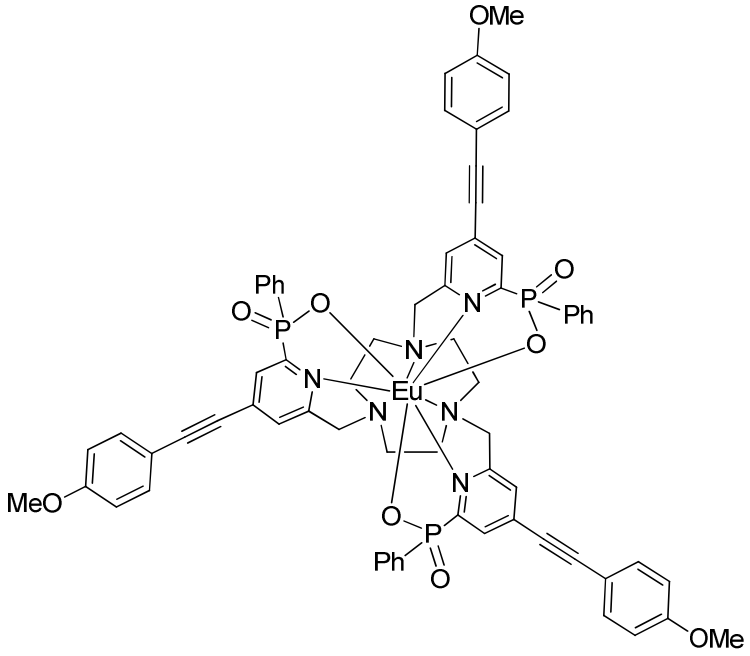

[Eu·L¹¹]

The tri-ethyl phenylphosphinate ester of ***L¹¹***, ***49*** (10 mg, 7.7 μmol) was dissolved in CD_3OD (3 mL) and NaOD (0.1 M in D_2O, 1 mL) was added. The solution was stirred at 60 °C and monitored by ^{1}H-NMR (loss of CH_3CH_2 peaks at 4.10 and 1.33 ppm) and ^{31}P-NMR (reactant 26.6 ppm, product 17.5 ppm) and stopped after 16 h. The pH of the solution was adjusted to 7 by addition of HCl (1M). $Eu(OAc)_3$ (3.4 mg, 8.5 μmol) in a H_2O : CH_3OH solution (0.5 mL, 1:1 v/v) was added and the solution was stirred at 50 °C for 24 h. The solvent was removed under reduced pressure and the crude material purified by column chromatography (silica, CH_2Cl_2 : 5 % CH_3OH) to give the *title product* as a white solid (2.5 mg, 24 %); *m/z* (HRMS$^+$) 1361.283 $[M(^{151}Eu) + H]^+$ ($C_{69}H_{61}O_9N_6P_3{}^{151}Eu$ requires 1361.291), 1363.299 $[M(^{153}Eu) + H]^+$ ($C_{69}H_{61}O_9N_6P_3{}^{153}Eu$ requires 1363.293); δ_P (CD_3OD) +17.5; R_f = 0.25 (silica, CH_2Cl_2 : 10 % MeOH). τ_{MeOH} = 1.30 ms, Φ^{em}_{MeOH} = 52 ± 10 %; ε_{MeOH} (332 nm) = 58, 000 M^{-1} cm^{-1}; t_R (*Method D*) = 11.5 min. Single crystals of [Eu·L^{11}] suitable for X-ray diffraction studies were grown by dissolving 2 mg of complex in CH_3OH (0.33 mL). Addition of H_2O (0.17 mL) led to crystal formation over 16 h.

[Tb·L¹¹]

An analogous procedure to that described for the synthesis of [Eu·L^{11}] was followed using the tri-ethyl phenylphosphinate ester of ***L¹¹***, ***49*** (10 mg, 7.7 μmol) and $Tb(OAc)_3$ (3.1 mg, 7.7 μmol) to give the title compound as a white solid (2.9 mg, 29 %); *m/z* (HRMS$^+$) 1369.301 $[M(^{159}Tb) + H]^+$ ($C_{69}H_{61}O_9N_6P_3{}^{159}Tb$ requires 1369.296); R_f = 0.25 (silica, CH_2Cl_2 : 10 % MeOH), t_R (*Method D*) = 11.5 min.

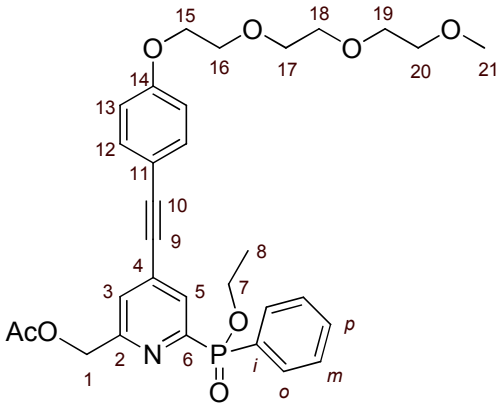

(6-[Ethoxy(phenyl)phosphoryl]-4-[2-(4-(2-[2-(2-methoxyethoxy)ethoxy]ethoxy)phenyl)ethynyl]pyridin-2-yl)methyl acetate, 50

(4-Bromo-6-[ethoxy(phenyl)phosphoryl]pyridine-2-yl)methyl acetate, ***45*** (540 mg, 1.36 mmol) was dissolved in dry THF (8 mL) and the solution was degassed (freeze-thaw cycle) three times. [2-(4-(2-[2-(2-methoxyethoxy)ethoxy]ethoxy)phenyl)ethynyl]trimethylsilane* (456 mg, 1.36 mmol) and NEt_3 (4 mL) were added and the solution was degassed once. Tetrakis(triphenylphosphine)palladium(0) (156 mg, 0.136 mmol) and CuI (26 mg, 0.136 mmol) were added and the solution was degassed a further three times. The solution was stirred under argon and tetrabutylammonium fluoride solution (1 M in THF, 1.9 mL, 2.04 mmol) was added. A colour change from yellow to a dark blue was observed and the mixture was stirred at 65 °C under argon. The reaction was monitored by TLC (silica; CH_2Cl_2 : 5 % CH_3OH, R_f(product) = 0.31, R_f(reactant) = 0.46) and stopped after 3 h. The solvent was removed under reduced pressure and the crude material purified by column chromatography (silica, CH_2Cl_2 : CH_3OH 0 – 1.5 % in 0.1 % increments) to give a yellow oil (575 mg, 73 %); δ_H ($CDCl_3$) 8.05 (1H, dd, $^3J_{H\text{-}P}$ 6.0 Hz, $^4J_{H\text{-}H}$ 1.6 Hz, H^5), 7.96 (2H, dd, $^3J_{H\text{-}H}$ 8.4 Hz $^3J_{H\text{-}P}$ 12.4 Hz, H^o), 7.50 (1H, t, $^3J_{H\text{-}H}$ 8.4 Hz, H^p), 7.44 (2H, d, $^3J_{H\text{-}H}$ 8.8 Hz, H^{12}), 7.43 (2H, td, $^3J_{H\text{-}H}$ 8.4 Hz $^4J_{H\text{-}P}$ 4.2 Hz, H^m), 7.42 (1H, d, $^4J_{H\text{-}H}$ 1.6 Hz, H^3), 6.88 (2H, d, $^3J_{H\text{-}H}$ 8.8 Hz, H^{13}), 5.21 (2H, s, H^1), 4.12 (2H, qd, $^3J_{H\text{-}H}$ 5.6 Hz $^3J_{H\text{-}P}$ 4.8 Hz, H^7), 4.11 (2H, t, $^3J_{H\text{-}H}$ 4.8 Hz, H^{15}), 3.83 (2H, t, $^3J_{H\text{-}H}$ 4.8 Hz, H^{16}), 3.71 (2H, t, $^3J_{H\text{-}H}$ 4.8 Hz, H^{17}), 3.65 (2H, t, $^3J_{H\text{-}H}$ 4.8 Hz, H^{18}), 3.63 (2H, t, $^3J_{H\text{-}H}$ 4.8 Hz, H^{19}), 3.61 (2H, t, $^3J_{H\text{-}H}$ 4.8 Hz, H^{20}), 3.34 (3H, s, H^{21}), 2.13 (3H, s, H^{OAc}), 1.34 (3H, t, $^3J_{H\text{-}H}$ 5.6 Hz, H^8); δ_C ($CDCl_3$) 170.6 (s, $C^{C=O(OAc)}$), 160.1 (s, C^{14}), 157.3 (d, $^3J_{C\text{-}P}$ 20 Hz, C^2), 154.7 (d, $^1J_{C\text{-}P}$ 165 Hz, C^6), 133.8 (s, C^{12}), 133.2 (d, $^2J_{C\text{-}P}$ 12 Hz, C^4), 132.7 (d, $^4J_{C\text{-}P}$ 5 Hz, C^p), 132.6 (d, $^2J_{C\text{-}P}$ 10 Hz, C^o), 130.1 (d, $^1J_{C\text{-}P}$ 139 Hz, C^i), 128.8 (d, $^3J_{C\text{-}P}$ 22 Hz, C^5), 128.6 (d, $^3J_{C\text{-}P}$ 12 Hz, C^m), 124.6 (d, $^4J_{C\text{-}P}$ 3 Hz, C^3), 115.1 (s, C^{13}), 114.1 (s, C^{11}), 96.2 (s, C^{10}), 85.5 (d, $^4J_{C\text{-}P}$ 2 Hz, C^9), 72.2 (s, C^{20}), 71.1 (s, C^{17}), 70.9 (s, C^{18}), 70.8 (s, C^{19}), 69.8 (s, C^{16}), 67.8 (C^{15}), 66.5 (s, C^1), 62.1 (d, $^2J_{C\text{-}P}$ 6 Hz, C^7), 59.3 (s, C^{21}), 21.1 (s, $C^{Me(OAc)}$), 16.7 (C^8); δ_P ($CDCl_3$) +26.0; *m/z* (HRMS$^+$) 582.2260 $[M + H]^+$ ($C_{31}H_{37}O_8NP$ requires 582.2257); R_f = 0.31 (silica, CH_2Cl_2 : 5 % MeOH).

*[2-(4-(2-[2-(2-methoxyethoxy)ethoxy]ethoxy)phenyl)ethynyl]trimethylsilane:

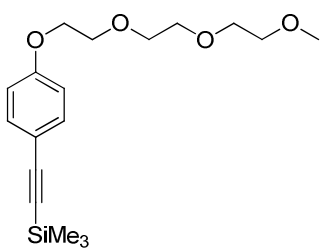

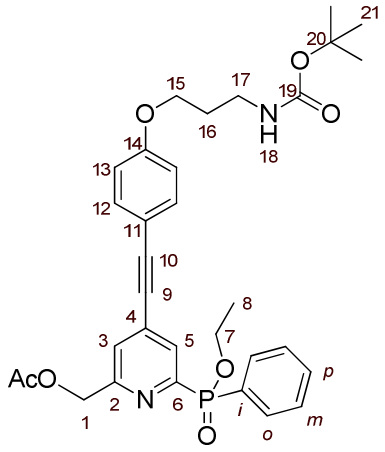

(4-(2-[4-(-([(Tert-butoxy)carbonyl]amino)propoxy)phenyl]ethynyl)-6-[ethoxy(phenyl)phosphoryl]pyridin-2-yl)methyl acetate, 51

(4-Bromo-6-[ethoxy(phenyl)phosphoryl]pyridine-2-yl)methyl acetate, ***45*** (170 mg, 0.43 mmol) was dissolved in dry THF (3 mL) and the solution was degassed (freeze-thaw cycle) three times. Tert-butyl N-(3-(4-[2-trimethylsilyl)ethynyl]phenoxy)propyl)carbamate* (148 mg, 0.43 mmol) and NEt_3 (1.5 mL) were added and the solution was degassed once. Tetrakis(triphenylphosphine)palladium(0) (49 mg, 0.043 mmol) and CuI (8 mg, 0.043 mmol) were added and the solution was degassed a further three times. The solution was stirred under argon and tetrabutylammonium fluoride solution (1 M in THF, 0.6 mL, 0.64 mmol) was added. A colour change from yellow to a dark blue was observed and the mixture was stirred at 65 °C under argon. The reaction was followed using TLC (silica; CH_2Cl_2 : 5 % CH_3OH, R_f(product) = 0.42, R_f(reactant) = 0.46) and stopped after 3 h. The solvent was removed under reduced pressure and the crude material purified by column chromatography (silica, CH_2Cl_2 : CH_3OH 0 – 1.5 % in 0.1 % increments) to give a yellow oil (174 mg, 69 %); δ_H ($CDCl_3$) 8.09 (1H, dd, $^3J_{H\text{-}P}$ 6.0 Hz, $^4J_{H\text{-}H}$ 2.0 Hz, H^5), 7.99 (2H, dd, $^3J_{H\text{-}H}$ 8.4 Hz $^3J_{H\text{-}P}$ 12.4 Hz, H^o), 7.54 (1H, t, $^3J_{H\text{-}H}$ 8.4 Hz, H^p), 7.47 (2H, d, $^3J_{H\text{-}H}$ 8.4 Hz, H^{12}), 7.45 (2H, td, $^3J_{H\text{-}H}$ 8.4 Hz $^4J_{H\text{-}P}$ 4.2 Hz, H^m), 7.45 (1H, d, $^4J_{H\text{-}H}$ 2.0 Hz, H^3), 6.88 (2H, d, $^3J_{H\text{-}H}$ 8.4 Hz, H^{13}), 5.24 (2H, s, H^1), 4.75 (1H, br s, H^{18}), 4.14 (2H, qd, $^3J_{H\text{-}H}$ 5.6 Hz $^3J_{H\text{-}P}$ 4.8 Hz, H^7), 4.05 (2H, t, $^3J_{H\text{-}H}$ 6 Hz, H^{15}), 3.33 (2H, m, H^{17}), 2.17 (3H, s, H^{OAc}), 1.92 (2H, q, $^3J_{H\text{-}H}$ 6 Hz, H^{16}), 1.44 (9H, s, H^{21}), 1.38 (3H, t, $^3J_{H\text{-}H}$ 5.6 Hz, H^8); δ_C ($CDCl_3$) 170.7 (s, $C^{C=O(OAc)}$), 160.0 (s, C^{14}), 157.3 (d, $^3J_{C\text{-}P}$ 20.3 Hz, C^2), 156.2 (s, C^{19}), 154.6 (d, $^1J_{C\text{-}P}$ 167 Hz, C^6), 133.9 (s, C^{12}), 133.2 (d, $^2J_{C\text{-}P}$ 12 Hz, C^4), 132.7 (d, $^4J_{C\text{-}P}$ 5 Hz, C^p), 132.6 (d, $^2J_{C\text{-}P}$ 10 Hz, C^o), 130.1 (d, $^1J_{C\text{-}P}$ 138 Hz, C^i), 129.1 (d, $^3J_{C\text{-}P}$ 23 Hz, C^5), 128.6 (d, $^3J_{C\text{-}P}$ 13 Hz, C^m), 124.6 (d, $^4J_{C\text{-}P}$ 3 Hz, C^3), 114.9 (s, C^{13}), 114.1 (s, C^{11}), 96.2 (s, C^{10}), 85.5 (d, $^4J_{C\text{-}P}$ 2 Hz, C^9), 79.5 (s, C^{20}), 66.5 (s, C^1), 66.1 (s, C^{15}), 62.1 (d, $^2J_{C\text{-}P}$ 6 Hz, C^7), 38.1 (s, C^{17}), 29.7 (s, C^{16}), 28.6 (s, C^{21}), 21.1 (s, $C^{Me(OAc)}$), 16.7 (C^8); δ_P ($CDCl_3$) +26.1; *m/z* (HRMS$^+$) 593.2435 $[M + H]^+$ ($C_{32}H_{38}O_7N_2P$ requires 593.2417); R_f = 0.42 (silica, CH_2Cl_2 : 5 % MeOH).

* Tert-butyl N-(3-(4-[2-trimethylsilyl)ethynyl]phenoxy)propyl)carbamate:

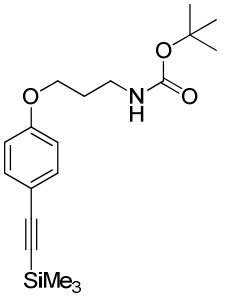

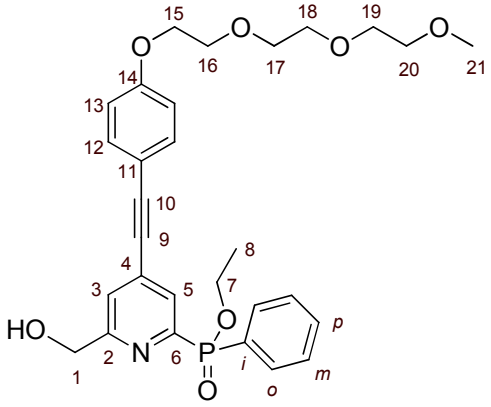

Ethyl-[6-(hydroxymethyl)-4-[2-(4-(2-[2-(2-methoxyethoxy)-ethoxy]ethoxy)phenyl)ethynyl]pyridin-2-yl](phenyl)phosphinate, 52

(6-[Ethoxy(phenyl)phosphoryl]-4-[2-(4-(2-[2-(2-methoxyethoxy)ethoxy]ethoxy)phenyl)ethynyl]pyridin-2-yl)methyl acetate, ***50*** (50 mg, 0.086 mmol) was dissolved in anhydrous CH_3CH_2OH (200 proof, 2.5 mL). A catalytic amount of sodium metal (~2 mg) was added and the solution was stirred at 40 °C under argon. The reaction was monitored by TLC (silica; CH_2Cl_2 : 5 % CH_3OH, R_f(product) = 0.19, R_f(reactant) = 0.31) and stopped after 40 min. To the crude reaction mixture CH_2Cl_2 (25 mL) was added and sodium salts were removed by filtration through a short silica plug. The silica was rinsed with CH_2Cl_2 : 10 % CH_3CH_2OH (300 mL) to ensure all material was desorbed from the silica. The solvent was removed under reduced pressure and the crude material was purified by column chromatography (silica, CH_2Cl_2 : CH_3OH 0 – 2.4 % in 0.2 % increments) to give a colourless oil (40 mg, 87 %); δ_H ($CDCl_3$) 8.06 (1H, dd, $^3J_{H\text{-}P}$ 6.0 Hz, $^4J_{H\text{-}H}$ 1.6 Hz, H^5), 7.95 (2H, dd, $^3J_{H\text{-}H}$ 8.4 Hz $^3J_{H\text{-}P}$ 12.4 Hz, H^o), 7.53 (1H, t, $^3J_{H\text{-}H}$ 8.4 Hz, H^p), 7.44 (2H, d, $^3J_{H\text{-}H}$ 8.8 Hz, H^{12}), 7.43 (2H, td, $^3J_{H\text{-}H}$ 8.4 Hz $^4J_{H\text{-}P}$ 4.2 Hz, H^m), 7.39 (1H, d, $^4J_{H\text{-}H}$ 1.6 Hz, H^3), 6.90 (2H, d, $^3J_{H\text{-}H}$ 8.8 Hz, H^{13}), 4.75 (2H, s, H^1), 4.14 (2H, qd, $^3J_{H\text{-}H}$ 5.6 Hz $^3J_{H\text{-}P}$ 4.8 Hz, H^7), 4.11 (2H, t, $^3J_{H\text{-}H}$ 4.8 Hz, H^{15}), 3.86 (2H, t, $^3J_{H\text{-}H}$ 4.8 Hz, H^{16}), 3.73 (2H, t, $^3J_{H\text{-}H}$ 4.8 Hz, H^{17}), 3.68 (2H, t, $^3J_{H\text{-}H}$ 4.8 Hz, H^{18}), 3.66 (2H, t, $^3J_{H\text{-}H}$ 4.8 Hz, H^{19}), 3.63 (2H, t, $^3J_{H\text{-}H}$ 4.8 Hz, H^{20}), 3.37 (3H, s, H^{21}), 1.37 (3H, t, $^3J_{H\text{-}H}$ 5.6 Hz, H^8); δ_C ($CDCl_3$) 160.4 (d, $^3J_{C\text{-}P}$ 19 Hz, C^2), 159.9 (s, C^{14}), 154.0 (d, $^1J_{C\text{-}P}$ 165 Hz, C^6), 133.6 (s, C^{12}), 133.0 (d, $^2J_{C\text{-}P}$ 12 Hz, C^4), 132.6 (d, $^4J_{C\text{-}P}$ 5 Hz, C^p), 132.3 (d, $^2J_{C\text{-}P}$ 10 Hz, C^o), 129.7 (d, $^1J_{C\text{-}P}$ 128 Hz, C^i), 128.6 (d, $^3J_{C\text{-}P}$ 22 Hz, C^5), 128.4 (d, $^3J_{C\text{-}P}$ 12 Hz, C^m), 123.8 (d, $^4J_{C\text{-}P}$ 3 Hz, C^3), 114.9 (s, C^{13}), 113.8 (s, C^{11}), 96.0 (s, C^{10}), 85.3 (d, $^4J_{C\text{-}P}$ 2 Hz, C^9), 71.9 (s, C^{20}), 70.9 (s, C^{17}), 70.7 (s, C^{18}), 70.6 (s, C^{19}), 69.6 (s, C^{16}), 67.5 (C^{15}), 63.9 (s, C^1), 61.8 (d, $^2J_{C\text{-}P}$ 6 Hz, C^7), 59.1 (s, C^{21}), 16.5 (C^8); δ_P ($CDCl_3$)

+26.6; *m/z* (HRMS$^+$) 540.2142 [M + H]$^+$ ($C_{29}H_{35}O_7NP$ requires 540.2151); R_f = 0.19 (silica, CH_2Cl_2 : 5 % MeOH).

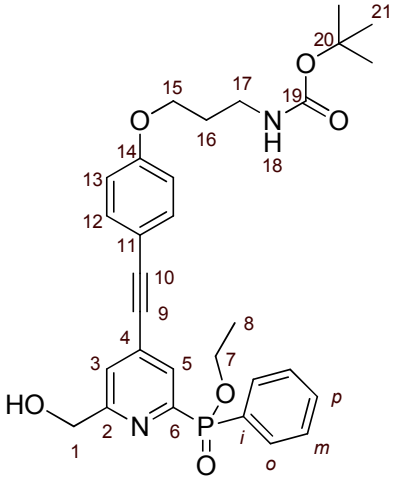

Tert-butyl N-(3-[4-(2-(2-[ethoxy(phenyl)phosphoryl]-6-(hydroxymethyl)pyridin-2-yl)ethynyl)phenoxy]propyl)carbamate, 53

(4-(2-[4-(-([(Tert-butoxy)carbonyl]amino)propoxy)phenyl]ethynyl)-6-[ethoxy(phenyl)phosphoryl]pyridin-2-yl)methyl acetate, ***51*** (32 mg, 0.054 mmol) was dissolved in anhydrous CH_3CH_2OH (200 proof, 2.5 mL). A catalytic amount of sodium metal (~2 mg) was added and the solution was stirred at 40 °C under argon. The reaction was monitored by TLC (silica; CH_2Cl_2 : 5 % CH_3OH, R_f(product) = 0.25, R_f(reactant) = 0.42) and stopped after 40 min. To the crude reaction mixture CH_2Cl_2 (25 mL) was added and sodium salts were removed by filtration through a short silica plug. The silica was rinsed with CH_2Cl_2 : 10 % CH_3CH_2OH (300 mL) to ensure all material was desorbed from the silica. The solvent was removed under reduced pressure and the crude material was purified by column chromatography (silica, CH_2Cl_2 : CH_3OH 0 – 2 % in 0.2 % increments) to give a colourless oil (24 mg, 80 %); δ_H ($CDCl_3$) 8.01 (1H, dd, $^3J_{H\text{-}P}$ 6.4 Hz, $^4J_{H\text{-}H}$ 2.0 Hz, H^5), 7.89 (2H, dd, $^3J_{H\text{-}H}$ 8.4 Hz $^3J_{H\text{-}P}$ 12.4 Hz, H^o), 7.48 (1H, t, $^3J_{H\text{-}H}$ 8.4 Hz, H^p), 7.40 (2H, d, $^3J_{H\text{-}H}$ 8.8 Hz, H^{12}), 7.39 (2H, td, $^3J_{H\text{-}H}$ 8.4 Hz $^4J_{H\text{-}P}$ 4.2 Hz, H^m), 7.33 (1H, d, $^4J_{H\text{-}H}$ 2.0 Hz, H^3), 6.81 (2H, d, $^3J_{H\text{-}H}$ 8.8 Hz, H^{13}), 4.73 (1H, br s, H^{18}), 4.69 (2H, s, H^1), 4.08 (2H, qd, $^3J_{H\text{-}H}$ 5.6 Hz $^3J_{H\text{-}P}$ 4.8 Hz, H^7), 3.97 (2H, t, $^3J_{H\text{-}H}$ 6 Hz, H^{15}), 3.26 (2H, m, H^{17}), 1.92 (2H, q, $^3J_{H\text{-}H}$ 6 Hz, H^{16}), 1.37 (9H, s, H^{21}), 1.31 (3H, t, $^3J_{H\text{-}H}$ 5.6 Hz, H^8); δ_C ($CDCl_3$) 160.3 (d, $^3J_{C\text{-}P}$ 18 Hz, C^2), 159.8 (s, C^{14}), 156.0 (s, C^{19}), 153.2 (d, $^1J_{C\text{-}P}$ 164 Hz, C^6), 133.7 (s, C^{12}), 133.0 (d, $^2J_{C\text{-}P}$ 11 Hz, C^4), 132.6 (d, $^4J_{C\text{-}P}$ 5 Hz, C^p), 132.3 (d, $^2J_{C\text{-}P}$ 10 Hz, C^o), 129.6 (d, $^1J_{C\text{-}P}$ 138 Hz, C^i), 128.6 (d, $^3J_{C\text{-}P}$ 18 Hz, C^5), 128.5 (d, $^3J_{C\text{-}P}$ 9 Hz, C^m), 123.8 (d, $^4J_{C\text{-}P}$ 3 Hz, C^3), 114.7 (s, C^{13}), 113.8 (s, C^{11}), 96.0 (s, C^{10}), 85.3 (d, $^4J_{C\text{-}P}$ 2 Hz, C^9), 79.3 (s, C^{20}), 65.9 (s, C^{15}), 63.8 (s, C^1), 61.9 (d, $^2J_{C\text{-}P}$ 6 Hz, C^7), 37.9 (s, C^{17}), 29.5 (s, C^{16}), 28.4 (s, C^{21}), 16.6 (C^8); δ_P ($CDCl_3$) +25.6; *m/z* (HRMS$^+$) 551.2290 [M + H]$^+$ ($C_{30}H_{36}O_6N_2P$ requires 551.2311); R_f = 0.25 (silica, CH_2Cl_2 : 5 % MeOH).

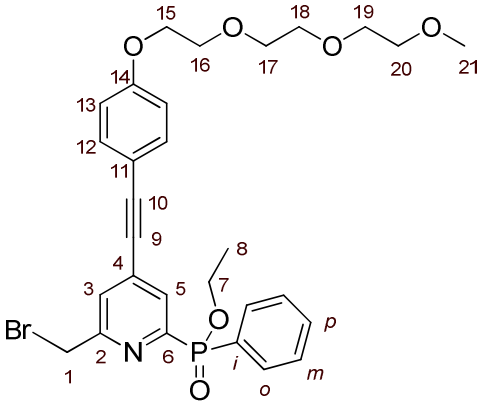

Ethyl-[6-(bromomethyl)-4-[2-(4-(2-[2-(2-methoxyethoxy)ethoxy]ethoxy)phenyl)ethynyl]pyridin-2-yl](phenyl)phosphinate, 54

Ethyl-[6-(hydroxymethyl)-4-[2-(4-(2-[2-(2-methoxyethoxy)-ethoxy]ethoxy)phenyl)ethynyl]pyridin-2-yl](phenyl)phosphinate, ***52*** (116 mg, 0.22 mmol) was dissolved in dry CH_2Cl_2 (5 mL) and the solution was stirred at 0 °C under argon. PBr_3 (30 µL, 0.33 mmol) was added and the solution was stirred for a further 1 h at 0 °C. The reaction mixture was allowed to warm to room temperature and monitored by TLC (silica; CH_2Cl_2 : 5 % CH_3OH, R_f(product) = 0.50, R_f(reactant) = 0.19). After 1 h at 20 °C the crude reaction mixture was immediately purified by column chromatography (silica, CH_2Cl_2 : 1 % CH_3OH) to give the *title product* as a yellow oil (95 mg, 73 %); δ_H ($CDCl_3$) 8.00 (1H, dd, $^3J_{H\text{-}P}$ 6.0 Hz, $^4J_{H\text{-}H}$ 1.2 Hz, H^5), 7.94 (2H, dd, $^3J_{H\text{-}H}$ 8.8 Hz $^3J_{H\text{-}P}$ 12.4 Hz, H^o), 7.51 (1H, d, $^4J_{H\text{-}H}$ 1.2 Hz, H^3), 7.48 (1H, t, $^3J_{H\text{-}H}$ 8.8 Hz, H^p), 7.41 (2H, d, $^3J_{H\text{-}H}$ 8.8 Hz, H^{12}), 7.40 (2H, td, $^3J_{H\text{-}H}$ 8.8 Hz $^4J_{H\text{-}P}$ 4.2 Hz, H^m), 6.85 (2H, d, $^3J_{H\text{-}H}$ 8.8 Hz, H^{13}), 4.48 (2H, s, H^1), 4.09 (2H, qd, $^3J_{H\text{-}H}$ 7.2 Hz $^3J_{H\text{-}P}$ 4.8 Hz, H^7), 4.08 (2H, t, $^3J_{H\text{-}H}$ 4.8 Hz, H^{15}), 3.81 (2H, t, $^3J_{H\text{-}H}$ 4.8 Hz, H^{16}), 3.67 (2H, t, $^3J_{H\text{-}H}$ 4.8 Hz, H^{17}), 3.63 (2H, t, $^3J_{H\text{-}H}$ 4.8 Hz, H^{18}), 3.59 (2H, t, $^3J_{H\text{-}H}$ 4.8 Hz, H^{19}), 3.49 (2H, t, $^3J_{H\text{-}H}$ 4.8 Hz, H^{20}), 3.31 (3H, s, H^{21}), 1.32 (3H, t, $^3J_{H\text{-}H}$ 7.2 Hz, H^8); δ_C ($CDCl_3$) 160.1 (d, $^3J_{C\text{-}P}$ 19 Hz, C^2), 159.9 (s, C^{14}), 154.3 (d, $^1J_{C\text{-}P}$ 165 Hz, C^6), 133.6 (s, C^{12}), 133.3 (d, $^2J_{C\text{-}P}$ 12 Hz, C^4), 132.4 (d, $^4J_{C\text{-}P}$ 5 Hz, C^p), 132.3 (d, $^2J_{C\text{-}P}$ 10 Hz, C^o), 129.7 (d, $^1J_{C\text{-}P}$ 128 Hz, C^i), 128.6 (d, $^3J_{C\text{-}P}$ 22 Hz, C^5), 128.4 (d, $^3J_{C\text{-}P}$ 13 Hz, C^m), 126.7 (d, $^4J_{C\text{-}P}$ 3 Hz, C^3), 114.9 (s, C^{13}), 113.8 (s, C^{11}), 96.3 (s, C^{10}), 84.9 (d, $^4J_{C\text{-}P}$ 2 Hz, C^9), 71.9 (s, C^{20}), 70.9 (s, C^{17}), 70.7 (s, C^{18}), 70.6 (s, C^{19}), 69.6 (s, C^{16}), 67.5 (C^{15}), 61.0 (d, $^2J_{C\text{-}P}$ 5 Hz, C^7), 59.1 (s, C^{21}), 33.1 (s, C^1), 16.6 (C^8); δ_P ($CDCl_3$) +24.8; *m/z* (HRMS$^+$) 602.1302 [M (^{79}Br) + H]$^+$ ($C_{29}H_{34}O_6NP^{79}Br$ requires 602.1302), R_f = 0.50 (silica, CH_2Cl_2 : 5 % MeOH).

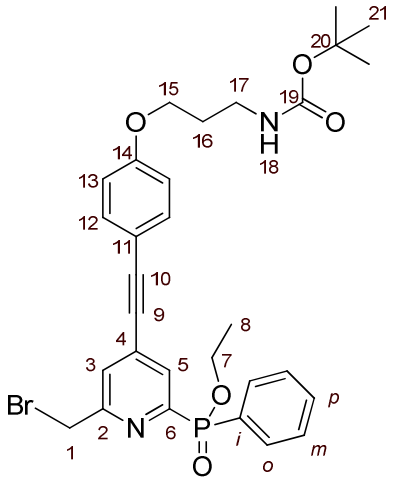

Tert-butyl N-[3(4-(2-[2-(bromomethyl)-6-[ethoxy(phenyl)phosphoryl]pyridin-4-yl]ethynyl)phenoxy)propyl]carbamate, 55

Tert-butyl N-(3-[4-(2-(2-[ethoxy(phenyl)phosphoryl]-6-(hydroxymethyl)pyridin-2-yl)ethynyl)phenoxy]propyl)carbamate, ***53*** (25 mg, 0.045 mmol) was dissolved in dry CH_2Cl_2 (3 mL) and the solution was stirred at 0 °C under argon. PBr_3 (4.3 µL, 0.045 mmol) was added and the solution stirred for a further 45 min at 0 °C. The reaction mixture was allowed to warm to room temperature and monitored by TLC (silica; CH_2Cl_2 : 5 % CH_3OH, R_f(product) = 0.45, R_f(reactant) = 0.25). After 30 min at 23 °C a precipitate formed. The precipitate was found to be the ammonium bromide salt of ***55*** resulting from loss of the BOC protecting group. This material was converted into ***55*** according to the procedure described below.* The supernatant, which contained some of the desired compound, was decanted and purified immediately by column chromatography (silica, CH_2Cl_2 : 0.8 % MeOH) to give the *title compound* as a colourless oil (8 mg).

*To the precipitate which formed was added dry CH_2Cl_2 (3 mL) and di-*tert*-butyl dicarbonate (19 mg, 0.087 mmol). *N*,*N*-Diisopropylethylamine (30 µL, 0.17 mmol) was added causing the ammonium bromide salt of ***55*** to dissolve. The mixture was stirred under argon at 0 °C for 30 min followed by 30 min at 23 °C. At this point the reaction mixture was immediately purified by column chromatography (silica, CH_2Cl_2 : 0.8 % MeOH) to give the *title compound* as a colourless oil (5 mg,).

Total *title compound* (13 mg, 47 %); δ_H ($CDCl_3$) 8.07 (1H, dd, $^3J_{H\text{-}P}$ 6.0 Hz, $^4J_{H\text{-}H}$ 1.2 Hz, H^5), 8.01 (2H, dd, $^3J_{H\text{-}H}$ 8.4 Hz $^3J_{H\text{-}P}$ 12 Hz, H^o), 7.58 (1H, d, $^4J_{H\text{-}H}$ 1.2 Hz, H^3), 7.55 (1H, t, $^3J_{H\text{-}H}$ 8.4 Hz, H^p), 7.47 (2H, td, $^3J_{H\text{-}H}$ 8.4 Hz $^4J_{H\text{-}P}$ 4.2 Hz, H^m), 7.46 (2H, d, $^3J_{H\text{-}H}$ 8.8 Hz, H^{12}), 6.89 (2H, d, $^3J_{H\text{-}H}$ 8.8 Hz, H^{13}), 4.72 (1H, br s, H^{18}), 4.55 (2H, s, H^1), 4.15 (2H, qd, $^3J_{H\text{-}H}$ 6.0 Hz $^3J_{H\text{-}P}$ 4.8 Hz, H^7), 4.05 (2H, t, $^3J_{H\text{-}H}$ 6 Hz, H^{15}), 3.33 (2H, m, H^{17}), 2.00 (2H, q, $^3J_{H\text{-}H}$ 6 Hz, H^{16}), 1.44 (9H, s, H^{21}), 1.38 (3H, t, $^3J_{H\text{-}H}$ 6.0 Hz, H^8); δ_P ($CDCl_3$) +25.8; *m/z* (HRMS$^+$) 613.1462 [M (^{79}Br) + H]$^+$ ($C_{30}H_{34}O_5N_2P^{79}Br$ requires 613.1462); R_f = 0.45 (silica, CH_2Cl_2 : 5 % MeOH).

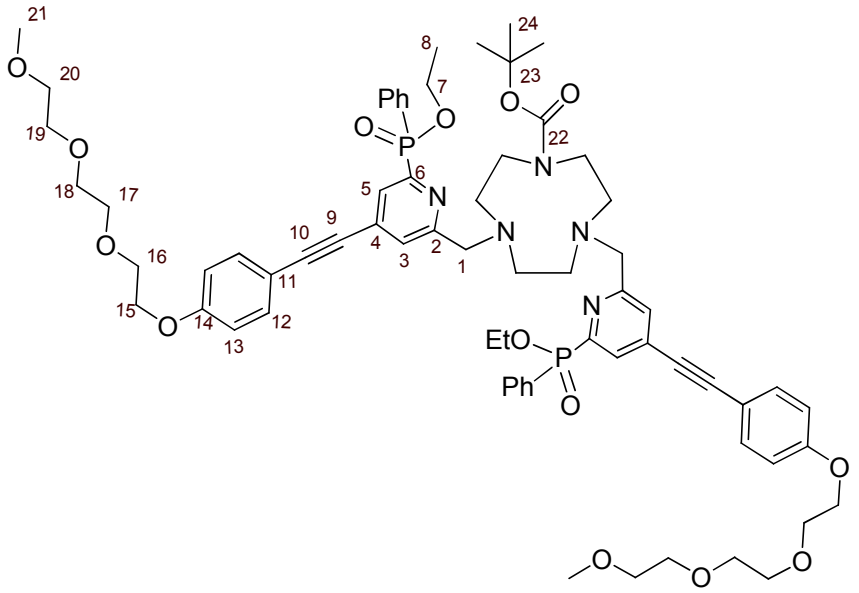

Tert-*butoxycarbonyl-protected di-ethyl phenylphosphinate ester of L[13], 57*

Tert-butyl-1,4,7-triazacyclononane-1-carboxylate* (22 mg, 0.096 mmol) and ethyl-[6-(bromomethyl)-4-[2-(4-(2-[2-(2-methoxyethoxy)ethoxy]ethoxy)phenyl)ethynyl]pyridin-2-yl](phenyl)phosphinate, ***54*** (95 mg, 0.16 mmol) were dissolved in CH_3CN (5 mL) and K_2CO_3 (27 mg, 0.19 mmol) was added. The mixture was stirred under argon at 50 °C and monitored by TLC (silica; CH_2Cl_2 : 10 % CH_3OH, R_f(product) = 0.41, R_f(reactant ***54***) = 0.81). After 1 h all of the starting material had been consumed and the reaction was cooled and the solution decanted from excess potassium salts. The solvent was removed under reduced pressure and the crude material purified by column chromatography (silica, CH_2Cl_2 : CH_3OH 0 – 5 % in 0.5 % increments) to give the *title product* as a yellow oil (58 mg, 59 %): δ_H ($CDCl_3$) 8.01 (2H, m, H^5), 7.95 (4H, m, H^o), 7.56 (2H, br s, H^3), 7.45 (2H, m, H^p), 7.41 (4H, d, $^3J_{H-H}$ 8.8 Hz, H^{12}), 7.40 (4H, m, H^m), 6.87 (4H, d, $^3J_{H-H}$ 8.8 Hz, H^{13}), 4.13 (4H, t, $^3J_{H-H}$ 4.8 Hz, H^{15}), 4.10 (4H, m, H^7), 3.85 (4H, s, H^1), 3.84 (4H, t, $^3J_{H-H}$ 4.8 Hz, H^{16}), 3.72 (4H, t, $^3J_{H-H}$ 4.8 Hz, H^{17}), 3.66 (4H, t, $^3J_{H-H}$ 4.8 Hz, H^{18}), 3.63 (4H, t, $^3J_{H-H}$ 4.8 Hz, H^{19}), 3.53 (4H, t, $^3J_{H-H}$ 4.8 Hz, H^{20}), 3.35 (6H, s, H^{21}), 3.24 (4H, br m, ring Hs), 2.97 (4H, br m, ring Hs), 2.53 (4H, br m, ring Hs), 1.45 (9H, s, H^{24}), 1.33 (6H, m, H^8); δ_C ($CDCl_3$) 161.6, 161.4 (d, $^3J_{C-P}$ 19 Hz, C^2), 159.7, 159.6 (s, C^{22}), 155.5 (s, C^{14}), 153.8, 153.7 (d, $^1J_{C-P}$ 165 Hz, C^6), 133.6, 133.5 (s, C^{12}), 133.3 (br m, C^4), 132.4 (br m, C^p), 132.3 (br m, C^o), 130.1 (d, $^1J_{C-P}$ 145 Hz, C^i), 128.1 (br m, C^5), 128.0 (br m, C^m), 126.2, 125.9 (d, $^4J_{C-P}$ 3 Hz, C^3), 114.9, 114.7 (s, C^{13}), 114.1, 114.0 (s, C^{11}), 95.4, 95.1 (s, C^{10}), 85.7, 85.5 (br m, C^9), 71.9 (s, C^{20}), 70.8 (s, C^{17}), 70.6 (s, C^{18}), 70.5 (s, C^{19}), 69.6 (s, C^{16}), 67.5 (C^{15}), 63.0 – 49.1 (br m, ring Cs), 61.6 (br m, C^7), 59.0 (s, C^{21}), 53.4 (br m, C^1), 28.7, 28.6 (s, C^{24}), 16.5 (C^8); δ_P ($CDCl_3$) +26.6, +26.5; *m/z* (HRMS$^+$) 1272.584 $[M + H]^+$ ($C_{69}H_{88}O_{14}N_5P_2$ requires 1272.580), R_f = 0.41 (silica, CH_2Cl_2 : 10 % MeOH).

* Tert-butyl-1,4,7-triazacyclononane-1-carboxylate:

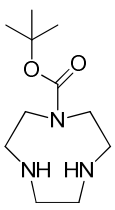

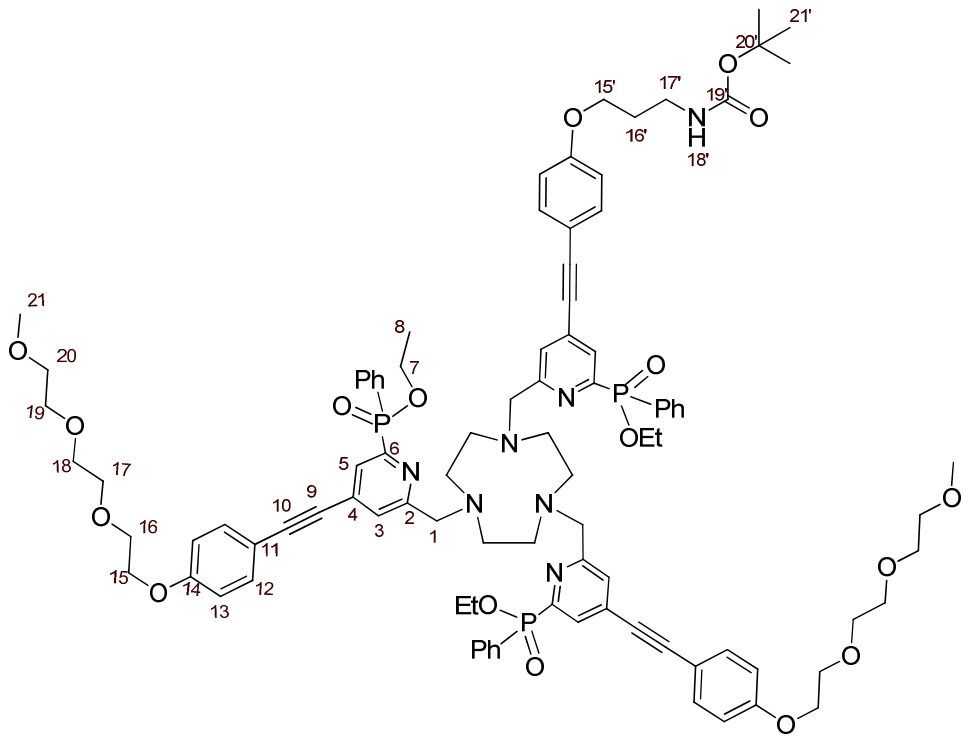

Tri-ethyl phenylphosphinate ester of L[12], 58

The t*ert*-butoxycarbonyl-protected di-ethyl phenylphosphinate ester of **L[13]**, ***57*** (47 mg, 0.037 mmol) was dissolved in anhydrous CH_2Cl_2 (1 mL) and trifluoroacetic acid (0.5 mL) was added. The solution was stirred under argon at 23 °C for 30 min. TLC (silica; CH_2Cl_2 : 10 % CH_3OH, R_f(product) = 0.10, R_f(reactant) = 0.41) and HRMS$^+$ (1172.528 $[M + H]^+$ $C_{64}H_{80}O_{12}N_5P_2$ requires 1172.527) were used to confirm protecting group removal had gone to completion. The solvent was removed under reduced pressure and the residue re-dissolved in CH_2Cl_2 (1 mL), which was again removed under reduced pressure. This process was repeated 5 times to ensure removal of excess trifluoroacetic acid. The residue was dissolved in CH_3CN (4 mL) and tert-butyl N-[3(4-(2-[2-(bromomethyl)-6-[ethoxy(phenyl)phosphoryl]pyridin-4-yl]ethynyl)phenoxy)propyl]carbamate, ***55*** (18 mg, 0.029 mmol) and K_2CO_3 (15 mg, 0.11 mmol) were added. The solution was stirred at 50 °C and the reaction monitored by LC-MS and TLC (silica; CH_2Cl_2 : 10 % CH_3OH, R_f(product) = 0.20, R_f(reactant ***55***) = 0.73). After 30 min all of the starting bromide ***55*** had been consumed and the reaction was cooled and the solvent removed under reduced pressure. The crude residue was purified by column chromatography (silica, CH_2Cl_2 : CH_3OH 0 – 10 % in 0.5 % increments) to give the *title product* as a yellow oil (25 mg, 50 %); δ_H ($CDCl_3$) 8.07 (3H, d, $^3J_{H\text{-}P}$ 6.0 Hz, H^5), 7.85 (6H, dd, $^3J_{H\text{-}H}$ 8.4 Hz $^3J_{H\text{-}P}$ 12 Hz, H^o), 7.48 (3H, m, H^3), 7.47 (3H, m, H^p), 7.46 (6H, d, $^3J_{H\text{-}H}$ 8.8 Hz, H^{12}), 7.39 (6H, m, H^m), 6.90 (6H, d, $^3J_{H\text{-}H}$ 8.8 Hz, H^{13}), 4.76 (1H, br s, $H^{18'}$), 4.14 (6H, m, H^7), 4.11 (4H, t, $^3J_{H\text{-}H}$ 4.8 Hz, H^{15}), 4.04 (2H, t, $^3J_{H\text{-}H}$ 6 Hz, $H^{15'}$), 3.94 (6H, br s, H^1), 3.87 (4H, t, $^3J_{H\text{-}H}$ 4.8 Hz, H^{16}), 3.73 (4H, t, $^3J_{H\text{-}H}$ 4.8 Hz, H^{17}), 3.68 (4H, t, $^3J_{H\text{-}H}$ 4.8 Hz, H^{18}), 3.65 (4H, t, $^3J_{H\text{-}H}$ 4.8 Hz, H^{19}), 3.54 (4H, t, $^3J_{H\text{-}H}$ 4.8 Hz, H^{20}), 3.37 (6H, s, H^{21}), 3.34 (2H, m, $H^{17'}$), 2.81 (12H, br m, ring Hs), 1.99 (2H, q, $^3J_{H\text{-}H}$ 6 Hz, $H^{16'}$), 1.43 (9H, s, $H^{21'}$), 1.34 (9H, t, $^3J_{H\text{-}H}$ 7.2 Hz, H^8); δ_C ($CDCl_3$) 160.8 (d, $^3J_{C\text{-}P}$ 19 Hz, C^2), 160.2 (s, $C^{19'}$), 156.2 (s, C^{14}), 154.6 (d, $^1J_{C\text{-}P}$ 165 Hz, C^6), 134.0 (s, C^{12}), 133.9 (br m, C^4), 132.9 (br m, C^p), 132.5 (d, $^2J_{C\text{-}P}$ 10 Hz, C^o), 130.2 (d, $^1J_{C\text{-}P}$ 138 Hz, C^i), 128.8 (br m, C^5), 128.7 (br m, C^m), 127.5 (br m, C^3), 115.1 (s, C^{13}), 113.9 (s, C^{11}), 97.0 (s, C^{10}), 85.3 (s, C^9), 79.6 (s, $C^{20'}$), 72.1 (s, C^{20}), 71.1 (s, C^{17}), 70.9 (s, C^{18}),

70.8 (s, C^{19}), 69.8 (s, C^{16}), 67.8 (C^{15}), 65.9 (s, $C^{15'}$), 62.0 (d, $^2J_{C\text{-}P}$ 6 Hz, C^7), 59.3 (s, C^{21}), 52.3 (s, C^1), 53.0 – 46.0 (br m, ring Cs), 37.9 (s, $C^{17'}$), 29.7 (s, $C^{16'}$), 28.6 (s, $C^{21'}$), 16.8 (C^8); δ_P ($CDCl_3$) +26.4; *m/z* (HRMS$^+$) 1704.741 $[M + H]^+$ ($C_{94}H_{113}O_{17}N_7P_3$ requires 1704.740), R_f = 0.20 (silica, CH_2Cl_2 : 10 % MeOH).

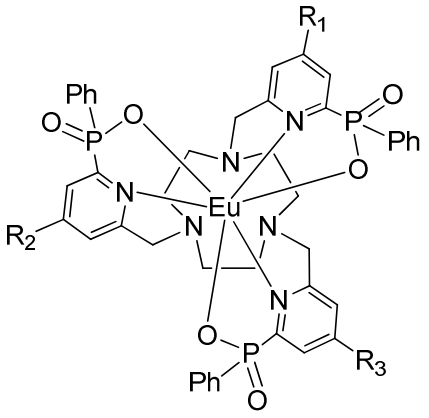

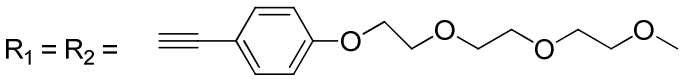

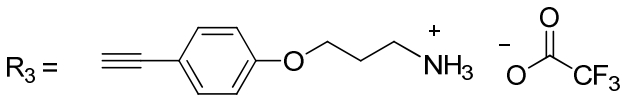

[Eu·L^{12}]

The tri-ethyl phenylphosphinate ester of ***L^{12}***, ***58*** (25 mg, 0.015 mmol) was dissolved in anhydrous CH_2Cl_2 (1 mL) and trifluoroacetic acid (0.5 mL) was added. The solution immediately underwent a change from colourless to yellow and was stirred under argon at 23 °C for 30 min. TLC was used to confirm that all starting material had been consumed. The solvent was removed under reduced pressure and the residue re-dissolved in CH_2Cl_2 (1 mL), which was again removed under reduced pressure. This process was repeated 5 times to ensure removal of excess trifluoroacetic acid. ^{1}H-NMR (loss of CH_3 peak at 1.43 ppm) and ESI-MS$^+$ (802.8 $[M + 2H]^{2+}$, 803.8 $[M(^{13}C) + 2H]^{2+}$) was used to confirm removal of the *tert*-butoxycarbonyl group. The residue was dissolved in CD_3OD (2.5 mL) and D_2O (1.5 mL) was added. The solution was heated to 60 °C and NaOD solution was added (0.5 M, 0.5 mL). The reaction was monitored by ^{1}H-NMR (loss of CH_3CH_2 peaks at 4.14 and 1.34 ppm) and ^{31}P-NMR (reactant 26.6 ppm, product 17.3 ppm) and stopped after 24 h. The pH of the solution was reduced to 7 by addition of HCl (1M). CH_3OH (1 mL) was added to ensure all material was in solution. $Eu(OAc)_3$ (7 mg, 0.016 mmol) in a H_2O : CH_3OH solution (0.5 mL, 1:1 v/v) was added and the solution was stirred at 50 °C for 14 h. The solvent was removed under reduced pressure and the crude material purified by column chromatography (silica, CH_2Cl_2 : 10 % CH_3OH : aq. NH_3 solution 0 – 1 % in 0.1 % increments) to give the *title product* as a white solid (9.1 mg, 34 %); *m/z* (HRMS$^+$) 1668.498 $[M - CF_3CO_2]^+$ ($C_{83}H_{90}O_{15}N_7P_3{}^{151}$Eu requires 1668.490); δ_P (CD_3OD) +17.5; R_f = 0.12 (silica, CH_2Cl_2 : 10 % MeOH : NH_3 1 %). $\tau_{MeOH} = 1.25$ ms, $\tau_{H_2O} = 0.96$ ms, $\tau_{D_2O} = 1.28$ ms, $\Phi^{em}_{MeOH} = 55 \pm 10$ %; ε_{MeOH} (332 nm) = 60, 000 M^{-1} cm^{-1}; t_R (*Method D*) = 11.5 min.

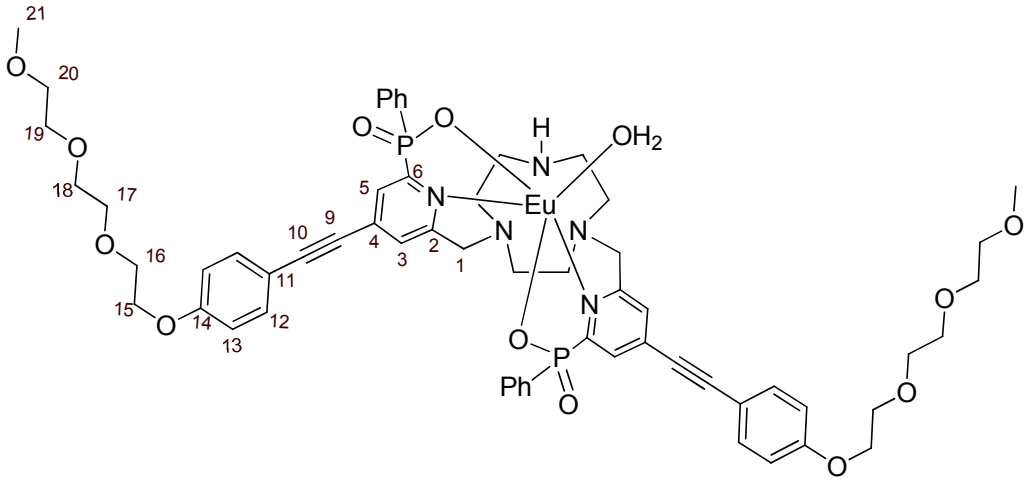

[Eu·L[13](H2O)]Cl

The *tert*-butoxycarbonyl-protected di-ethyl phenylphosphinate ester of ***L[13]***, ***57*** (20 mg, 0.016 mmol) was dissolved in anhydrous CH_2Cl_2 (1 mL) and trifluoroacetic acid (0.5 mL) was added. The solution was stirred under argon at 23 °C for 30 min. TLC (silica; CH_2Cl_2 : 10 % CH_3OH, R_f(product) = 0.10, R_f(reactant) = 0.41) and HRMS$^+$ (1172.528 $[M + H]^+$ $C_{64}H_{80}O_{12}N_5P_2$ requires 1172.527) were used to confirm removal of the *tert*-butoxycarbonyl group. The solvent was removed under reduced pressure and the residue re-dissolved in CH_2Cl_2 (1 mL), which was again removed under reduced pressure. This process was repeated 5 times to ensure removal of excess trifluoroacetic acid. The residue was dissolved in CD_3OD (2 mL) and D_2O (1 mL) was added. The solution was heated to 60 °C and NaOD solution was added (0.5 M, 0.5 mL). The reaction was monitored by ^{1}H-NMR (loss of C*H*$_3$C*H*$_2$ peaks at 4.13 and 1.34 ppm) and ^{31}P-NMR (reactant 26.6 ppm, product 16.6 ppm) and stopped after 18 h. The pH of the solution was adjusted to 7 by addition of HCl (1M). CH_3OH (1 mL) was added to ensure all material was in solution. $Eu(OAc)_3$ (7 mg, 0.016 mmol) in a H_2O : CH_3OH solution (0.5 mL, 1:1 v/v) was added and the solution was stirred at 50 °C for 16 h. The solvent was removed under reduced pressure and the crude material purified by preparative-HPLC to give the *title product* as a white solid (7.8 mg, 38 %); *m/z* (ESI-MS$^+$) 1266.391 $[M]^+$ ($C_{60}H_{69}O_{12}N_5P_2{}^{153}Eu$ requires 1266.363); δ_P (CD_3OD) +25.8, +13.6; $\tau_{H_2O} = 0.33$ ms, $\tau_{D_2O} = 0.50$ ms, $\Phi^{em}_{MeOH} = 18 \pm 10$ %; ε_{MeOH} (332 nm) = 44, 000 M^{-1} cm^{-1}; t_R (*Method D*) = 9.5 min.

8.3 References

1. A. Beeby, I. M. Clarkson, R. S. Dickins, S. Faulkner, D. Parker, L. Royle, A. S. de Sousa, J. A. G. Williams and M. Woods, *J. Chem. Soc. Perkin Trans. 2*, 1999, 493-503.
2. L. Porres, A. Holland, L. O. Palsson, A. P. Monkman, C. Kemp and A. Beeby, *J. Fluoresc.*, 2006, **16**, 267-272.
3. J. Carmichael, W. G. Degraff, A. F. Gazdar, J. D. Minna and J. B. Mitchell, *Cancer Res.*, 1987, **47**, 936-942.
4. G. M. Sheldrick, *Acta Crystallographica Section A*, 2008, **64**, 112-122.
5. O. V. Dolomanov, L. J. Bourhis, R. J. Gildea, J. A. K. Howard and H. Puschmann, *J. Appl. Crystallogr.*, 2009, **42**, 339-341.
6. E. E. Kilbourn and M. C. Seidel, *J. Org. Chem.*, 1972, **37**, 1145-1148.

Appendix 1.

HPLC Methods and Traces

Reverse phase HPLC analysis was performed at 298 K on a Perkin Elmer system, comprising a Perkin Elmer Series 200 pump, Perkin Elmer Series 200 autosampler, Perkin Elmer Series 200 UV/Vis detector and Perkin Elmer Series 200 fluorescence detector.

Column 1: Phenomenex Synergi 4u Fusion-RP 80i 150 × 4.66 mm 4 μm particle size.
Column 2: XBridge C18 100 × 5.00 mm 3.5 μm particle size.

Method A:

Time (min)	H_2O + 0.1 % HCO_2H	CH_3CN + 0.1 % HCO_2H
0	95	5
2	95	5
15	0	100
17	0	100
22	95	5

Method B:

Time (min)	H_2O + 0.1 % HCO_2H	CH_3CN + 0.1 % HCO_2H
0	95	5
2	95	5
20	0	100
23	0	100
28	95	5

Method C:

Time (min)	H_2O + 0.1 % HCO_2H	CH_3CN + 0.1 % HCO_2H
0	95	5
1	95	5
8	0	100
11	0	100
13	95	5

Method D:

Time (min)	H_2O + 0.1 % HCO_2H	CH_3CN + 0.1 % HCO_2H
0	95	5
2	95	5
13	0	100
15	0	100
17	95	5

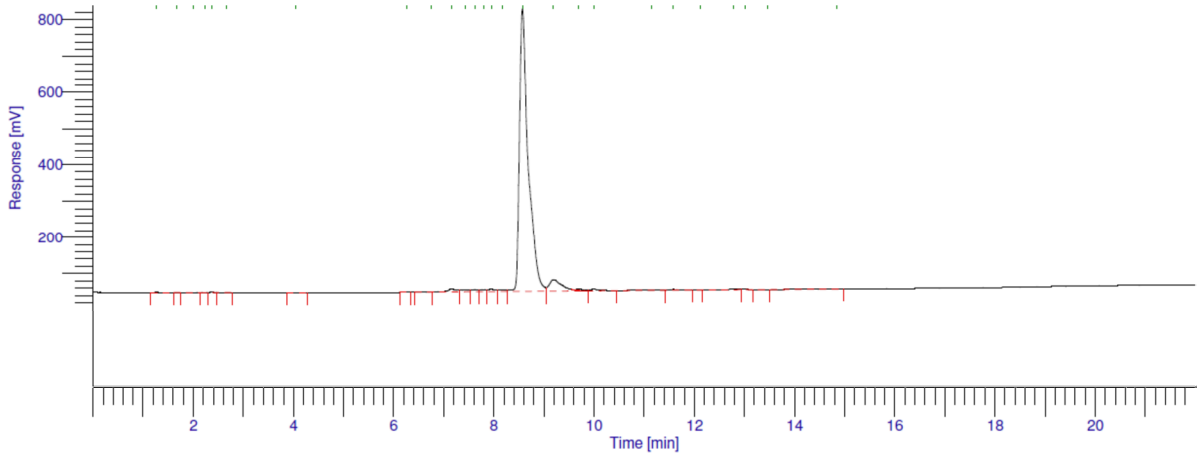

a) HPLC analysis of **[EuL^1]**, *Method A*, *Column 1* λ_{abs} = 328.

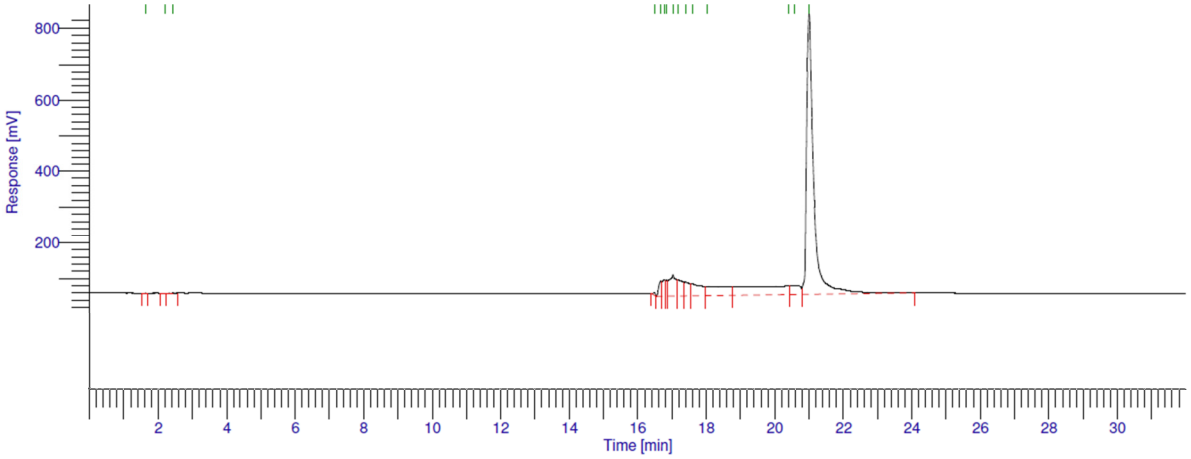

b) HPLC analysis of **[TbL^1]**, *Method A*, *Column 2*, λ_{abs} = 328.

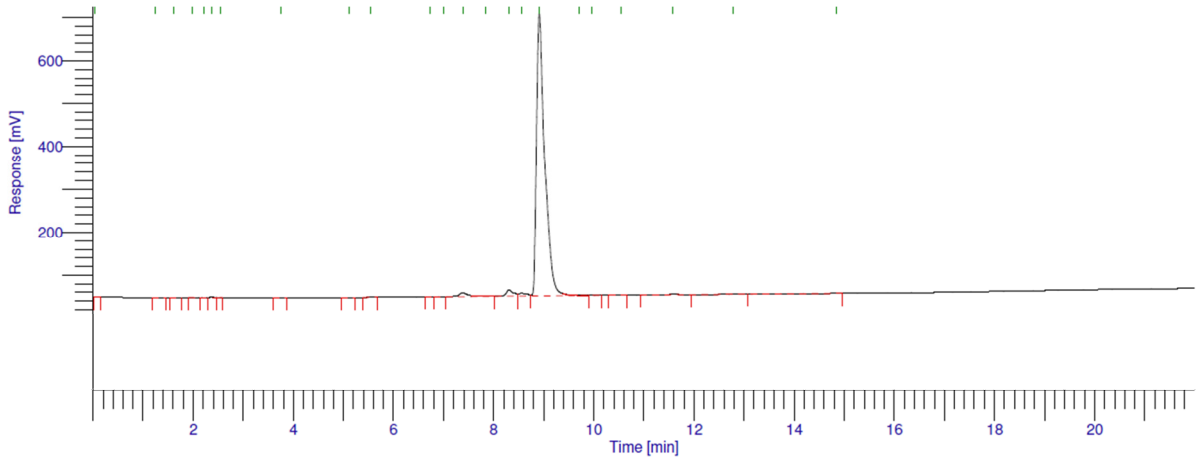

c) HPLC analysis of **[EuL^2]Cl**, *Method A*, *Column 1*, λ_{abs} = 328.

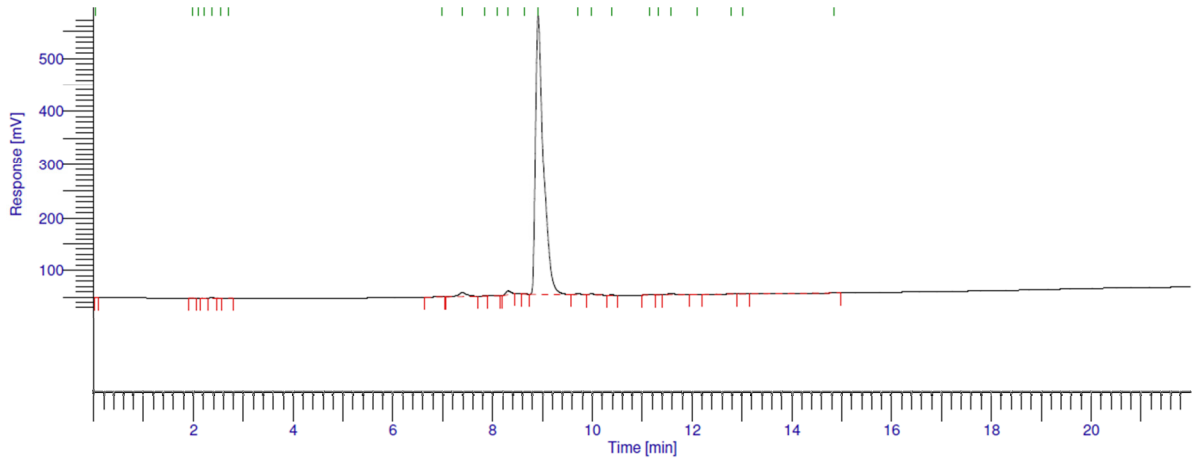

d) HPLC analysis of **[TbL^{2}]Cl**, *Method A*, *Column 1*, λ_{abs} = 328.

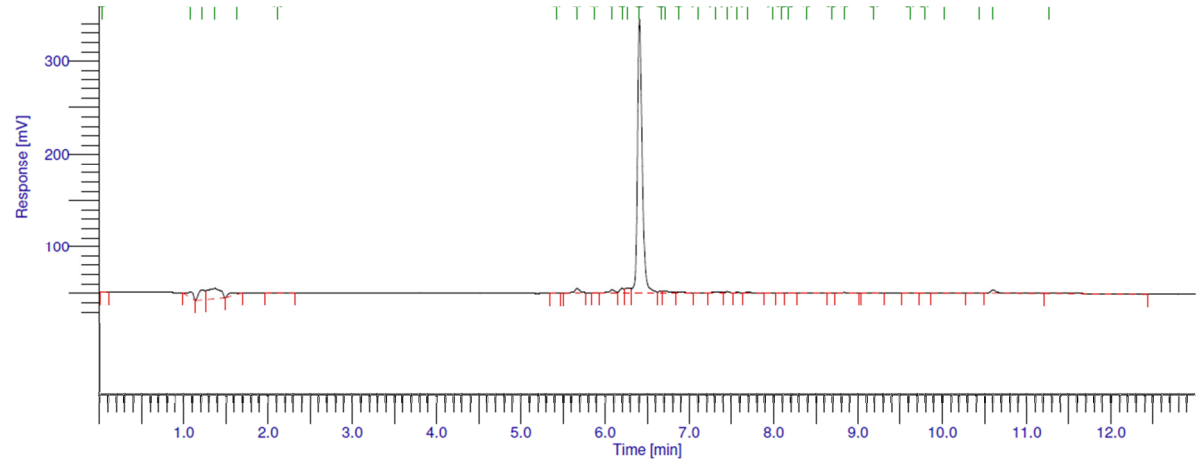

e) HPLC analysis of **[EuL^{2b}]Cl**, *Method C*, *Column 2*, λ_{abs} = 368.

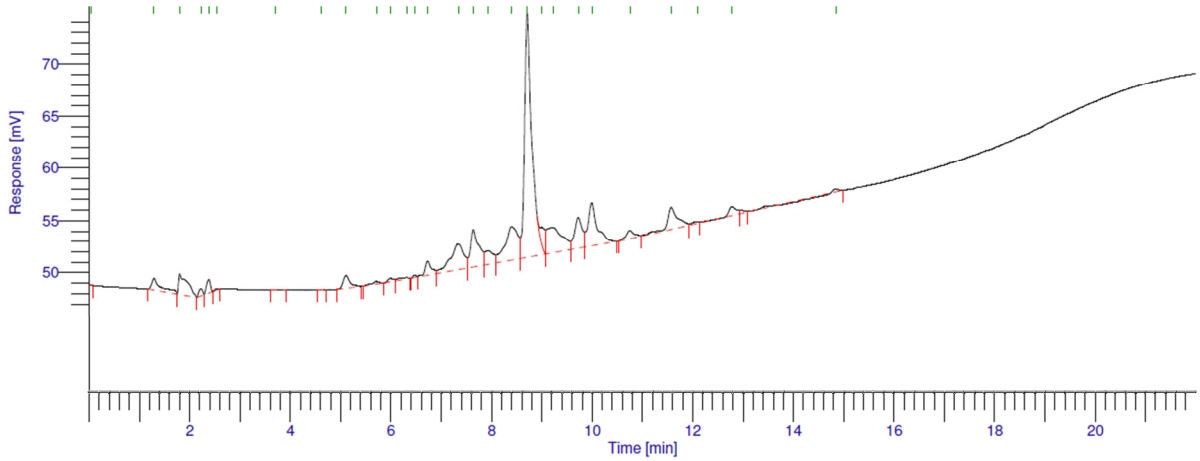

f) HPLC analysis of **[EuL^{3}]Cl$_2$**, *Method A*, *Column 1*, λ_{abs} = 328.

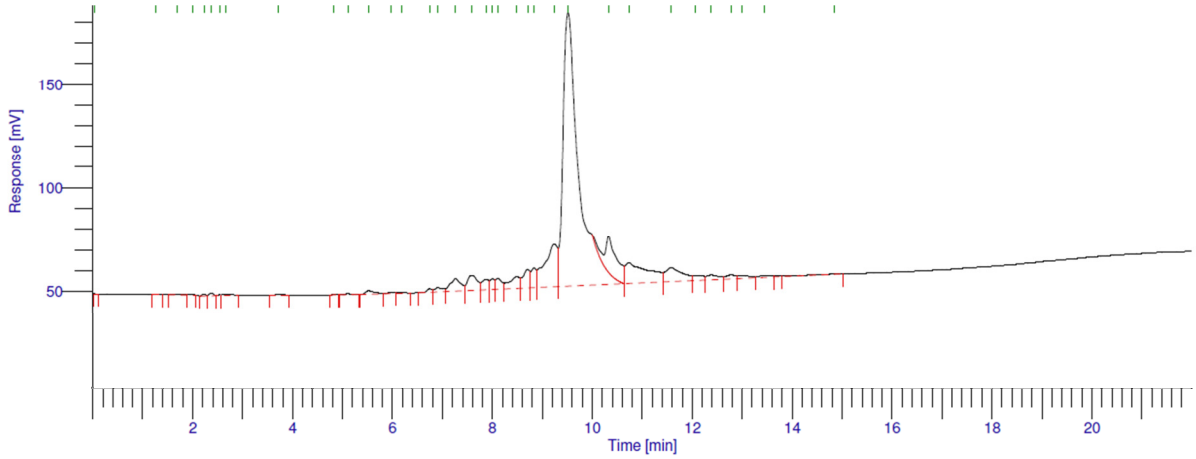

g) HPLC analysis of **[EuL^4]Cl$_3$**, *Method A*, *Column 1*, λ_{abs} = 328.

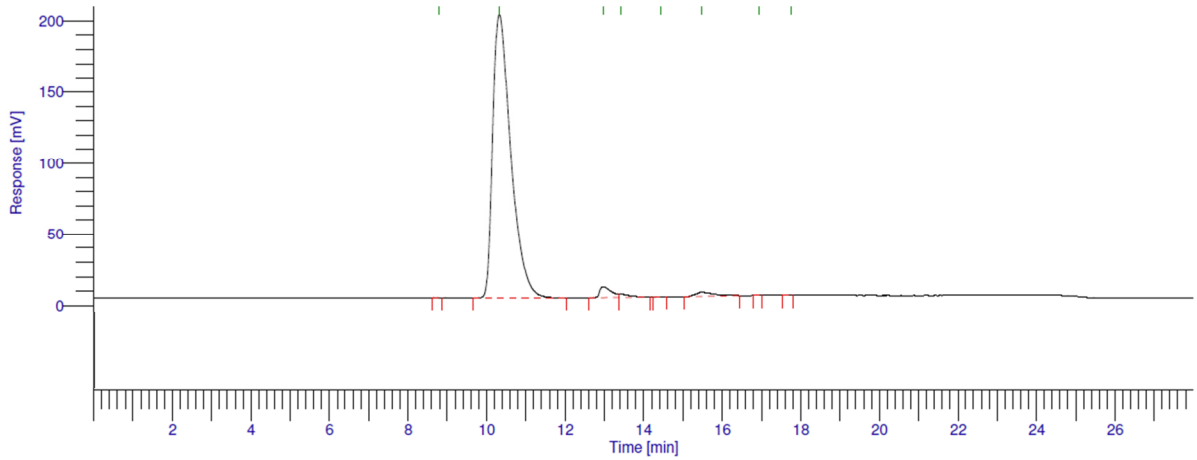

h) HPLC analysis of **[EuL^5]**, *Method B*, *Column 1*, λ_{abs} = 275.

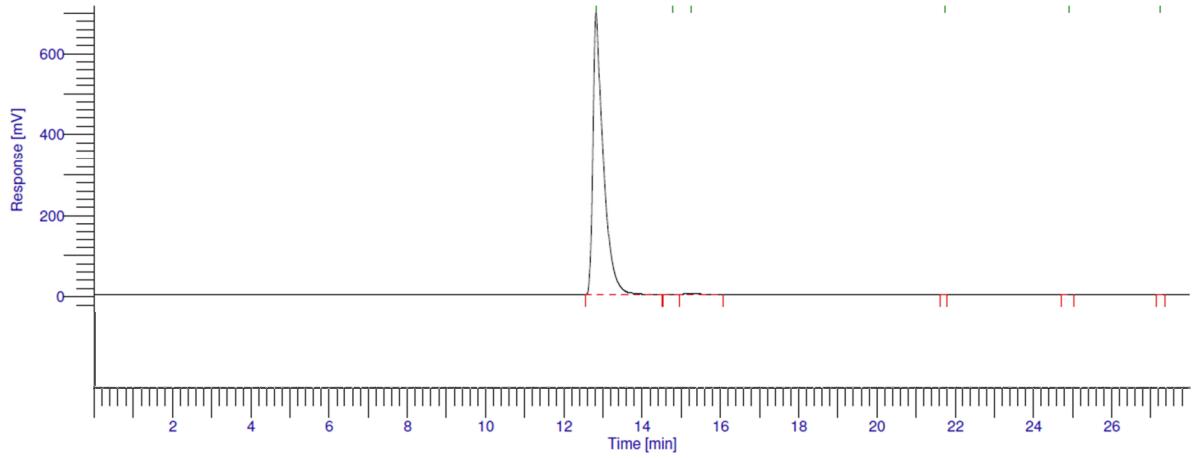

i) HPLC analysis of **Na[EuL^6]**, *Method B*, *Column 1*, λ_{abs} = 275.

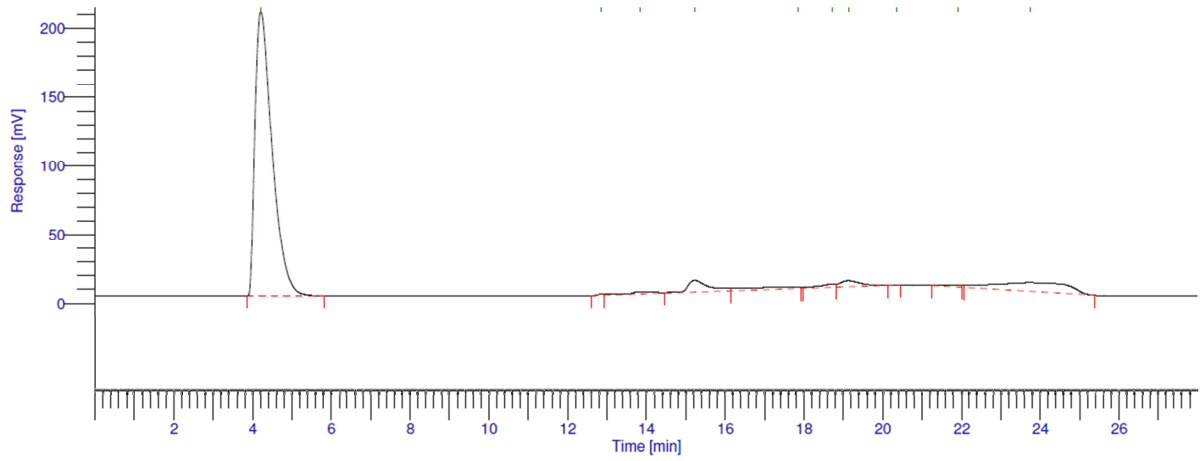

j) HPLC analysis of **Na[EuL^{7}]**, *Method B*, *Column 1*, λ_{abs} = 275.

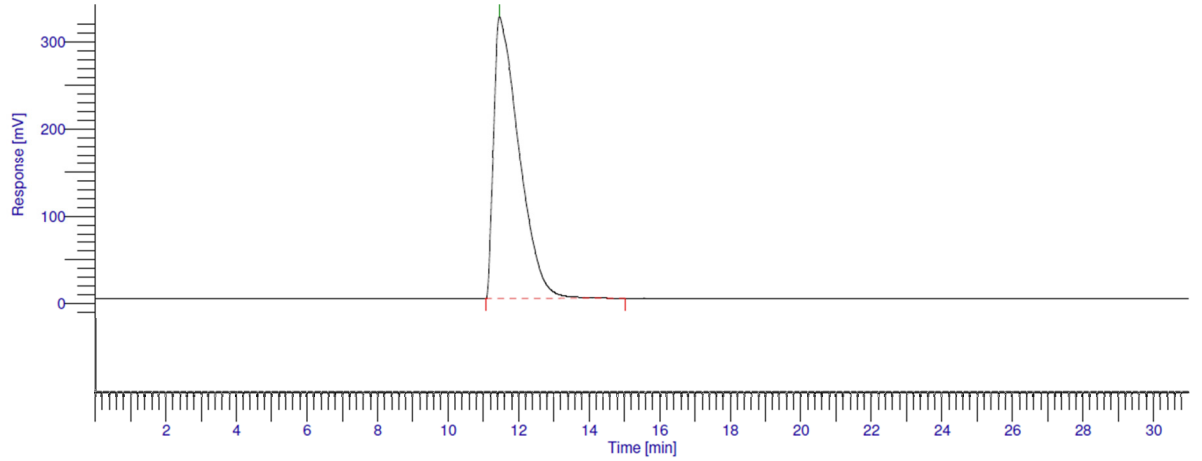

k) HPLC analysis of **Na[EuL^{8}]**, *Method B*, *Column 1*, λ_{abs} = 275.

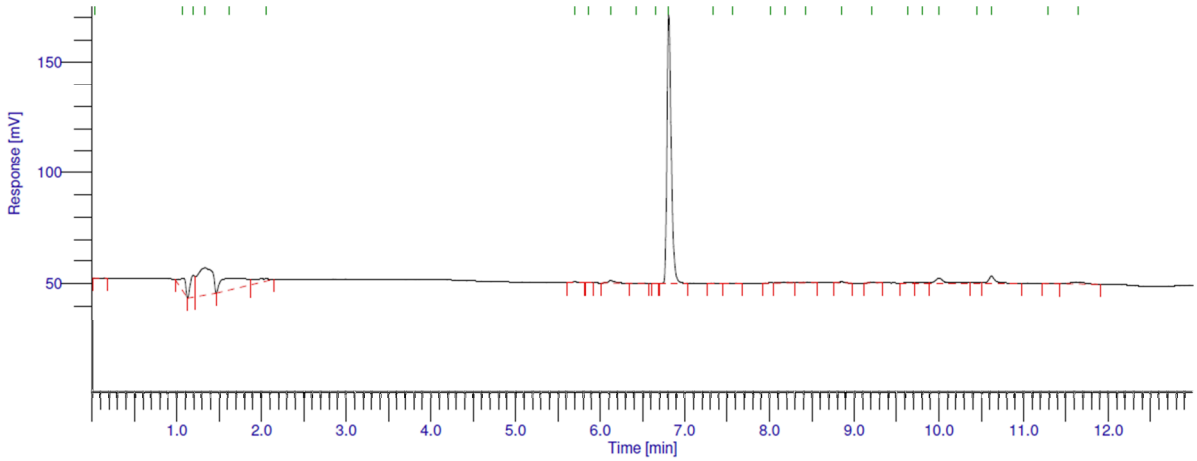

l) HPLC analysis of **[EuL^{9}]**, *Method C*, *Column 2*, λ_{abs} = 275.

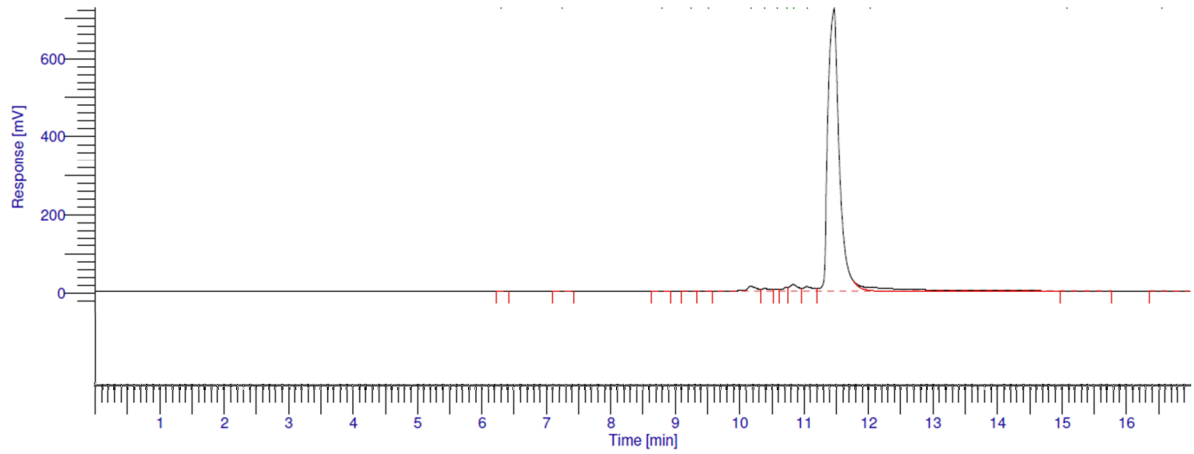

m) HPLC analysis of **[EuL^{11}]**, *Method D*, *Column 1*, λ_{abs} = 332.

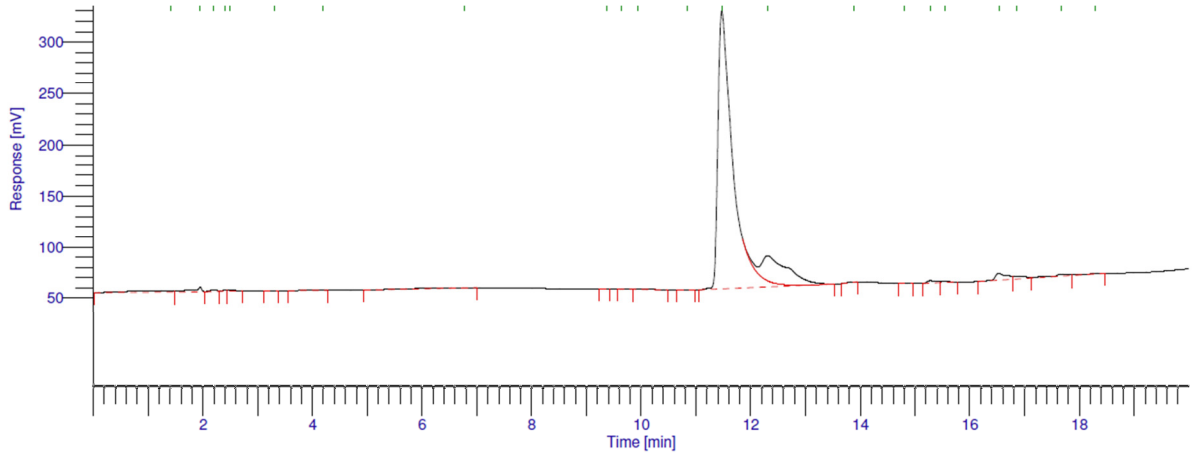

n) HPLC analysis of **[EuL^{12}]**, *Method D*, *Column 1*, λ_{abs} = 332.

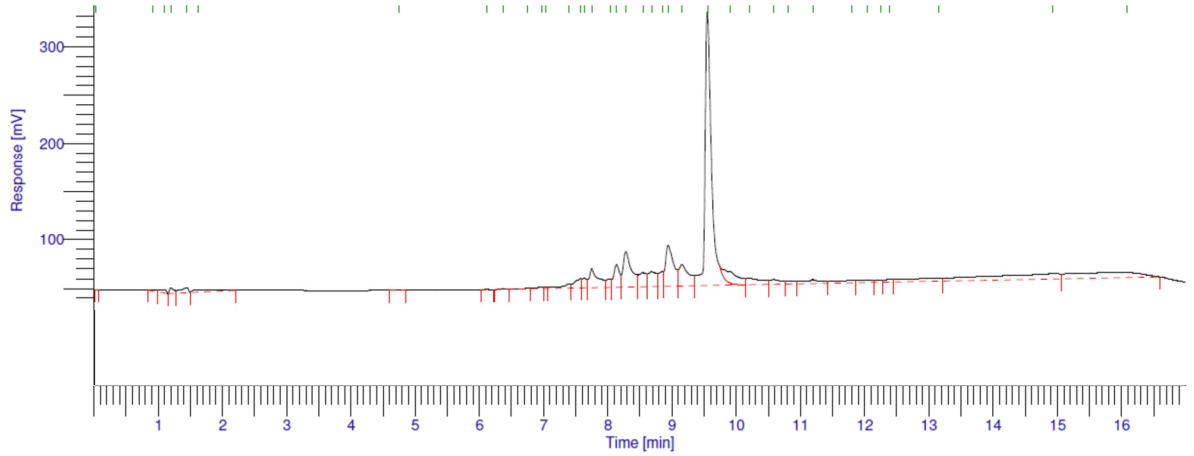

o) HPLC analysis of **[EuL^{13}]Cl**, *Method D*, *Column 1*, λ_{abs} = 332.

Appendix 2.

Stability Assays for Each Complex

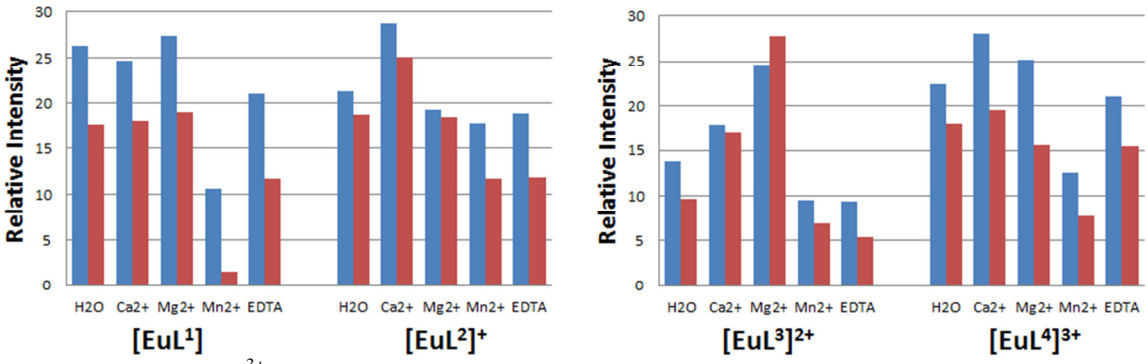

a) Changes in Eu^{3+} emission intensity after 15 min (*blue*) or 18h (*red*) in the presence of the stated additives (10nM complex, 20mM additive, λ_{ex} = 335 nm, λ_{ex} = 620 nm).

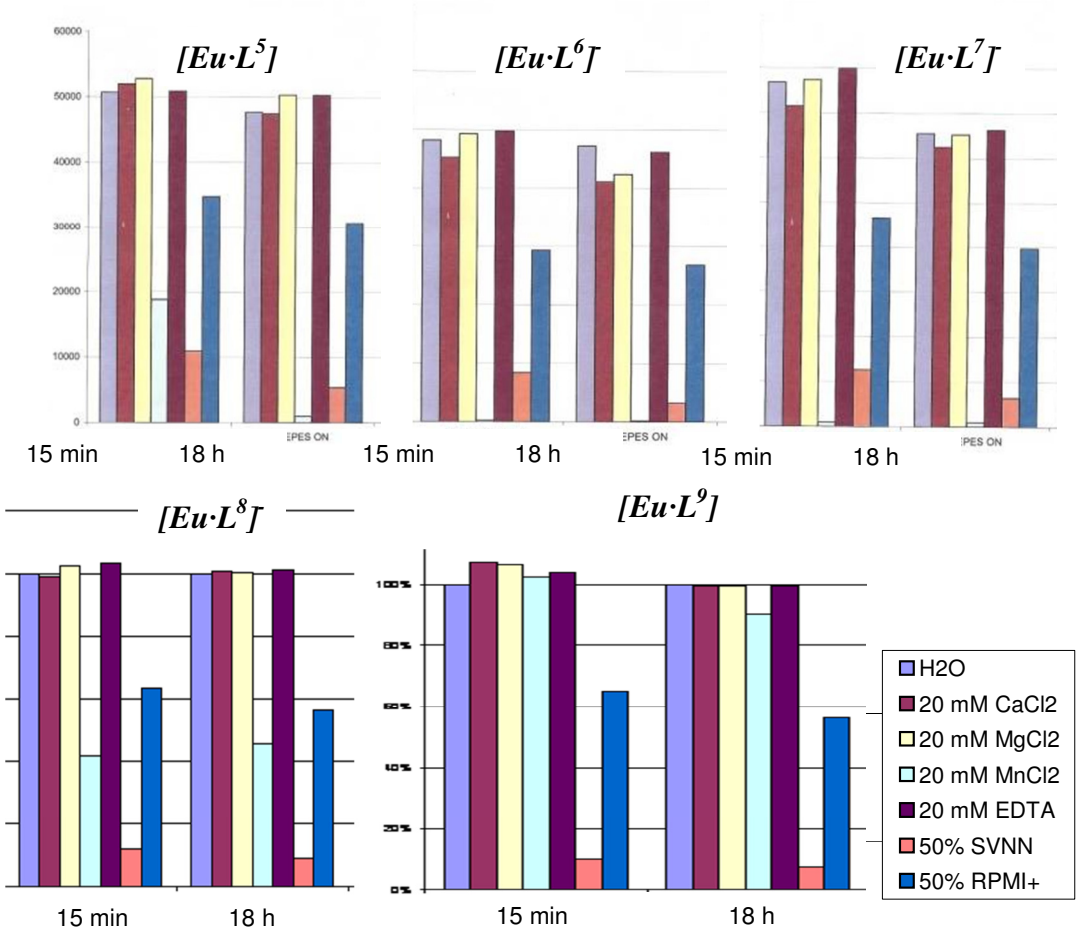

b) Changes in Eu^{3+} emission intensity after 15 min or 18 h in the presence of the stated additives (10nM complex, 20mM additive, λ_{ex} = 335 nm, λ_{ex} = 620 nm).

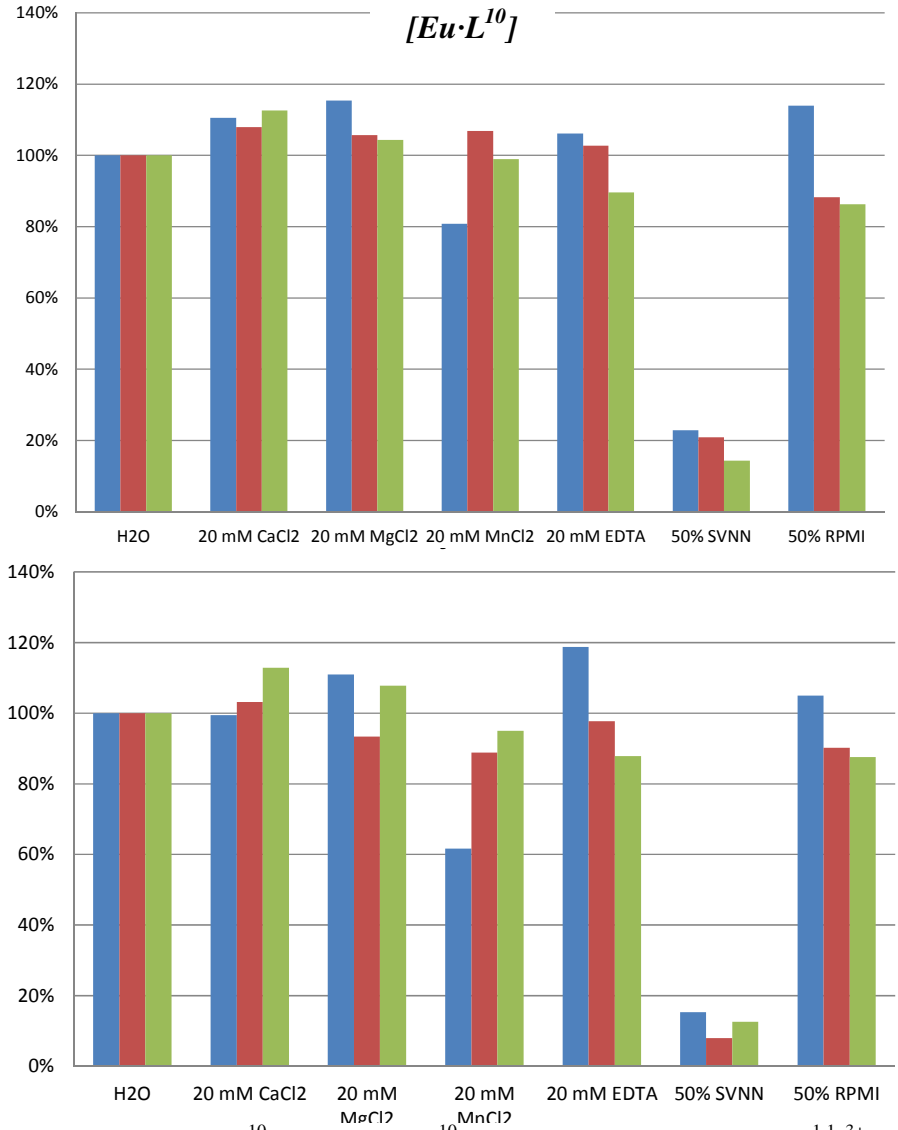

c) Stability assay for [Eu·L^{10}] (*blue*), [Eu·L^{10}] in 0.4 M KF (*red*) and [Eu·$L^{1.1}$]$^{3+}$ (*green*) after 10 min (*upper*) and 18 h (*lower*) (10nM complex, 20mM additive, λ_{ex} = 335 nm, λ_{ex} = 620 nm).

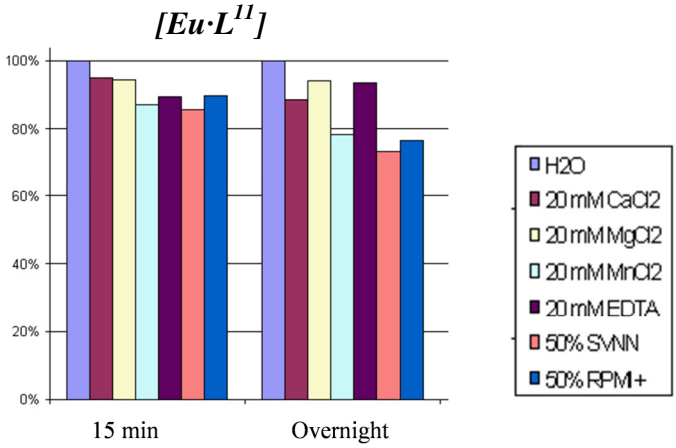

d) Changes in Eu^{3+} emission intensity after 15 min or 18 h in the presence of the stated additives (10nM complex, 20mM additive, λ_{ex} = 335 nm, λ_{ex} = 620 nm).

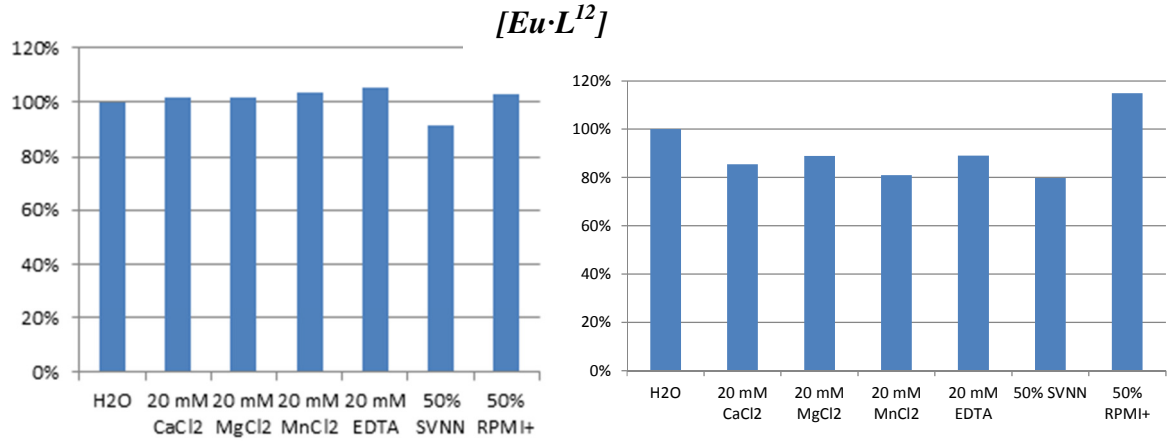

e) Changes in Eu^{3+} emission intensity after 15 min (*left*) or 18 h (*right*) in the presence of the stated additives (10nM complex, 20mM additive, λ_{ex} = 335 nm, λ_{ex} = 620 nm).

Appendix 3.

List of Complexes

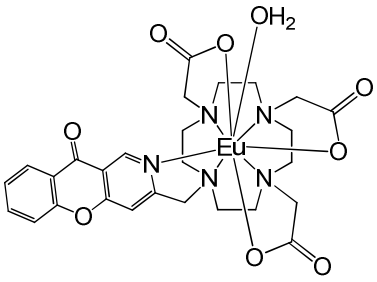

[Eu·L^{1}]

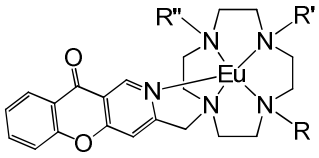

[Eu·L^{2}]$^{+}$: R' = 3-Azaxanthone
R, R'' = $CH_2CO_2^-$

[Eu·L^{3}]$^{2+}$: R, R'' = 3-Azaxanthone
R' = $CH_2CO_2^-$

[Eu·L^{4}]$^{3+}$: R, R', R'' = 3-Azaxanthone

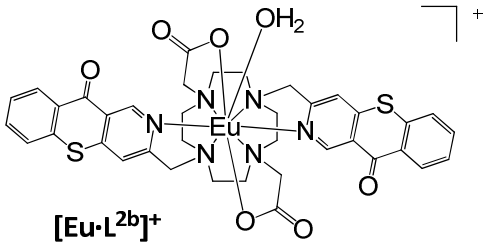

[Eu·L^{2b}]$^{+}$

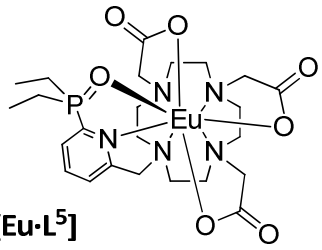

[Eu·L^{5}]

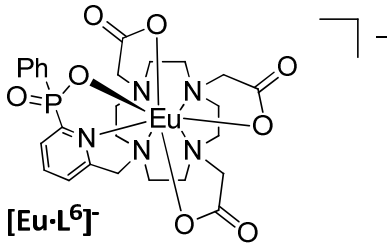

[Eu·L^{6}]$^{-}$

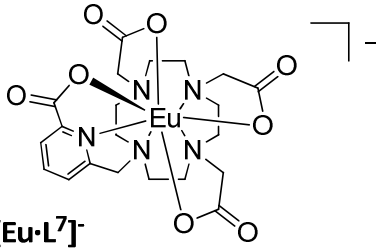

[Eu·L^{7}]$^{-}$

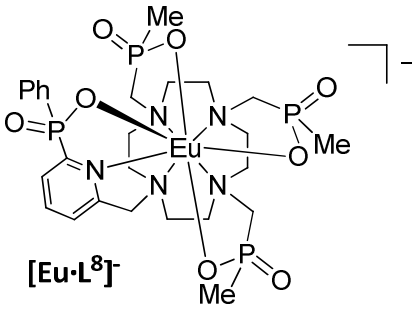

[Eu·L^{8}]$^{-}$

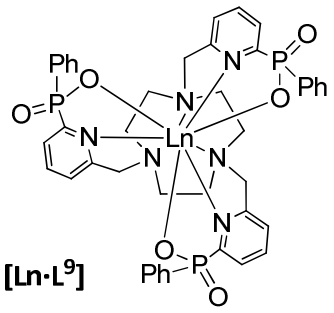

[Ln·L^{9}]

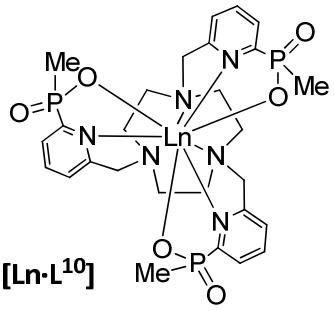

[Ln·L^{10}]

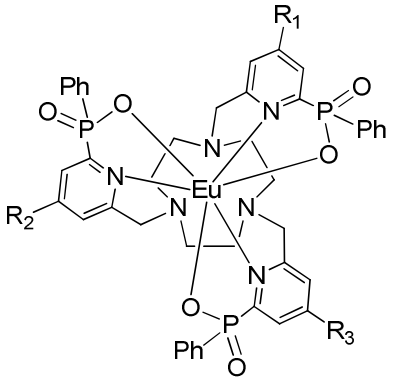

[Eu·L^{11}]

[Eu·L^{12}]

$R_1 = R_2 = R_3 =$ 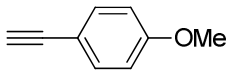

$R_1 = R_2 =$ 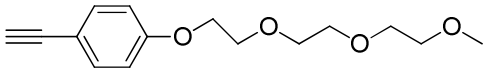

$R_3 =$ 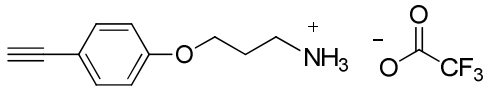

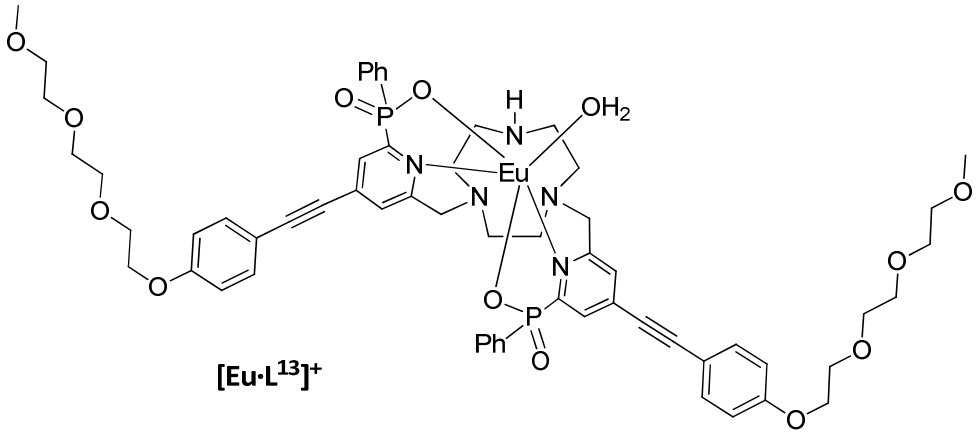

[Eu·L^{13}]$^{+}$